Technical Report No. 32-396

Radar Exploration of Venus: Goldstone Observatory Report for October–December 1962

Edited by
R. Goldstein
R. Stevens
W. K. Victor

JET PROPULSION LABORATORY
CALIFORNIA INSTITUTE OF TECHNOLOGY
PASADENA, CALIFORNIA

March 1, 1965

Technical Report No.32-396

Radar Exploration of Venus: Goldstone Observatory Report for October–December 1962

Edited by

R. Goldstein

R. Stevens

W. K. Victor

E. Rechtin

Assistant Laboratory Director for Tracking and Data Acquisition

JET PROPULSION LABORATORY

CALIFORNIA INSTITUTE OF TECHNOLOGY

PASADENA, CALIFORNIA

March 1, 1965

Prepared Under Contract No. NAS 7-100
National Aeronautics & Space Administration

CONTENTS

CONTENTS (Cont'd)

CONTENTS (Cont'd)

TABLES

FIGURES

FIGURES (Cont'd)

FIGURES (Cont'd)

FIGURES (Cont'd)

FIGURES (Cont'd)

FIGURES (Cont'd)

FIGURES (Cont'd)

ABSTRACT

Venus returned for another conjunction with the Earth in the fall of 1962 and was once again the object of extensive study by the Goldstone radar observatory. Radiometer studies, spectral studies, frequency-time mapping, amplitude-modulated ranging, automatic frequency tracking, and polarization studies were undertaken.

The average radar cross-section was found to be 10%, and there was a noticeable variation from day to day. Velocity tracking and time-of-flight measurements definitely confirmed the value of the astronomical unit which was found during the previous conjunction, and refined its accuracy somewhat. Polarization studies show negligible polarization rotation through both the interplanetary medium and the ionosphere of Venus at a wavelength of 12½ cm.

Three separate methods were used to determine the rotation period of Venus: tracking of a spectral feature across the disk, estimation of a set of spectral base-bandwidths, and measuring the widths of range-gated spectrums. The estimated period is 250 ±50 days *retrograde,* with the axis of rotation nearly perpendicular to the orbit.

I. INTRODUCTION

S. Golomb

In the spring of 1961, from March 10 to May 12, the Jet Propulsion Laboratory, using equipment of the Deep Space Instrumentation Facility's Goldstone Tracking Station, conducted radar experiments on a daily basis involving reflection of a continuous wave S-band signal from the surface of the planet Venus. Two 85-ft antennas at the Goldstone Station, approximately seven miles apart, were used as transmitter and receiver. The detection of the Venus reflection on March 10, 1961, was the first time successful real-time radar detection of another planet had been accomplished from the Earth. From the series of experiments, a number of conclusions about characteristics of Venus, in particular, and the solar system, in general, could be inferred. Thus, values were obtained for the reflectivity of Venus and the surface roughness of that planet. However, the most important achievement was improvement in the knowledge of the Astronomical Unit by approximately two and one-half orders of magnitude. A complete description of the objectives, instrumentation, data obtained, and conclusions reached in that series of experiments is contained in Ref. 1. At least four other radar investigations of the planet Venus, independent of the JPL experiments, were conducted in the spring of 1961 and reported on, involving antenna sites in Massachusetts (Ref. 2), New Jersey (Ref. 3), England (Ref. 4), and the Soviet Union (Ref. 5).

In an attempt to supplement the information obtained in the 1961 radar experiment, and as an inspiration for a further improvement in the performance capabilities of the Deep Space Instrumentation Facility equipment, it was decided to undertake another series of radar experiments during the time period of the November 12, 1962, inferior conjunction of Venus. This set of tests began with a successful detection of a radar echo from Venus on October 1, 1962, and continued on an almost daily basis until December 15, 1962.

For this new series of tests, it was felt that further improvement of tracking information (i.e., refinement of the Astronomical Unit and the planetary ephemeris) was no longer the principal objective. Indeed, the considerable improvement in knowledge of the Astronomical Unit resulting from the use of radar rather than optical measurements had already been adequately exploited. As an adjunct to the Jet Propulsion Laboratory's program for the exploration of the planets (*Mariner II* was en route to its successful rendezvous of December 14, 1962, with Venus during the entire duration of the 1962 Venus radar experiment), the primary emphasis was placed on obtaining "planetary science" information about Venus.

From a careful study of the doppler spreading of the returning signal, it was hoped that more could be learned about the rotation period and axis tilt of Venus. It was also hoped that surface characteristics could be deduced from reflectivity data and polarization experiments.

For the 1962 experiments, a monostatic system, involving an 85-ft azimuth-elevation mounted antenna at the new Goldstone "Venus site" was employed, using a continuous wave S-band signal, which was keyed on and off for intervals equal to the round trip propagation time from Goldstone to Venus. This 3-db loss in duty cycle, as compared with the bistatic 1961 system, was more than offset by improvements elsewhere in the system, including better signal processing techniques, lower receiver temperatures, and higher antenna aperture efficiency.

The data gathered were of the following types:

1. The power of the echo was observed by using the receiver in the configuration of a radiometer.
2. The spectrum of the echo was obtained, pure CW being transmitted.
3. The range-gated spectrum was observed, i.e., regions of Venus were selected and the spectra of the echoes returning only from those regions were measured.
4. The effect of changing the mode of linear and circular polarization on the received power and spectrum was measured.
5. The relative Goldstone-Venus velocity was measured by the receiver in a phase-locked configuration.
6. The time-of-flight was measured by comparing the phases of the transmitted and received modulation.
7. The temperature of Venus was observed by its black-body radiation.

Several conclusions were reached from the 1962 Venus radar experiment. First, the value of the Astronomical Unit computed from the 1961 data was positively confirmed to an accuracy of 5 parts per million. Second, the measurements of surface reflectivity and roughness from the 1961 experiment were repeated, with some refinment in the measuring accuracy. Finally, the 1961 conclusion that the rotation rate of Venus is "slow" (not more than one rotation per 100 Earth days) was refined significantly, so that it now appears that the rotation of Venus is *retrograde*, with one *retrograde* revolution every 250 ± 50 days.

II. GENERAL SYSTEM DESCRIPTION

W. K. Victor

The 1961 Venus radar experiment (Ref. 1) utilized two 85-ft-diameter antennas which were located at the Echo and Pioneer sites (see Fig. 1). The two-antenna system was operated as a bistatic radar, transmitting with the Echo antenna and receiving with the Pioneer antenna. During the 1962 Venus radar experiment a single 85-ft-diameter antenna at the Venus site (see also Fig. 1) was utilized because the Echo and Pioneer antennas could not be made available by the DSIF owing to the need to track and communicate with the *Mariner 2* spacecraft on its way to Venus.

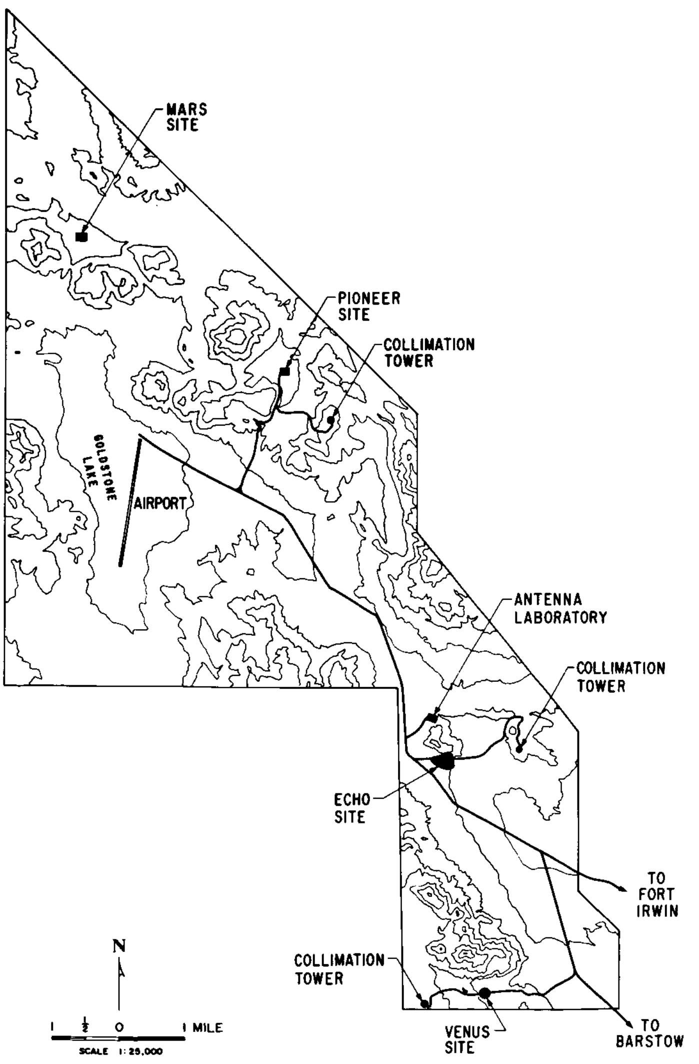

Fig. 1. Map showing Venus site in relation to Echo and Pioneer sites

The 1962 monostatic radar differed from the 1961 bistatic radar in the following ways:

1. The 1962 monostatic radar required a high-power/low-noise duplexer in order to accommodate both the transmitter and the receiver on the same antenna. A method of switching the duplexer automatically to compensate for the changing Earth-Venus range was also incorporated in the 1962 system.
2. A digital integrator at the output of the 1962 receiver was needed to replace the 1961 analog integrator in order to provide memory from one receive cycle to the next.
3. Precision range rate information was programmed into the 1962 digital closed-loop ranging system in order to carry the loop over from one receive cycle to the next, whereas the 1961 analog closed-loop ranging system did not require this added feature.
4. An automatic method of turning the klystron beam voltage off and on was incorporated in the 1962 transmitter to prevent the klystron beam noise from entering the receiver through the duplexer.
5. Continuous counting of rf doppler cycles was not feasible for the 1962 experiment because transmission (and reception) had to be interrupted.
6. Because half of the on-Venus time was taken up in transmission and half for reception, the 1962 monostatic radar was only half as efficient as the 1961 system in the gathering of data.
7. The 1962 single-antenna radar was simpler to operate and easier to maintain than the 1961 dual-antenna radar.

A photograph of the 1962 monostatic radar system at the Venus site is shown in Fig. 2.

The functional block diagram of the 1962 Venus radar system is shown in Fig. 3. The antenna was normally slaved to a Venus angle ephemeris provided on punched paper tape. However, it could be pointed manually by positioning the crosshairs of a telescopic television camera on Venus. The angle ephemeris was a list of time-tagged azimuth and elevation angles sampled at 64-sec intervals.

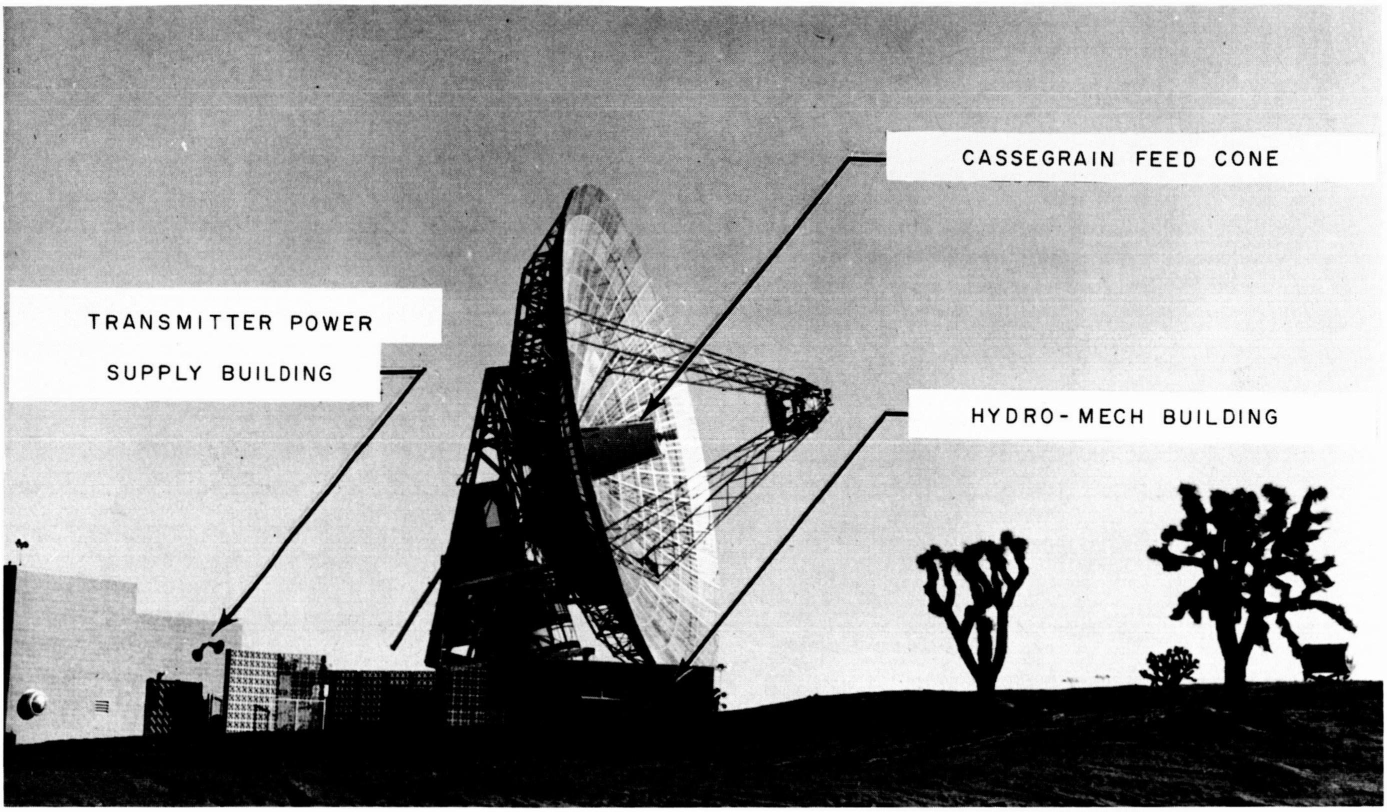

Fig. 2. Venus site antenna

The transmitter was capable of a continuous-wave output of 13 kw at a frequency of 2388 Mc; however, it could be keyed off intermittently to permit the receiver to distinguish the signal more easily from the background noise. The radio frequency power was delivered to the Cassegrain feed system which, with the help of the 85-ft-diameter paraboloidal reflector, concentrated the signal into a conical searchlight beam about 0.35 deg wide in the direction of the planet. The normal polarization of the transmitted signal was right-hand circular.

The normal polarization of the received signal was left-hand circular. The normal signal power at the output of the antenna was approximately 10^{-20} watts (-170 dbm). After amplification in a maser followed by a parametric amplifier, the signal was processed either in a continuous-wave receiver employing synchronous detectors exclusively, or in an amplitude modulation receiver which utilized square-law or envelope diode detectors.

Each type of receiver could be operated either open-loop or closed-loop. Therefore, four different receiver configurations were utilized, and four different types of data were gathered: (1) received signal level, (2) power spectrum and range-gated power spectrum of the Venus-reflected signal, (3) Venus-Earth velocity, and (4) Venus-Earth range. The signal level data and power spectra were obtained using the open-loop receiver configurations; the velocity and range data were obtained with the closed-loop configurations.

The receiving system was connected as shown in Fig. 4 to measure the signal level and power spectrum of the Venus-reflected signal. The transmitted signal was keyed *on* for approximately 1 sec and *off* for the same length of time in order to make the received signal measurements insensitive to slow variations in amplifier gain. The shaded blocks in Figure 4 show the portion of the amplitude modulation open-loop receiver that was modified for the 1962 experiment. As mentioned earlier, the postdetection integration was performed digitally in order to simplify the problem of holding the integrated value of signal level during the several-minute transmit cycle. However, other changes include (1) the use of an amplitude detector followed by a digital squarer to convert the number to power as opposed to the use of a square-law detector for the 1961 receiver and (2) the use of a digital low-pass filter as opposed to an analog filter

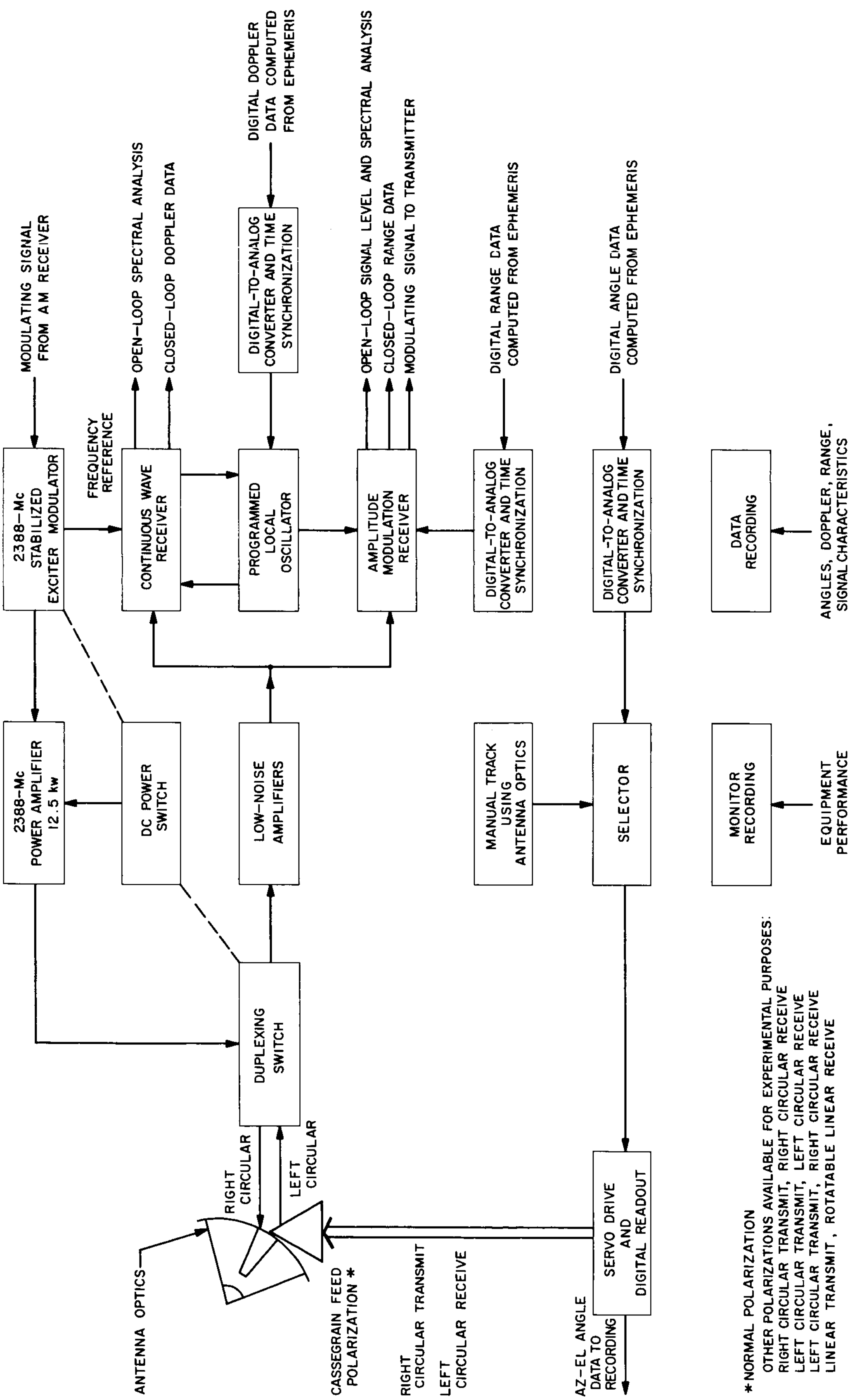

Fig. 3. Functional block diagram

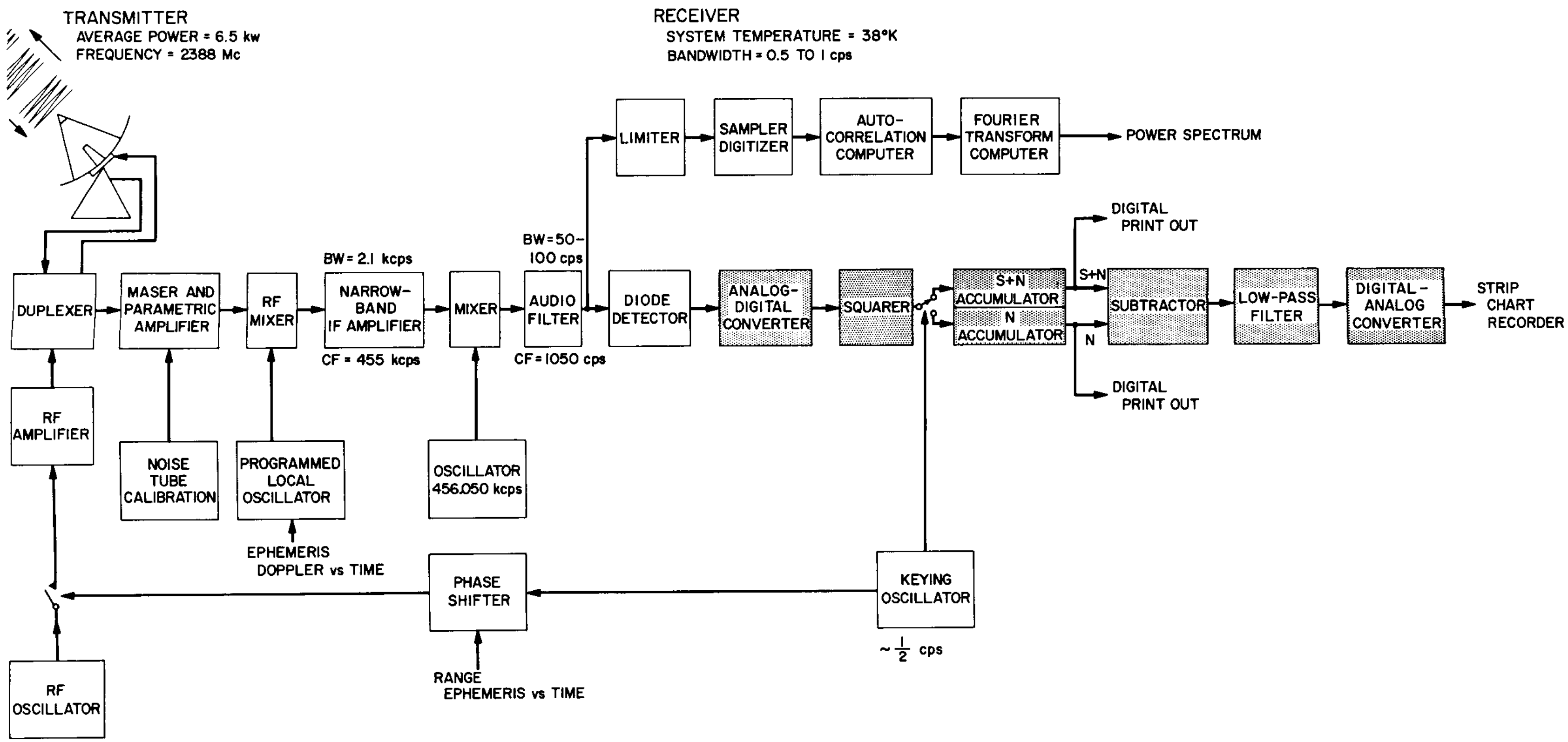

Fig. 4. Venus radar with amplitude modulation open-loop receiver

for the 1961 system. There were no changes in the spectrum analyzer portion of the receiver except to provide a computer for transforming the autocorrelation coefficients to a power spectrum at the end of each receive cycle for the operator to use as a check on the performance of the radar system. This system is discussed in greater detail in Sec. IV-A.

The balanced modulation open-loop receiver shown in Fig. 5 is a modification of the amplitude modulation receiver shown in Fig. 4 and was not a part of the 1961 receiver system. The balanced modulation system provides a power spectrum at selected intervals in range. This system is also discussed in greater detail in Sec. IV-A.

The system shown in Fig. 6 utilizes synchronous detectors throughout and detects the presence of a CW signal in noise by a standard autocorrelation computation method using a general purpose computer. This system provides a second and independent method of measuring the power spectrum of the Venus-reflected signal. It also provides an indirect method of measuring signal level when the noise spectral density is known. This system is very similar to that utilized in the 1961 Venus radar experiment and is discussed in Sec. IV-B.

Direct measurements of Venus-Earth velocity were made using the continuous-wave synchronous closed-loop receiver shown in Fig. 7. The frequency of the Venus-reflected signal was compared with the transmitted frequency, and the doppler-shifted echo—variable from 0 to 200,000 cps—was measured with a standard digital frequency counter using a gating-time of 1 sec. The accuracy of the measurement is affected by thermal receiver noise, internal transmitter/receiver oscillator noise, and signal distortion caused by anomalous surface reflection characteristics of the planet. The synchronous closed-loop receiver for this experiment is the same equipment as that used in the 1961 experiment and is described in Ref. 1 and Sec. V-A. The use of the doppler data in checking the previously determined value of the Astronomical Unit is described in Sec. VIII.

The closed-loop ranging equipment for this experiment (see Fig. 8) is completely different from that used in the 1961 experiment. The closed-loop portion of the 1961 equipment was part analog and part digital in order to expedite its design, fabrication, testing, and installation at Goldstone; the closed-loop portion of the 1962 equipment is all digital to achieve greater stability and flexibility and narrower tracking bandwidths. The 1962 digital system has the capability of accepting ephemeris range rate information which (1) updates the loop during the several-minute transmit cycle when there is no signal to which the loop can lock and (2) aids the loop during the receive cycle by requiring it to control displacement only. The width of the closed-loop range gate was 19 millisec, and the accuracy of the time-of-flight measurement is about 19 millisec in a typical round-trip flight time of 3×10^5 millisec, limited principally by thermal noise and calibration uncertainty. The pseudonoise-coded closed-loop ranging system is described in Sec. V-B.

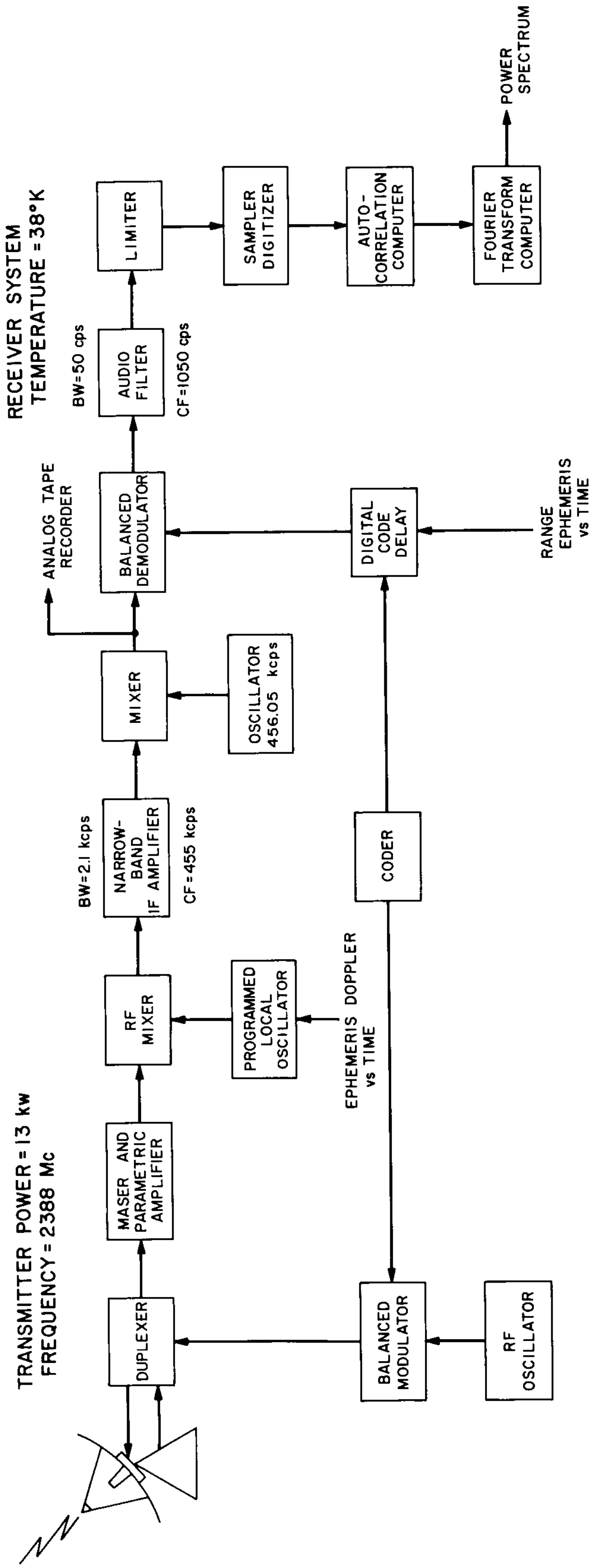

Fig. 5. Venus radar with balanced modulation open-loop receiver

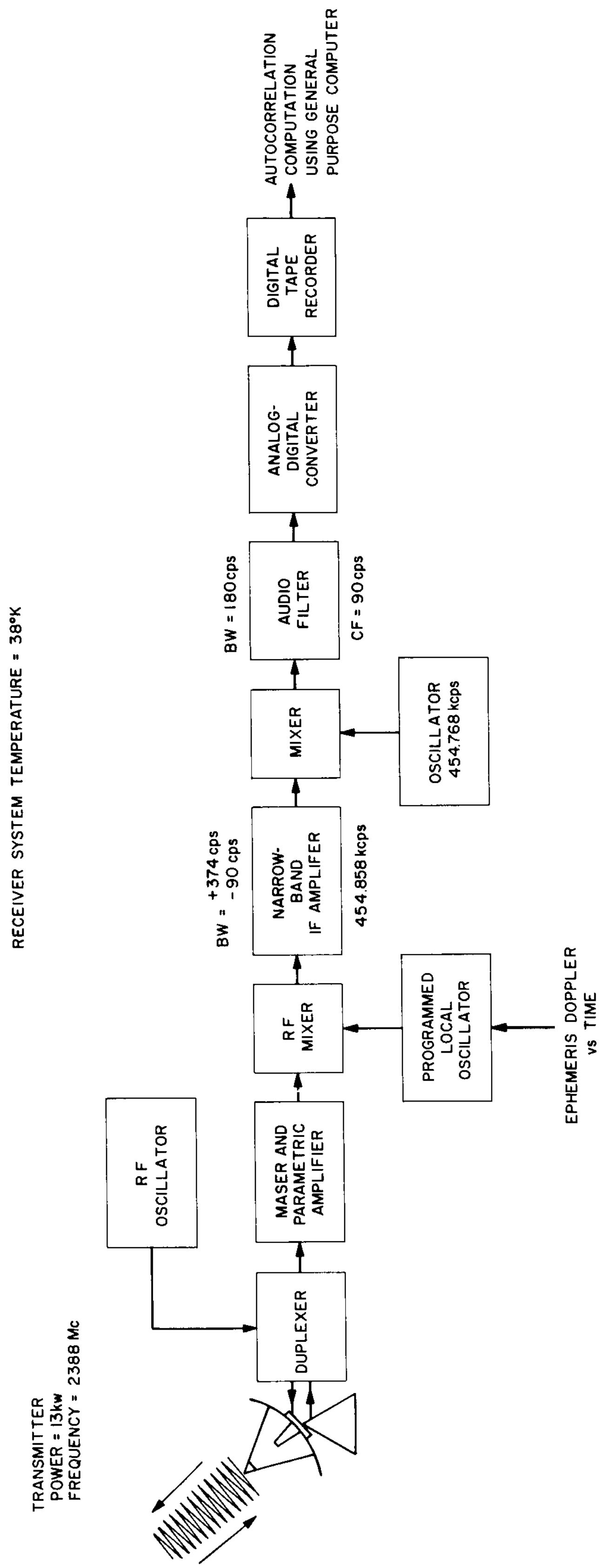

Fig. 6. Venus radar with continuous wave open-loop receiver

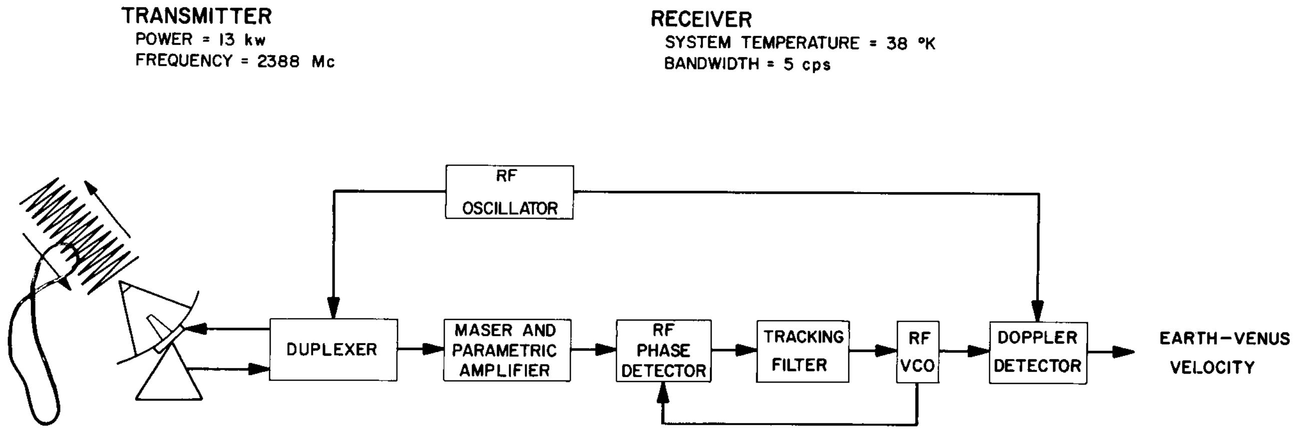

Fig. 7. Venus radar with continuous wave closed-loop receiver

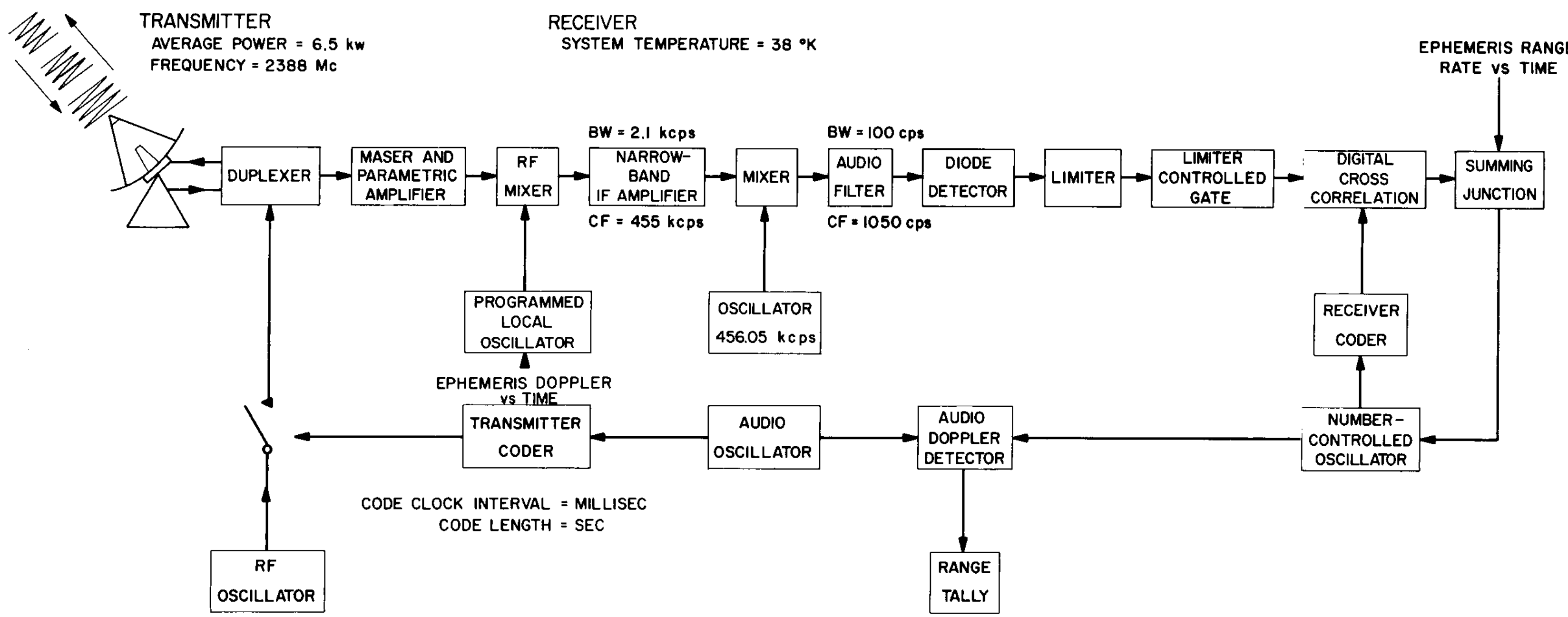

Fig. 8. Venus radar with amplitude modulation closed-loop ranging system

III. SYSTEM CAPABILITY AND CRITICAL COMPONENTS

A. Résumé

R. Stevens

Several improved components and subsystems were incorporated in the Goldstone planetary radar for the 1962 Venus experiment. Also, the one-antenna-system configuration required components not used in the earlier two-antenna system. Although the time-sharing transmit-receive duplexing cycle resulted in a 3-db loss of data per unit time relative to the 1961 radar system capability, the loss was more than compensated by a 3.5-db increase from better antenna aperture efficiency, less feed line loss, and lower system noise temperature, and from better transmitter stability, more precise receiver tuning, and more accurate and reliable antenna steering.

A comparison of the principal parameters of the 1961 and 1962 planetary radar systems is given in Table 1. The use of a Cassegrain feed system provided a good installation for the radio frequency portion of the duplexing system and for the low-noise portion of the receiver system. By very careful design of the microwave optics and transmission line system substantial improvements in the noise temperature and gain of the 85-ft antenna were obtained (item 1 of Table 1 and Sec. III-A).

The principal shortcomings of the earlier maser installation were gain instability from antenna motion, low gain resulting in significant system temperature degradation by the follow-on amplifier, and rather high noise temperature contribution from the maser itself. A dual-cavity-maser system was designed and constructed for the 1962 radar receiver which had significantly improved performance. The follow-on parametric amplifier was also redesigned and showed improved long-term stability and a lower noise temperature than obtained with its predecessor (items 2 and 3 of Table 1 and Sec. III-B and III-C).

The net improvement in receiver system performance from the better antenna efficiency, lower antenna temperature, and lower maser/paramp temperature was 2.8 db (item 5 of Table 1 and Sec. III-E). Calculated receiver thresholds are given in items 6 and 7 of Table 1.

The Cassegrain feed system gave increased gain and allowed a very low-loss transmission line system (item 8 of Table 1). Thus, even though the 1961 transmitter had to be used (item 9 of Table 1) a net increase in radiated power density was obtained (item 10 of Table 1). Calculated S/N ratios for the radar system on Venus are given in Item 11 of Table 1.

The accuracy of the doppler velocity measurement depends upon the frequency stability of the transmitter over the signal time-of-flight (5-10 min); the accuracy and resolution of the spectral measurement depend upon the stability of the transmitter and the precision of the receiver tuning over the time of a measurement (5 min to 10 hr). The use of a rubidium-vapor frequency standard and a reliable automatic local oscillator tuning machine improved the system measurement capability (items 12 and 13 of Table 1). The rubidium-vapor frequency standard was very reliable, more so than the atomic frequency standard previously used in the system.

The basic technique used for slaved steering with optical monitoring of the 85-ft antenna was similar to that used previously. Lacking the coordinate converter computer of the 1961 system, it was necessary to feed the angle comparator from an ephemeris tape reader in Az-El coordinates. The slaved tracking of the antenna was demonstrated to be good (see Sec. III-H). A new addition to the system block diagram was a tape driven range tracking loop, which automatically provided properly phased signal decoding waveforms and properly timed control functions for the transmit-receive cycle (see Sec. III-I).

B. Antenna Feed and Polarizer

P. Potter

A Cassegrainian feed system (Ref. 6) was utilized for the 1962 Venus radar experiment. The system provided a low effective antenna noise temperature, good aperture efficiency, and a convenient configuration for mounting receiver instrumentation on the antenna. Design and evaluation of a 960-Mc Cassegrainian feed system (Ref. 7) for one of the Goldstone 85-ft antennas were completed in late 1961 and demonstrated the suitability of the general approach.

The same general techniques utilized in design of the 960-Mc Cassegrain system were invoked for design of the 2388-Mc Venus radar feed. The subreflector design includes a non-optical beam-shaping flange (Ref. 7),

Table 1. Parameters of Venus radar systems

Component	1961 system	1962 system	Ratio of 1962 to 1961 performance
1. Receiver antenna	53.4-db net gain (including 0.2-db feed line attenuation) 15°K antenna temp. +14°K feed line temp.	54.2-db net gain (including 0.1-db feed line attenuation) 11°K antenna temp. + 8°K feed line temp.	0.8 db gain 1.8 db temp.
2. Preamplifier (maser)	2.5 Mc BW at 20-db gain, 26°K noise temperature (includes 1°K instrumentation noise)	2.7 Mc BW at 27-30 db gain. 21°K noise temperature (includes ~½°K instrumentation noise)	—
3. Postamplifier (parametric amplifier)	300°K noise temperature (400°K with cable) 4°K contribution to system temperature	290°K noise temperature (317°K with receiver). ½°K contribution to system temperature	—
4. Total system noise temperature	64°K (average of measurements during experiment)	40°K (average of measurements during experiment)	+2.0 db
5. Receiving system figure of merit, $M_r = \frac{\text{effective aperture}}{\text{system temperature}}$ $\left(\text{db relative to } \frac{1\ \text{ft}^2}{1\,^\circ\text{K}}\right)$	+16.7 db	+19.5 db	+2.8 db[2]
6. Synchronous receiver threshold S/N = 1 (5-cps BW)	173.6 dbm	−175.6 dbm	+2.0 db
7. Nonsynchronous receiver threshold S/N = 1 (for 25 cps predetection BW, post detection τ = 68 sec)	−181.2 dbm	−183.2 dbm	+2.0 db
8. Transmitter antenna	53.4 db net gain (including 0.4-db feed line attenuation). Separate transmitting and receiving antennas used	54.1 db net gain (including 0.2-db feed line attenuation). Single antenna used for both transmitting and receiving	+0.7 db[2]
9. Transmitter output power	13 kw (+71.1 dbm)	13 kw (+71.1 dbm)	0.0
10. Radiated power density	218×10^6 watts/steradian (+113.4 dbm/steradian)	256×10^6 watts/steradian (+114.1 dbm/steradian)	+0.7 db
11. Calculated S/N on Venus at 31×10^6 mi for Venus power reflection coefficient of 9% a. in minimum closed-loop BW b. For 25-cps input BW, τ = 68 sec	 +2.8 db[1] +10.6 db	 +6.3 db[1] +14.1 db	 +3.5 db +3.5 db
12. Transmitter stability	~$1{:}10^{10}$ for 10 min	~$2{:}10^{11}$ for 10 min	5
13. Receiver tuning accuracy	~$1{:}10^{9}$ continuously	~$2{:}10^{10}$ for 10 min	5

[1]This calculated S/N would be approached only for a very pure received signal spectrum i.e., spectrum width ≪ 5 cps. Since the spectrum of the Venus returned signal had a 3 db width of 5 to 10 cps the actual S/N achieved could not be determined.

[2]Total improvement in transmitter/receiver/antenna rf system performance is 3.5 db = improvement in: Radiated power density + receiving system figure of merit.

optimized by scale model pattern tests to reduce rearward spillover and therefore lower the antenna noise temperature. A sketch of the feed system configuration is shown in Fig. 9.

A new type of feed horn was developed for the 2388-Mc feed system. This feed horn (Ref. 8), referred to as a dual-mode conical horn, has improved sidelobe performance, thus increasing the feed-system aperture

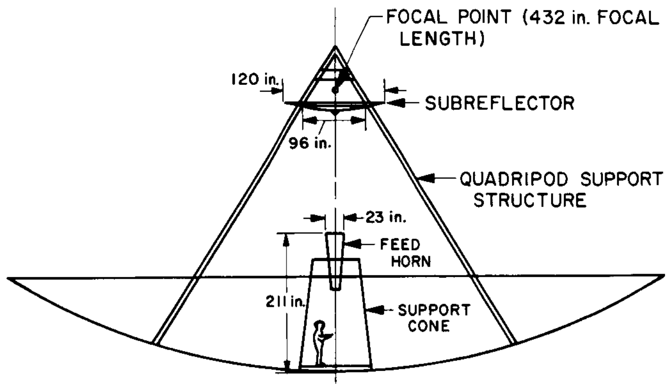

Fig. 9. Feed system configuration

efficiency and reducing the antenna spurious forward sidelobe level. Use of this type of feed horn reduces the forward spillover from approximately 12% (960-Mc Cassegrain system) to 4%.

To provide means for efficient and accurate polarization experiments during the radar experiments, sophisticated and versatile microwave circuitry was utilized (see pp. 25–26 of Ref. 9). Figure 10 shows the circuitry. Use of the two high-power rotary joints[1] permitted performance of a Faraday rotation experiment as well as rapid evaluation of celestial radio source polarization at 2388 Mc. For this linear polarization mode of operation, the turnstile junction (Ref. 10) required a manual change of its short circuits (approximately ½ hr operation) from the normally used short circuits. In the normal mode of radar operation, transmitter power entered one port of the turnstile junction and was radiated as right-handed circular polarization (*IRE* definition). The normal received signal was therefore left-handed circular polarization which appeared at the opposite port of the junction and entered the receiver system when both the polarization and transmit receive high-power switches[2] were reversed. For depolarization experiments only the transmit-receive high-power switch was reversed between transmit and receive operation.

A system was installed for remote control and readout of the polarizer and the three switches (see pp. 27–30 of Ref. 9). This system provided manual control and visual indication of the switch positions, manual control and synchro readout of the polarization position, and an analog voltage output indication of the polarization. During normal operations switching was accomplished automatically by ephemeris tape control. For this mode of operation, logic circuitry (see pp. 27–30 of Ref. 9) prevented the transmitter from being on when the switch positions were incorrect. Figure 11 is a photograph of the switch and polarization control rack as it was installed in the control trailer.

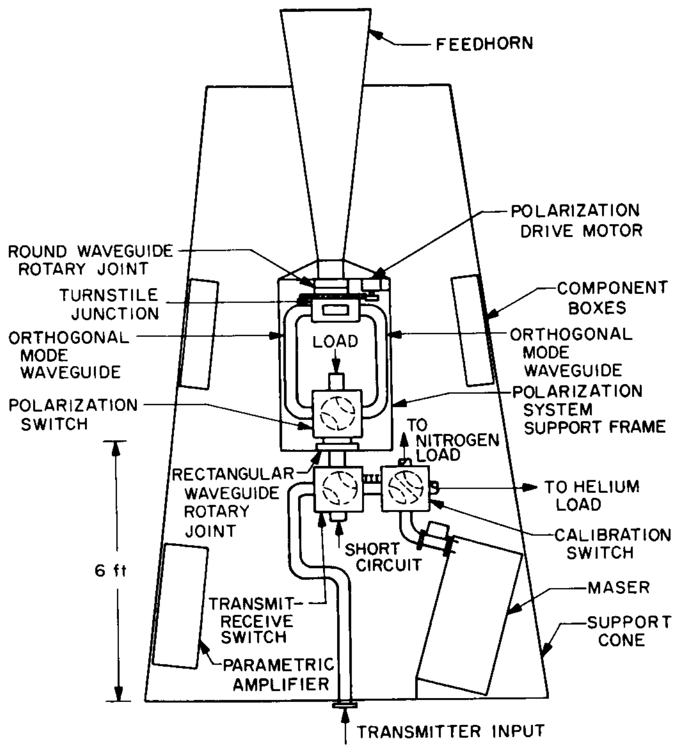

Fig. 10. Microwave circuitry

Cryogenic loads were utilized in the standard manner (Ref. 11) to determine the zenith antenna temperature and to calibrate the system noise temperature. Both liquid helium and liquid nitrogen loads were developed (see pp. 22–24 of Ref. 9) and used during the experiment, providing a method of accurate calibration in the range of 5 to 80°K. Detailed insertion loss tests were performed (see pp. 26–27 of Ref. 9) to determine reference temperatures at the calibration switch. This instrumentation, together with the maser, was used with the Y-factor method (see Sec. III-E) to evaluate the antenna temperature as a function of elevation angle.

The measured antenna temperature as a function of elevation angle θ is shown in Fig. 12, averaged over 3 runs taken at azimuths between 90 and 110 deg, and also at the collimation tower azimuth.

[1]Built by Canoga Corp., Van Nuys, Calif.
[2]Built by MCS Corp., Monrovia, Calif.

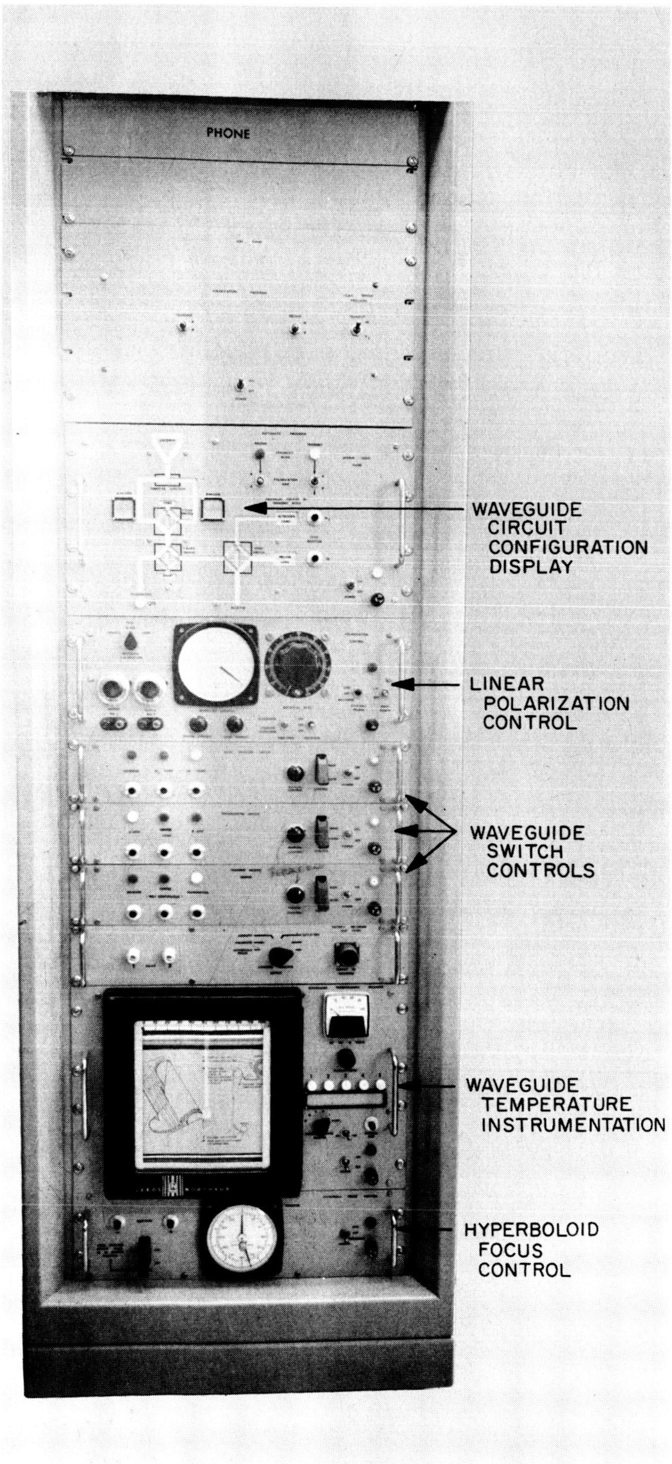

Fig. 11. Switch and polarizer control instrumentation

Aperture efficiency tests were made by the source flux method using the 1961 JPL Venus radar source calibrations as the reference. A summary of pertinent feed system performance data is shown in Table 2.

Table 2. Feed system data (2388 Mc)

Parameter	Measured value and estimated accuracy
Gain at feedhorn output	54.3 db ± 1 db p.e.
Aperture efficiency	64% ± 13% p.e.
Transmission line loss between feedhorn output and maser	0.12 db ± 0.01 db p.e.
Transmission line noise contribution	8.2°K ± 0.7°K p.e.
Zenith noise temperature at feedhorn output	11.0°K ± 1°K p.e.
Transmission line loss between feedhorn output and transmitter	0.20 db ± 0.05 db p.e.
Normal polarization	Right circular transmit Left circular receive

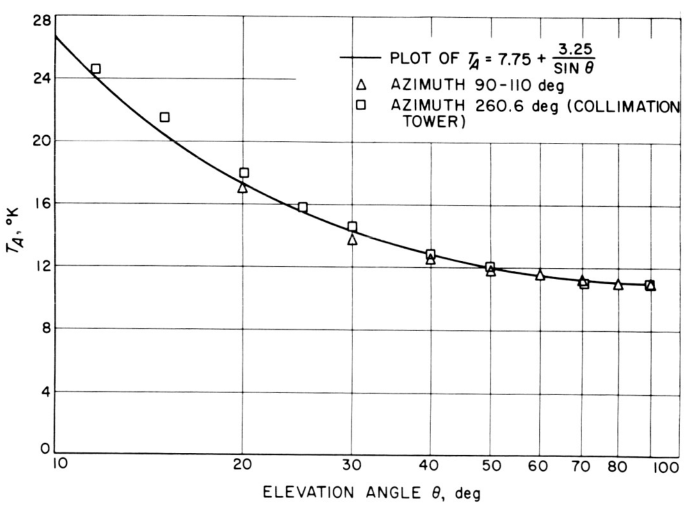

Fig. 12. Antenna temperature vs elevation angle

C. *Maser Amplifier*

W. Higa and R. Clauss

A dual-cavity ruby maser was used as a low-noise preamplifier for the radar receiver. The important advantage of the dual-cavity maser is improvement in gain stability over a single-cavity unit operating with the same total gain. The following discussion illustrates how this improvement results.

An inherent difficulty with all reflection-type amplifiers is the sensitivity of gain to changes in source or load impedances. Let g_1 represent the power gain of the first maser under ideal conditions (see Fig. 13); then the actual gain, G_1, of the first stage is given approximately by

$$G_1 \cong g_1 + 2\alpha_1 g_1^{3/2} \quad (1)$$

Where the second term is due to the reflection resulting from mismatches at the ports of the ideal circulator. Here α_1 is the magnitude of the voltage reflection coefficient (a fixed phase factor is assumed for simplicity). Even if the internal gain of the maser remained constant, it is noted that fluctuations in α_1 due to environmental conditions can cause large gain fluctuations:

$$\delta G_1 = 2g_1^{3/2}\,\delta\alpha_1 \quad (2)$$

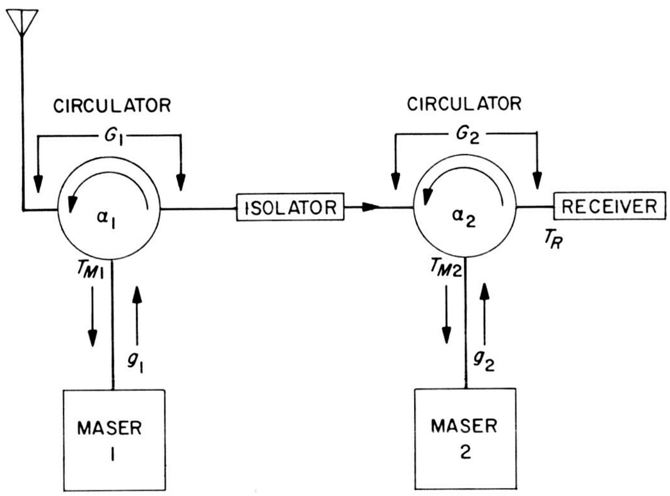

Fig. 13. Dual cavity maser

T_{m1}, T_{m2}, T_r are equivalent noise temperatures at the input terminal of each respective stage

Equation (2) shows clearly that a single cavity maser will have serious stability problems at high gains. Consider for example: $g_1 = 26$ db, and a change in effective VSWR from 1.04 ($\alpha = 0.02$) to 1.05 ($\alpha = 0.025$, then

$$\delta G = 2\,(400)^{3/2} \times 5 \times 10^{-3} = 80$$

or

$$\delta G = 0.78 \text{ db}$$

The stability of a cascaded pair of masers can be improved by use of a good isolator between stages as shown in Fig. 13. The fluctuation for each stage is independent and the total gain variation is given by

$$\delta G = \delta(G_1\,G_2) = G_1\,\delta G_2 + G_2\,\delta G_1 \quad (3)$$

where δG_1 and δG_2 are given by expressions similar to Eq. (2). In order to compare with a single cavity maser with the same total gain, Eq. (3) may be written approximately as

$$\delta G \cong 2g_1\,\delta G_1 = 4g_1^{5/2}\,\delta\alpha_1 \quad (4)$$

where identical units for the two stages are assumed. If a single-stage maser is to provide the same total gain, the fluctuation is given by

$$\delta G^1 \cong 2g_1^3\,\delta\alpha_1 \quad (5)$$

Thus the degradation over a dual-cavity maser is

$$\rho = \delta G^1 \,/\, \delta G = g_1^{1/2}/\,2 \quad (6)$$

As a typical example, if $g_1 = g_2 = 13$ db for a total gain of 26 db, the dual-cavity master will be twice as stable as a single-cavity unit with the same total gain.

The 2388-Mc maser, which was designed and built for the radar receiver, consists of two complete single-cavity amplifiers in one dewar with a common magnet (2450 gauss) and klystron pump supply. Figure 14 shows the dual-cavity head. The first unit with a WR430 waveguide circulator and a ¾-in.-outside-diameter stainless steel transmission line has 18-db gain. The second unit has an "N" connector circulator, 5/16-in. transmission line, and 13-db gain.

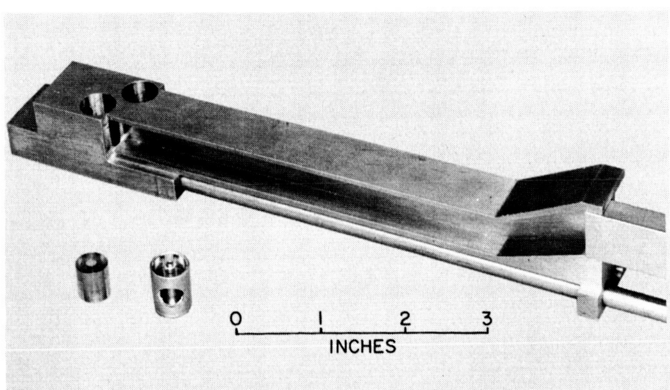

Fig. 14. Dual cavity maser structure

Shown in foreground are ruby cylinder and coaxial cavity

Two 0.010-in. wall stainless steel wave guides supply the pump power. The coxial lines and pump wave guides provide support for a machined brass structure, which contains the cavities. Figure 15 illustrates the manner in which signal coupling and frequency adjustments are made. Pump power enters the ruby through an iris in the outer conductor of the coaxial cavity.

Because the orientation of the C axis with respect to the magnetic field determines the necessary field strength for resonance, the two rubies must be aligned very accurately with respect to each other. Figure 16 illustrates the manner in which this is accomplished. The maser structure is rotated in the magnetic field until the horizontal C axis of one ruby reaches the identical angle as created between the vertical C axis of the other ruby and the magnetic field. The structure is sealed to keep liquid helium from entering the assembly. Thus, instability caused by boiling helium in the maser cavities and impedance changes due to shifting liquid levels are eliminated. Laboratory checks indicated less than ½-db gain drift during an 8-hr period.

The maser gain instability due to antenna motion during normal tracking was less than ½ db peak-to-peak. Figure 17 is a plot of the maser gain taken with the antenna moving at 0.15 deg/sec in elevation. The maser was initially tested without an isolator between the two stages, and small variations in source impedance caused troublesome gain variations. For example, rotation of the antenna feed polarizer with a VSWR 'wow' of ~1.01 produced 0.3-db gain variations; after adding the isolator (see Fig. 13), the gain variations from that source were reduced to <0.05 db.

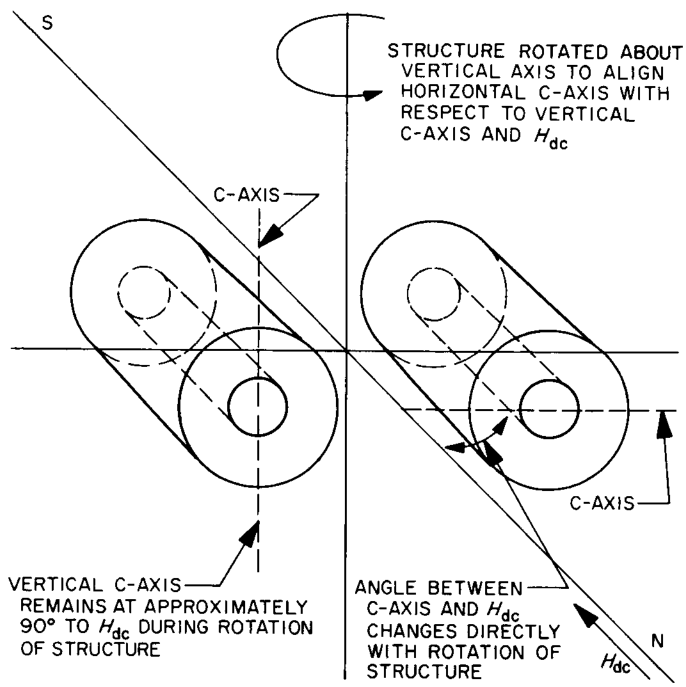

Fig. 16. Illustration of C-axis alignment of ruby cylinders

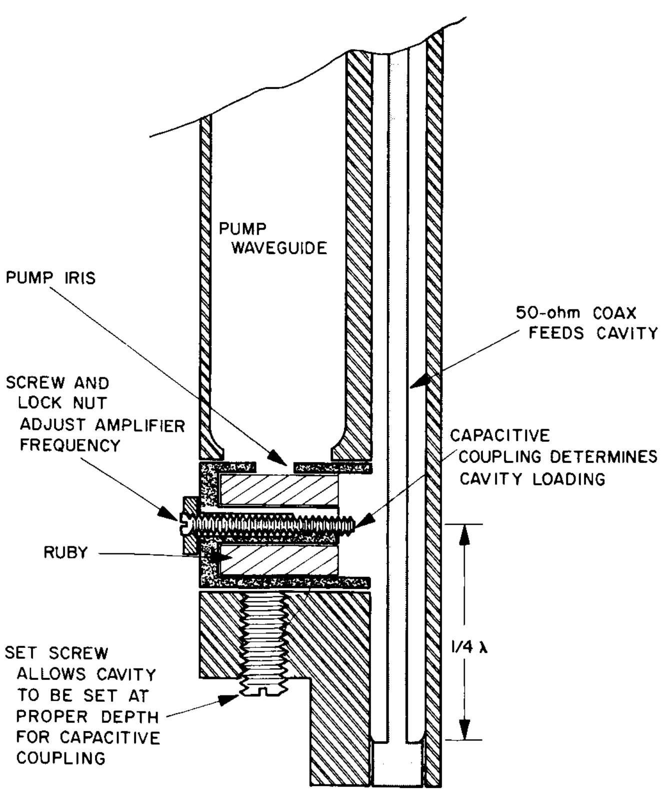

Fig. 15. Machined brass structure for 2-cavity maser

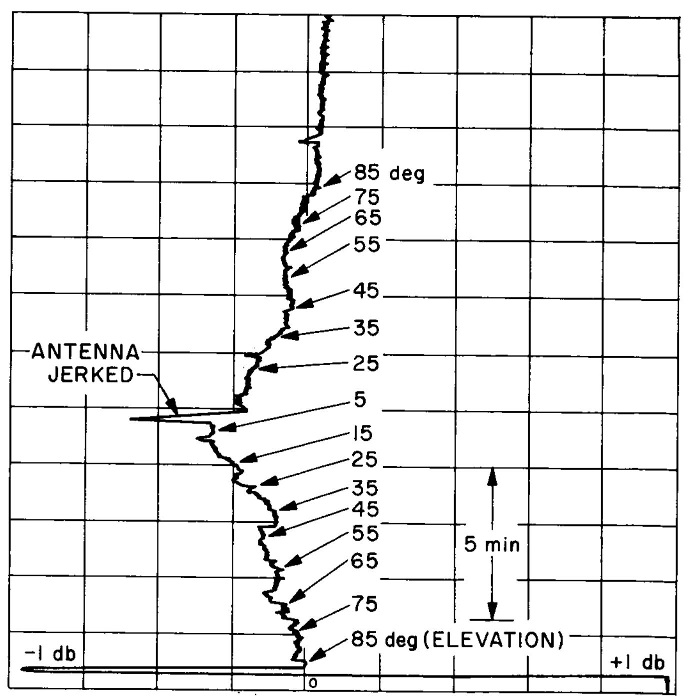

Fig. 17. Moving antenna maser gain stability recording

The equivalent noise temperature of the maser system is given by

$$T_M = T_{M1} + \frac{T_{M2}}{G_1} + \frac{T_r}{G_1 G_2} \qquad (7)$$

where all quantities are defined in Fig. 13. The second term in Eq. (7) indicates that the two-cavity maser should not be operated at low gains. A photograph of the maser installed in the Cassegrainian cone on the ground at the Goldstone Venus Site is shown in Fig. 18. The maser is filled once a day with liquid nitrogen and liquid helium from outside the cone through a small door. A failure in the feed line to the second cavity caused some minor erratic behavior during the last part of the experiment, resulting in day to day gain variations of as much as 3 db. Table 3 summarizes the performance of the system during the Venus experiment.

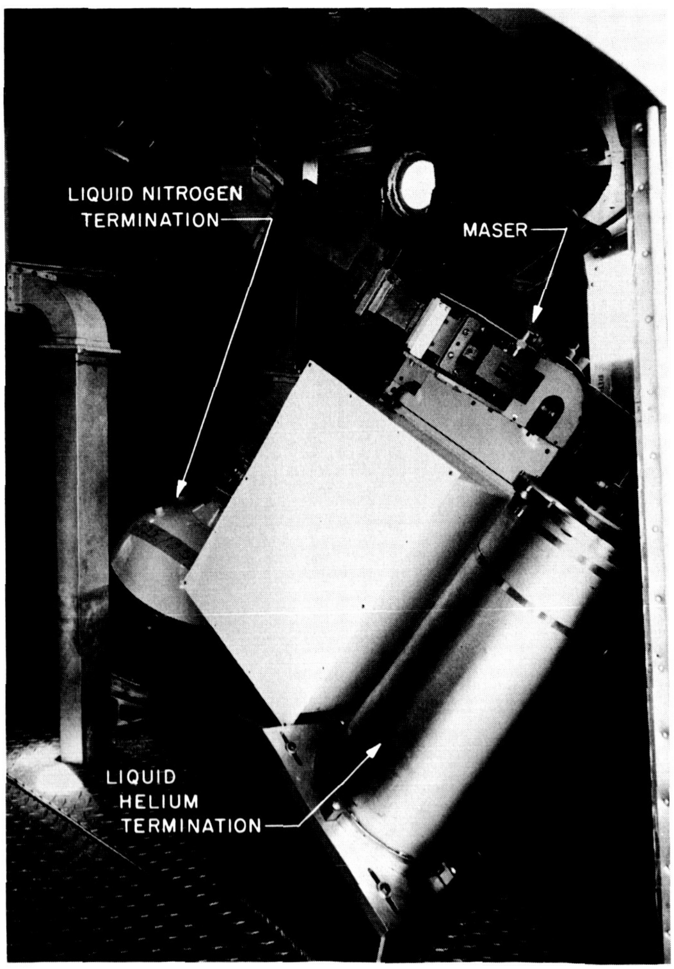

Fig. 18. 2388 Mc maser installed in Cassegrainian cone

Table 3. Performance of dual-cavity maser for radar receiver

Frequency, Mc	2388
Gain, db	27-30
Bandwidth, Mc	2.7
Maser temperature ($T_{m1} + T_{m2}/G_1$), °K	21
Gain stability:	
Long term (hr), db	±0.5
Short term (min), db	±0.02

D. Parametric Amplifier

H. R. Buchanan

The S-band parametric amplifier for the Venus radar receiver was developed and designed to serve as the post-amplifier following the 2388-Mc maser amplifier. The design objectives were 300°K noise temperature, 5-Mc bandwidth, and 20-db gain with particular emphasis to be placed on gain stability over the fairly severe ambient temperature range encountered at the Goldstone site.

The parametric amplifier is a one-port nondegenerate type utilizing a circulator in the signal port. The pump frequency of 9600 Mc was chosen to make use of the extremely stable source that has been used for earlier parametric amplifiers at Goldstone. Detailed discussion of the parametric amplifier and pump source design is given in Ref. 12, 13, and 14. Figure 19 shows the block diagram of the paramp system.

Particular emphasis has been placed on temperature regulation and pump level regulation of the paramp system in order to achieve long-term gain stability. All temperature-sensitive components of the system are mounted in a temperature-controlled "inner" chamber as indicated in Fig. 19. This inner chamber is thermally insulated from the paramp case by a 1½-in.-thick layer of foam potting insulation on all sides. Insulated control shafts extend through the thermal insulation to permit tuning adjustments to be made without upsetting the thermal balance inside the box.

The pump amplitude regulator has also been incorporated as shown in Fig. 19. The open-loop gain of the feedback network is 960 at dc. All elements of the regulator, including the zener diode voltage reference, are mounted in the temperature-controlled chamber to enhance the gain stability of the parametric amplifier. More detailed information on the construction of the temperature-controlled box and design parameters of the

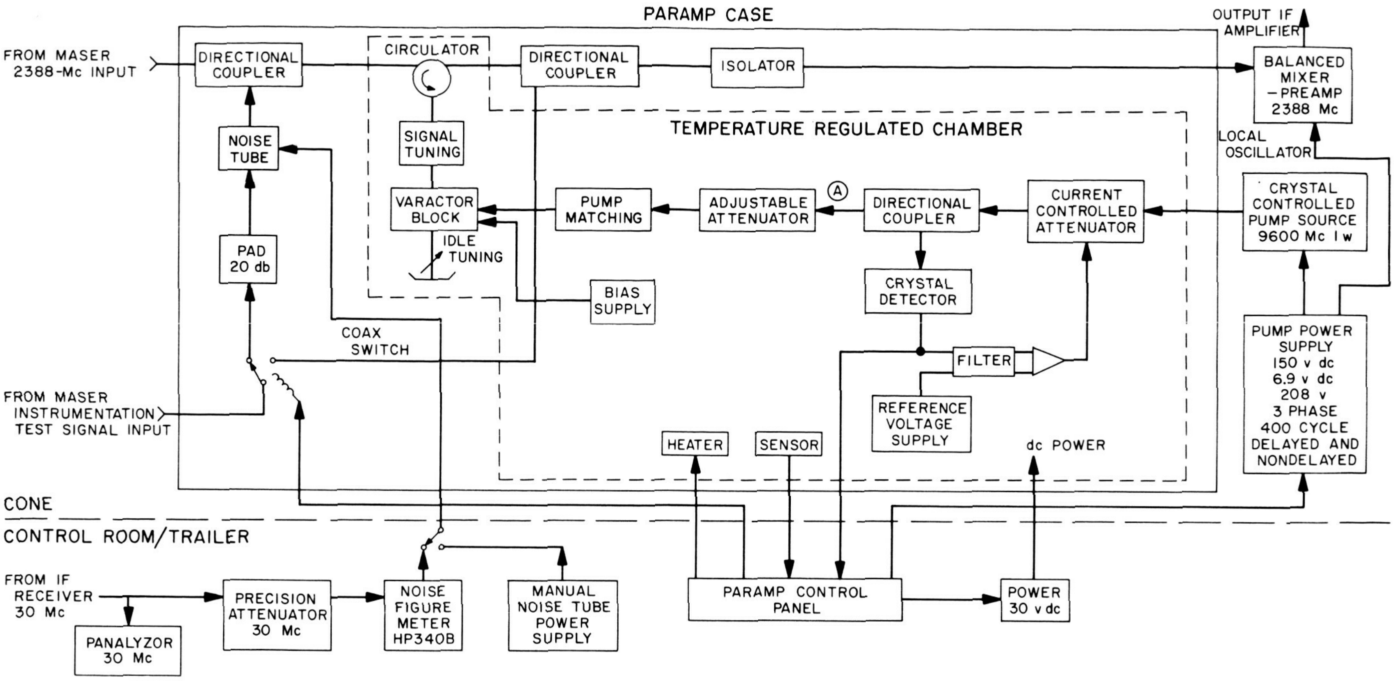

Fig. 19. Block diagram of S-band parametric amplifier system

pump regulation network have been given in a previous report (Ref. 12).

Instrumentation mounted in the nontemperature-regulated half of the paramp case permits remote monitoring of the paramp noise temperature and gain (see pp. 27–29 of Ref. 12 for a detailed description). Figures 20 and 21 show the interior views of the temperature-regulated chamber and instrumentation chamber, respectively. An instrumentation and control rack for remotely operating the parametric amplifier is located in the control trailer complex; it includes the paramp control panel, temperature controller and indicator, a 30-Mc spectrum analyzer, an automatic noise figure meter, a precision 30-Mc attenuator, and a manual noise tube power supply.

The measured performance data of the parametric amplifier after installation is summarized in Table 4.

During the Venus radar experiment the parametric amplifier was operated approximately 500 hr. No maintenance was required on the paramp unit during this period of operation. On two occasions it was necessary to replace the X12 UHF cavity frequency multiplier in the pump

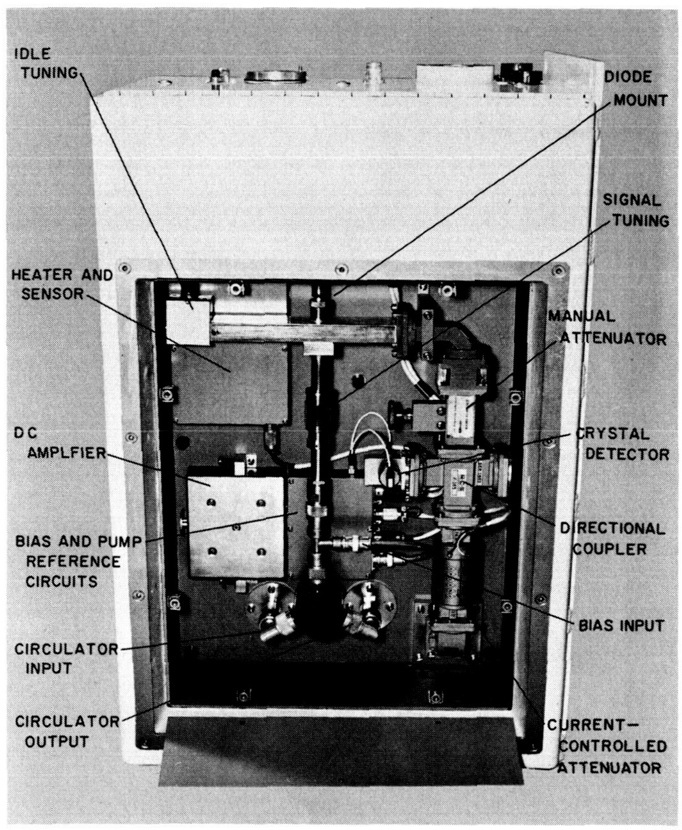

Fig. 20. Temperature-controlled chamber of parametric amplifier

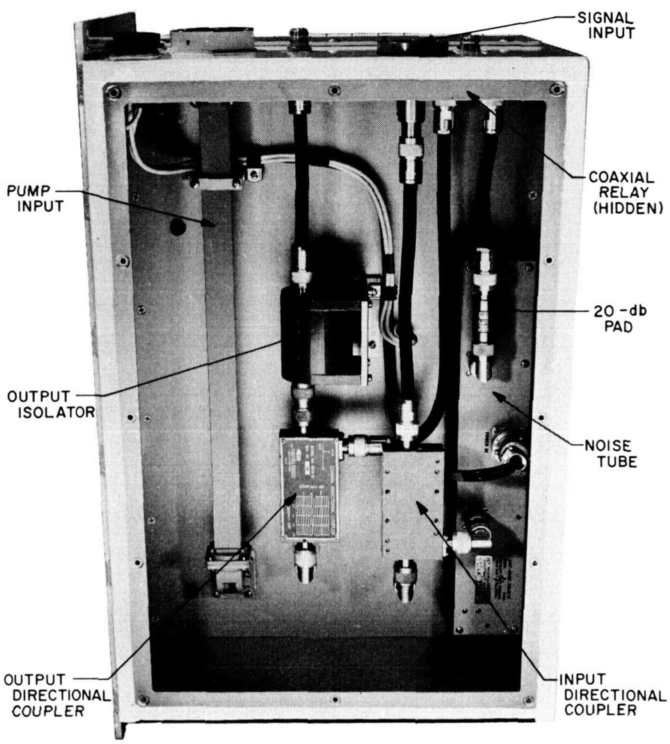

Fig. 21. Parametric amplifier instrumentation

source chain because of low emission of the type-6442 tubes used in this module. As a result, the 9600-Mc output was too low for the pump regulator in the paramp box to function.

The gain of the paramp was monitored daily during the 10-week experiment. The measured gain variation during the experiment was ± 1.5 db, about an average gain of 19.5 db. The average day-to-day gain change was less than 0.8 db.

The parametric amplifier performance met the experimental objectives reasonably well. The two failures of the pump source point up the desirability of a solid-state pump source to improve the long-term reliability of the system.

Table 4. Paramp measured performance data

Noise temperature of paramp (referred to circulator input port), °K	211
Noise temperature of paramp (referred to case input terminal), °K	290
Noise temperature of paramp plus follow-up receiver, °K	317
Case terminal-to-terminal gain (equal output for both positions of the coaxial relay), db	18.8
Bandwidth, Mc	5
Pump power at varactor diode, mw	24

E. System Temperature Instrumentation and Results

C. T. Stelzried

The 2388-Mc Venus radar receiving system instrumentation is shown in the block diagram of Fig. 22. The maser amplifier, noise box, and associated waveguide were mounted on the antenna in the Cassegrain cone (see Fig. 18), and the instrumentation control racks were located in the maser trailer (Fig. 23).

Maser gain is measured by injecting a signal before and after the maser through directional couplers and noting the difference in the signal generator attenuator for the same output signal level. Gain stability is normally measured by recording the total output noise level with a constant temperature termination on the maser amplifier input.

Figures 24 and 25 show recordings of the gain stability of the monitor receiver and maser-monitor receiver, respectively. The 3-db bandwidth of the detector is ½ Mc for these recordings. The maser-monitor receiver short-term (1–2 min) peak-to-peak gain stability was about 0.02 db. The resolution of this combination for measuring rapid changes in antenna temperature for a system temperature ~40°K, is, therefore, 0.1–0.2°K. This system has been used as a "total power" radiometer (see Sec. VI-D) to measure the black-body radiation from Venus.

Figure 26 shows a gain stability recording of both the maser-monitor receiver and maser-paramp-trace receiver combination on the same recording for comparison. Although the system temperature is slightly higher using the monitor receiver as a follow-up amplifier, the recording shows that the combination has an overall advantage for total-power radiometric measurements.

The equivalent noise temperature of the receiving system was measured daily from October 1 to December 17, 1962; *Y*-factor ratios were determined before and after the daily radar experiments with the antenna pointed at zenith and during the experiments with the antenna pointed at Venus. The *Y*-factor method consists of adjusting the precision attenuator for the same power level indication after firing a noise source or switching terminations. Figure 27 shows a simplified block diagram of the receiving system for noise-measurement evaluations

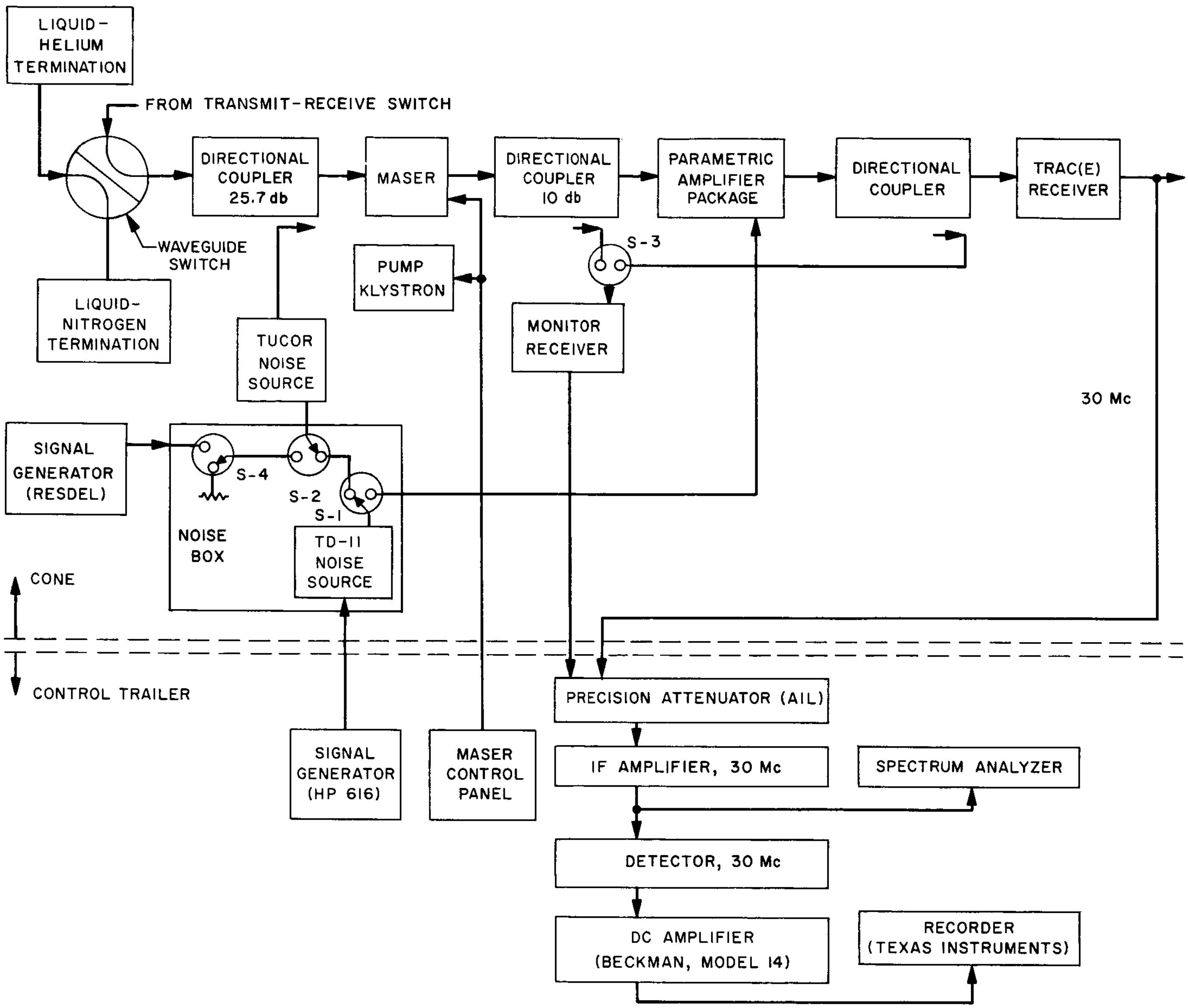

Fig. 22. 2388-Mc maser instrumentation for Venus radar

where all temperatures are referred to the maser input (Fig. 28). Firing the noise source is represented by the equations

$$\frac{T_{SA} + T_E}{T_{SA}} = Y_A \tag{8}$$

$$\frac{T_{SH} + T_E}{T_{SH}} = Y_H \tag{9}$$

$$\frac{T_{SN} + T_E}{T_{SN}} = Y_N \tag{10}$$

Manipulation of Eq. (8), (9), and (10) yields, respectively,

$$T_{SA} = \frac{T_E}{Y_A - 1} \tag{11}$$

$$T_{SH} = \frac{T_E}{Y_H - 1} \tag{12}$$

$$T_{SN} = \frac{T_E}{Y_N - 1} \tag{13}$$

Equations (9) and (10) with $T_{SH} = T_R + T_H''$ and $T_{SN} = T_R + T_N''$ result in

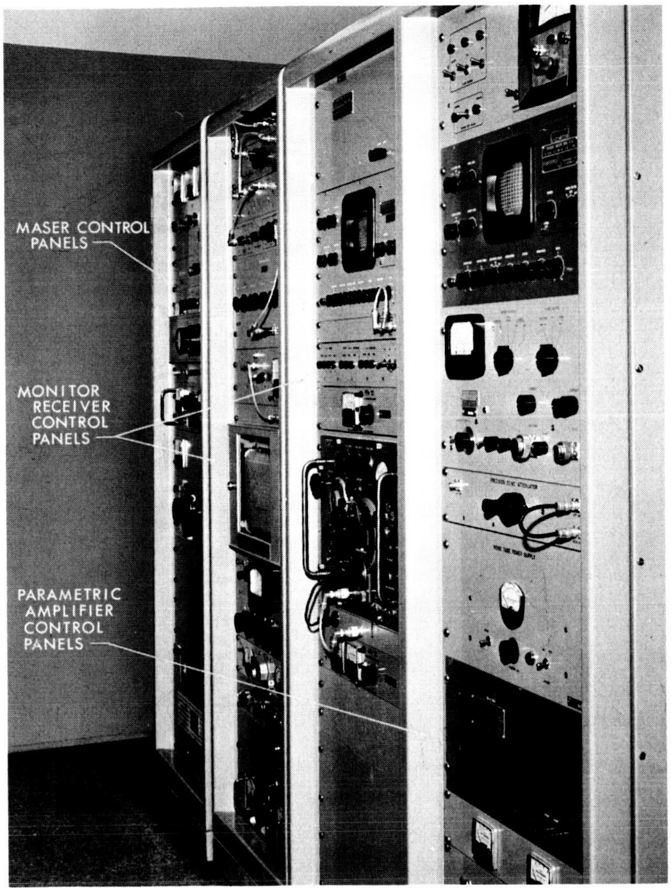

Fig. 23. Maser and monitor-receiver control panels

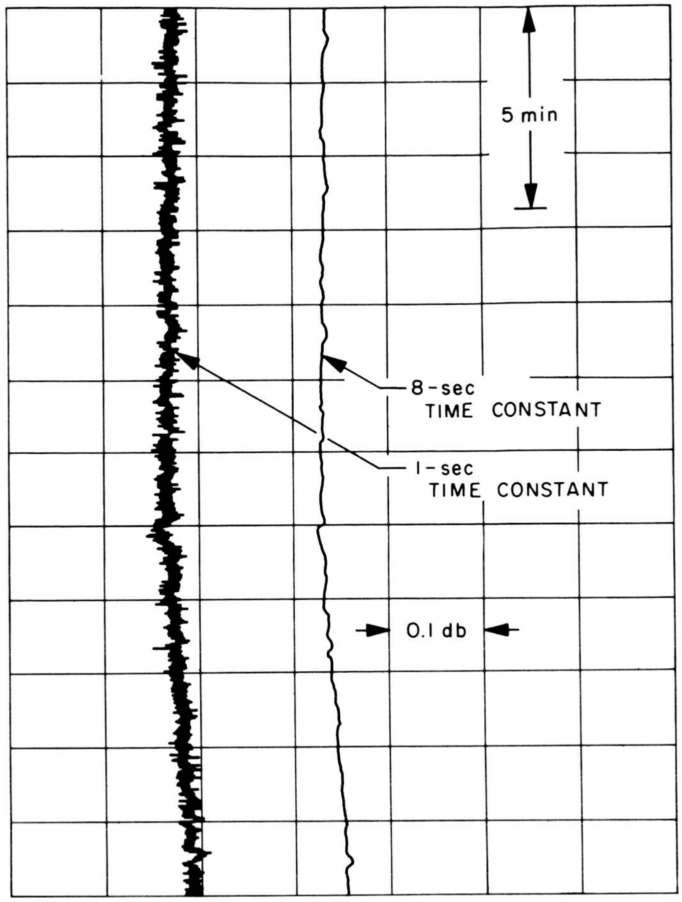

Fig. 24. Monitor-receiver gain stability recording

$$T_E = \frac{(Y_H - 1)(Y_N - 1)(T_N'' - T_H'')}{Y_H - Y_N} \quad (14)$$

$$T_R = \frac{T_N''(Y_N - 1) - T_H''(Y_H - 1)}{Y_H - Y_N} \quad (15)$$

where

T_E = excess noise of gas tube injected into maser amplifier

T_R = equivalent noise temperature of receiver (includes the effect of post amplifier)

T_H'', T_N'' = equivalent noise temperature referred to the maser input of the liquid helium or liquid nitrogen cooled terminations, respectively

T_{SA}, T_{SH}, T_{SN} = system temperature defined at the maser input when switched to the antenna, liquid helium or liquid nitrogen cooled terminations, respectively

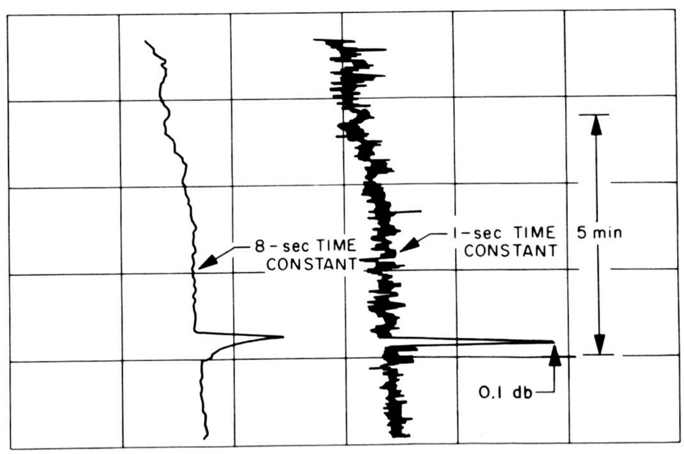

Fig. 25. Maser and monitor-receiver gain stability recording

Y_A, Y_H, Y_N = power ratio as determined with the precision attenuator when the noise source is fired and switched to antenna, liquid helium or liquid nitrogen cooled terminations, respectively

The postcalibration noise temperatures are shown plotted in Fig. 29 using $T_E = 56°K$. The value of T_E is obtained from the average of determinations from Eq. (14), which is based on the absolute temperature values determined for the liquid helium and liquid nitrogen cooled terminations: $T_H'' = 12.3°K$, $T_N'' = 88.7°K$ (Oct. 1—Oct. 19), $T_N'' = 86.3°K$ (Oct. 20—Dec. 17). The temperatures of the cooled loads were determined from calculations and insertion loss measurements (see Fig. 28 and pp. 26–27 of Ref. 9). The liquid nitrogen cooled termination waveguide run was modified on October 19, changing T_N'' to 86.3°K. During the period the parametric amplifier was inoperative (Nov. 21–28), the maser was connected directly to the Trace receiver with a subsequent increase in system temperatures and a decrease in measurement accuracy. Commencing on November 1, 1962, Y-factor measurements were also taken, switching between the cooled terminations with results consistent with the data shown.

The equivalent noise temperatures of the receiving system referred to the maser input obtained from averaging the measurement data shown in Fig. 23 (disregarding data taken during the period the parametric amplifier or cooled terminations were inoperative) are:

$$T_E = 56°K$$

$$T_{SA}\,(\text{zenith}) = 40°K$$

$$T_{SH} = 35°K$$

$$T_{SN} = 108°K$$

$$T_R = 22°K$$

The precision of the measurements is about ±1°K and the absolute accuracy about ±3°K.

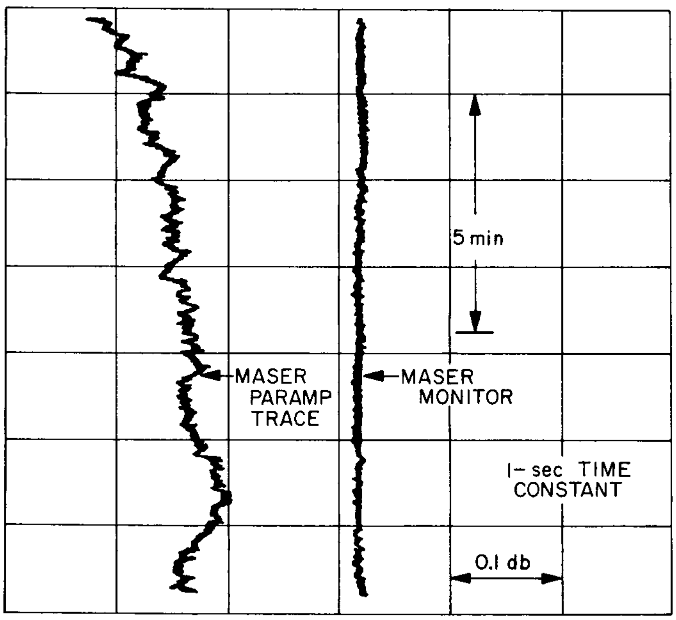

Fig. 26. Maser-monitor receiver and maser-paramp-Trace receiver combination simultaneous gain stability recordings

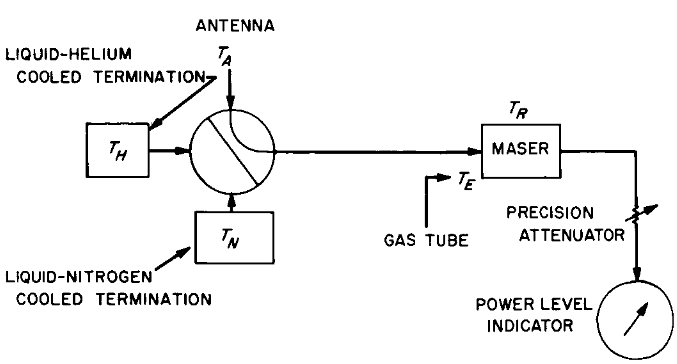

Fig. 27. Simplified block diagram of Venus radar receiving system for noise temperature evaluations

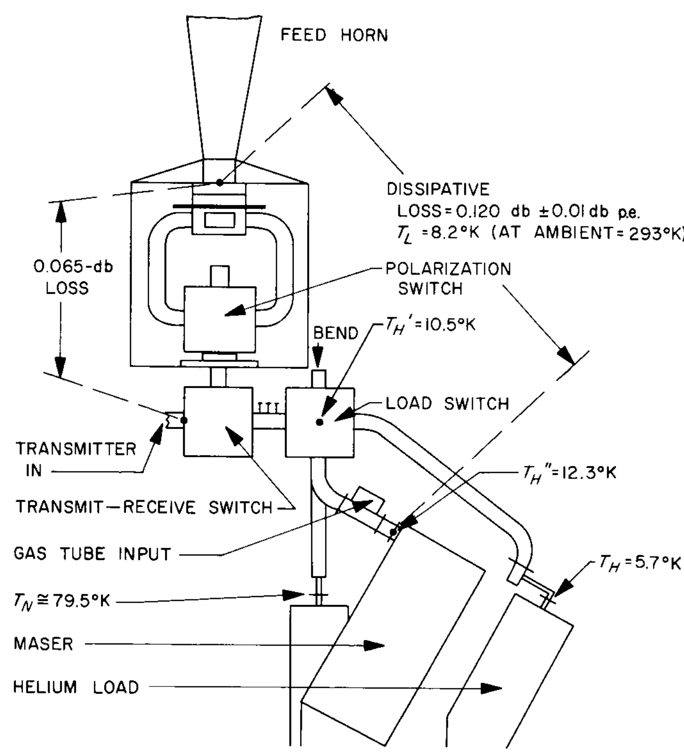

Fig. 28. Insertion loss and excess temperature diagram

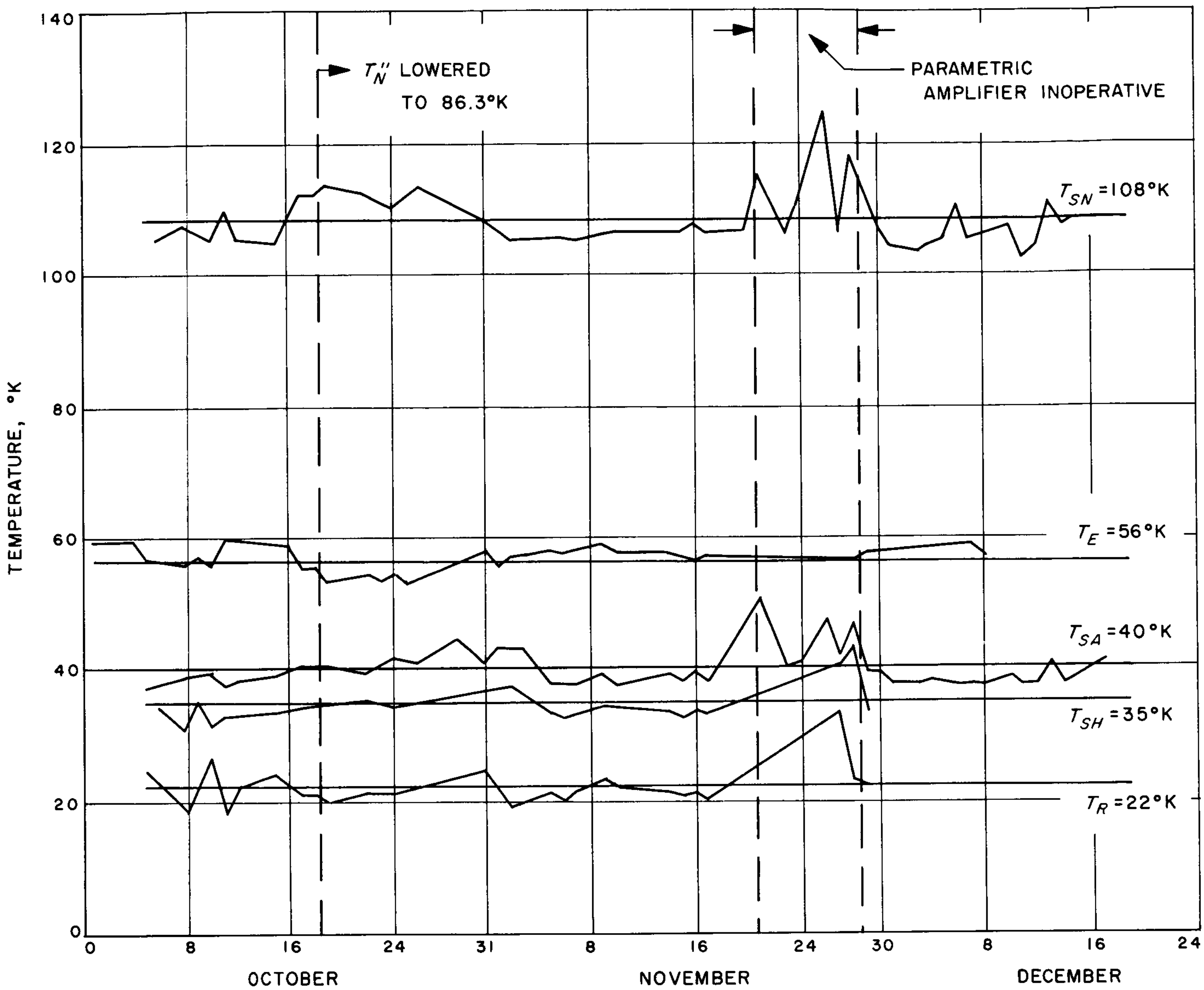

Fig. 29. Plot of receiving system equivalent noise temperatures

F. Transmitter Oscillator System

R. L. Sydnor

All frequencies used in the transmitter and receiver were obtained by synthesis directly from a rubidium-vapor frequency standard. This standard has a stability of 1×10^{-11} standard deviation for one-second averaging time and 5×10^{-11} standard deviation for one year. The accuracy of the frequency depends on the adjustment of the unit and the accuracy of the reference used. For the Venus experiment the frequency was adjusted in reference to two Atomichrons available at JPL. Since this adjustment could be made very precisely, the accuracy was limited to the quoted accuracy of the Atomichrons, i.e., $\pm 20 \times 10^{-10}$ (see Ref. 15). The actual frequency was set to a value corresponding to A1 time, 76 parts in 10^{10} higher than the Atomichron output frequency and 130 parts in 10^{10} higher than UT 2 for 1963. A1 was chosen for the time scale because it is invariant whereas UT 2 changes from year to year.

The block diagram of the transmitter oscillator system is shown in Fig. 30. The 75th submultiple of 2.388 Gc was synthesized from the 1-, 100-, and 10-kc outputs of the frequency divider driven by the frequency standard. This 31.84 Mc was filtered to obtain the necessary spectral purity by means of a narrow band ($2B_L = 3$ cps)

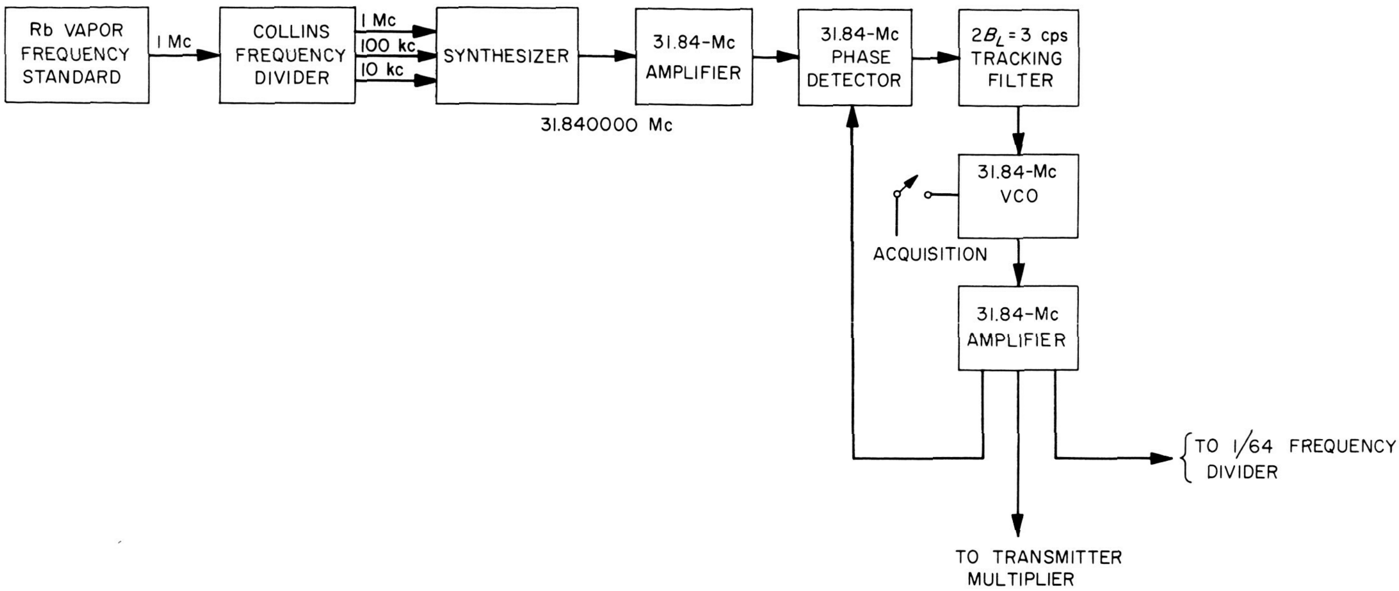

Fig. 30. Block diagram of atomically-stabilized transmitter oscillator

phase-locked loop. Reference frequencies supplied to the receiver are 1 Mc from the frequency standard and 497.5 kc obtained by dividing 31.84 Mc by 64.

This system is nearly the same as was used during the 1961 Venus experiment (see pp. 29–31 of Ref. 1) with the exception of the replacement of the Atomichron by the rubidium-vapor standard and some changes in the monitoring and control panel to simplify operation of the unit.

The complete transmitter subsystem, less the 1/64 divider, is shown in Fig. 31. In this rack are shown the frequency standard power supply, the frequency standard, the acquisition and monitoring control panel for the rf units, a swing-out door on which the rf units are mounted, and power supplies for the rf units. Not shown are the frequency divider, which is mounted in the rear of the rack with the alarm circuitry that indicates loss of lock in the frequency standard. Stand-by batteries for operating the frequency standard during power losses, which were rather frequent, were mounted under the trailer.

The only failure in the transmitter oscillator system during the 2½ months of the experiment was a power supply for the vacuum-tube phase detector.

G. Programmed Local Oscillator

R. Winkelstein

The programmed local oscillator consists of a digital control subsystem and a receiver local oscillator subsys-

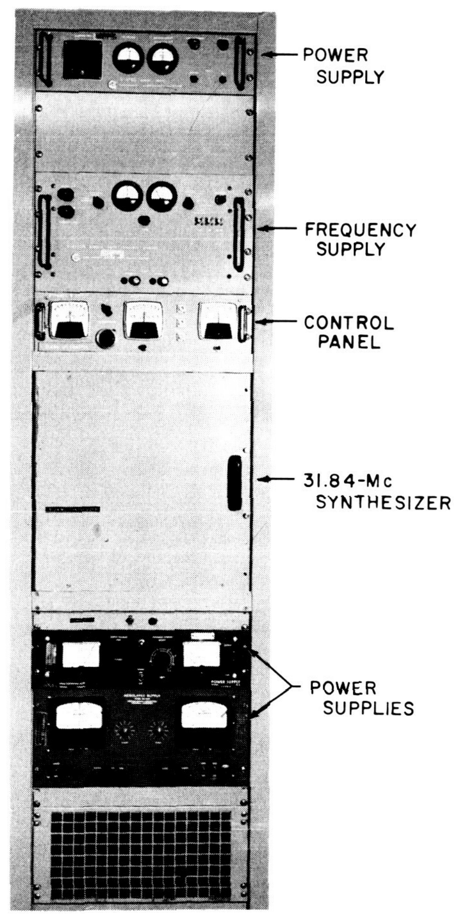

Fig. 31. Transmitter oscillator system

tem. The purpose of the digital control subsystem it to tune the local oscillator of the Venus radar receiver to the exact frequency of the doppler-shifted radar echo within an accuracy of $5:10^{10}$, or approximately 1 cps at a received S-band frequency of 2.388×10^9 cps. Because the received radar signal has a doppler frequency component which may vary as much as 14 kc over the period of a single day's viewing, and 200 kc over the period of the experiment, the digital control must smoothly vary the local oscillator frequency to match this changing doppler frequency component within the above-stated accuracy.

To accomplish its purpose, the digital control subsystem reads in the required frequency information from punched paper tape as it is needed during real-time operation. Each day's tape is previously prepared and the frequency information calculated from a Venus-Earth ephemeris. The frequency of the local oscillator is compared with the frequency read in from the tape, and a control voltage to the local oscillator is generated which causes its frequency to change in a manner forcing the difference frequency error to approach zero.

Figure 32 shows the combined configuration of the programmed local oscillator in block diagram form. The receiver local oscillator subsystem generates the highly accurate and phase-stable doppler-controlled frequency which, when processed by the receiver multiplier circuits, becomes the receiver local oscillator signal. In addition, a spectrally pure reference frequency is provided to permit generation of the controlled doppler frequency required to close the programmed local oscillator feedback loop.

The physical equipment comprising the programmed local oscillator is shown in Fig. 33. Four cabinets are used, the right two containing the digital control subsystem, and the left two containing the receiver local oscillator subsystem. Details of the digital display and control sections are shown in Fig. 34 and 35, respectively.

1. Digital Control Subsystem

Figure 36 is a block diagram of the digital control subsystem. The timing, clock, and control block synchronizes the remaining blocks of the digital control and ensures proper registration between the controlled doppler frequency and universal time (UT). Shown in Fig. 34 is the display of UT labeled *clock*, together with pushbuttons for synchronizing the clock to an internal manually set value or to an external standard.

After each 10-sec time interval, the tape reader system is caused to read in a block of information from the paper tape in preparation for the next frequency comparison. Two words of information are contained in a block: doppler frequency and the associated UT. The block information is also brought out to display panels shown in Fig. 34 labeled *tape time* and *tape frequency*. Information may be inserted manually into the system by means of the *manual load* pushbuttons shown in Fig. 34 and the

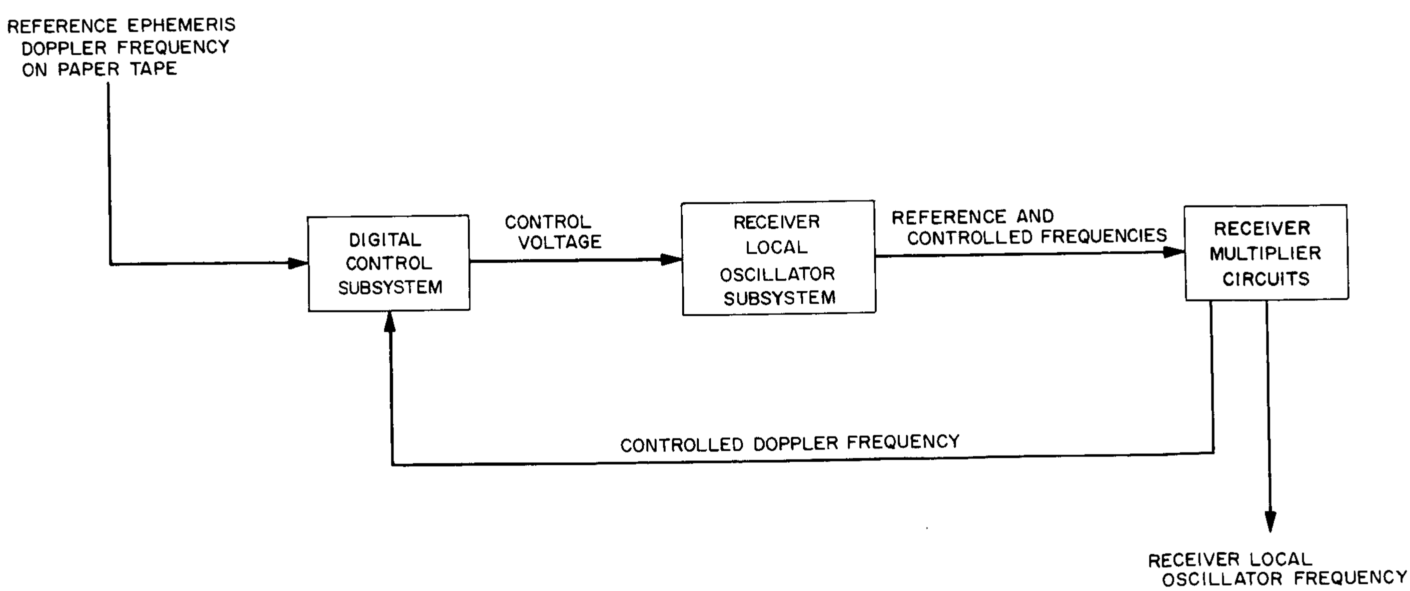

Fig. 32. Block diagram of programmed local oscillator

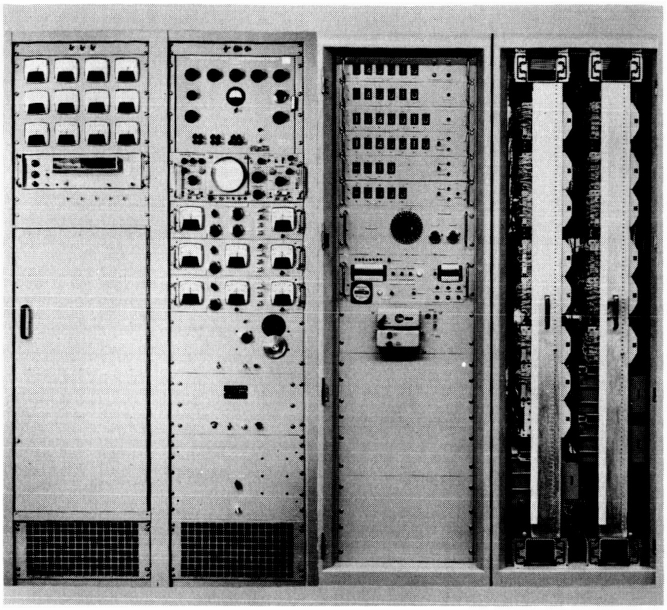

Fig. 33. Programmed local oscillator equipment

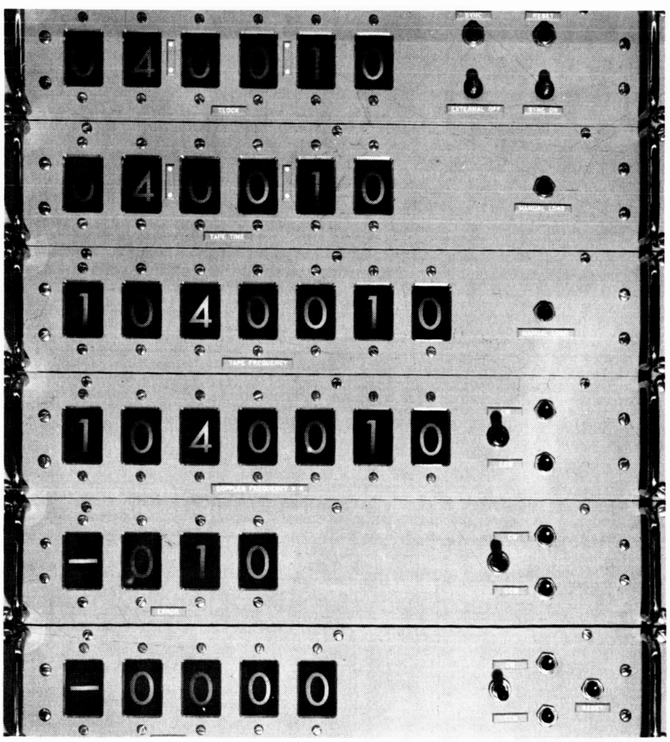

Fig. 34. Display section

manual entry digit switch shown in Fig. 35. Also shown in Fig. 35 are controls for manually reading in one block from the tape or searching for a block with the particular time word set in the *manual entry* digit switch.

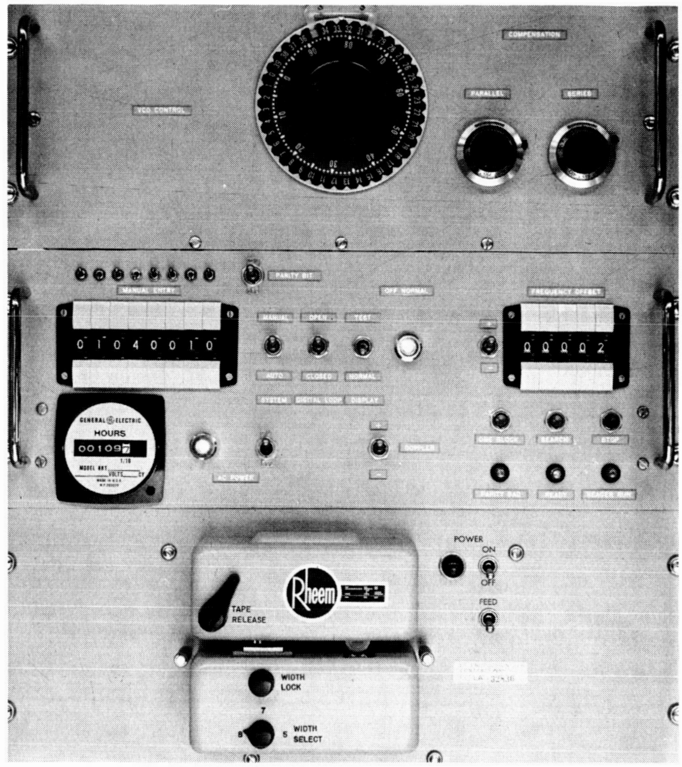

Fig. 35. Control section

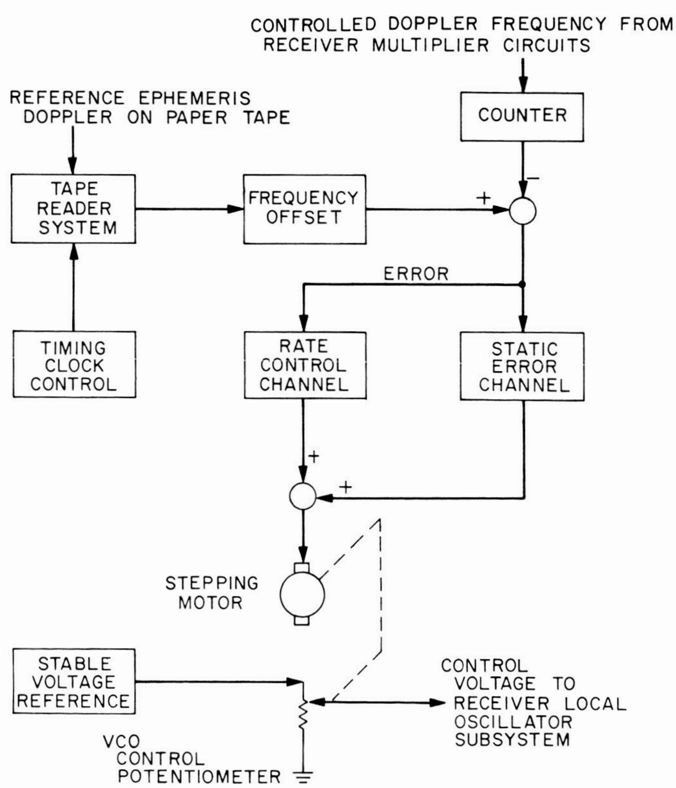

Fig. 36. Block diagram of digital control subsystem

The frequency offset block adds or subtracts a fixed value to the tape frequency. This value is the one dialed into the *frequency offset* digit switch shown in Fig. 35. A range of $\pm 10^5$ quarter-cycles is provided to an accuracy of one quarter-cycle.

Controlled doppler frequency from the receiver multiplier circuits is counted by the counter block during the last 4 sec of each 10-sec time interval. Counting for 4 sec reduces the error due to counter uncertainty and increases overall system accuracy because each unit of the 4-sec totalization is equivalent to a quarter-cycle of doppler frequency. For this reason, tape frequency, offset frequency, and error frequency values are all in quarter-cycle units.

The error frequency, which is the difference between the counter and frequency offset block outputs, is fed to the static-error and rate-control channels. The value of the error in quarter-cycles is converted by the static-error channel to an equal number of pulses which are fed to the digital stepping motor at the maximum motor rate of 200 cps. A display of *error* is shown in Fig. 34.

The rate-control channel feeds pulses to the digital motor at a constant rate, the value of which is modified by each 10-sec frequency error. The rate range can vary in multiples of 1 pulse per 10 sec to a maximum of 800 pulses per 10 sec. A given error will change the 10-sec rate by a quantity equal to the error. Thus, an error of +3 quarter-cycles will add +3 pulses per 10 sec to the rate. The *rate* display is the bottom display shown in Fig. 34 and is given as an octal number.

A pulse from either the static-error channel or rate-control channel causes the stepping motor shaft to rotate 18 deg in the proper direction. The VCO control potentiometer is coupled to the motor through a step-down gear ratio of 100. The 40-turn continuous-wire potentiometer covers a single doppler range of 16,800 cps.

Because of the VCO nonlinear control characteristic, series and parallel compensating load potentiometers are used (Fig. 35). The use of the motor-driven continuous-wire potentiometer digital-to-analog conversion technique permits the attainment of an extremely fine resolution of better than $1{:}10^5$. Additional details of the system and its analysis are given in Ref. 9 (pp. 32–38).

Table 5 outlines the digital control subsystem experimental capabilities together with the applicable Venus radar experiment requirements. Figure 36 presents a block diagram of the digital control subsystem. In all cases, experimental capabilities exceed requirements. The large excess-error correction and doppler rate capability facilitate initial program acquisition during system startup.

Table 5. Local oscillator digital control system capabilities

	Control system	Requirements
Doppler range for single day's viewing, cps	16,800	14,200
Sampling period, sec	10	—
Doppler frequency counting time	last four seconds of sampling period	—
Doppler frequency accuracy, cps	¼	1
Doppler frequency resolution, cps	¼	1
Maximum doppler frequency static error correction after one sampling time, cps	240	5
Maximum rate of doppler change, cps/sec	20	½

2. Receiver Local Oscillator Subsystem

The receiver local oscillator subsystem consists mainly of the equipment used in the 1961 Venus experiment, with some changes made for improved reliability in power supplies and to better suit the system for use with the new digital control system and monostatic radar operation. The control and monitor equipment was entirely rebuilt for increased ease of use. A block diagram of the subsystem is shown in Fig. 37.

The input reference frequency is generated by phase-locked synthesizers within the receiver which retain the basic stability and accuracy of the rubidium-vapor frequency standard used as the station standard. A narrow-band ($2B_L = 3$ cps) loop is used to filter this reference signal for improved spectral purity.

The following two phase-locked loops are used to generate the local oscillator frequency, which must vary continuously over a range of frequencies of ± 3 kc centered at 29.476875 Mc. The second phase-locked loop is wideband to maintain the spectral purity of the input signal. The output frequency of this loop is shifted down in frequency by 475 kc plus the slowly changing component of doppler by the 475-kc VCO controlled by the digital equipment.

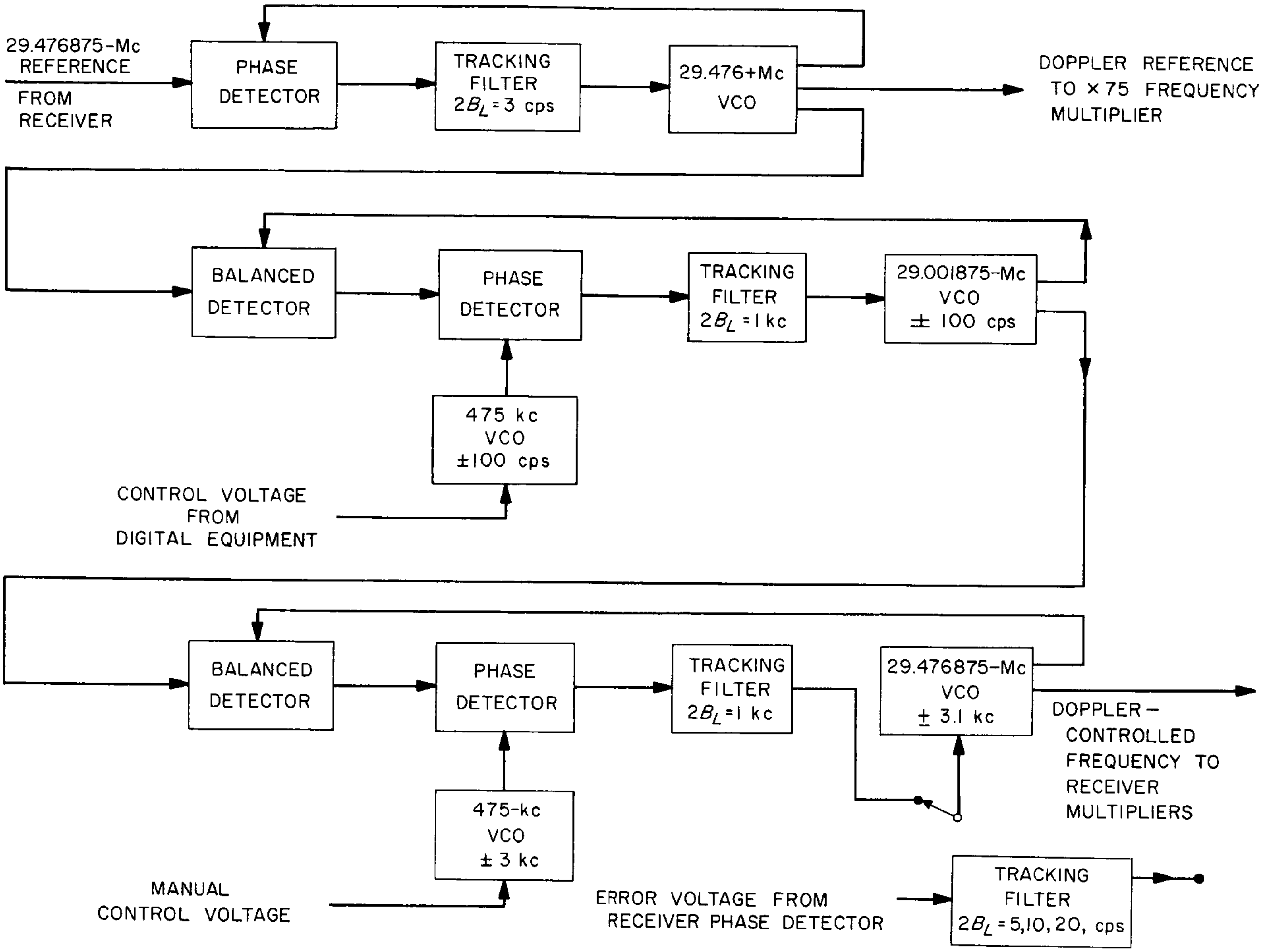

Fig. 37. Block diagram of receiver local oscillator subsystem

The third phase-locked loop is also a wideband loop to maintain the purity of the input signal. The output frequency of this loop is shifted up in frequency by 475 kc plus a component of the doppler, which represents the median doppler offset for any one day. Because of the large excursion of this doppler, ±3 kc at 29.476875 Mc, a total of 40 crystals were required in the 475-kc VCO and 5 crystals in the 29.476875-Mc VCO (see p. 34 of Ref. 16).

For use in the synchronous-receiver mode of operation, it is possible to switch the input of the last VCO to the output of the main receiver tracking filter, which has selectable bandwidths of 5, 10, and 20 cps.

The phase noise of the entire system, as well as the tracking performance of the system in the programmed mode, has been measured; these data are presented in Table 6.

Table 6. Phase noise and tracking performance data

System characteristic	Specified	Achieved
Phase noise in loop bandwidth $2B_L = 5$ cps	≦0.1 rad rms	0.05 to 0.066 rad rms
Tracking accuracy in programmed mode	$\leqq 1 \times 10^{-9}$	Best case: 0.26 cps at 2388 Mc (0.11×10^{-9}); Worst case: 0.74 cps at 2388 Mc (0.31×10^{-9})

3. Receiver Multiplier Circuits

In order to complete the programmed local oscillator feedback loop, certain frequency multiplier circuits within the main receiver section are used as shown in Fig. 38. The controlled doppler frequency consists of the difference between the 75th multiple of the reference frequency and the 75th multiple of the doppler controlled frequency. Because a multiplication factor of 80 is used to produce the receiver local oscillator signal, the actual value of the controlled doppler frequency is 75/80 times the true doppler component of the received Venus radar signal.

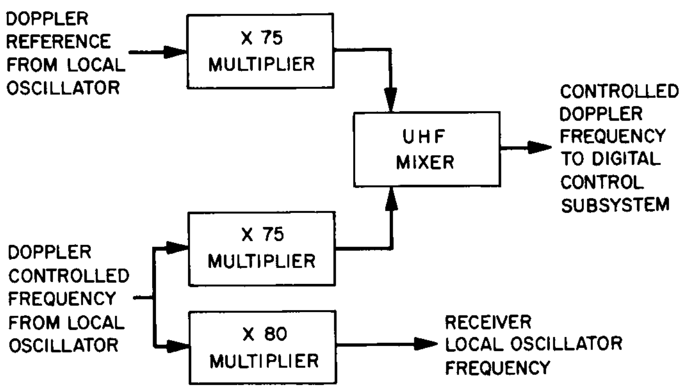

Fig. 38. Receiver multiplier circuits

H. Digital Angle-Pointing System

G. A. Morris and D. McClure

For the planetary radar experiment, the 85-ft Az-El antenna was controlled by the digital angle slave pointing system shown in Fig. 39. This system is similar to the system used in the 1961 Venus radar experiment (Ref. 1) and the *Echo* communication satellite experiment (Ref. 17). In the previous system, the digital comparator was supplied with information from the coordinate converter computer; angle information is now supplied to the digital comparator from the ephemeris tape reader. This change of input to the digital comparator is essentially the only change made in the digital angle pointing system.

1. Ephemeris Tape Reader

The input to the ephemeris tape reader is a punched paper tape. This paper tape contains time in binary coded decimal form, and azimuth and elevation angles in octal form as fractions of a circle divided into 2^{18} parts. The tape is prepared by the IBM 7090 computer at JPL. Every 64 sec (64 sec in advance of real time) the tape is read into the ephemeris tape reader as time, azimuth, and elevation. A linear interpolation is performed on adjacent 64-sec samples to present prediction information to the digital comparator at 2-sec intervals.

2. Digital Comparator

The digital comparator is designed to receive azimuth and elevation information every two seconds and to extrapolate from this information until new angles are received. The digital comparator takes the difference between the present angle and the last angle and divides this difference into 2048 parts. This difference is multiplied by a number n that ranges from 1 to 2048 and is added to the last angle θ_t supplied to the computer such that the present angle $\theta = [\theta_t + n(\theta_t - \theta_{t-2\,\mathrm{sec}})/2048]$. In the digital comparator the antenna position read-outs from the data system are subtracted from the commands (which can include manually inserted offsets) to generate a digital position error. The manual offsets are introduced by the servo operator to position the optical image of Venus in the correct position on the television screen (to correct boresight bias errors). After digital-to-analog conversion, the position error is used to control the antenna servo system.

There is no provision on-site to check the angles delivered to the digital comparator for accuracy such as was employed in the coordinate converter computer for the 1961 experiment (see Ref. 1). However, the tapes are checked at JPL on the IBM 7090 before being delivered to Goldstone.

3. Servo and Control System

The servo system for the 85-ft-diameter antenna consists of hydraulic drive motors for each axis, with hydraulic fluid provided from electrical induction motor driven pumps. The control channels have electronic amplifiers to provide mixing of feedback signals and amplification of control commands to a suitable level to actuate the hydraulic servo valves. A control console provides synchro and digital angle read-outs, hand wheels for manual control, start-stop control and indications, and operational mode selection. The operating modes are: brake, manual, aided track, auto (not used in this experiment; requires tracking feed), and slave to the ephemeris tape commands. A panel containing azimuth and elevation keyboards provides a means of introducing manual offsets to the ephemeris angles.

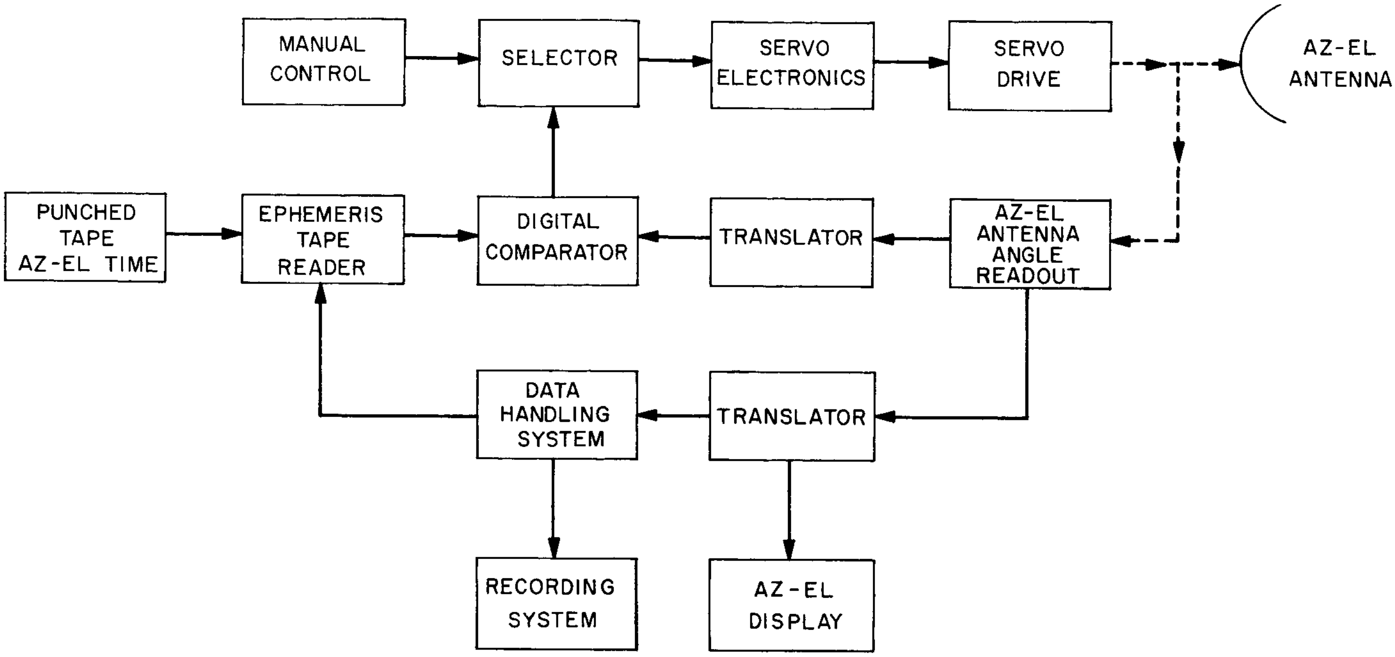

Fig. 39. Digital angle-pointing system

4. Angle Readouts and Translators

The angular encoding system installed on the Az-El antenna provides digital representation of the angular position of the axes of the antenna. The angular position of each axis is represented in binary digital form for input to the digital comparator. Also, a binary coded decimal representation is provided for data handling purposes. A complete description of the antenna axes readout system is contained in Ref. 17.

5. Tracking Performance

During the experiment, data were taken to determine the average operational dynamic tracking characteristics of the angle pointing system.

The angle error voltages from the digital comparator, as seen at the output of the servo slave mode preamplifiers, were recorded for 5-min periods at 1-hr intervals during the tracking operations. Figure 40 is a typical recording; it was taken on October 31, 1962. Noted on the recording are the azimuth and elevation angles, time (GMT), wind conditions, and the recorder calibration of ±0.0879 deg. Calibration was accomplished by setting in a known offset momentarily.

A total of 43 azimuth and 37 elevation error recordings were usable for data reduction. Only the standard deviation and the maximum and minimum deviations were computed because of the slow recorder speed (1 mm/sec). The total standard deviation for all recordings was 0.0029 deg for azimuth and 0.0019 deg for elevation. Azimuth and elevation standard deviation for each 5-min interval as a function of azimuth and elevation angle are presented in Fig. 41 and 42 respectively. Since Venus was never above 35 deg elevation, there are no data for the higher elevation angles. There appear to be no significant changes in standard deviation of azimuth and elevation errors for any particular azimuth or elevation angle.

Figure 43 shows the azimuth and elevation standard deviation as a function of wind velocity. During this period the wind velocity was generally less than 10 mph; thus, no definite conclusion can be reached regarding the effects of wind velocity on the dynamic tracking characteristics.

I. Range Ephemeris

P. H. Schottler

1. Introduction

The Mod IV Ranging Equipment performs several functions in addition to the measurement of Earth-Venus range, which is the closed-loop ranging experiment (see Sec. V-B). One such function is to provide correctly timed signals for use in correlation detection of radar

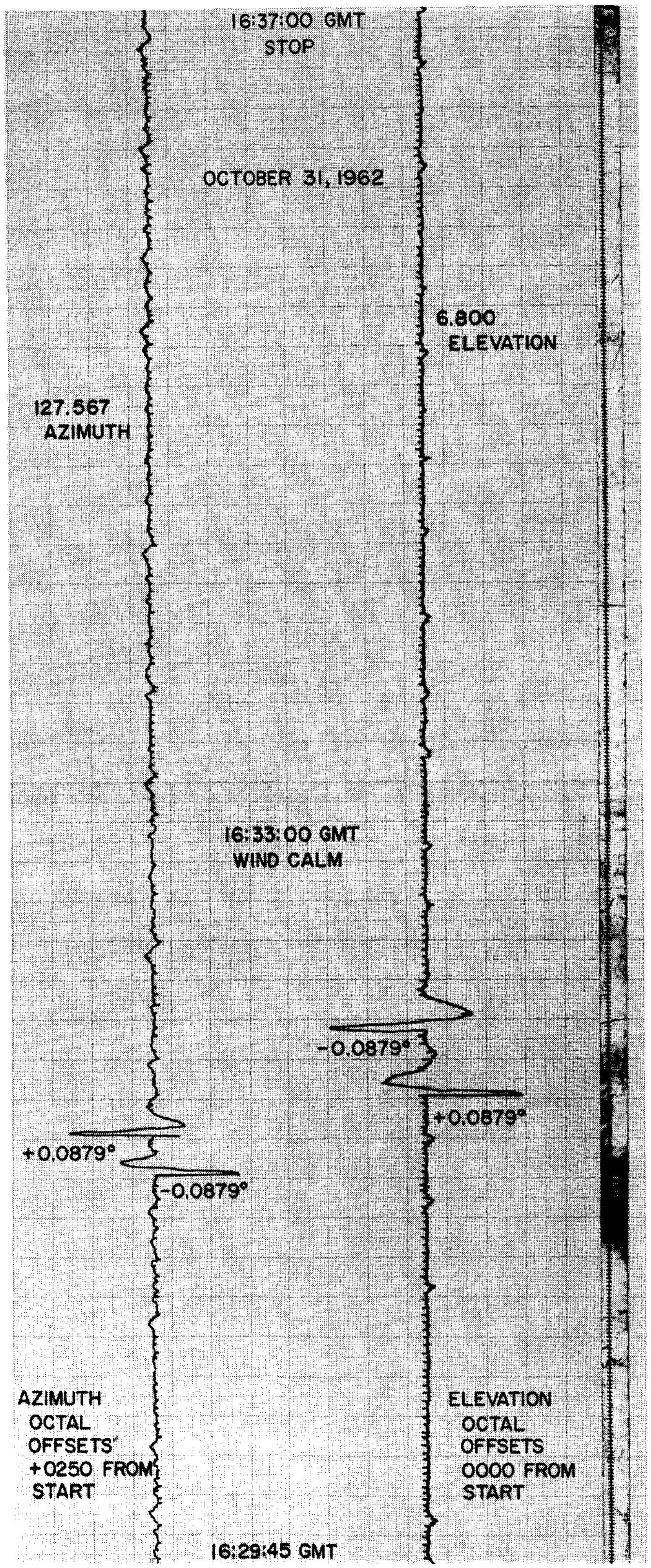

Fig. 40. Typical Sanborn recording of azimuth and elevation errors

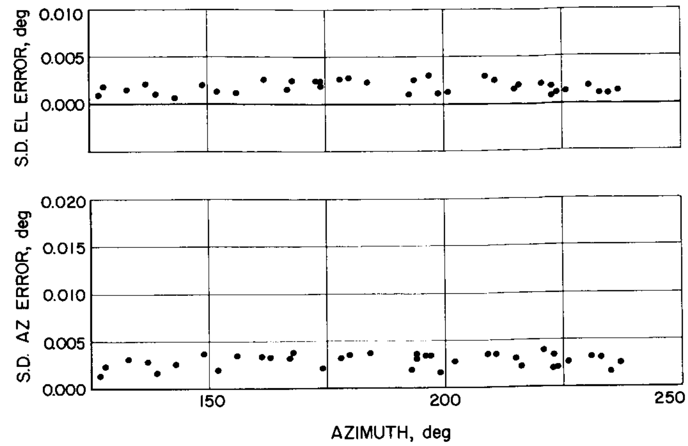

Fig. 41. Standard deviation of azimuth and elevation errors vs azimuth

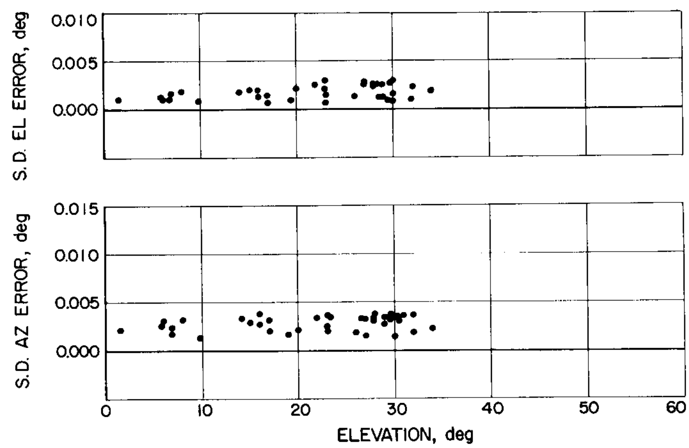

Fig. 42. Standard deviation of azimuth and elevation errors vs elevation

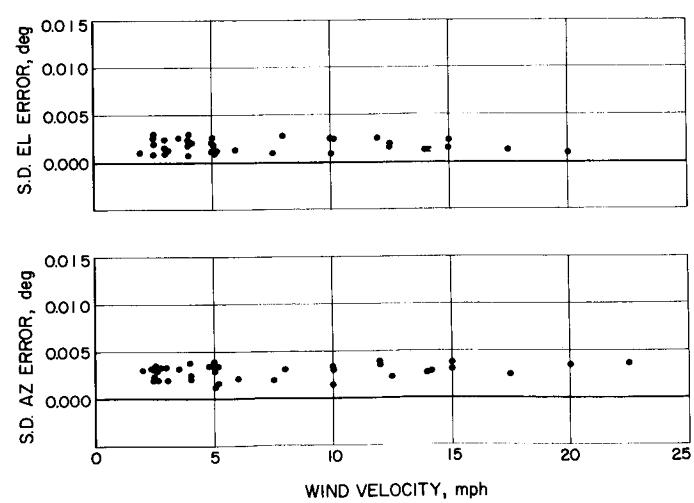

Fig. 43. Standard deviation of azimuth and elevation errors vs wind velocity

echoes from Venus; these signals are derived from a digital tracking loop which tracks a precomputed range ephemeris. A second function is to provide transmit-receive keying signals to control the alternate connection of transmitter and receiver to the single antenna. The period of the on-off keying signals is determined from the range to Venus as given by the range ephemeris.

2. Ephemeris Programmed Signals

The phase of the echo signal waveform from Venus at the input to the receiver is determined by the length of the round-trip path which the signal traverses. For correlation detection, a local model of the transmitted signal waveform is required at the same phase as the received signal. Since the length of the signal path is continuously changing, the local signal waveform must be continuously advanced or delayed in phase according to whether the Earth-Venus distance is decreasing or increasing.

In the case of a carrier which is on-off amplitude modulated by a square wave or a pseudonoise (PN) sequence, the phase of the local signal modulation can be advanced or delayed by deleting or repeating digit periods or fractions of digit periods in the modulating sequence. Commands to the local-signal generator to change the phase of its modulation output are derived from a digital control loop which tracks the range ephemeris. The loop consists of a binary subtractor, a number-controlled oscillator (NCO), and a range tally register (Fig. 44). The input to the loop is a binary number, the ephemeris range number, which gives the Earth-Venus round-trip distance in units of light microseconds as determined from the range ephemeris. The range tally register displays the loop value of range number. The difference between these two numbers, that is, ephemeris range number minus the tally range number, is the error signal to the NCO. The error signal represents the number of light microseconds by which the loop must compensate so that the tally displays the ephemeris range number. The NCO operates on the error number to produce shift pulses which increment or decrement the tally according to whether the range to the target is increasing or decreasing. Since a change in target range implies a change in the phase of the local signal, the shift pulses from the NCO also serve to delay or advance the phase of the local signal by the same number of microseconds that the tally number has been changed.

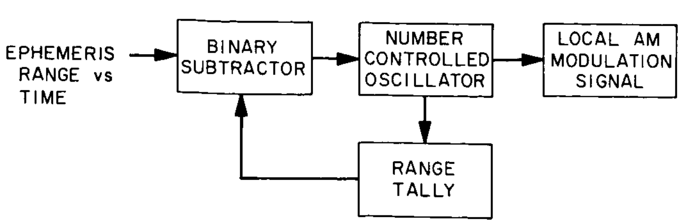

Fig. 44. Block diagram of ephemeris tracking loop

Ephemeris range information is read into the loop from a punched paper tape at intervals of 8 sec. Each read of the tape yields a 6-digit number which gives the tape time (as GMT) and a 9-digit number which gives the round-trip time to Venus in units of light microseconds. Time from the tape is displayed so that the tape may be synchronized with local time. The range number which is read from the tape at a particular value of tape time, say T, is the round-trip time to Venus 8-sec later, that is, at time $T + 8$ sec. The loop compensates during the interval T to $T + 8$ sec, so that at time $T + 8$ sec the loop displays the ephemeris value of range number corresponding to time $T + 8$ sec.

The tape is read just prior to an 8-sec time tick which provides fundamental timing for the operation of the tracking loop. The range number is inserted into a register, the Eph_{t+8} register, where it remains until just prior to the next 8-sec time tick. Following the occurrence of an 8-sec time tick, the range number in the tally register, Tally_t, is subtracted from the Eph_{t+8} number and the difference stored in a register called the shift control number register (see Fig. 45). The sign of the shift control number is stored in a flip-flop, the logical "0" representing a positive error. A new shift control number is formed at the start of each 8-sec interval, but the shift control number for any particular interval remains constant throughout that interval.

The absolute value of the shift control number is added into a register called the shift control accumulator every 50 microsec. Following each addition, the content of the shift control accumulator is compared to a constant number. If the content of the shift control accumulator is less than the constant number, the addition process continues. If the content of the shift control accumulator is $\geq$ the constant number, a comparison-true pulse (shift pulse) is produced, and the value of the constant number is subtracted from the content of the shift control accumulator. The addition process then repeats. The shift pulse performs two functions, viz., if the shift control number is positive, the shift pulse increments the tally by one unit and delays the phase of the local signal by one microsecond. If the shift control number is negative, the shift pulse decrements the tally by one unit and advances the phase of the local signal by one microsecond.

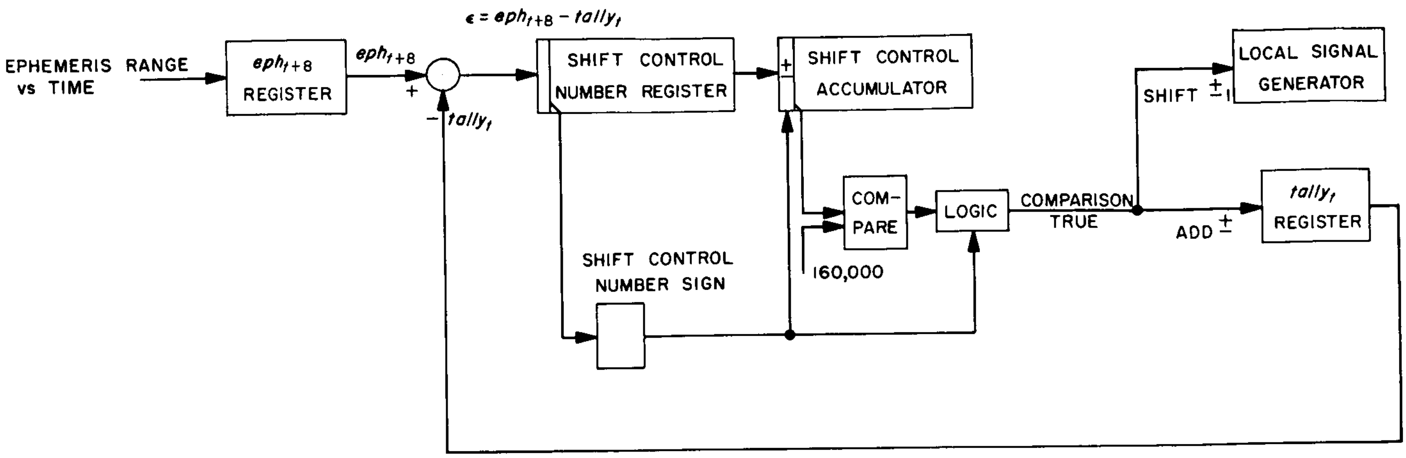

Fig. 45. Ephemeris tracking loop

The value of the constant number with which the content of the shift control accumulator is compared is determined as follows: The smallest nonzero shift control number possible is ±1. Assume that the shift control number formed at the start of an 8-sec interval is +1. Then the tally must be incremented by one unit prior to the start of the next 8-sec interval. If the value +1 is added into the shift control accumulator every 50 microsec during the 8-sec interval, the content of the shift control accumulator will be 160,000 at the end of the interval. The constant for comparison is taken to be this value (actually slightly less because of the time consumed in forming the shift control number), hence the shift pulse occurs just at the end of the 8-sec interval. If the errer were +2, one shift pulse would be produced at the end of 4 sec and a second shift pulse at the end of the 8-sec interval.

3. Transmit-Receive Keying Signals

Signals to control the alternate connection of transmitter and receiver to the single antenna are provided

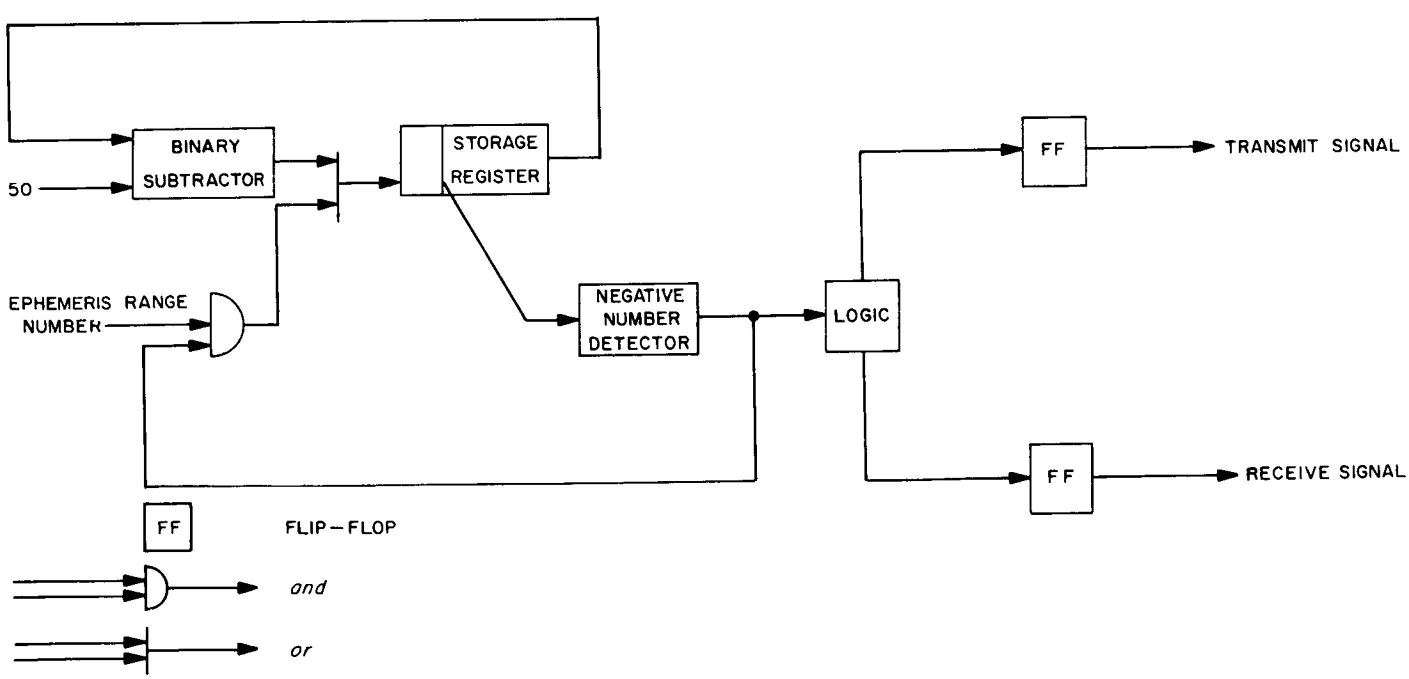

Fig. 46. Block diagram of keyer control

from the keyer control, a subsystem of the Mod IV Ranging Equipment. Each transmit period lasts a sufficient length of time to exactly fill the space to and from Venus with energy. The receiver then listens for an equal length of time before the next transmit period starts. The length of a particular transmit period starting, say, at time T is the ephemeris range number on the punched paper tape corresponding to tape time $T - 8$ sec.

The keyer control consists of a binary subtractor, a storage register, a negative-number detector, and a pair of output flip-flops (see Fig. 46). An ephemeris range number is loaded into the storage register at the start of each transmit period and each receive period. Every 50 microsec thereafter, the number 50 is subtracted from the content of the storage register until the remainder in the register becomes negative. When the sign of the remainder changes, the negative number detector produces an output which complements the pair of output flip-flops. The output flip-flops provide the control signals to the transmitter and receiver, the logical *one* representing the *on* condition. Additional logic provides that the transmit and receive output flip-flops run out of phase with one another. The output of the negative number detector also resets the storage register and reloads a new value of the ephemeris range number so that the countdown process can start again.

IV. OPEN-LOOP RECEIVER SYSTEM EXPERIMENTS

A. Amplitude Modulated System

R. M. Goldstein

1. Introduction

In the design of a radar experiment, one may control both the form of the transmitted signal and the type of processing applied to the echo. It is this possibility which gives radar its unique potential of gathering facts about Venus, as the planet may be expected to interact differently with different incident waveforms. The design problem is to select a suitable waveform-receiver combination to extract the desired information from Venus. As usual, the overwhelming difficulty in this problem is caused by the extremely feeble power contained in the echo, which is immersed in strong background noise. Thus every step of signal processing must be carefully considered so as to conserve signal-to-noise ratio.

Radio astronomers have developed a technique to measure such weak signals. Called a switched radiometer (see Ref. 18), the receiver alternately listens to the signal plus noise and then to noise only. It detects the small resulting change in output and is thus free (to first order) of drifts and gain changes which are slow compared to the switching rate. Switching the input of a receiver brings about some formidable engineering problems that can be avoided altogether in the radar case by switching the transmitter off and on.

Thus an appropriate transmitted signal is a slow modulation, on and off, of the carrier; the corresponding receiver is a radiometer, and the measurement made is the strength of the echo signal. The measurement can be interpreted in terms of the radar cross-section of Venus. The radar cross section is a Venerian feature of great interest. How the cross section varies with time, with matched and crossed circular polarization, and matched and rotated linear polarization, will be discussed subsequently.

The transmission of a pure sinusoid, coupled with spectral analysis at the receiver, has proven to be a fruitful combination to study surface roughness and rotation characteristics of Venus. This is so because angular velocity imparts to each element of Venerian territory a specific line-of-sight velocity which manifests itself as a doppler shift of frequency in the received spectrogram. The magnitude of the shift depends on both the position of the reflecting element and the rotation of Venus, while the strength of the echo depends upon the element's ability to reflect at its particular inclination to the line of sight (the back-scatter function; Ref. 19).

Thus, in principle, both the component of rotation perpendicular to the line of sight and the backscatter function can be determined from a spectrogram. Although the backscatter function cannot tell precisely what the Venerian surface is made of, it can be used as a criterion to test hypotheses and so to eliminate some possibilities. However, small errors in estimating the perpendicular component of rotation from a spectrogram yield large errors in estimating the corresponding backscatter function.

A transmitter-receiver pair exists which can specifically extract the rotation component from Venus. It is a combination of a range-gate and a spectrometer. A range-gate is a device which accepts signals from a specified distance and rejects those from closer or farther ranges. This is accomplished by modulating the transmitter with a wide-band waveform and using the waveform's inverse (delayed by just the time of flight) to remove the modulation at the receiver. In this manner, echoes from the proper distance pass through the system unaltered, while those from other ranges remain wide-band and may be removed by filtering.

Spectral analysis of the output of the range-gate then reveals the line-of-sight velocity of the selected portion of Venus. From this the rotation component can be calculated independently of the scattering law.

Such information, combined with the spectrograms mentioned above, produce an unambiguous backscatter function. In addition, by observing the component of rotation for several months as Venus swings by the Earth, enough information is available, in principle, to infer the complete rotation vector of Venus.

2. Radiometer

The radiometer is essentially a power-measuring device. This is normally done by squaring the received signal and then averaging the results. However, in the Venus radar case, by far the largest source of power is the thermal noise of the antenna and the receiver. In order to eliminate that large component, the transmitter is switched on and off, and the change of receiver power is noted.

The block diagram of the radiometer (Fig. 47) illustrates this method. The keying period is about 2 sec. The signal is converted to a final IF of 1 kc before being squared. The bandwidth, determined by a plug-in filter, was chosen to be as narrow as possible to eliminate the most noise but wide enough to let all of the signal power through. During the experiment, 100- and 50-cps filters proved to be the most convenient.

The average output of the square-law device is proportional to the total power of its input, but the instantaneous value fluctuates widely about this average because of noise in the input. This signal is then smoothed by one of two accumulators (integrators) depending upon whether the signal contains the echo power from Venus or only the noise. Thus the receiver switch of Fig. 47 must be delayed from the transmitter switch by precisely the time of flight. The proper delay is computed from the Venus and Earth ephemerides. The method of generating this delay is described in Sec. III-I.

After smoothing for about 2 sec, the contents of the noise-only accumulator is subtracted from that of the signal-plus-noise accumulator. The result, proportional to the signal power, is filtered by a simple RC circuit and displayed on a strip chart recorder. Because of the low signal-to-noise ratio, a long time constant of 60 sec was used.

All of the operations, from the receiver output on, were performed on a small general-purpose computer (Packard-Bell PB250). The receiver output was sampled at a rate of 300 samples per second (an ample rate for the 100-cps bandwidth) by an analog-to-digital converter and then fed directly to the computer. The use of a computer provides many advantages other than the usual ones of freedom from drifts and gain changes, etc. For example, the computer simulates a square-law device with high accuracy. Hence the output is truly linear in power, which is a great convenience. Also, the long time constant of the RC filter is realized by a simple recursion formula in the computer without the problem of charge leaking off of the condenser during the alternate 5 min when the transmitter is on and the receiver is off.

At the end of a 5-min receive cycle the computer types out the signal power, the noise power, and their ratio. Additional runs can either be computed accumulatively or successively.

The signal power can be calibrated by keying in a known amount of power from a separate source. It can also be calibrated by multiplying the signal-to-noise ratio by kTB where T is the system noise temperature. The second method was used for the Venus experiment as it is relatively insensitive to time-varying system gain; and the temperature measurement was quite stable and accurate.

A plot of how the radar cross section, as a percentage of the geometric cross section, of Venus changed during

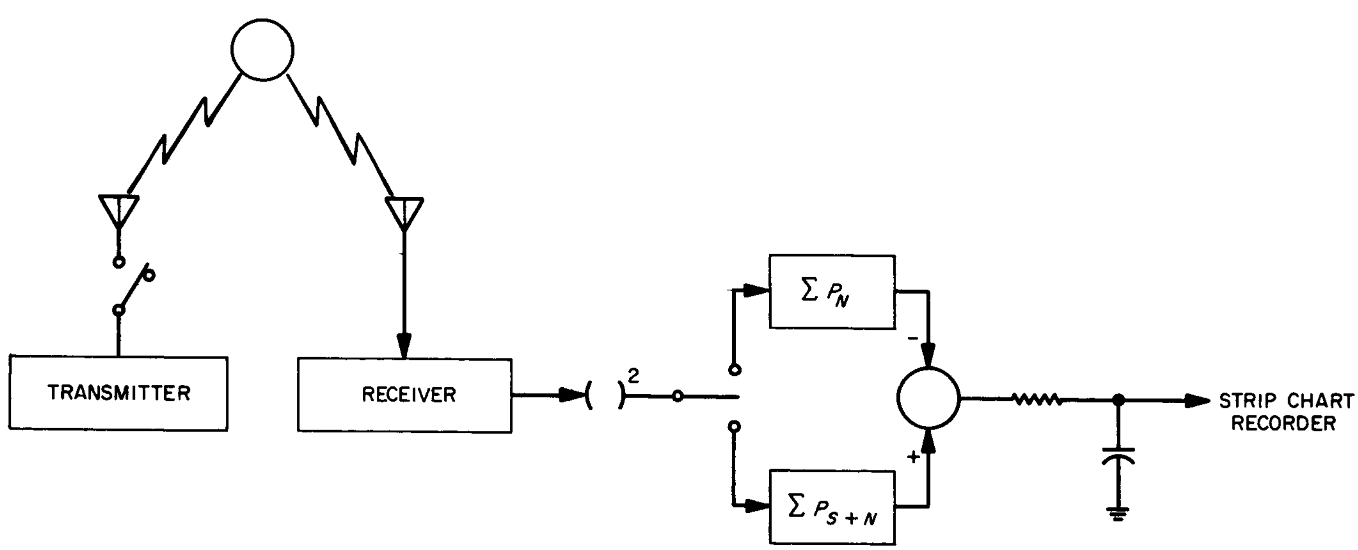

Fig. 47. Radiometer

the course of the experiment is given in Fig. 48. A typical sample of the strip chart recorder, showing signal power (through the 60-sec time constant) as a function of time, is given in Fig. 49. Another advantage of digital techniques is apparent in that figure—instead of going off scale at the top, the reading just starts over again from the bottom.

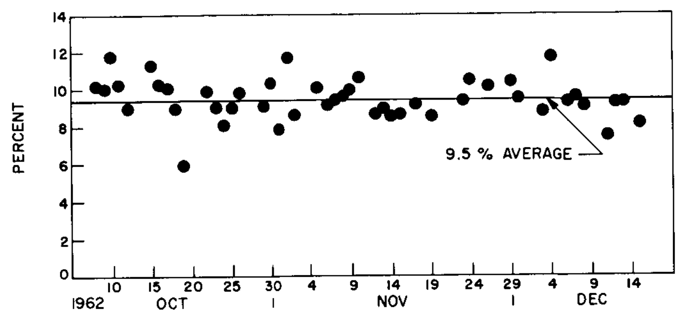

Fig. 48. Radar cross section

3. Spectrometer

The correlation approach is used to find the power spectrum of the echo. That is, the autocorrelation function of the signal is measured, and the spectrum is then calculated by Fourier transformation. The theory behind spectral measurement and the correlation approach is well covered in Ref. 20. It is shown there that increased spectral resolution can be obtained only at the cost of signal-to-noise ratio, and that, in any case, accurate spectrograms inherently require great amounts of input data. High accuracy is quite necessary in this application since the Venus echo is only a perturbation of the thermal background noise. Some of the spectrograms shown in the data section (Appendix A) represent the processing of up to 4 hr of signal.

A block diagram of the spectrum analyzer is given in Fig. 50. There the entire maser, paramp, programmed local oscillator, several stages of conversion and IF amplification, etc., have all been reduced to one block labeled band-pass filter. The center frequency is 1 kc and the width is controlled by a plug-in filter. As in the case of the radiometer, 100- and 50-cps filter bandwidths proved most convenient. The output of the filter is sampled at the Nyquist rate for the bandwidth used. The spectrum of the sampler output (see Fig. 50) is thus periodic, the signal appearing in the frequency intervals of 0 to B cps, and B to $2B$, $2B$ to $3B$, etc. Because of this effect, the signal does not have to be heterodyned down to the desired range of 0 to B cps.

The limiter is used as an analog-to-digital converter, quantizing to only two levels. This is the major innovation of this method. The digital correlator computes the autocorrelation function of the signal at y (see Fig. 50) by forming the sums:

$$R_k = \sum_{n=1}^{N} y_n \, y_{n+k} \qquad k = 0, 1, \cdots, 44$$

where y_n is the nth sample of the signal at y. Because of the limiter, the values of y_n are always either ± 1 so that the correlator can calculate the terms in the equation above at a rate of 3 million per sec. The correlator is a special purpose machine which computes 45 points on the autocorrelation function, at a maximum sampling rate

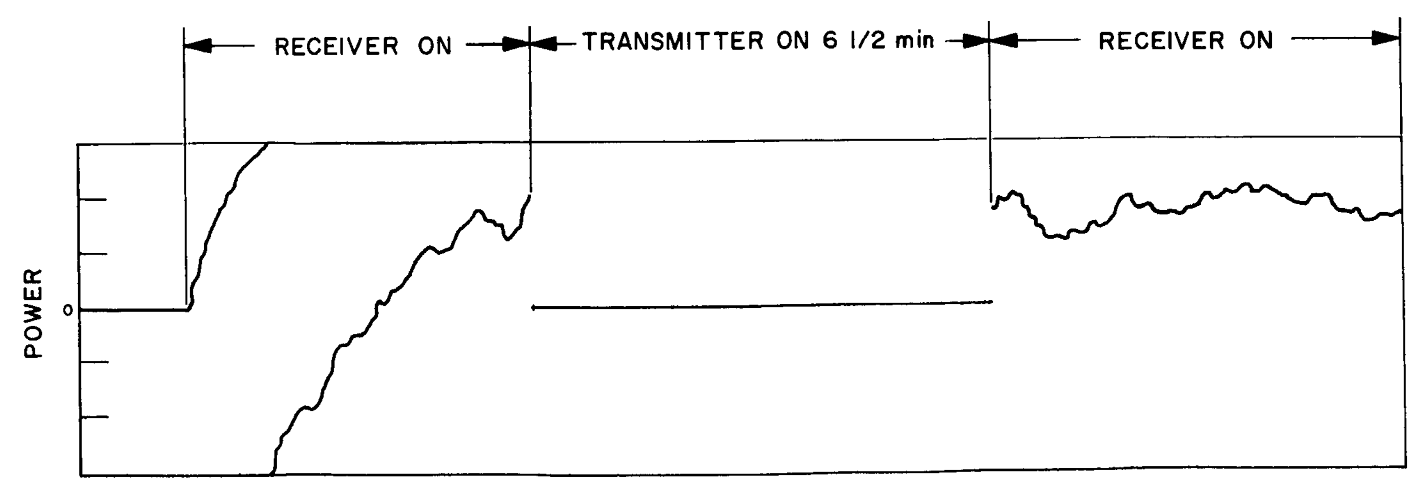

Fig. 49. Signal power

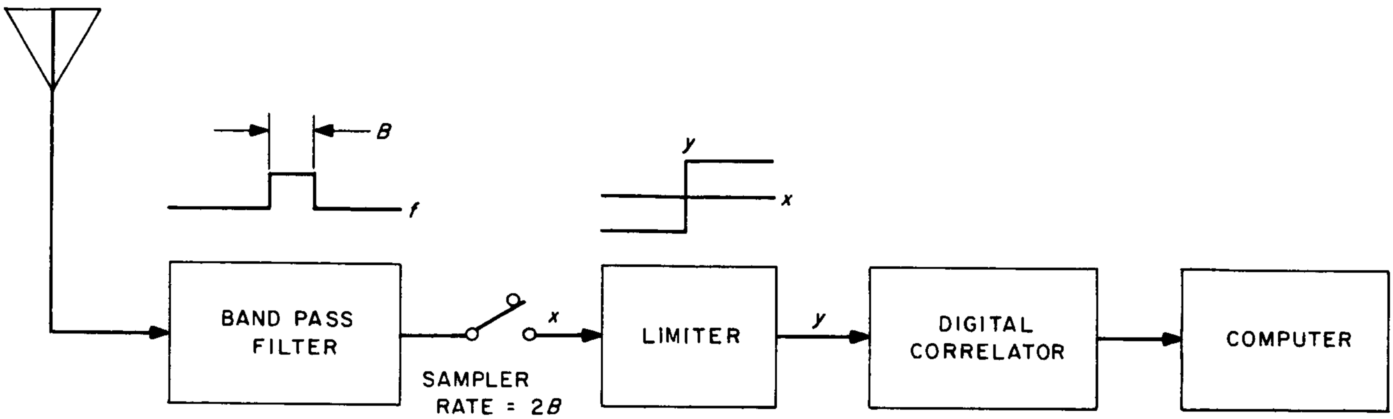

Fig. 50. Spectrum analyzer

of 66⅔ kc and can integrate (at that rate) for weeks without an overflow. It is described in detail in Ref. 21 (p. 111).

It is the correlation function at x (see Fig. 50) which is desired but that at y which is measured. One might think that the action of the limiter would alter the spectrum at x beyond recovery. Fortunately, this is not so, and a simple correction formula (Ref. 1) applied to the autocorrelation function at y suffices. The correction and the Fourier transformation are performed on the same general-purpose computer (Packard-Bell PB250) that is used for the radiometer.

The spectrum that is produced is the sum of the desired signal and the ubiquitous noise. To provide meaningful results, the noise-only spectrum is computed separately and subtracted from the total spectrum. It must be measured to the same accuracy as the total spectrum, however, so the same technique that is used in the radiometer is applied. Because the transmitter is keyed, one second on and one second off, the calculation of signal-plus-noise and noise-only spectra can be interleaved and the two resulting spectra are subtracted.

The action of the limiter complicates this procedure somewhat, since the limiter output has a constant power regardless of whether or not the signal is present in the noise. This is accounted for by using the output of the radiometer to determine the magnitude of the noise spectrum to be subtracted.

The radiometer and spectrometer experiments thus run simultaneously. During the nominal 5-min receiving cycle the PB250 acts as the radiometer, and the special-purpose machine measures the autocorrelation function of the signal. During the transmitting cycle the PB250 corrects and transforms the autocorrelation function and displays the resulting spectrum on an x-y plotter.

Permanent records are kept by means of the computer's typewriter. A complete set of the spectrograms taken during the experiment are given in Appendix A of this report.

4. Range-Gated Spectrum

The very narrow bandwidths of the echo signal spectrograms, determined by the method of Sec. IV-A-3, pose an interesting question: does Venus have a rough surface (allowing echoes to be heard from the limbs) and rotate very slowly; or is the surface shiny and the rotation faster? A combination range-gate and spectrometer enables this question to be answered.

The geometry of the range-gate is shown in Fig. 51. The first zone corresponds to the front of the planet, seen as a disk on the right-hand view. The second, third, etc., zones are seen as annular rings of increasing radius. Power from just one of the 111-mile zones is accepted by

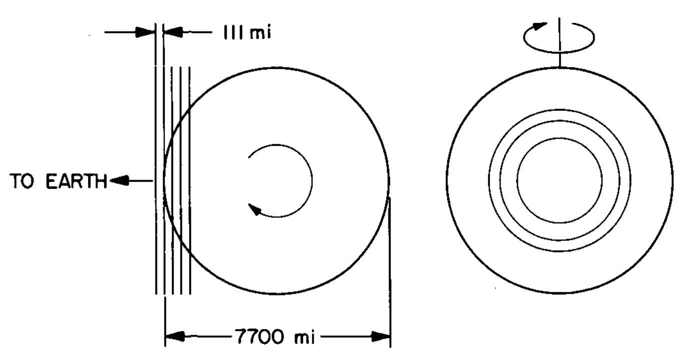

Fig. 51. Range-gate geometry

the range-gate. This power is analyzed into its frequency spectrum by the method of Sec. IV-A-3. The width of this spectrum, together with the knowledge of the position of the corresponding zone, enables the perpendicular component of the angular velocity of Venus to be calculated directly.

The method of accomplishing the range-gate is diagrammed in Fig. 52. The transmitted carrier is multiplied by a code. The code chosen for the Venus experiment is a pseudo-random square wave, generated by a shift-register of length five. The clock frequency is variable, but 840 cps was convenient, producing zone depths on Venus of 111 miles. The transmitted signal is thus wide band.

At the receiver the signal is multiplied by a very carefully delayed version of the same pseudo-random wave, thereby cancelling out the modulation impressed at the transmitter and leaving the signal narrow band. If the echo originated from the center of the zone, the timing would be perfect and the cancellation complete. If the echo occurs in the zone, but away from the center, cancellation is only partial. Hence part of the signal power remains narrow band and part wide band. The magnitude of the narrow-band component can be shown to be the square of the autocorrelation function, for the appropriate delay, of the code waveform.

The two-level autocorrelation function of the pseudo-random square wave is thus ideal for this application. "Cross-talk" between zones is virtually eliminated. Power from the "wrong" zones is wide band and appears as noise to the spectrometer where it is negligible as compared to the thermal noise already present.

During some of these experiments, the signal was recorded on tape (before being multiplied), along with the code, so that the same signal could be examined for its content in each range-zone. It was an advantage to have a high-speed correlator since 3 hr of signal data were processed in only 10 min (for each zone).

The range-gated spectrograms are displayed in Appendix A of this report. The perpendicular component of rotation was calculated for each of these spectrograms and is presented in Fig. 53. The abscissa is marked off in the days of the experiment, and the ordinate in the rotation component, measured in cps of the limb-to-limb Doppler broadening. The solid curve is a theoretical one, calculated from the Venus and Earth ephemerides on the basis of the rotation axis being perpendicular to the orbit, and the rotation period being 250 days retrograde.

It is interesting to note that the theoretical doppler broadening for synchronous rotation or any forward rotation faster than synchronous and for any tilt of the axis,

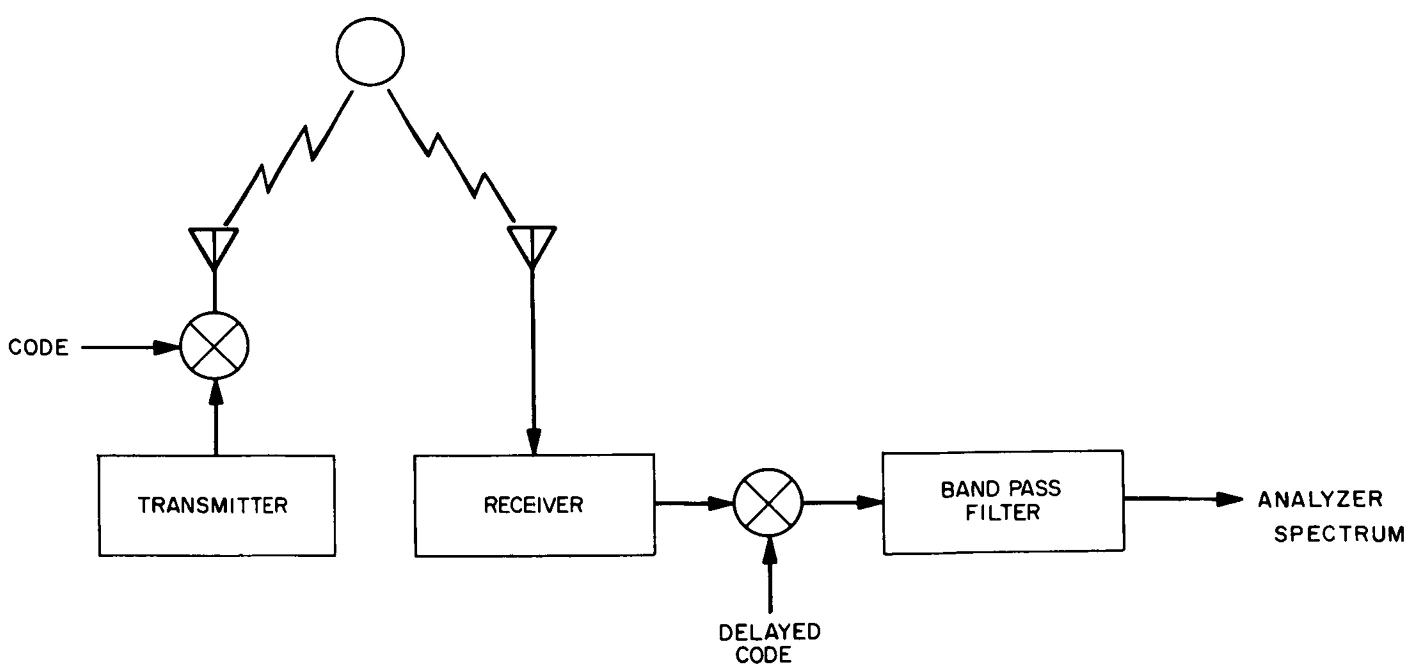

Fig. 52. Range-gate

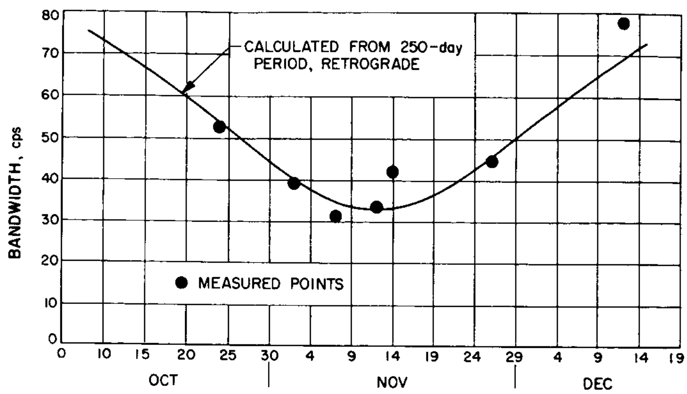

Fig. 53. Perpendicular component of rotation

must be greater than 88 cps on the day of conjunction (November 12, 1962).

The maximum bandwidth possible, under the 250-day retrograde assumption, has been marked off by arrows on all of the spectrograms (Cf Appendix A). As can be seen, they are quite consistent with this assumption

B. Continuous Wave System

R. L. Carpenter

The major objective of the CW experiment was to obtain high resolution broadband spectra of the signal reflected by Venus in order to investigate the planet's period and direction of rotation. This objective is the same as that of the AM system spectrum measurements discussed in Sec. IV-A. The techniques and some of the instrumentation for these measurements are different and thus provide a second independent spectrum determination. The results of the 1961 CW radar experiment suggested that Venus might have a slow retrograde rotation (p. 56 of Ref. 22). The equipment for this year's experiment provided higher resolution and wider bandwidth coverage than was available previously. The data obtained do indeed suggest that Venus has a slow retrograde rotation.

1. Experimental Procedure

For the CW measurements, the 2388-Mc, 13-kw transmitter was switched on and radiated continuously for the duration of the signal's round-trip time to Venus. The radar system was then switched from its transmit to its receive mode for the duration of the echo return.

The received rf signal was very stably heteodyned down to 89.9 cps, low-pass filtered with a sharp cut-off at 167 cps, and recorded on magnetic tape. For the spectra obtained prior to October 23 the positioning of the signal in the audio region was changed from day to day to determine an optimum location. The stable heterodyning was done by offsetting the ephemeris controlled local oscillator subsystem as described in Sec. III-G.

Between each complete transmit-receive cycle a noise run was recorded with the system in its receive mode, but with no echo present. The noise runs were used to remove the distortion in the spectrum caused by the receiver. The magnetic tapes were sent to JPL for processing. The tapes were played back and sampled at 375 samples per second by an analog-to-digital converter; the A/D converter generated a second tape in the correct format to be read into the IBM 7094.

A special program was written to compute the spectrum of the recorded signal. This program was designed to utilize either the full 16-bit amplitude resolution of the A/D converter or 4 bit or binary resolution. The binary resolution case was used for all spectral computations in this report; however, both the 16-bit and the 4-bit resolutions were tried as a check on the accuracy of the computed spectra. The only difference between the binary and the 4- and 16-bit cases was that in the binary case the fluctuations on the spectrum were more exaggerated. The results confirmed the analysis by R. Goldstein that 2½ times more data is needed for a binary resolution computation if one is to obtain a spectrum as smooth as one computed with full amplitude resolution. Even though more data is needed in the binary case than otherwise for spectra of comparable smoothness, the saving of computer time was essential. The running time required in the binary case is 8 times less than the full resolution case even though 2½ times more data must be used. The fact that the true spectrum of the signal can be obtained using only binary resolution requires that the amplitude probability distribution of the signal is Gaussian (Ref. 23), which is the case for Venus's radar echo. The *frequency* resolution of all the computed signal spectra was 1 cps, while the noise spectra were computed with only 5-cps resolution. The noise spectra were computed with coarser resolution (and consequently were smoother) so as not to introduce noise into the signal spectra when they were corrected for the distortion caused by the receiving system.

Figure 54 shows the spectrum obtained when Venus was closest to the Earth (November 13, 1962). It was computed from approximately 47 min of recorded signal data. The ordinate is relative signal power per unit bandwidth, and the abscissa is frequency. The plot can be

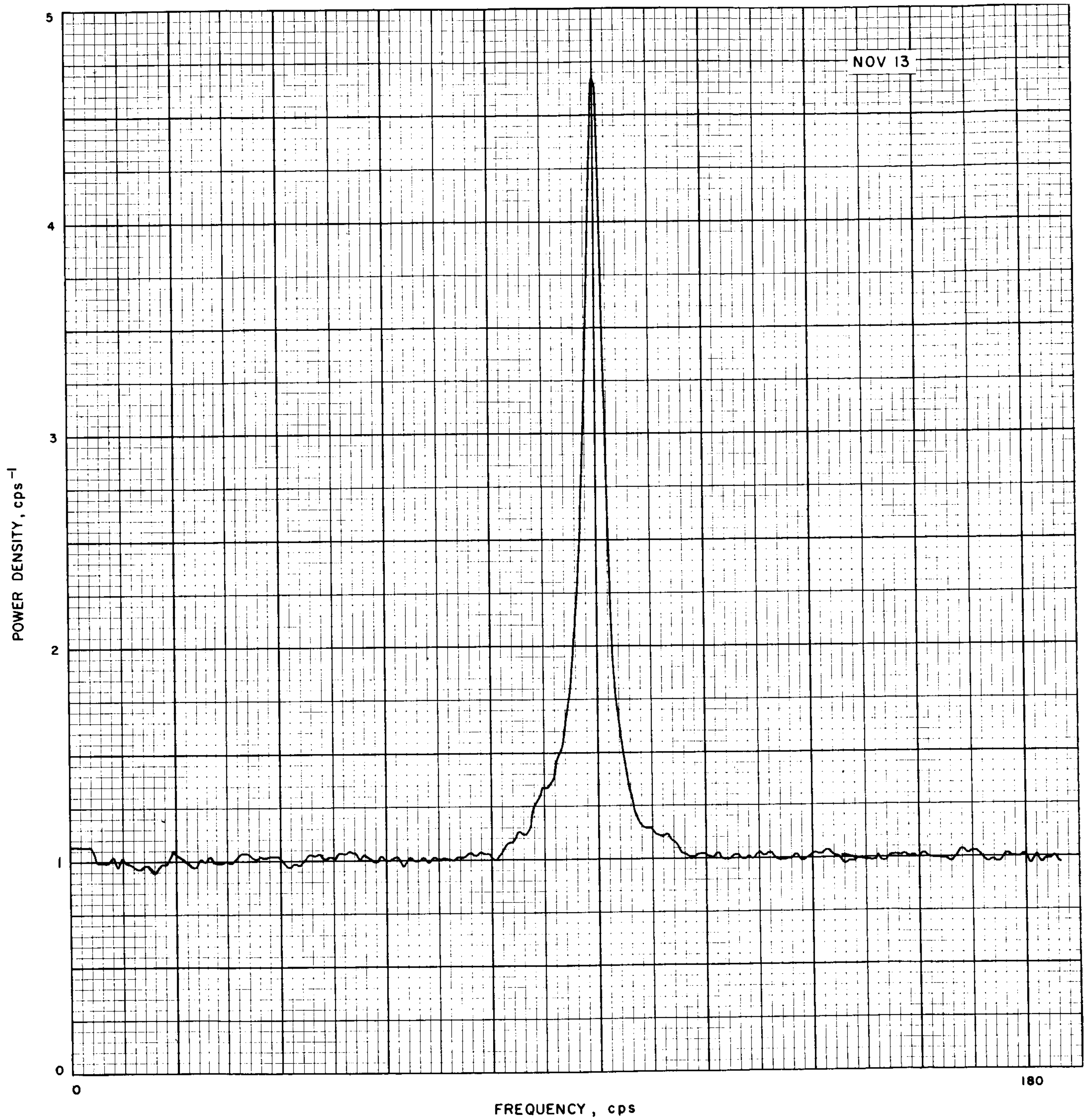

Fig. 54. Venus spectrum: November 13, 1962

equally interpreted as signal power vs the radial velocity of Venus' surface due to rotation. The peak corresponds to zero radial velocity. The spectrum has a resolution of 1 cps, or a radial velocity resolution of about 6.3 cm/sec.

2. Measurement of Bandwidth and Signal Level

The spectral analysis program was designed to provide a large part of the desired data reduction for each spectrum. Three different bandwidths and the relative signal level were determined for each of the spectra. The bandwidth determinations consisted of the 3-db, 6-db, and effective bandwidth. The effective bandwidth is the width of a rectangle that has the same height and area as Venus' spectrum. The 3- and 6-db bandwidths were found by first determining the best fit horizontal line through the noise skirts on each side of the spectral peak. This line established a zero reference level and represents the best estimate of the base of the spectrum. The bandwidths were measured at the half- and quarter-power levels relative to this base. The effective bandwidth was derived by dividing the area bounded by the spectrum and its base by its height. The measurable part of the spectrum was taken to lie within ±40 cps of the peak.

3. Relative Signal Level and Planet Reflectivity

The ratio between the areas of the signal spectrum and the background noise spectrum is a measure of the received signal-to-noise ratio. This ratio may be used to determine the power level of the returned signal. The radar cross section σ of the planet may then be found from the radar equation:

$$\sigma = \frac{(4\pi)^3\, d^4\, P_r}{G_t\, G_r\, \lambda^2\, P_t} \tag{16}$$

where

d = distance to Venus

P_r = received power

G_r = gain of the receiving antenna (54.2 db ± 1 db)

G_t = gain of the transmitting antenna (54.1 db ± 1 db)

λ = wavelength

P_t = transmitter power

The receiver power P_r is obtained from the measured signal-to-noise ratio and the measured system noise temperature:

$$P_r = (S/N)\, kT, \tag{17}$$

where

(S/N) = the signal-to-noise ratio per cycle of bandwidth

k = Boltzmann's constant

T = system noise temperature.

The radar cross section of a uniformly rough planet is

$$\sigma = \pi R^2\, g\rho, \tag{18}$$

where R is the radius of the planet, ρ is the power reflectivity of the surface material, and g is the directivity (the ratio of the power scattered back toward the receiver to the average power per unit solid angle scattered in all directions). The directivity is dependent on the roughness of the planet's surface; it is unity for a smooth sphere and 8/3 for a Lambert scattering sphere (Ref. 24).

Equation (18) shows that the reflectivity of the surface cannot be obtained directly from a measurement of the radar cross section; only the product $g\rho$. The $g\rho$'s obtained during the experiment are shown in Fig. 55. The mean value is

$$g\rho = 0.0975^{+0.026}_{-0.020}$$

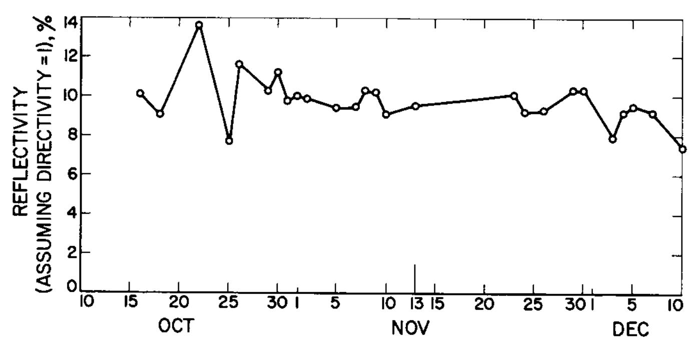

Fig. 55. Venus reflectivity (g = 1 assumed)

The dielectric constant k of the reflecting surface, assuming zero conductivity, is given by

$$k \approx \left(\frac{1+\sqrt{\rho}}{1-\sqrt{\rho}}\right)^2 \tag{19}$$

Hence, assuming $g = 1.0$,

$$k = 3.75^{+0.55}_{-0.25}$$

For illustration, a few dielectric constants for various terrains (Ref. 25) are shown in Table 7.

4. Bandwidth Measurements

From a study of the changes in bandwidth of the returned signal, it is possible to determine the direction and period of rotation of Venus *if* the inhomogeneities in the scattering characteristics of its surface are not

Table 7. Dielectric constants for various terrain features

Terrain	k
Sea or fresh water	80
Agricultural land, low hills	15
Mountainous (hills up to 3000 ft)	5
Desert sand	3

too extreme. This possibility arises from the fact that the apparent angular velocity of Venus as seen from the Earth changes as it passes from one side of conjunction to the other. The apparent angular velocity is the projection on to a plane perpendicular to the line of sight of the sum of two rotational components: (1) a component due to the rotation of Venus on its own axis and (2) a component due to an apparent rotation caused by Venus passing the Earth. The latter component is a maximum at the time of conjunction and gives the planet an apparent forward rotation rate. If Venus were rotating forward the two components add, giving rise to a maximum in the apparent angular velocity at conjunction assuming that the axis is roughly perpendicular to its orbit. If Venus were rotating backwards, then the two components would counteract each other and the apparent angular velocity would be a minimum at conjunction.

Figures 56 and 57 show the theoretical and observed variation in the bandwidth during the course of the experiment. Consider the two theoretical curves first. The upper set of curves in Fig. 56 corresponds to the 6-db bandwidth; the lower set corresponds to the 3-db bandwidth. The theoretical curves for the effective bandwidth are shown in Fig. 57. All curves were computed utilizing the ephemeris of the Earth and Venus and with the axis of Venus assumed perpendicular to its orbit. The sidereal rotation periods are for synchronous rotation (224.7 day forward) and 150, 200, and 250 days retrograde. The spectrum bandwidths for shorter rotation periods, both forward and retrograde, were also computed, which gave relatively flattened curves. This is to be expected since the broadening due to rapid rotation will mask out the slower apparent rotation arising from the orbital motion of

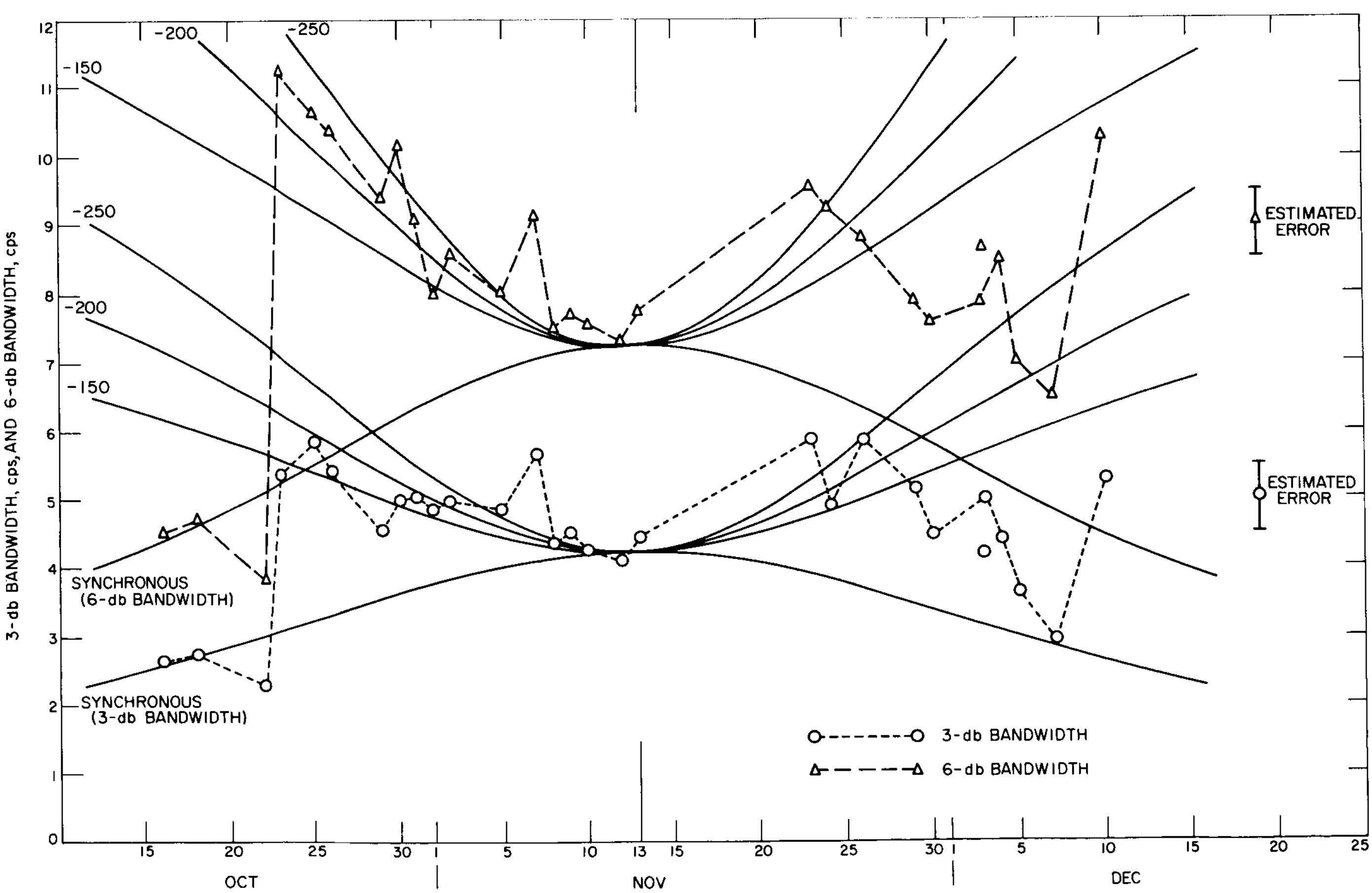

Fig. 56. 3- and 6-db bandwidths of Venus spectrum

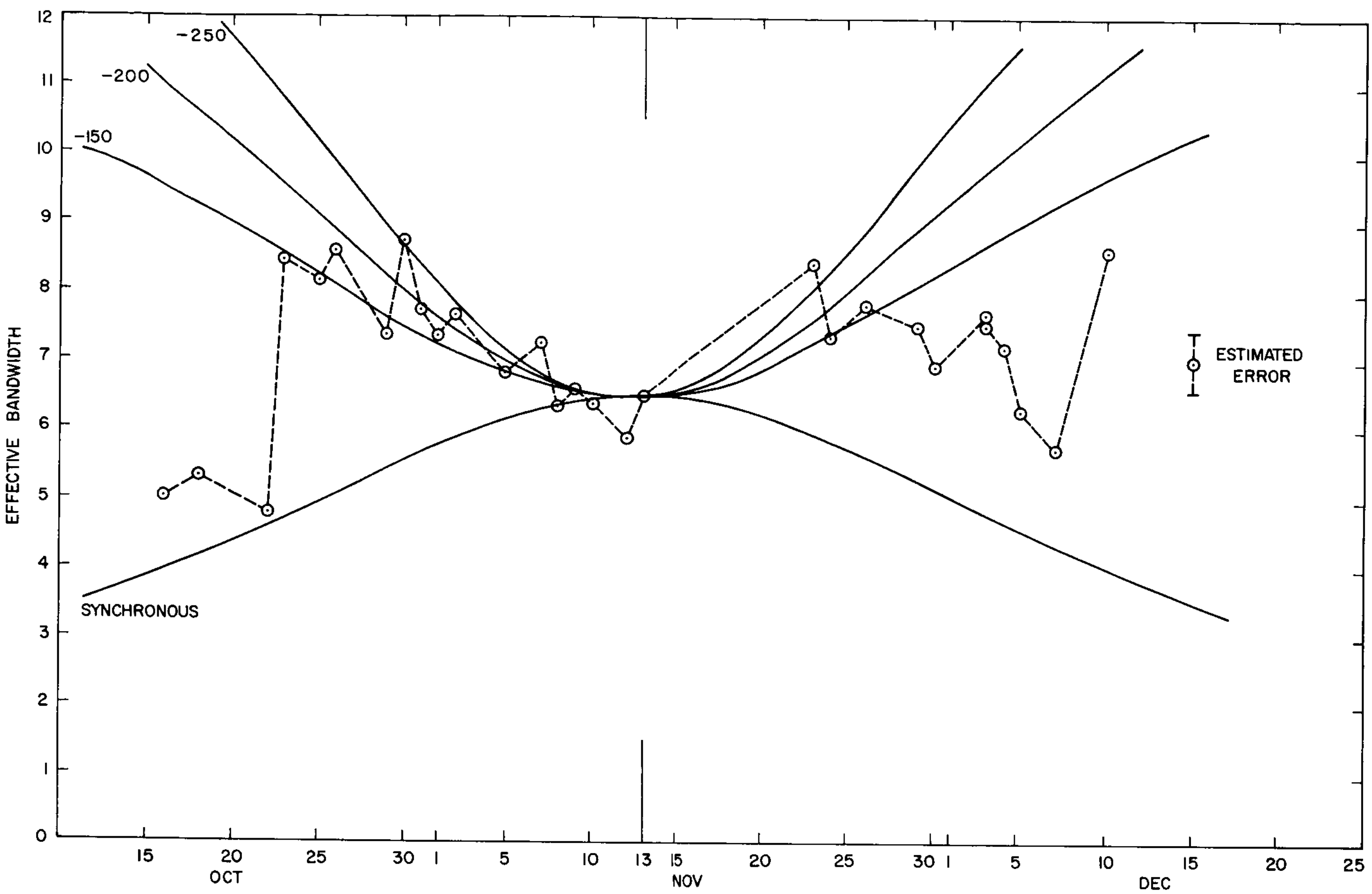

Fig. 57. Effective bandwidth of Venus spectrum

Venus. The shorter rotation period curves are not shown; however, they would fall between the synchronous and retrograde 150-day curves. For example, a 14-day period would be practically a straight horizontal line with a bandwidth equal to that observed at conjunction. All of the bandwidths have been normalized by dividing the limb-to-limb bandwidth by an appropriate constant so that the bandwidth at conjunction was approximately equal to the observed bandwidth. This allows comparing the observed bandwidth with the theoretical bandwidth without requiring the knowledge of the scattering characteristics of the planet's surface; however, it does assume that the scattering is approximately the same from point to point over the surface.

The observed bandwidths are also shown in Fig. 56 and 57. The probable error of each point for the 3- and 6-db bandwidth is estimated to be $\pm\frac{1}{2}$ cps, and for the effective bandwidth, $\pm\frac{3}{8}$ cps. (The absence of data between November 13 and 23 was due to an improper setting on the ephemeris controlled oscillator.) It appears that the scattering characteristics of the surface are not homogeneous and that there may be a rather marked variability in the topography of Venus. As a consequence, no conclusion regarding the direction and period of rotation seems justified based on the CW spectral bandwidth measurements alone. The extreme change that occurred between October 22 and 23 (Fig. 56 and 57) is difficult to understand without assuming that some small highly reflecting region passed through the center of the disc of the planet during the week prior to October 23. This conjecture is supported by the appearance of the spectrum on October 22 (Fig. 58) and particularly in comparison with the spectrum of October 23 (Fig. 59). The October 22 spectrum is fairly broad except for the central spike. The 3-db, 6-db, and effective bandwidth measurements are markedly reduced by the presence of the spike.

5. Spectral Detail

Of particular interest is the possible detection of an actual surface feature on Venus. Figures 60 and 61 show the spectrum for November 8 and 10, 1962. Note the

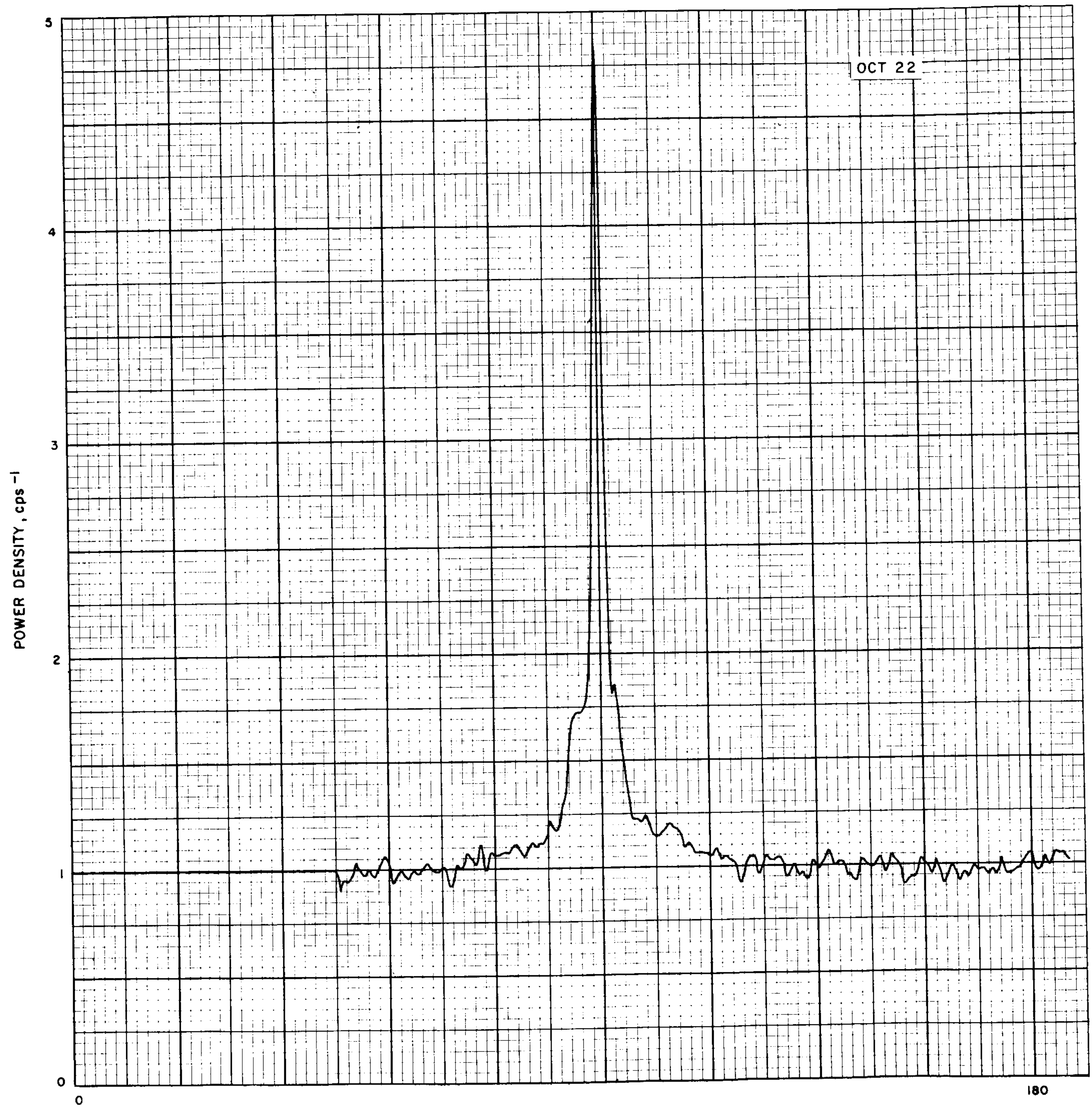

Fig. 58. Venus spectrum: October 22, 1962

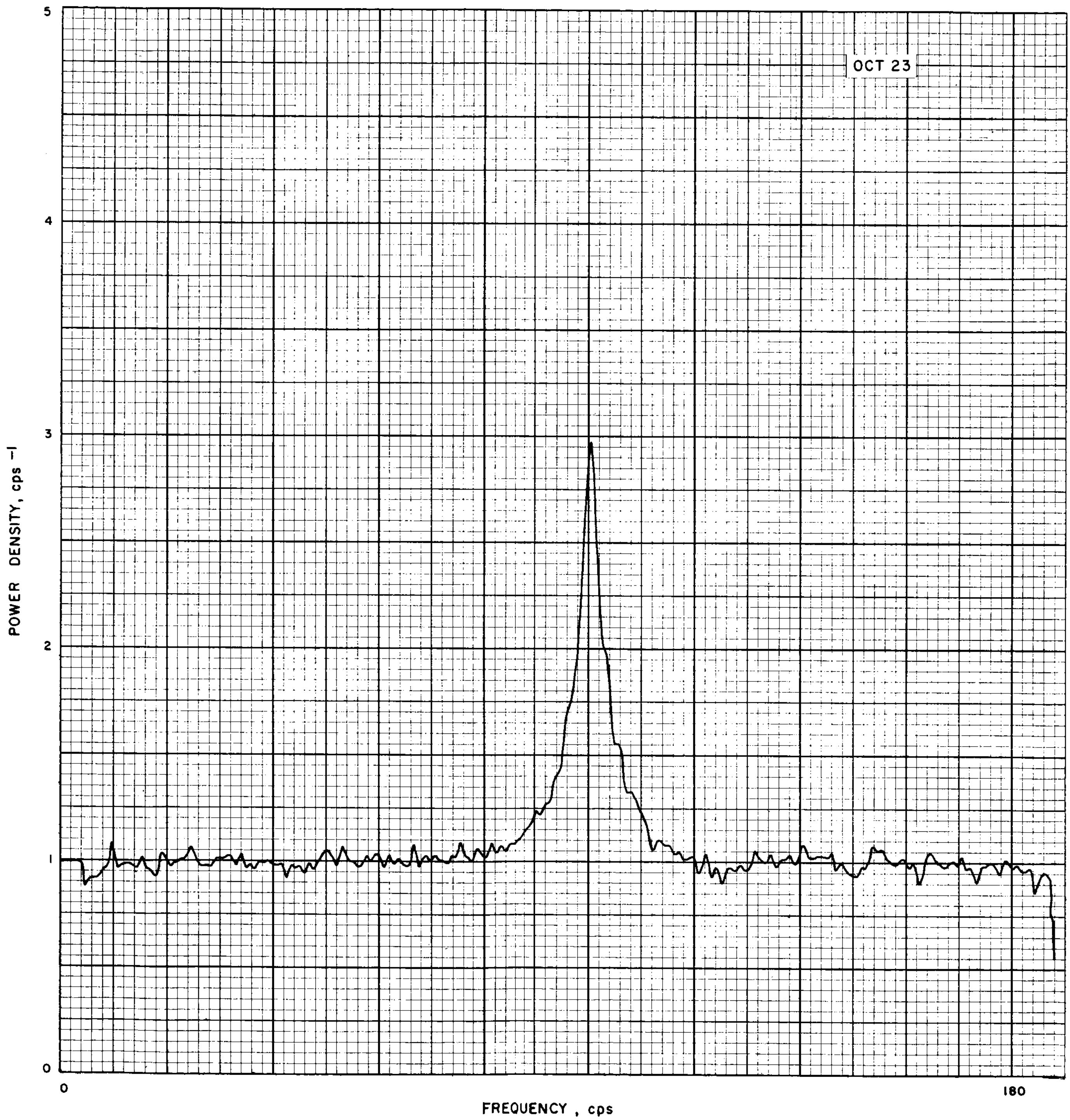

Fig. 59. Venus spectrum: October 23, 1962

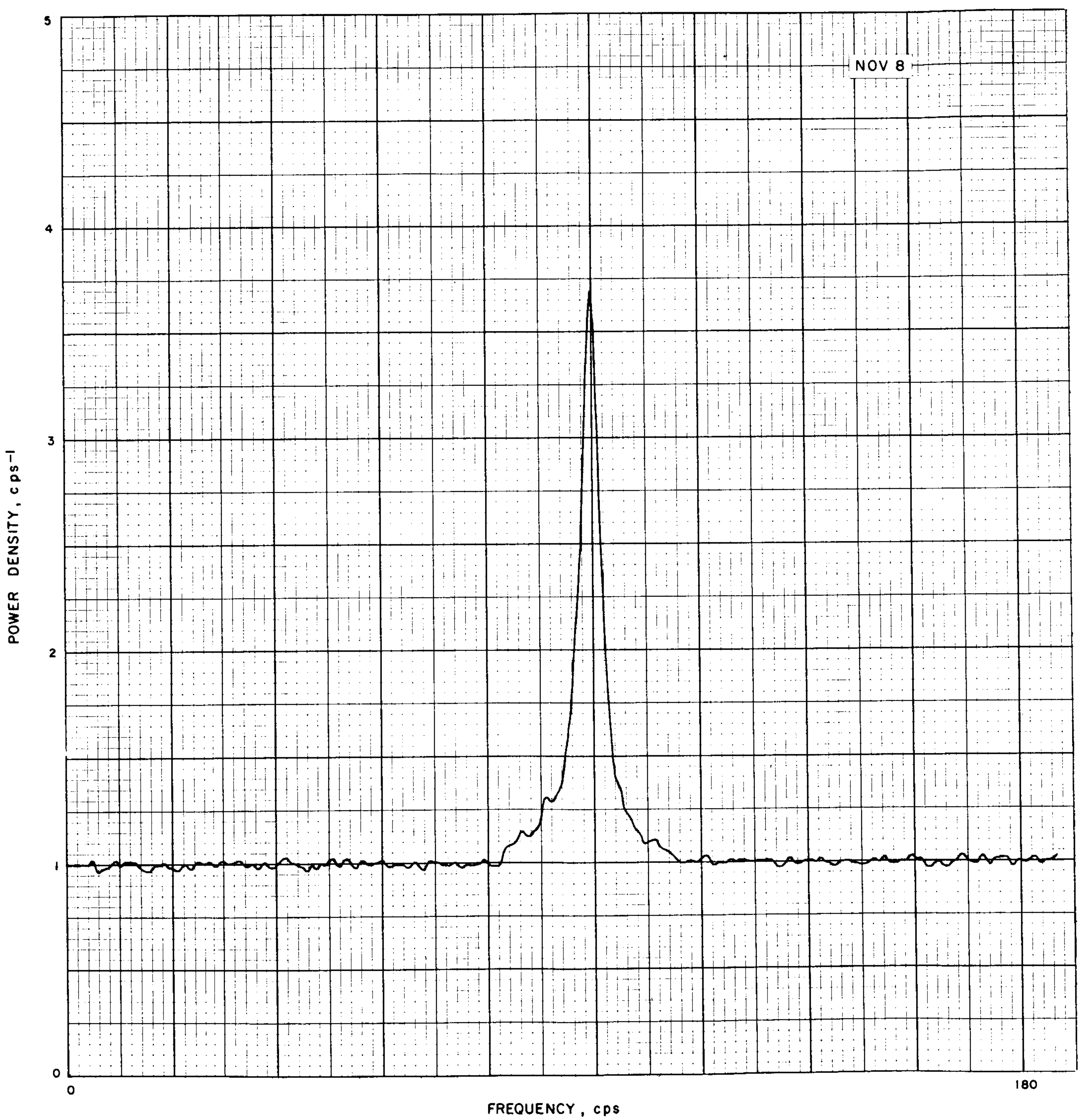

Fig. 60. Venus spectrum: November 8, 1962

Fig. 61. Venus spectrum: November 10, 1962

detail on the lower left side of each spectrum. It is approximately 5.2 db above the average peak of the background noise and 1 db above the adjacent part of the spectrum. At least a suggestion of a similar detail was found on all but a few of the spectra obtained in the month preceding conjunction (see Appendix B). Figure 62 shows the position of various details relative to the peak of the spectrum. The ordinate is the date of the observation and the abscissa is the frequency difference in cps between the peak and detail. The width of the boxes corresponds to the approximate width of the detail. The filled boxes are considered good identifications, while the unfilled and dotted ones are fair and poor, respectively. There appears to be a significant continuity in the position of the best identified details, which strongly suggests that they represent one and the same spectral detail which has moved slowly across one side of the spectrum. If this detail is the result of an actual topographic structure on the surface of Venus, then the rate at which it moves may be used to estimate the planet's rotation period. The relation between the detail's rate and the planet's angular velocity, assuming it to be perpendicular to the line of sight, is

$$\dot{\theta} = \left(\frac{\lambda}{2R} \sec \Phi \sec \theta \, f\right)^{1/2} \tag{20}$$

where

$\dot{\theta}$ = apparent angular velocity of the planet

θ = longitude of feature

Φ = latitude of feature

f = rate at which feature moves across spectrum (measured in cps of doppler shifts per unit time)

λ = signal wavelength

R = radius of planet

To obtain the angular velocity, the latitude and longitude of the feature relative to the center of the planet's disc must be known. By measuring the position of the detail, relative to the maximum observable half-width of the spectrum's base, its longitude may be estimated. This assumes that the spectrum extends to the limb of the planet. If this is not the case, the longitude will be overestimated which will result in overestimating the rotation rate. Fortunately, the derived rotation rate varies as the square root of the secant of the latitude and longitude; hence, the rate is insensitive to the detail's position if it is within 45 deg of the center of the disc.

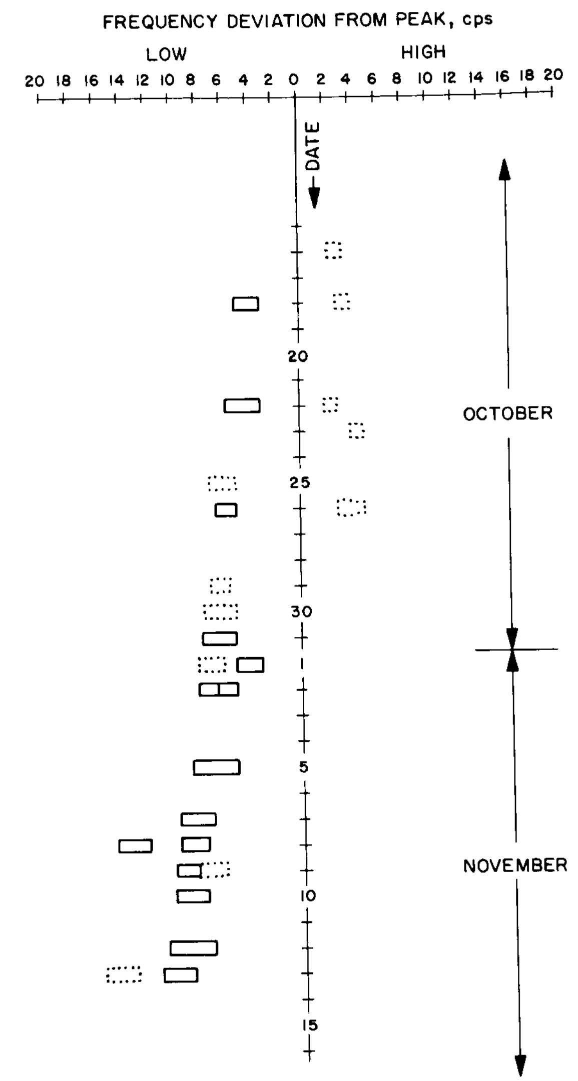

Fig. 62. Frequency deviation from peak of detail on spectrum

Using a composite spectrum constructed by averaging the spectra of November 7, 8, 9, and 10, the estimated longitude of the detail was 23 deg ±3 deg. The given set of spectra was chosen because it fell in the middle of the period of the best position estimates of the detail. The latitude of the detail cannot be found from the current data, and it will be assumed equal to 23 deg also. The estimated rate at which the detail was moving across the spectrum for the week prior to conjunction is $0.028^{+0.30}_{-0.10}$ cycles per day. This corresponds to an apparent angular velocity of $2.0^{+0.87}_{-0.41} \times 10^{-7}$ rad/sec. Synchronous rotation would be approximately 4.5×10^{-7} rad/sec. If it is assumed that the axis of Venus is perpendicular to its orbit, then the angular velocity found corresponds to a sidereal rotation period of over 1000 days forward or 230^{+40}_{-50} days retrograde. The latter period is equivalent to a synodic period (rotation relative to the Sun) of 114^{+8}_{-14} days retrograde. The 1000 days forward can be rejected because it leads to a maximum possible bandwidth of about 20 cps for the spectra taken several weeks before and after conjunction, and such a narrow bandwidth definitely was not observed.

The effect of tipping the axis in different directions is under study; however, a tip of nearly 70 deg toward the Earth would be required to give the apparent angular velocity obtained above if Venus were rotating synchronously (225 days forward). The axis would have to be tipped even more for faster rotation rates. Preliminary analysis of both the current data and the results of the 1961 radar experiment suggest that the axis is indeed approximately perpendicular to the orbit and would not change the derived sense of rotation or change the period significantly.

6. Limb-to-Limb Bandwidth

As was stated in the discussion of the effective bandwidth, it was not possible to deduce the direction and period of rotation from the 3-db, 6-db, and effective bandwidth measurements because of their wide fluctuations. However, if the signal-to-noise ratio were good enough it would be possible to estimate the limb-to-limb bandwidth by measuring the width of the spectra at their base, i.e., where they fade into the noise. Knowing the limb-to-limb bandwidth, the apparent angular velocity is found easily from the doppler equation. Since the signal-to-noise ratio was the greatest near conjunction, we should at that time see closer to the limb than before or after; consequently, there should be a systematic bias in the estimates of the limb-to-limb bandwidth in the direction favoring synchronous rotation. The measurements of the base bandwidths are shown in Fig. 63.

The curves in Fig. 63 show the theoretical limb-to-limb bandwidth for synchronous and 230-day retrograde rotation. They were computed assuming that the axis of Venus is perpendicular to its orbit. It must be emphasized that the curve for 230 days retrograde was not derived from the base bandwidth measurements but from the motion of the spectral detail discussed earlier. The fact that the two methods are in fair agreement gives added weight to the retrograde interpretation.

The anomalous points at the beginning and end of the experiment are disturbing; however, these spectra are quite noisy and thus the only part of the spectrum that can be detected is the central peak.

Three weeks before and after conjunction the limb-to-limb bandwidth for both synchronous and retrograde 230 days were approximately the same and equal to about 63 cps, whereas the bandwidths are different by 50 cps at conjunction. As a consequence, if the base width of the spectra taken 3 weeks before and after conjunction are compared with the base width of the spectra taken near conjunction, then the consistency of the data with 230 days retrograde and inconsistency with synchronous is readily apparent. Figure 64 shows the lower part of the spectra obtained on October 22, 23, and 25, three weeks before conjunction. Figures 65, 66, and 67 show the spectra obtained on December 3, 4, and 5, three weeks after conjunction. The two bars below each spectrum show the expected limb-to-limb bandwidth for synchronous and 230-day retrograde rotation, assuming that the rotation axis is perpendicular to the orbit of Venus. Note that in all six spectra the base extends at least half way to the limb as defined by the computed bandwidths. If one of the two rotation periods obtains, it is apparent that energy is being received almost to the limb. Note that both the narrowest (October 22) and the broadest (October 23) spectrum as defined by the 3- and 6-db bandwidths are included among the six spectra. Now consider three spectra obtained near conjunction. These are shown in Fig. 68, 69, and 70; they are for November 8, 10, and 13. The bars below each spectrum are again for synchronous and 230 days retrograde. It is clear that the motion corresponding to a sidereal period of 230 days retrograde is the more consistent with the data.

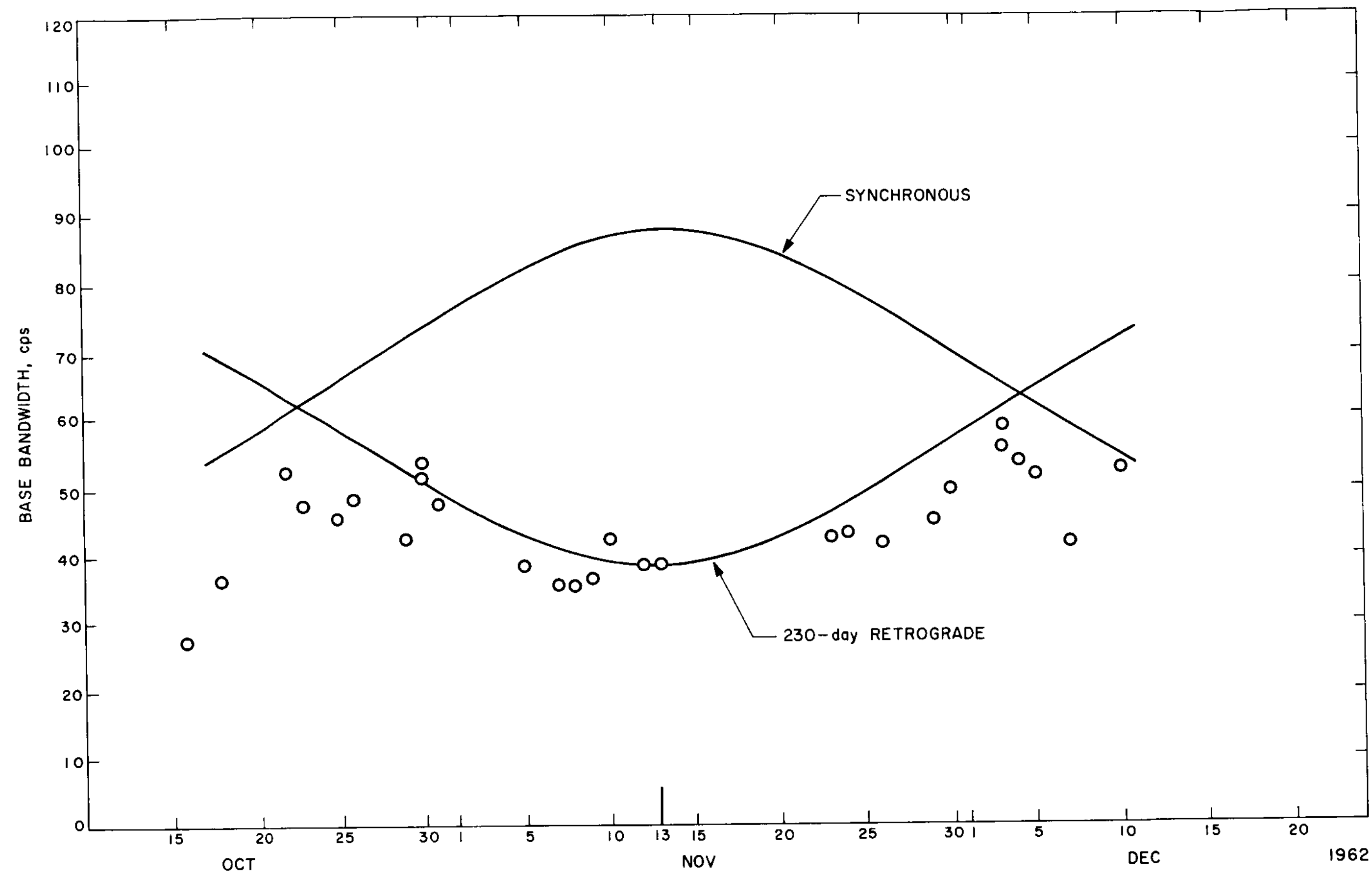

Fig. 63. Base bandwidth of Venus spectrum

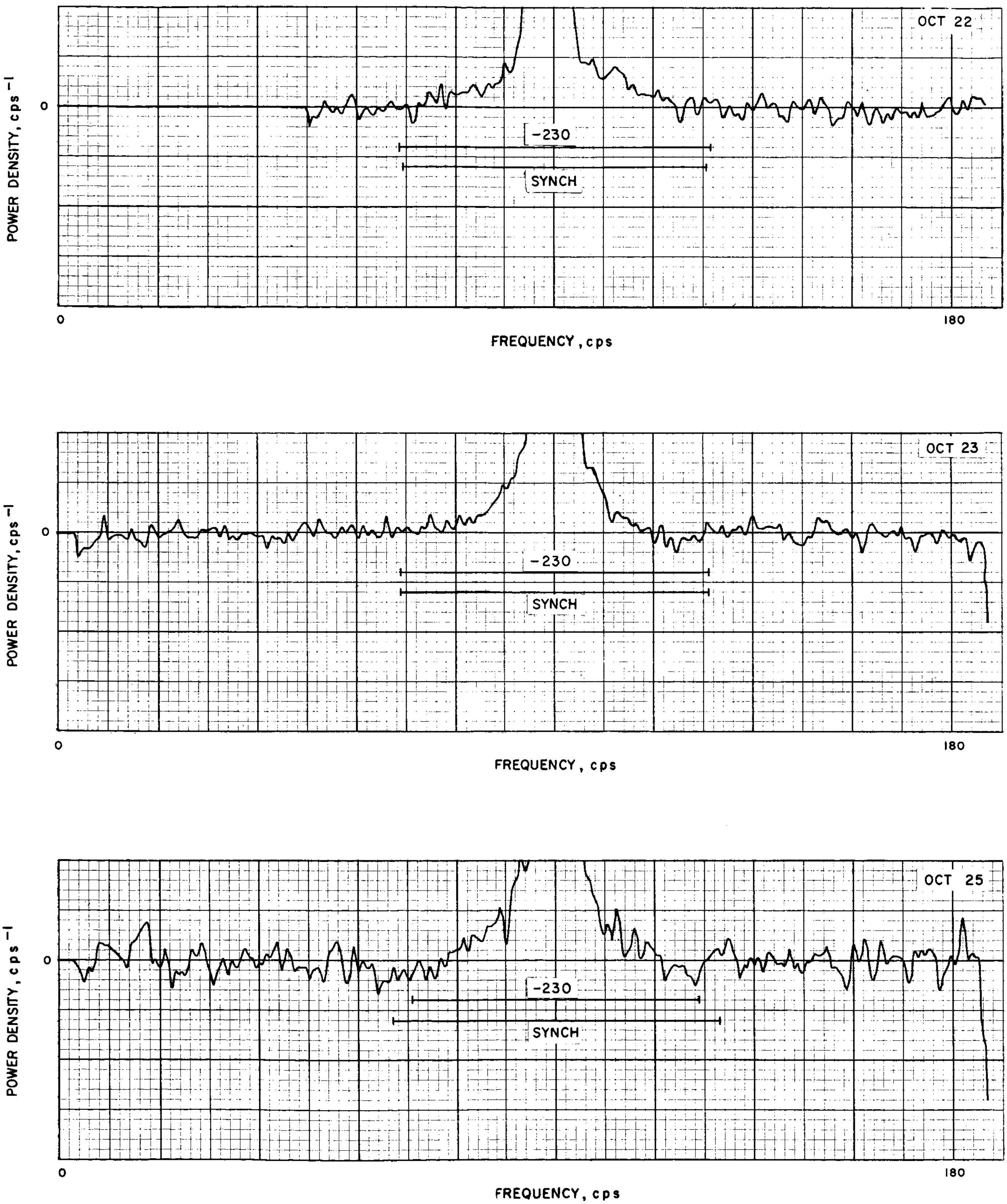

Fig. 64. Venus spectrum: October 22, 23 and 25, 1962

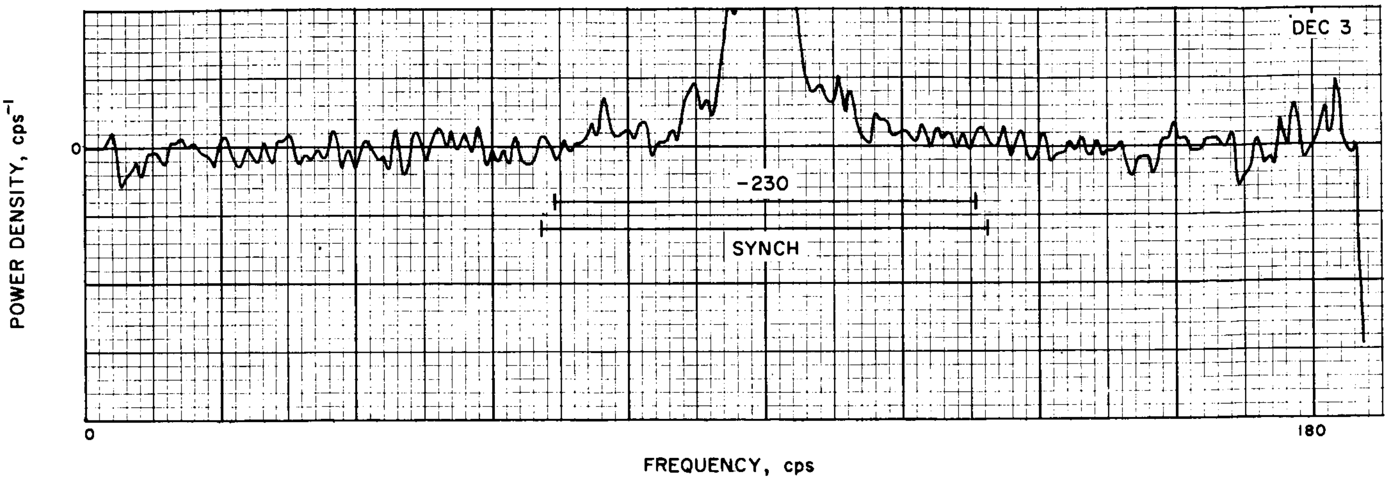

Fig. 65. Venus spectrum: December 3, 1962

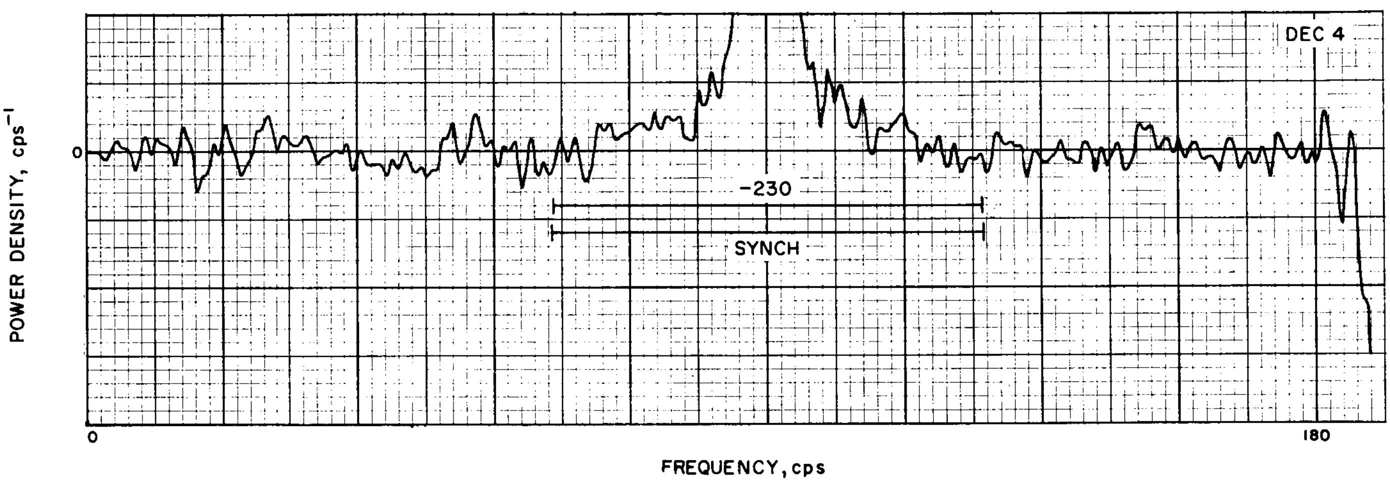

Fig. 66. Venus spectrum: December 4, 1962

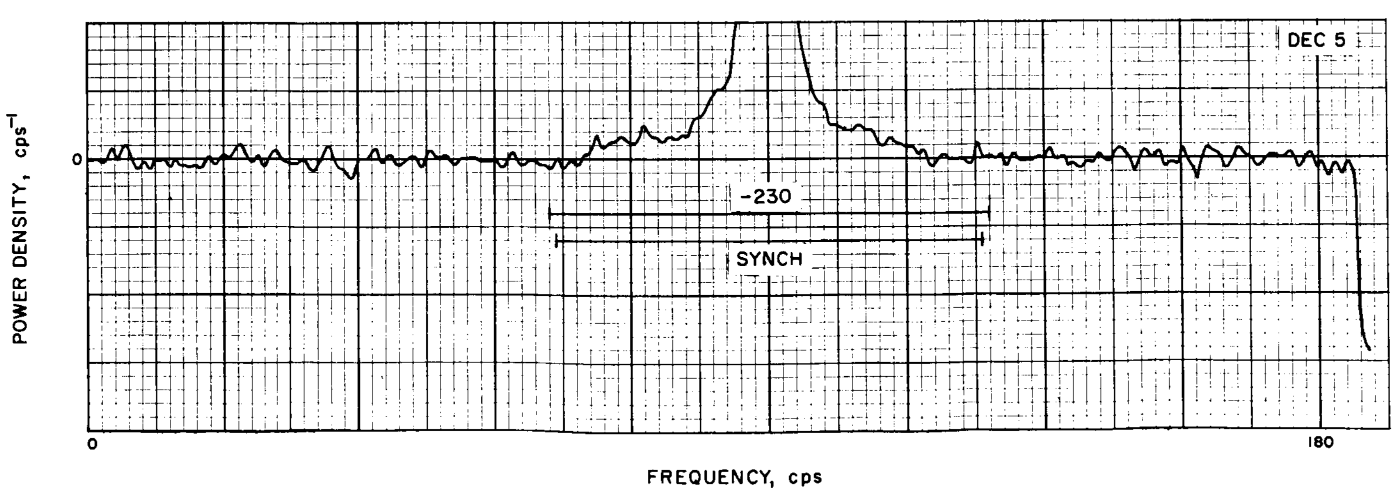

Fig. 67. Venus spectrum: December 5, 1962

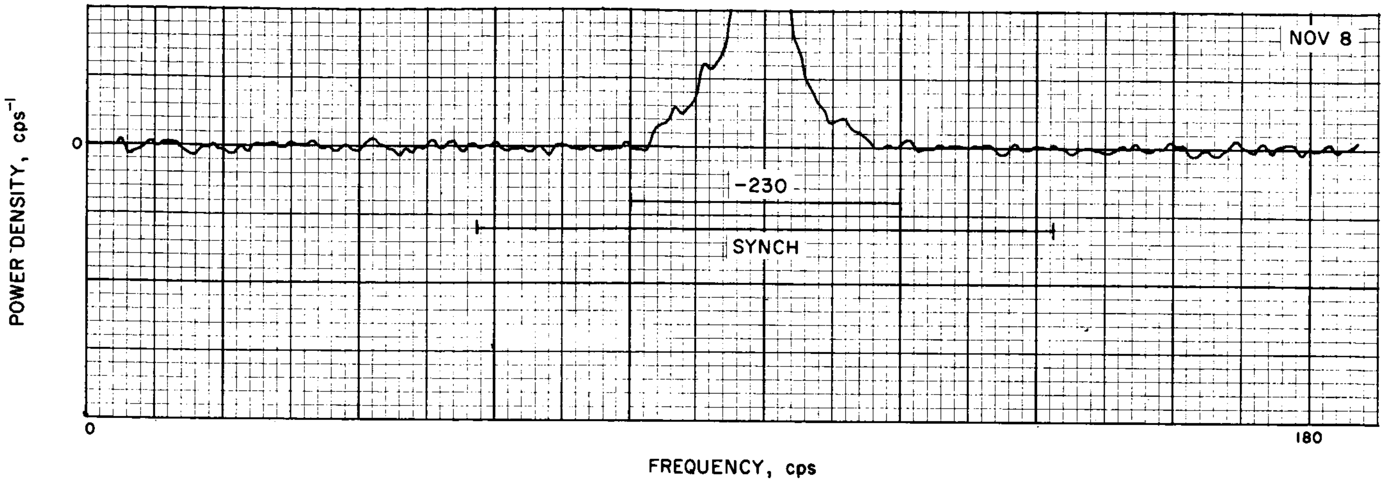

Fig. 68. Venus spectrum: November 8, 1962

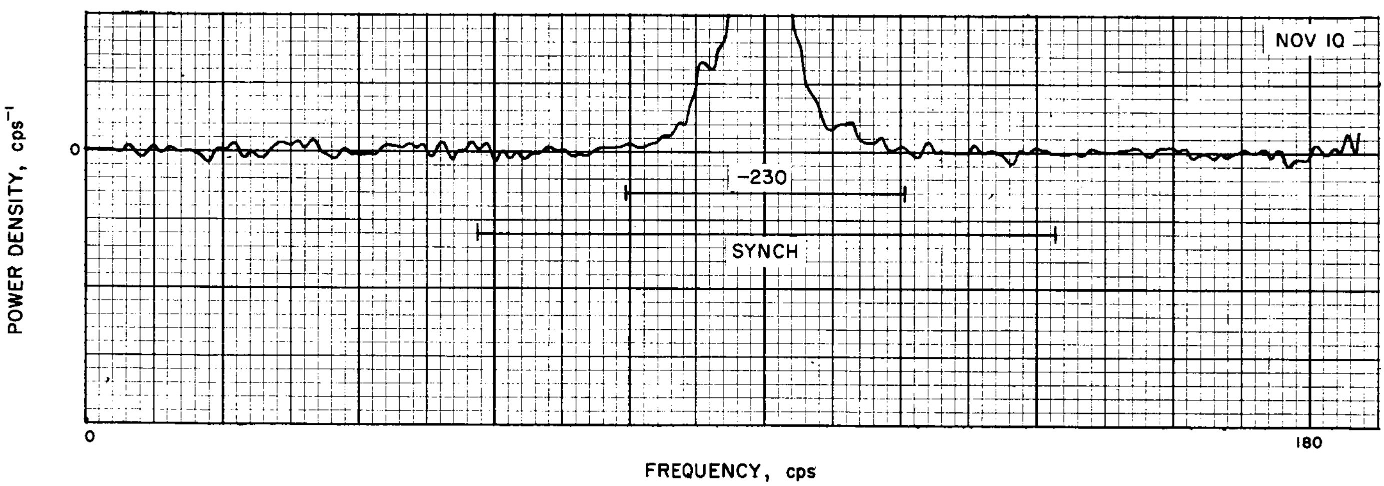

Fig. 69. Venus spectrum: November 10, 1962

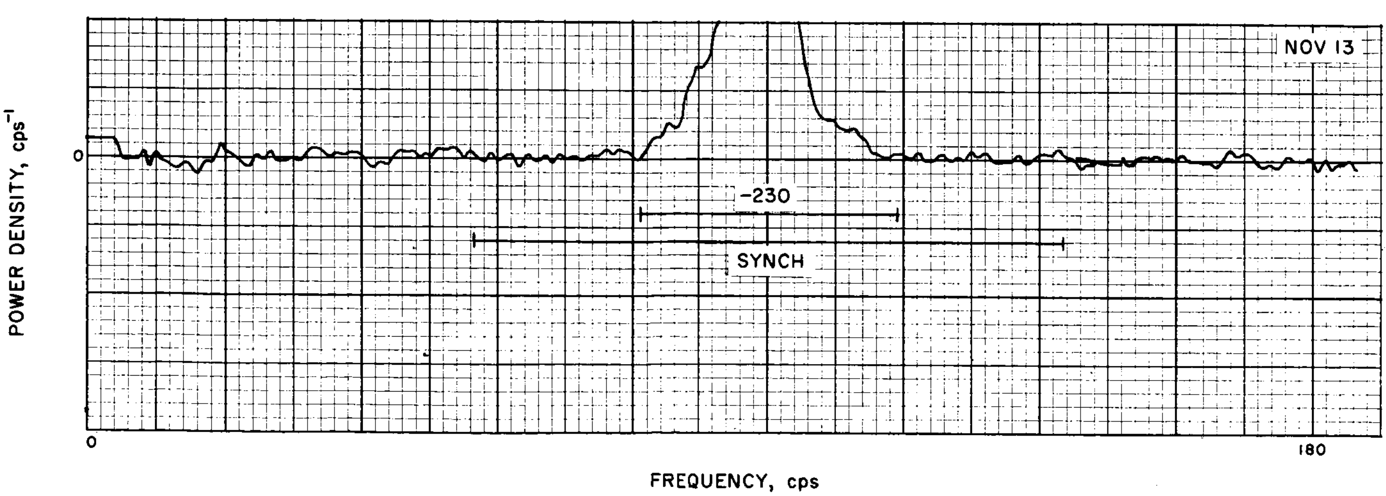

Fig. 70. Venus spectrum: November 13, 1962

V. CLOSED-LOOP RECEIVER SYSTEM EXPERIMENTS

C. P. Wiggins and W. Gillmore

A. Continuous-Wave Velocity-Measuring System

The relative velocity between Venus and the Earth can be determined by measurement of the change in frequency (doppler shift) of the received signal with respect to the transmitted signal. Phase-coherent comparison of received and transmitted signals provides a two-way doppler frequency measurement of extreme accuracy.

One antenna was used for the experiment, on a time-shared basis, for transmitting and receiving. The transmitter was operated for approximately 6 min, the time-of-flight to Venus and return, then switched off. The receiver was switched on, the received signal acquired, and doppler frequency recorded. This cycle was repeated with equal transmitting and receiving periods.

Figure 71 is a simplified functional block diagram of the system. The atomic frequency standard and synthesizer supplied phase-coherent references to both transmitter and receiver, affording maximum stability and minimizing the system contribution to doppler frequency error. In the transmitting mode the 31.84-Mc oscillator is phase-locked to the synthesizer. The oscillator frequency is multiplied 75 times to 2.388 gc, amplified to 13 kw, and radiated by the antenna. In the receiving mode, the antenna is switched to the receiver, and the received signal is amplified by the maser and parametric amplifier. The voltage controlled oscillator in the coherent receiver removes the doppler component of the incoming signal at the first mixer. This permits use of a predetection bandwidth much narrower than the doppler shift. The first mixer converts the signal to 29.85 Mc where it is amplified and then converted to 455 kc in the second mixer using a 30.305-Mc reference. The 455-kc IF amplifier contains a band-pass filter which establishes the predetection bandwidth of 500 cps. The IF amplifier drives the phase detector. The phase detector output is filtered and applied as a phase-error correction voltage to the

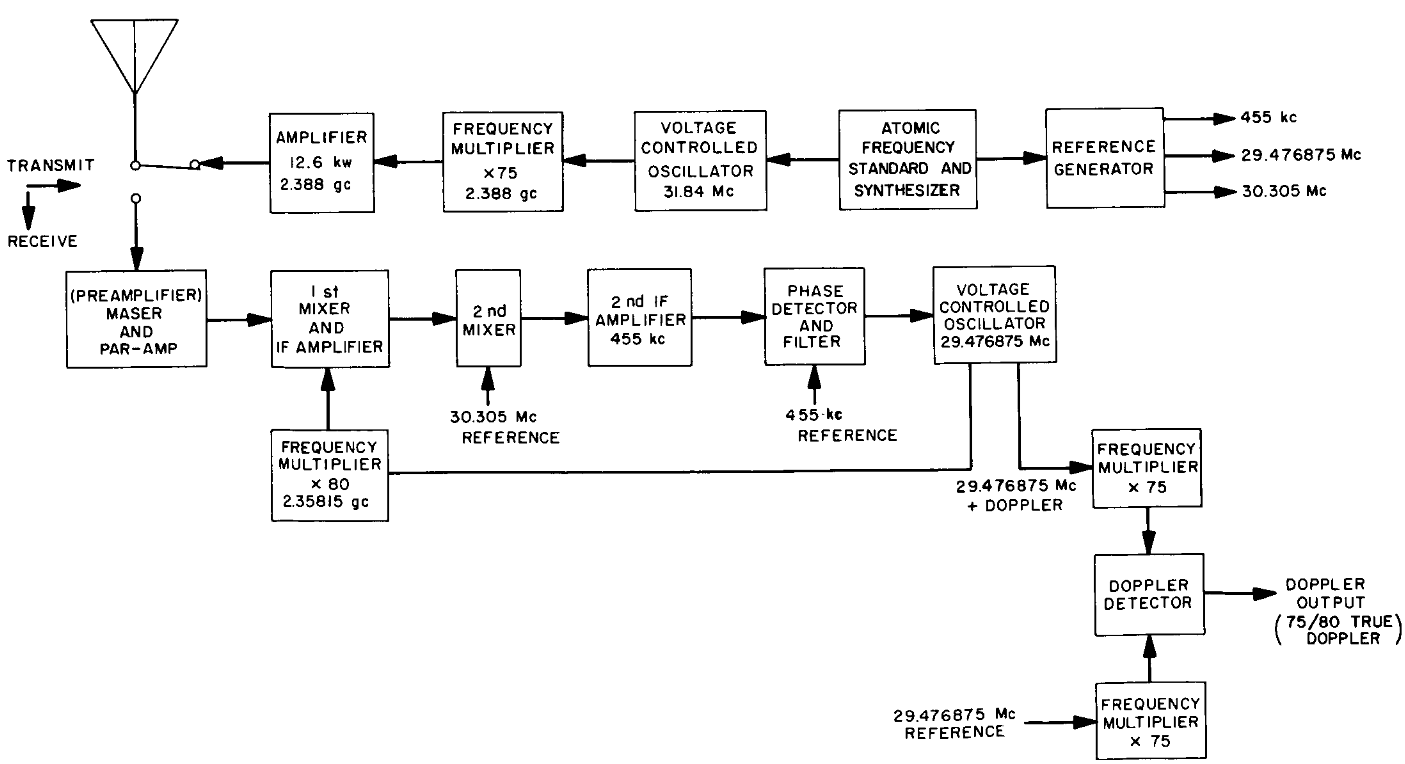

Fig. 71. Simplified functional block diagram closed-loop, continuous-wave, velocity-measurement experiment

VCO. The VCO output is multiplied to 2.35815 gc and supplied to the first mixer.

The UHF doppler signal is generated by frequency multiplying both the 29.476875-Mc reference and the RF loop VCO outputs by 75 and then detecting them. The detector output is 75/80 of the received doppler. The RF loop VCO is phase-locked to the received signal; hence, it differs in frequency by the amount of the doppler from the 29.476875-Mc reference. References necessary for receiver operation are generated in the coherent reference generator section of the receiver. A complete description of the 2.388 gc receiver, exciter, and transmitter is given in Ref. 26 (pp. 43–47).

1. Equipment Description

The receiver was physically divided into two parts, the antenna-mounted part and the control room part. The antenna-mounted components, shown in Fig. 72, were housed in a water-tight box located in the Cassegrain feed cone. The box contains the preselector, first mixer, 29.85-Mc IF preamplifier, HF amplifier, X16 frequency multiplier, and an attenuator for setting the local oscillator power level injected into the mixer.

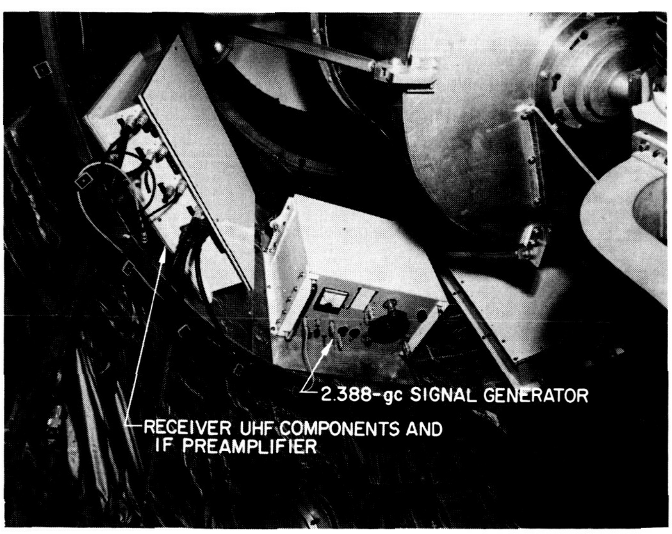

Fig. 72. Antenna mounted components of 2.388-gc receiver

Control room components were contained in a 4 cabinet assembly (Fig. 73). The left-hand cabinet houses the coherent reference generator and the UHF doppler detection system; the right-hand cabinet, the second mixer and 455-kc IF amplifier channels. The two center cabinets hold control panels, instrumentation, and power supplies.

2. System Calibration

A new approach to receiver calibration was used for the 1962 Venus Radar experiment. A signal generator was fed directly into the system by a closed path; formerly calibration was performed by space transmission, using a remote transmitter and antenna. This change was made possible by the development of a stable, low leakage signal generator (see pp. 43-47 of Ref. 26). The signal generator was mounted in the Cassegrain feed cone, adjacent to the receiver components (Fig. 72). Calibration was much more convenient than the space transmission method, and daily signal level vs AGC voltage curves were run. The validity of the substitution was established by comparative tests with a remote transmitter and collimation tower antenna which gave substantial agreement (Fig. 74).

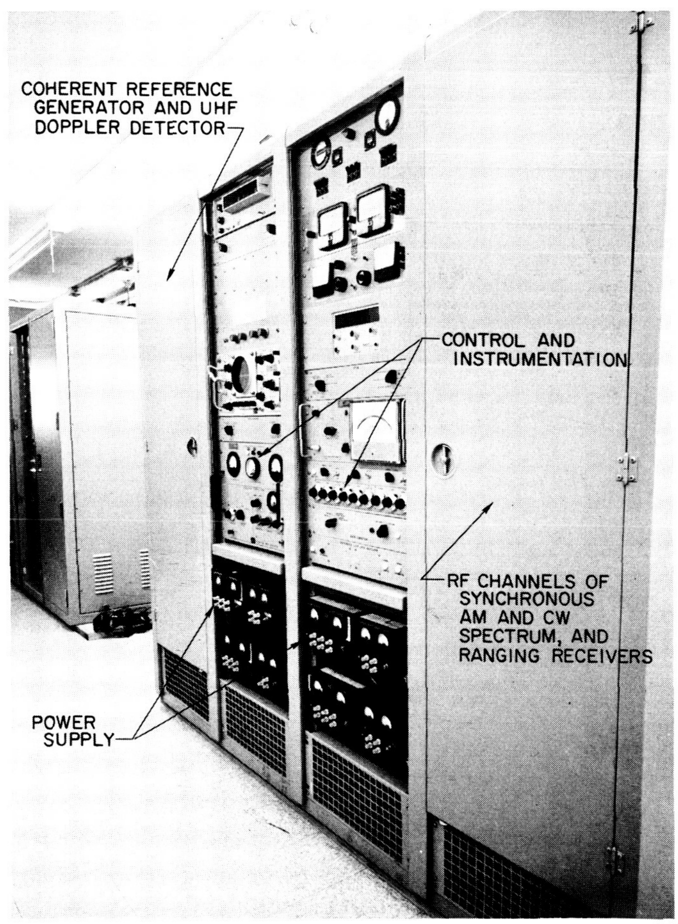

Fig. 73. Mod II planetary radar receiver, control room section

Performance of the basic receiver only (not including the maser and paramp) was not the limiting factor in the system gain stability; spot checks throughout the experiment showed gain variations of the basic receiver to be about ±½ db over a 3-month period.

3. Experimental Results

Data from the closed-loop receiver system was recorded on punched paper tape. Later the data were transferred to IBM cards. In this form it was easier to edit the data and delete bad data points. Finally the card images were recorded on magnetic tape so that the data could be processed on an IBM 7090 digital computer.

For each good data point taken during the experiment, a residual Δ was calculated. This residual is defined by the following equations:

$$\Delta = f_r' - \frac{75}{80} f_c$$

$$f_r' = \frac{75}{80} f_r$$

$$f_r = \frac{2\dot{r}}{\lambda_0}$$

where

- Δ is the doppler residual
- f_r' is the experimentally measured UHF doppler frequency
- f_c is the doppler shift in cps from nominal 2388-Mc carrier frequency computed from an ephemeris
- f_r is the true doppler shift in cps from the nominal 2388-Mc carrier frequency
- r is the Earth-Venus distance in meters
- $\dot{r}$ is the velocity of Venus relative to the Earth in meter/sec
- λ_0 is the wavelength of the (nominal 2388 Mc) transmitted signal in meters

Normally the UHF doppler f_r' was measured by counting the UHF doppler detector output for a period of 1 sec. During the following 9 sec this number was recorded and the counter was reset. This cycle was repeated throughout the experiment.

A slightly different procedure was used on files 3130 to 3510, which were recorded between November 10 and December 17, 1962. Here the UHF doppler detector output counted for 10 sec alternately on one of two counters while the number on the other was recorded and then reset to zero. For all of these runs the recorded data was actually $10f_r'$ rather than f_r' itself.

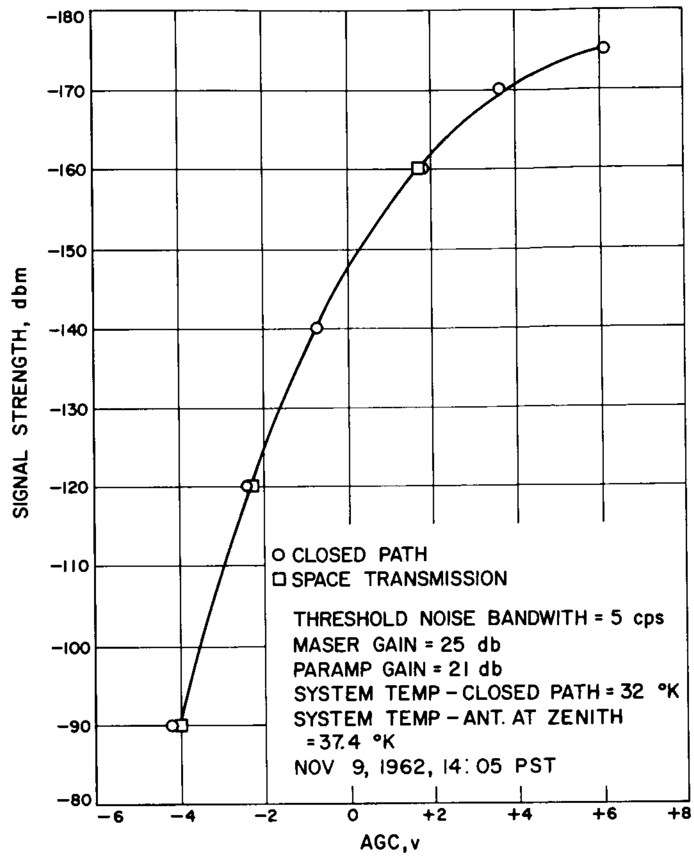

Fig. 74. Sensitivity of 2.388-gc synchronous receiver

The doppler shift f_c requires certain constants for its calculation; the constants used are listed in Table 8.

Table 8. Constants required for doppler-shift calculations

Astronomical unit, km	149598845
Earth radius for lunar ephemeris, km	6378.145
Velocity of light, km/sec	299793.0
Earth/Moon mass ratio	81.450
Radius of Venus, km	6100
Rotation rate of Earth, deg/sec	$\left(\frac{0.00417807417}{1 + (5.21)\,10^{-13}\,d}\right)$
Ephemeris time minus universal time, sec	34
Geocentric north latitude of radar, deg	35.064560
East longtiude of radar, deg	243.205989
Geocentric radius of radar, km	6372.1307

The astronomical unit listed in the table is the best value obtained from the previous 1961 Venus radar experiment; the quantity d represents the number of days since 1950.0.

All of the residuals are plotted on curves in Appendix C. The computer was programmed to discard points for which the doppler residual Δ for a 1-sec count was larger than 100. On those runs where 10-sec counts were used, residuals 10 Δ as large as 1000 were allowed. It was experimentally found that this criterion almost completely eliminated data runs exhibiting improper operation somewhere in the system. Curves showing the doppler residuals during typical runs are given in Fig. 75 and 76 for 1- and 10-sec counts, respectively. All of the curves in Appendix C are scaled in this same fashion to facilitate comparison.

Residuals from both the one second and the 10-sec data show a considerable amount of time variation (see Fig. 75 and 76). This may be a significant result. At radio frequencies surface features of the planet Venus probably emit glints from many regions which add to give a reflection of fluctuating amplitude and frequency. The net effect is that the received signal is modulated rapidly in both amplitude and phase.

It seems reasonable to think of the signal returned from Venus as a stochastic process; the coherent receiver attempts to follow the signal phase. Sudden changes in the phase result in sudden changes in the phase error. If the magnitude of the phase error does not exceed 90 deg, the system will attempt to catch up with and lock on to the original phase. Larger changes in phase may cause a jump of a cycle or more in the UHF doppler. This effect can be seen in the doppler residual curves (see Fig. 75 and 76).

In order to compare the closed-loop receiver data with other data taken during the experiment, the mean, rms, and standard deviation of the doppler residuals were computed. The equations used to define these quantities are given below:

$$\text{mean} = \frac{1}{N}\sum_{i=1}^{N}\Delta_i$$

$$\text{rms} = \sqrt{\frac{1}{N}\sum_{i=1}^{N}\Delta_i^2}$$

$$\text{standard deviation} = \sqrt{\frac{1}{N}\sum_{i=1}^{N}\Delta_i^2 - \left(\frac{1}{N}\sum_{i=1}^{N}\Delta_i\right)^2}$$

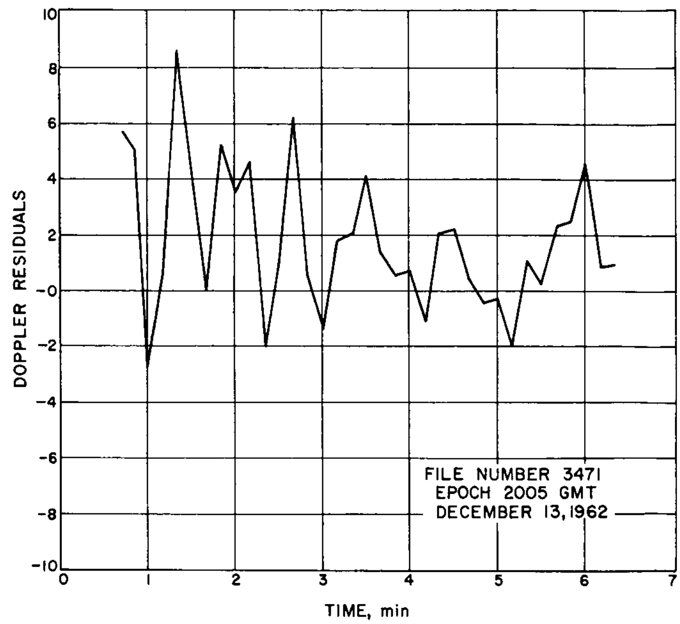

Fig. 75. Doppler residuals during a typical data run using 1-sec count periods

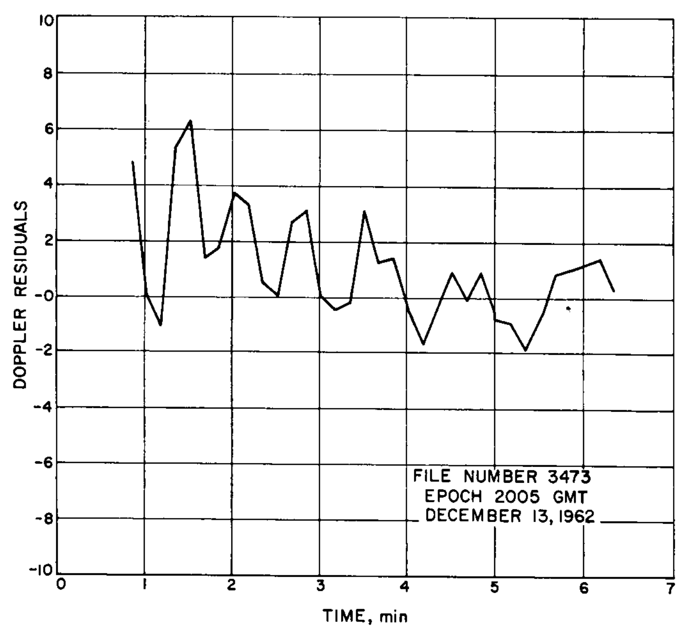

Fig. 76. Doppler residuals during a data run using 10-sec count periods

In these equations N represents the number of good data points, and Δ_i represents one of the previously defined doppler residuals. Curves comparing daily doppler residual statistics are given in Fig. 77.

Comparison of these summations with the predicted received signal strength shows an expected decrease in

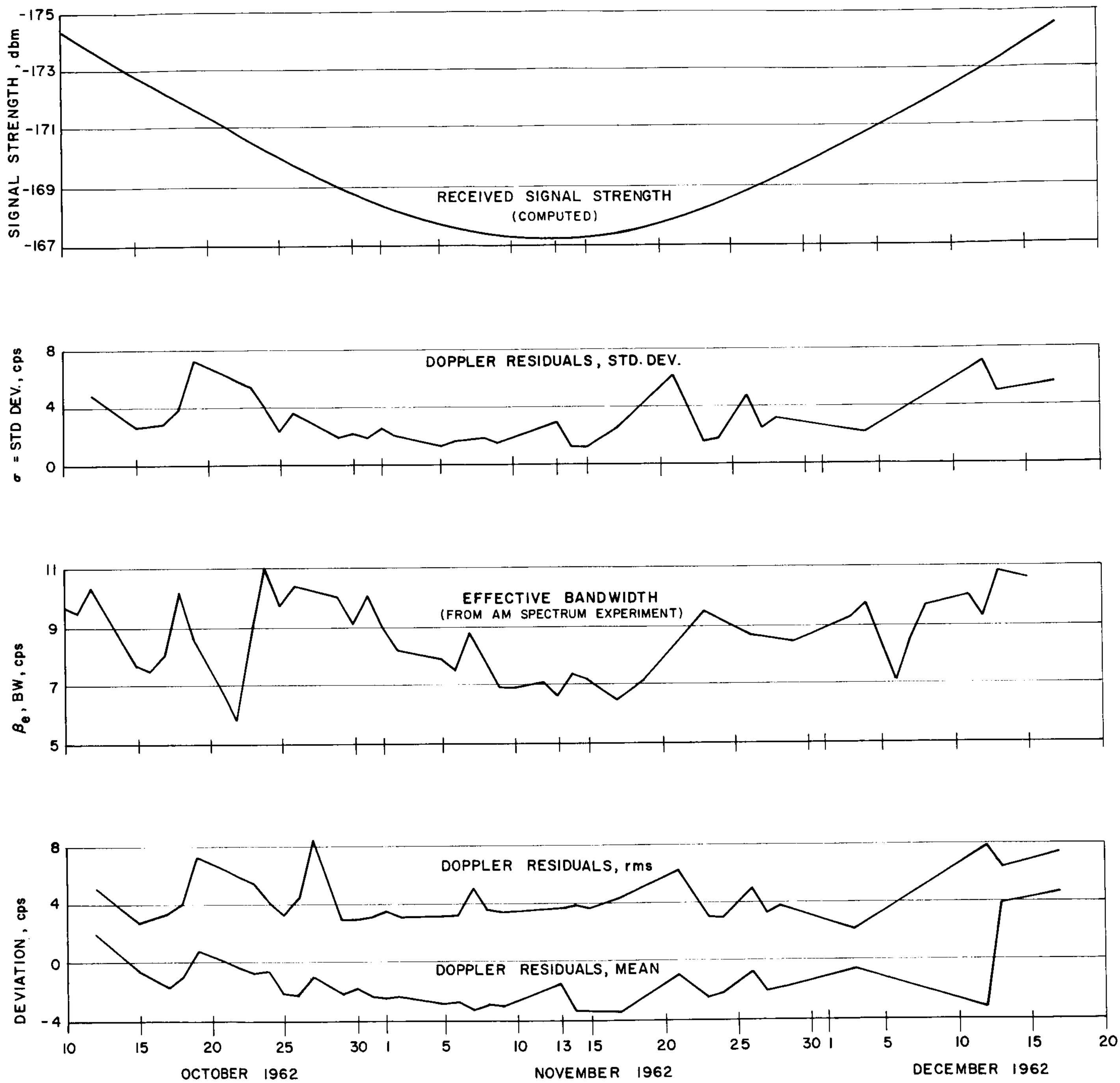

Fig. 77. Doppler residuals compared to received signal strength and bandwidth

the jitter near conjunction, when the signal was strongest (see Fig. 77). There appears to be some correlation between the received signal bandwidth (measured by the AM spectrum experiment) and the standard deviation curve of doppler residuals. Small variations in the received signal bandwidth do not have an obvious effect on the doppler jitter which is considered to result from the fact that the receiver bandwidth was narrower than the spectrum of the narrowest received signal.

4. System Measurement Accuracy

Accuracy of the closed-loop doppler measurement is determined by transmitter stability, thermal noise, signal distortion, and the recording frequency counter round-off error. Transmitter instability during time of flight of the signal (approx. 6 min.) will result in an incorrect comparison of received signal and reference. The transmitter exciter local oscillator and the doppler reference oscillator are phase-locked to the Varian VA 700 rubidium vapor standard and have the same stability as the standard. (See pp. 38-40, 55 of Ref. 9 and p. 30 of Ref. 12). Thus,

$$\text{Transmitter stability} = \pm 0.4 \times 10^{11} \sim 8 \text{ min average}$$
$$\cong \pm 0.01 \text{ cps at } 2.388 \text{ gc}$$
$$\cong \pm 0.12 \text{ cm/sec}$$

Tests of the synchronous receiver-transmitter oscillator system indicate a phase instability of approximately 9–10 deg peak to peak, or approximately 1.5–2.5 deg rms in the closed-loop bandwidth ($2\beta_{LO} = 5$ cps, (pp. 38–40, 55 of Ref. 9). This instability was due to the oscillators and multipliers, exclusive of thermal noise contributions.

Instability in the doppler measurement due to thermal noise is given by

$$\sigma_n = [\Phi_n \, 2\beta_L]^{\frac{1}{2}}$$

where

σ_n = theoretical rms phase noise for a given signal level, Ps

Φ_n = noise power spectral density

$2\beta_L$ = loop bandwidth for signal level, Ps

For example, using a system temperature on Venus of 40°K, the calculated signal level corresponding to $\sigma_n = 1$ radian rms is $Ps = -175.5$ dbm (threshold). The signal level one month before and after conjunction (Oct. 14 and Dec. 12) was approximately −173.0 dbm; the 40°K system temperature gives a calculated σ_n of 0.717 radian. Similarly at conjunction (April 13) a signal level of −167.2 dbm and 40°K system temperature corresponds to a thermal noise jitter of $\sigma_n = 0.313$ radian. The 2π radian per cycle conversion gives a σ_n of 0.05 cycles for the −167.2 dbm signal (see Fig. 78).

The deterioration of receiver performance due to signal distortion cannot be analyzed quantitatively with the available data. An intuitive appreciation of the effect of signal distortion may be gained by consideration of the coherent AGC voltage developed during the closed-loop doppler experiment (see Fig. 79). While the AGC voltage is an indication of the data condition and received signal characteristics, it cannot be used as an absolute measure of the Venus-reflected signal strength. This is because the spectrum of the signal is wider than the receiver RF loop noise bandwidth, and the relationship between AGC voltage developed by a broad spectrum signal and that developed by a narrow spectrum is not known quantitatively. Fig. 79 shows that the receiver is suffering momentary loss-of-lock due to noise bursts (as indicated by the downward spikes in the loop-condition curve during the receive mode); the AGC voltage (Fig. 79) is equivalent to that produced by a pure −174 dbm signal from the signal generator; but it is developed by a −167 dbm signal from Venus.

Round-off error in the frequency counter used to record the received doppler signal is ±1 cps. Since the thermal noise and oscillator instabilities are negligible and the total jitter is typically a standard deviation of 2-5 cps (see Fig. 78) the contribution from signal distortion is approximately (total instability −1 cps) = ~ 1-4 cps.

5. Comparison in Accuracy — Open vs Closed Loop

In the open-loop receiver, the transmitter accuracy is the same as stated for the closed-loop case. The phase noise due to oscillators is slightly higher (approx. ± 15° peak to peak). Tests with the system tracking an ephemeris tape (open-loop receiver mode) show the frequency jitter to be about ±1.5 cps peak or $\pm 0.6 \times 10^{-9}$. Laboratory tests with new oscillators substituted in the equipment demonstrate stabilities of ±0.4 cps or $\pm 0.2 \times 10^{-9}$. Thus, with new oscillators in the open-loop unit, the stability of the open and closed loop systems will be the same order of magnitude.

B. *Amplitude-Modulated Range-Measuring System*

M. Esterling

1. Introduction

The amplitude-modulated range-measuring system used in the 1961 Venus experiment was derived from the system used in the 1961 Venus experiment (Ref. 1). The planetary range measurement system is an application of techniques that have been under development at JPL for several years for radio guidance of missiles and spacecraft. In the original development of these techniques for missile and spacecraft use, the emphasis was placed on high-resolution low ambiguity phase-modulated range-measuring-systems. However, it was necessary to change to amplitude-modulation for the 1961 Venus system because the radio wave was distorted during reflection by

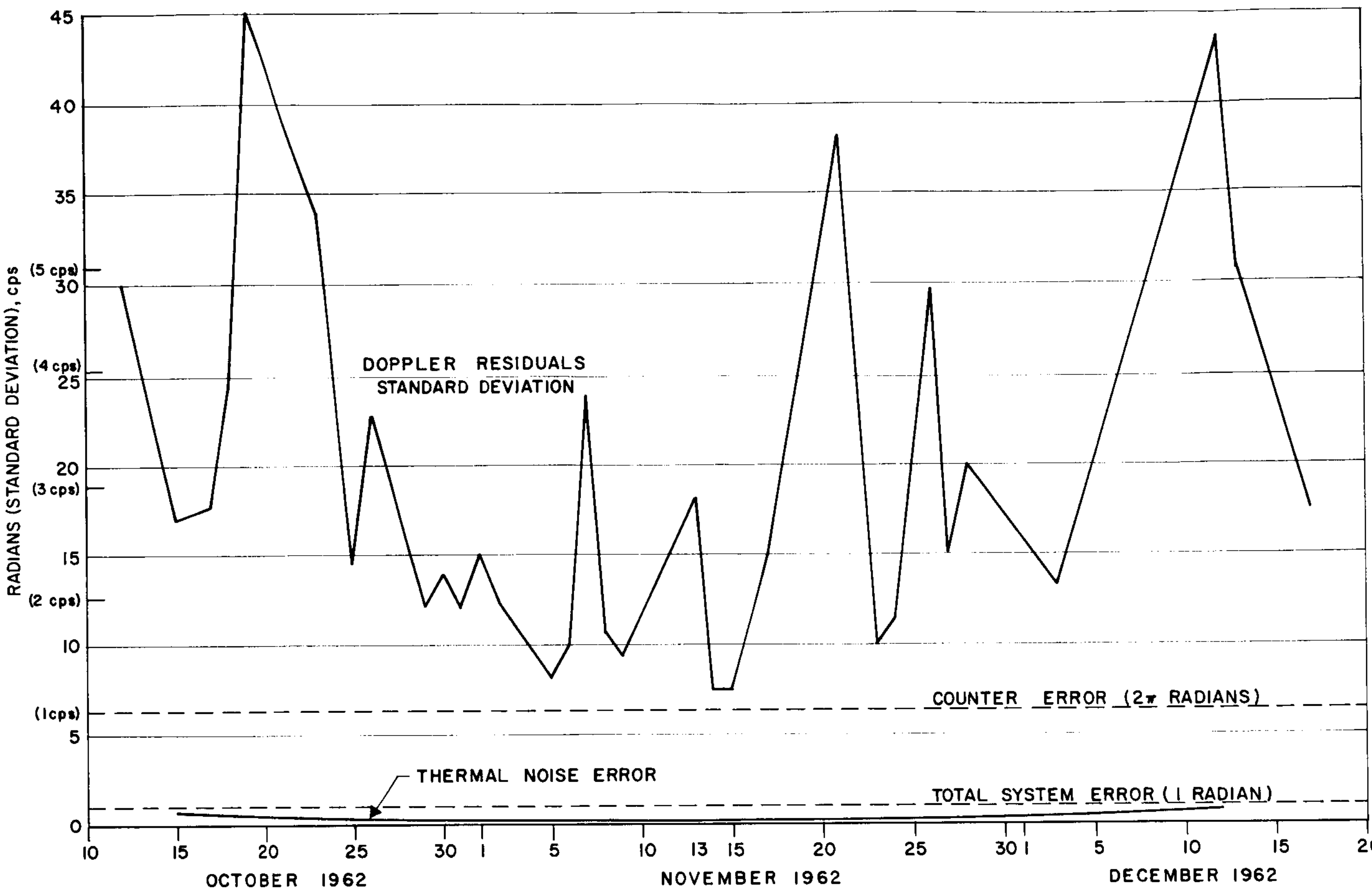

Fig. 78. System contribution to doppler residuals

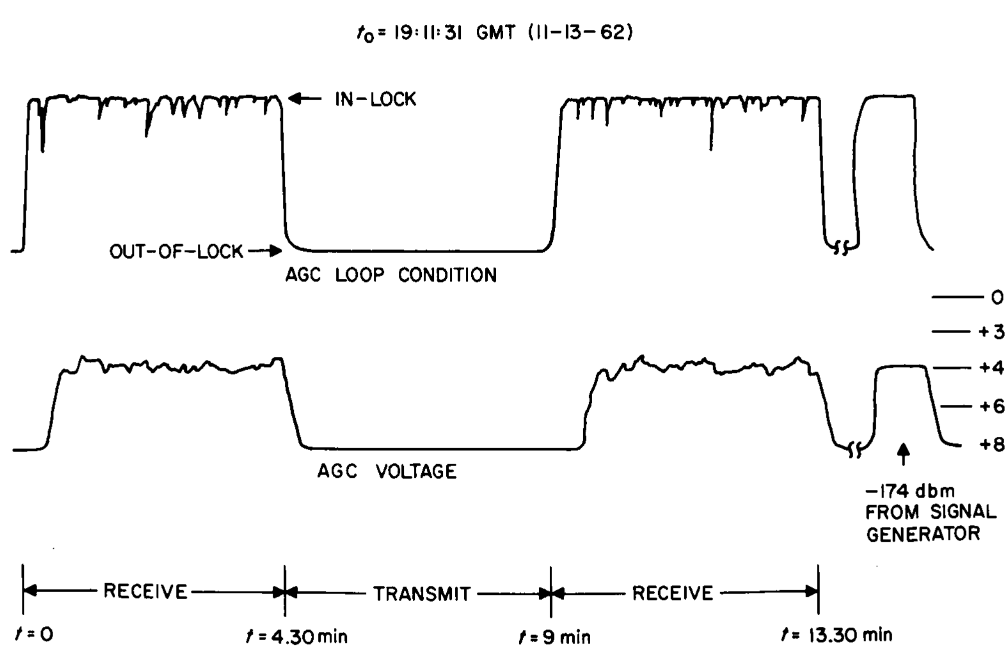

Fig. 79. AGC voltage developed by synchronous receiver

the planet; equipment orginally designed for use in the phase modulated system was, at that time, adapted for use in the amplitude-modulated system. The 1962 Venus experiment used the amplitude-modulated techniques essentially as used in 1961; however, new equipment especially designed for an amplitude modulated system was constructed. This equipment not only contains the digital equipment necessary for ranging but also provides modulation, timing, and keying services for the radar and for other experiments as described in Sec. III-I.

2. Description of the Ranging System

The block diagram of the range-measuring system is shown in Fig. 80. The system operates as follows: The transmitter is amplitude-modulated by the transmitter code, a long pseudo-random binary waveform. In the ranging receiver, the receiver coder forms a local model for correlation detection of the received signal waveform. When the received code has been acquired—that is, when the local model is in phase with the received code—the phase difference between the transmitter code and the receiver code is a measure of the propagation time to the planet and back. This propagation time is a measure of the range for a known propagation velocity. The ranging receiver tracks the received code, and the phase measuring device operates to provide a continuous real-time measure of range.

The 1962 system differs from the 1961 system in three significant ways (see Ref. 1):

1. The transmitter and receiver both use the same antenna.
2. Rate aided tracking is used in the range-tracking loop.
3. The range-tracking loop is entirely digital.

The use of one antenna by both transmitter and receiver requires that each be active for only one-half the time; this creates the requirement that the range loop continue tracking during receiver-off periods. The use of rate-aided tracking meets the requirement. During receiver-on time, the tracking loop utilizes both receiver-generated phase error and ephemeris range-rate signals. During receiver-off time, the tracking loop utilizes only ephemeris range-rate signals. It should be noted that, although the range ephemeris may not be quite correct, the range-rate derived from the ephemeris is very accurate. Thus, rate tracking through the receiver-off time means that the phase error at the end of the off time is essentially the same as the phase error at the beginning of the off time.

The digital tracking loop, although necessarily discrete, uses sufficiently fine quantization and sufficiently rapid sampling that it can be discussed in terms of the linear continuous system upon which it was modeled. The model system, shown in Fig. 81, is a first-order phase tracking servo with rate aiding. The functional equivalent of the tracking loop is shown in Fig. 82. The digital devices in Fig. 80 can be related to the blocks in Fig. 81 and 82 as follows: The multiplier in Fig. 80 is equivalent to the phase detector in Fig. 81 and the subtracter in Fig. 82. The shift-rate generator adds the rate to the phase difference to perform the summing operation shown in Fig. 81 and 82. In addition, the shift-rate generator together with the shift control and clock generator act as the VCO in Fig. 81 or the integrator in Fig. 82. The coder performs the same functions in Fig 80 and 81 but does not appear in Fig. 82 because it has no dynamic function. The range tally tallies the phase shifts of the receiver code. Since all operations start with the two coders synchronized and the tally set to zero, the range tally always shows the phase of the receiver code relative to the transmitter code. The range tally, therefore, performs exactly the function of the integrator shown in Fig. 81. In Fig. 82, the integration performed by the VCO and the integration performed by the output phase integrator are shown combined into one unit.

Except for the three points discussed above, the operation of the 1962 system is essentially the same as the operation of the 1961 system described in Ref. 1. The codes used in the two systems are identical. For convenience, two of the parameters used in the 1961 system were altered. The filter immediately preceding the detector was reduced from 200 to 100 cps and the clock frequency was reduced from 61 to 26 cps. The bandwidth of the tracking loop is a function of the signal to noise ratio because of the limiter in the system; it was approximately 0.002 cps for Venus signals.

3. Operation and Calibration

The availability of a good ephemeris greatly simplified the operation of the system compared to the operation of the 1961 system. Acquisition was accomplished by tracking the ephemeris with a range offset approximately equal to the calibration value which caused the receiver code to have very nearly the correct phase. The technique for inserting the range offset is described in Sec. III-I. Code acquisition was verified by observing the signal level on a strip chart recorder (see Fig. 80). The loop was then closed and it automatically tracked out the

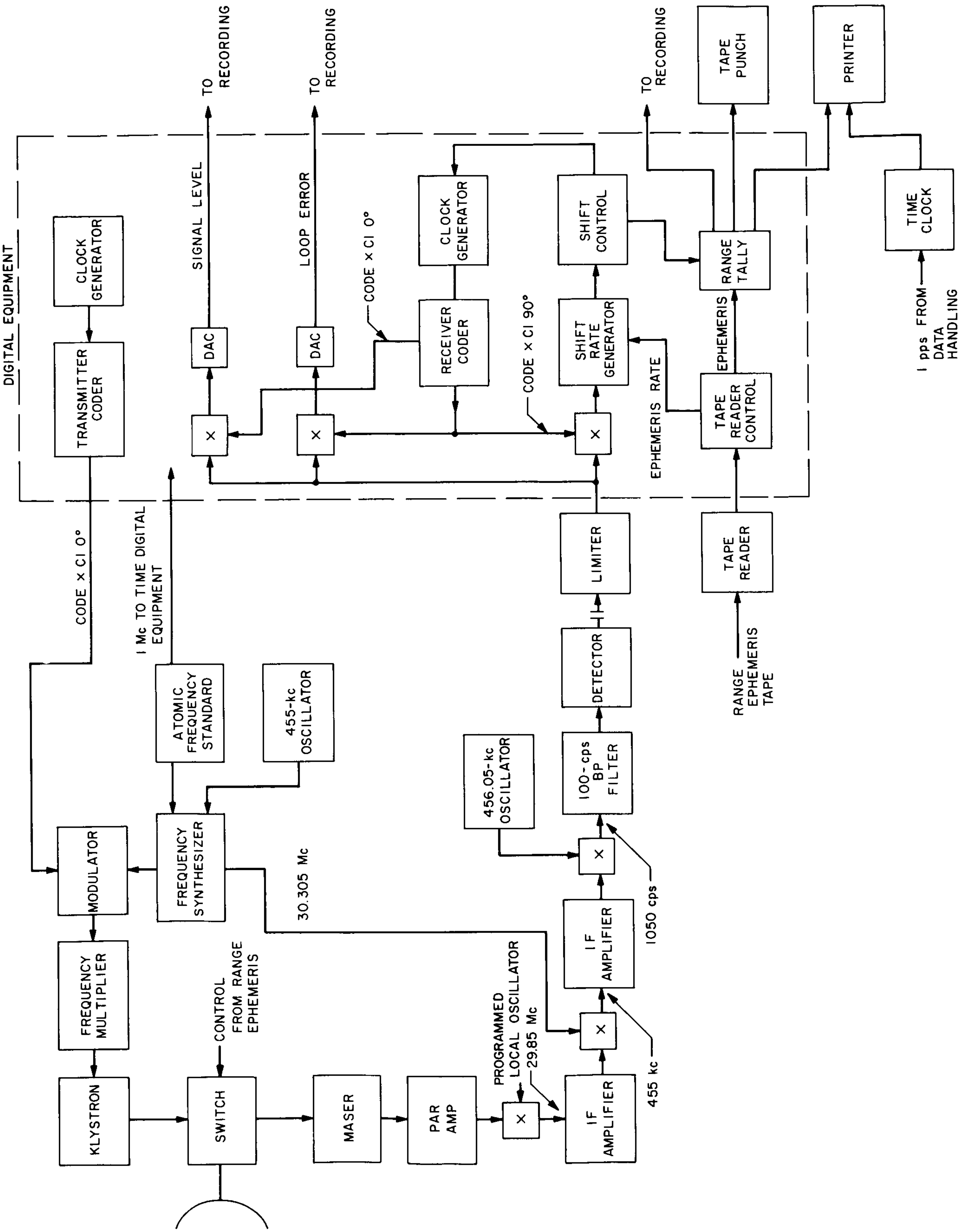

Fig. 80. Amplitude-modulated range-measuring system

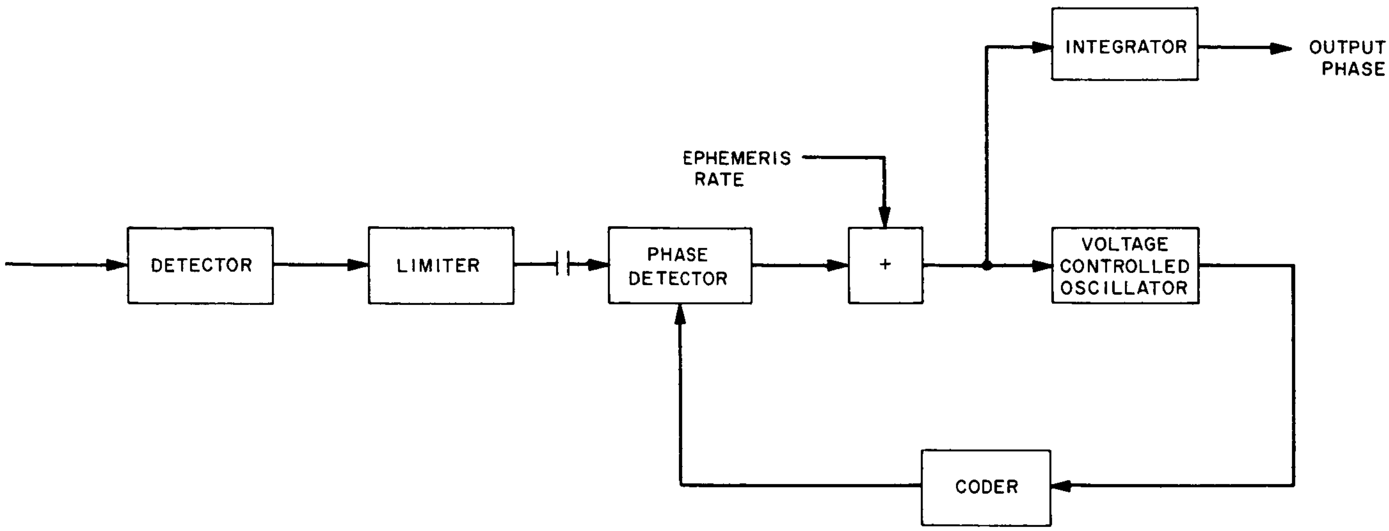

Fig. 81. Linear continuous model of the phase-tracking loop

phase error. During the operation, performance was monitored by observing both the signal level and the loop error as recorded on a strip chart.

The measurement actually made by the ranging system is the phase displacement in microseconds of the receiver code relative to the transmitter code. When the range receiver loop is locked up and tracking, the phase displacement is a measure of the time taken for a signal to propagate over a path which includes the transmitter, the path from the antenna to the planet, the path from the planet back to the antenna, and the receiver. The desired portion of this measurement is the propagation time from the antenna to the planet and back. This is obtained by subtracting the measured value of the propagation time through the transmitter and receiver. This calibration measurement is made by connecting the output of the transmitter at a low power point into the receiver input through an appropriate attenuator, arranging for both the transmitter and the receiver to be on simultaneously, and then making a range measurement. The ephemeris rate is

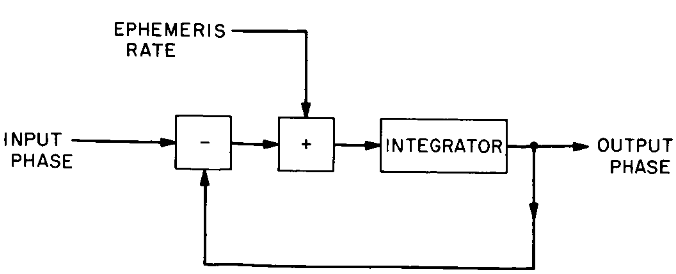

Fig. 82. Functional block diagram of the phase-tracking loop

set to zero during the calibration. Although it would be desirable to subtract the measured system delay in the tally and record only the measured propagation time to the planet and back, the operational arrangements did not normally allow time for processing the calibration data before starting the track of the planet. Therefore, the recorded value of the propagation time includes the system delay which was removed during the data processing.

4. Form and Quantity of Data

The use of one antenna for the 1962 Venus radar introduced severe problems of leakage and self-jamming. Because of the nature of the system these problems were solved last on the amplitude-modulated range-measuring system. This delayed the obtaining of Venus ranging data until November 8. Further problems were encountered in the ranging calibration mode because the transmitter and receiver must be operated simultaneously. The first fully satisfactory calibration runs were not made until November 28. Although some of the tracking runs made between November 8 and November 28 may be calibrated from later calibration runs, only data supported by calibration runs taken within a few hours of the tracking runs are presented in this report, i.e., the six runs made between November 29 and December 15.

The amplitude-modulated range-measuring system measures the round-trip propagation time from the antenna to the planet and back. The measurement is made in microseconds and is made continuously. The measurement is sampled for recording once per 8 sec, and the mechanization is such that the sampled value can never differ by more than a few microseconds from the "true" measurement, i.e., the mechanization errors are at most a few microseconds. The propagation time recorded is the propagation time for the wave that arrives back at the antenna at the time of sampling.

The basic measurement made by the system consists of the sum of the round-trip propagation time and the propagation time through the transmitter and receiver. To facilitate recording, monitoring, and initial data processing, the ephemeris value of the round-trip time is subtracted from the measurement before recording. Because it is later added back in, this introduces no additional uncertainty into the data. Finally, to assure that the recorded quantity is never negative, a bias of 50,000 μsec is added. The recorded quantity is given by Eq. (21).

$$Q_R(t) = T_M(t) + T_S(t) - T_E(t) + 50{,}000 \qquad (21)$$

where

$Q_R(t)$ is the quantity recorded at time t (μsec)

$T_M(t)$ is the measured round-trip propagation time of the wave that arrives back at the antenna at time t (μsec)

$T_S(t)$ is the propagation time through the system at time t (μsec) and is based on previous calibration

$T_E(t)$ is the round-trip propagation time of the wave that arrives back at the antenna at time t as obtained from the ephemeris (μsec)

The form of the calibration data is similar. In the calibrate mode, only the system propagation time is being measured and the ephemeris time is set to zero. The recorded calibration quantity is given by Eq. (22).

$$Q_C(t) = T_S(t) + 50{,}000 \qquad (22)$$

where

$Q_C(t)$ is the calibration quantity recorded at time t (μsec)

$T_S(t)$ is the measured propagation time through the system at time t (μsec)

5. Initial Data Processing

The initial processing of the ranging data has three objectives:

1. The separation of data from dross.
2. The evaluation of the data.
3. The extraction of the round trip propagation time measurements from the recorded quantities.

The initial processing is not concerned with the use of the data for scientific purposes, e.g., to correct the ephemeris or calculate an astronomical unit. Thus, the initial processing is in a sense a part of the measuring process itself, and the data from the initial processing should be considered "raw" data for scientific purposes.

The real-time data from the ranging system consist of the recorded quantity punched in paper tape in an octal format, the same quantity plus time printed on an adding machine type of paper tape in decimal digits, and auxiliary strip chart recordings of the received signal strength and the error in the tracking loop. The strip chart record also shows whether the system is in the transmitting or receiving mode and a one minute time tick. The initial processing operates on the data from the system by a combination of machine and manual operations to accomplish the three objectives given above.

There are two sets of operations on the data associated with each ranging run on the planet, one set which applies to the calibration runs, and one set which applies to the ranging run itself. The operations performed on the calibration runs consist of the following:

1. The data is transferred to cards, one data point per card, and machine-plotted. The 50,000 μsec bias is removed in this step.
2. The mean and rms of the data from each run are computed.
3. By examination of the plots, the strip chart, and the computed values, together with the notes taken during the operation, the experimenter selects those runs or portions of runs which represent valid data.
4. The mean and rms of the data selected from each run is computed.
5. A weighted mean of the data from each set of runs is computed and this mean is the calibration number used for the corresponding tracking run.

Examples of calibration runs made at three different signal levels are shown in Fig. 83. The calibration was found to be insensitive to signal level and remarkably stable with time. Figure 84 shows the calibration number for the calibration runs associated with all of the tracking runs. The variation in calibration number over a two-week period is only 250 μsec, about 1% of the total cali-

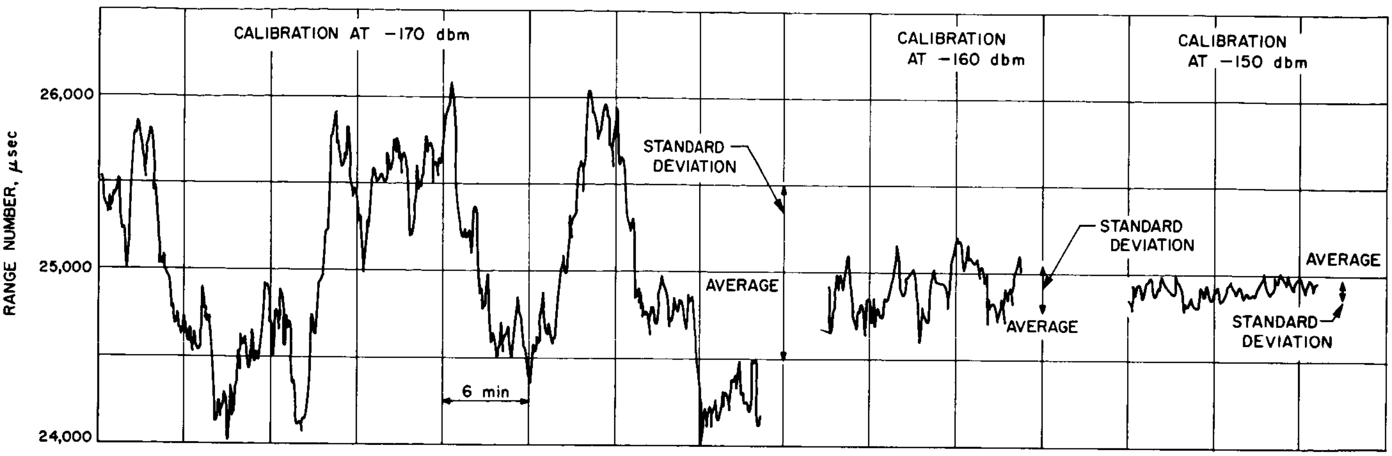

Fig. 83. Calibration runs at three signal levels

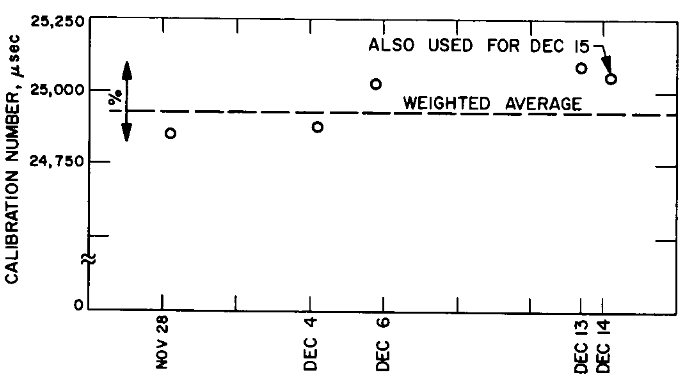

Fig. 84. Calibration numbers

bration number (250-μsec error corresponds to about 25 miles of one-way range error).

The operations performed on the tracking runs are similar to those performed on the calibration runs, and consist of the following:

1. The data is transferred to cards, one data point per card, and machine plotted. The 50,000-μsec bias is removed in this step.
2. By examination of the plots, the strip chart, and notes taken during the operation, the experimenter selects those portions of each run which represent actual data. The points recorded during the time the transmitter is on are rejected.
3. The mean and rms are computed.
4. The data are corrected by having the calibration number subtracted and are converted to propagation time by having the ephemeris propagation time originally subtracted added back in. An example of a portion of a range tracking run plot is shown in Fig. 85. Those portions retained as data are indicated. Figure 86 shows the means and standard deviations of the data for each day. The data show that a correction should probably be made in the

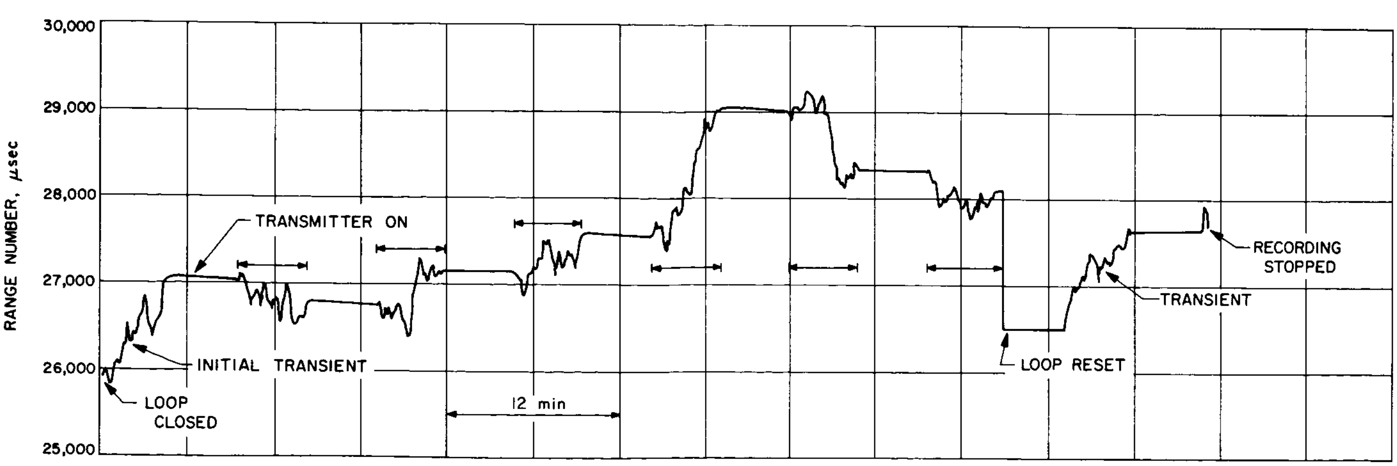

Fig. 85. Example of a tracking run

ephemeris because the consistency among the data is much better than the consistency between the data and the ephemeris. The nature of the correction is not considered here. The complete final data from the amplitude-modulated range-measuring system are presented in Appendix D.

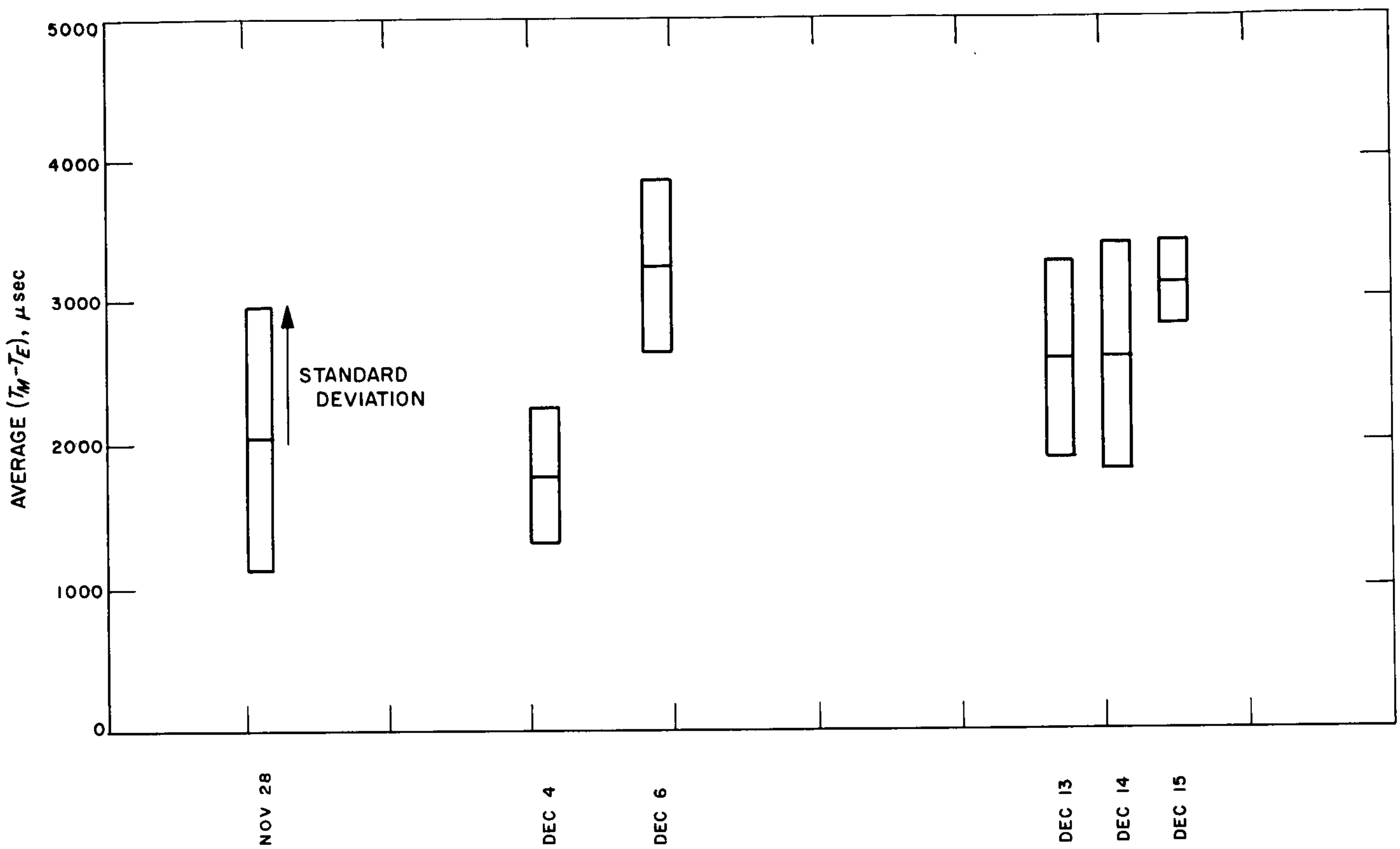

Fig. 86. Comparison of tracking data and ephemeris

VI. ADDITIONAL EXPERIMENTS

A. Résumé

R. Stevens

The principal experiments have been described in Sec. IV and V; additional supporting experiments were conducted on the polarization characteristics of the Venus reflected signal and the 2.4-kMc thermal radiation of Venus.

Polarization diversity was provided by the turnstile junction and waveguide switching arrangement in the Cassegrain feed system so that either sense of circular polarization could be transmitted and either sense could be received. Thus, all combinations of circular polarization could be used with the radar. Measurements of the relative strength of the matched and mismatched polarization components showed an average ratio of about 11.5 db; a result which substantiates the (less accurate) 1961 experiment results. A number of individual measurements of the mismatched polarization signal spectrum has provided a weak but interesting 'average' spectrum of the mismatched polarization signal—the spectrum indicates a rather diffuse Lambert/Lommel-Seeliger-like scattering (see Sec. VI-B).

By changing the pair of shorts on the turnstile junction the antenna feed could be converted to rotatable linear polarization. Thus, measurements of the rotation of a linearly polarized signal suffered during its travel to Venus and return could be made. Also, the relative strength of the depolarized linear energy could be measured by determining the polarization null depth. The total polarization rotation which was a few degrees can be ascribed to Faraday rotation within the Earth's ionosphere. Variations in the polarization null depth were observed, presumedly arising from variations in the scattering characteristics of the Venus surface (see Sec. VI-C).

Black-body radiation measurements of Venus were made on several occasions to calibrate the system and possibly provide data of scientific interest. The observed temperatures at the receiver were lower than expected and further analysis and verification of the data are needed before conclusions as to the Venus temperature can be made (see Sec. VI-D).

B. Depolarization Experiments

G. Levy

The polarization switching equipment (p. 26 of Ref. 9) permitted remote automatic selection of the sense of circularity independently for both transmit and receive. During most of the radar experiment the feed system on the 85-ft antenna was set so that right-handed circularly polarized energy (RCP) was transmitted and left-handed circularly polarized energy (LCP) was received (specular reflection reverses the sense of rotation of circularly polarized energy). Several times during the experiment, however, RCP was both transmitted and received. If the reflection mechanism were purely specular we would expect to get no depolarized return. The depolarized component was found to be approximately 11.5 db below the matched component, a result confirming the measurements made during the 1961 JPL radar experiment (Ref. 1).

The axial ratio of the polarization ellipse was measured by rotating a linear antenna at the collimation tower about 1 mile away; the result was 0.45 db for both RCP and LCP. An additional test of ellipticity was made by using a circularly polarized horn with 1-db ellipticity at the collimation tower and measuring the isolation between the RCP and LCP outputs of the 85-ft antenna feed. The minimum isolation was found to be 22.5 db as compared to 21.2 db calculated. In a later test the axial ratio of the illumination horn was improved to 0.25 db, and the minimum isolation was found to be 25.5 db as compared to 24.5 db calculated.

Measurements were made of the strength and spectrum of the matched and mismatched polarization signals. The standard deviation of signal-to-noise ratio for a single mismatched polarization run for each day was computed. This deviation from the daily mean of mismatched polarization runs was plotted (Fig. 87). The ratio of mismatched to matched polarized signal was then plotted in percent for each run (approximately 5 min). It was found that about 65% of the points fell within 1σ limits of the daily mean (Fig. 87). This indicates that the apparently highly variable data on a short-term basis may actually be the result of a low signal-to-noise ratio. The standard deviation of the daily mean is also indicated for each day. The variation of the daily mean indicates that the reverse polarized reflection coefficient is changing with time.

Spectral data were obtained from two modes of radar system operation—AM (Fig. 88) and CW (Fig. 89). The integrated matched and mismatched spectra are plotted on the same scale for each day. The mismatched mode has extremely low signal-to-noise ratio. In the matched

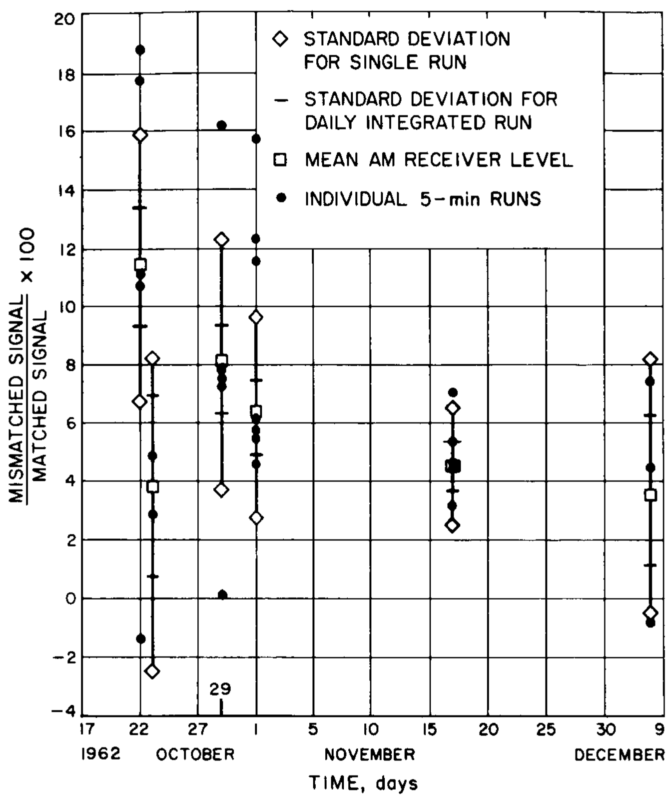

Fig. 87. Relative magnitude of depolarized signal from Venus

mode a very narrow-band specular spike is the most marked feature. In the depolarized case the spike is not apparent.

Usable matched and mismatched polarized spectra were obtained by algebraically summing the data from October 20, and November 1, 21, and 30, 1962. The resulting spectra are presented in Fig. 90. The estimated limb-to-limb doppler bandwidth for each day based on a 250-day retrograde orbit is respectively 46, 42, 39, and 42 cps. For the purposes of this data analysis it was assumed that the doppler bandwidth was constant for all 4 days. Goldstein (Ref. 19) has shown that the frequency backscattering function has an angular cosine series transform. The frequency backscattering function $P(f)$ is given by:

$$P(f) = \left[\frac{2R^2}{f_0}\right]\left[a_1 b_1 \left(1 - \frac{f^2}{f_0^2}\right)^{1/2} + a_2 b_2 \left(1 - \frac{f^2}{f_0^2}\right) + a_3 b_3 \left(1 - \frac{f^2}{f_0^2}\right)^{3/2} + \cdots + a_n b_n \left(1 - \frac{f^2}{f_0^2}\right)^{n/2}\right]$$

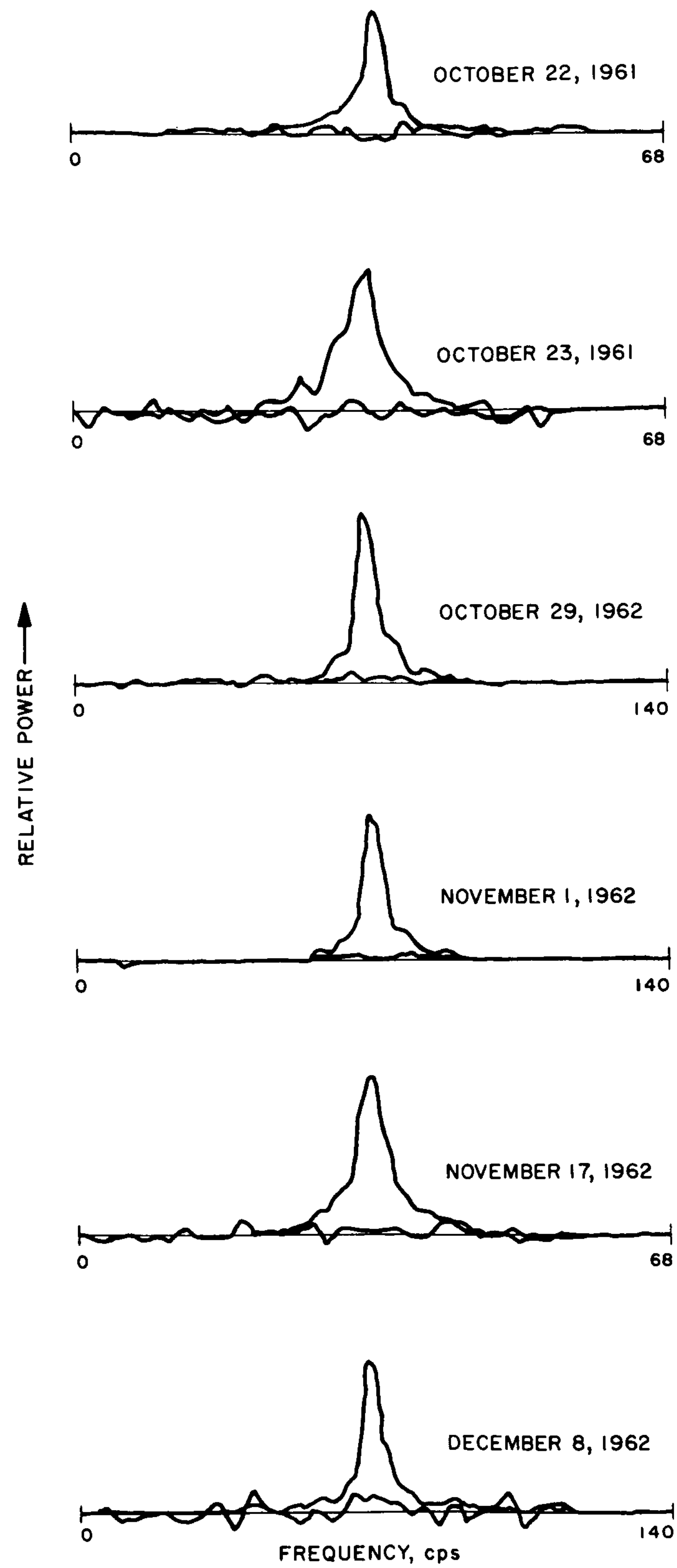

Fig. 88. Matched and mismatched polarized spectra AM receiver

where

f_0 = ½ total limb-to-limb doppler spread

R = Venus radius

If only the first term in the series were present the scattering would be Lommel-Seeliger scattering or that from a uniformly illuminated disc. If only the second term were present it would be Lambert scattering where the energy reflected per unit area is proportioned to the cosine of the angle (θ) formed by the incident ray and the surface normal. The angular scattering function may be represented by a cosine series:

$$F(\theta) = b_1 \cos\theta + b_2 \cos^2\theta + b_3 \cos^3\theta + \cdots$$

where the first and second terms have the same significance as in the $P(f)$ expression.

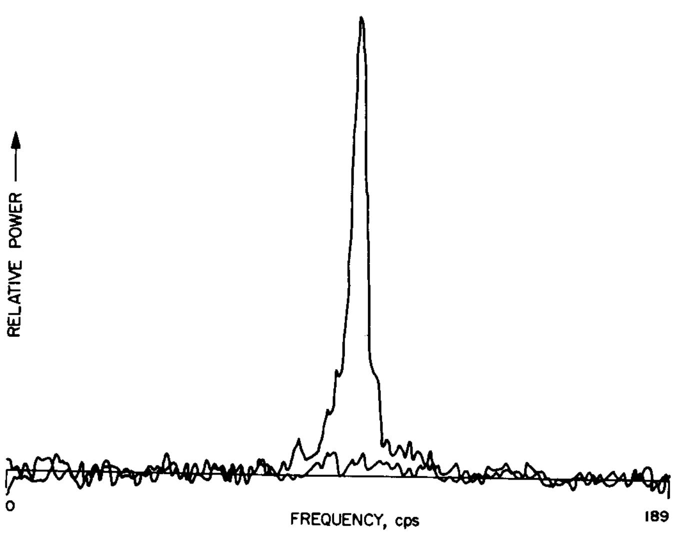

Fig. 89. Matched and mismatched polarized spectra CW receiver November 1, 1962

The matched and mismatched spectra have been replotted in Fig. 91 on log paper with the abscissa adjusted to produce a straight line for any integral power of

$$\left(1 - \frac{f^2}{f_0}\right)^{n/2}$$

where the slope of the line is a function of $n/2$, the power of the term. Since both spectra were asymmetric, and the logarithmic plot folds the spectrum at its center, both sides of each spectrum are plotted.

The mismatched polarized signal appears to follow approximately a Lambert scattering law from 0 to 50 deg

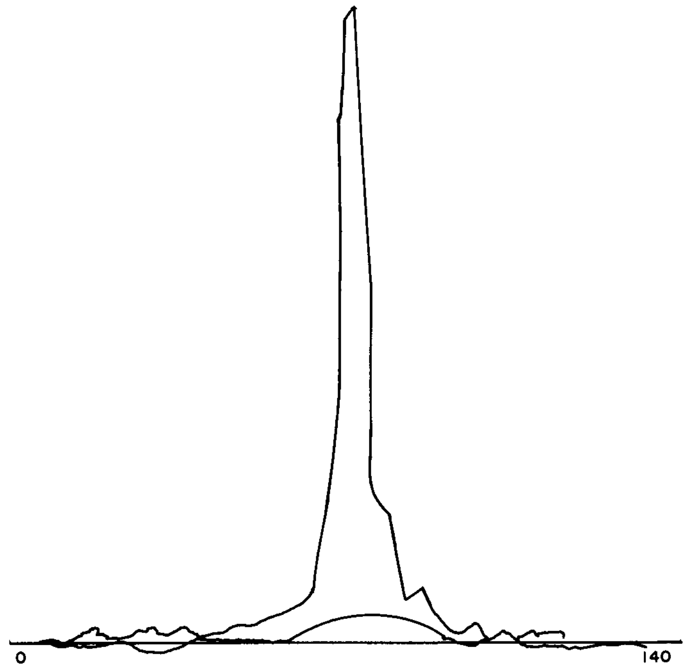

Fig. 90. Integrated matched and mismatched circularly polarized Venus echoes, Oct. 29 and Nov. 1, 21, and 30, 1962—AM receiver

(although the spread in the data is such that a Lommel-Seeliger law should not be ruled out). The data is usable only to 50 deg because the signal-to-noise ratio becomes too small at larger angles. The matched polarization signal appears to be composed of a specular as well as a diffuse component. The diffuse component seems to be somewhere between a Lommel-Seeliger and Lambert scattering law.

Taylor and Peake obtained the points indicated by X's by measuring the matched and mismatched backscattering cross section of gravel with an average diameter of ⅓ of a wavelength and well-rounded edges.[1] The relative magnitude of the angular backscattering function and the amplitude difference between polarizations are presented.

The depolarization observed, although very weak, appears to be similar to what one would expect from a rough surface scattering phenomenon. Although there is insufficient data to draw any firm conclusions, a comparison with the backscattering data of Taylor and Peake shows a very interesting correlation.

[1]Private communication.

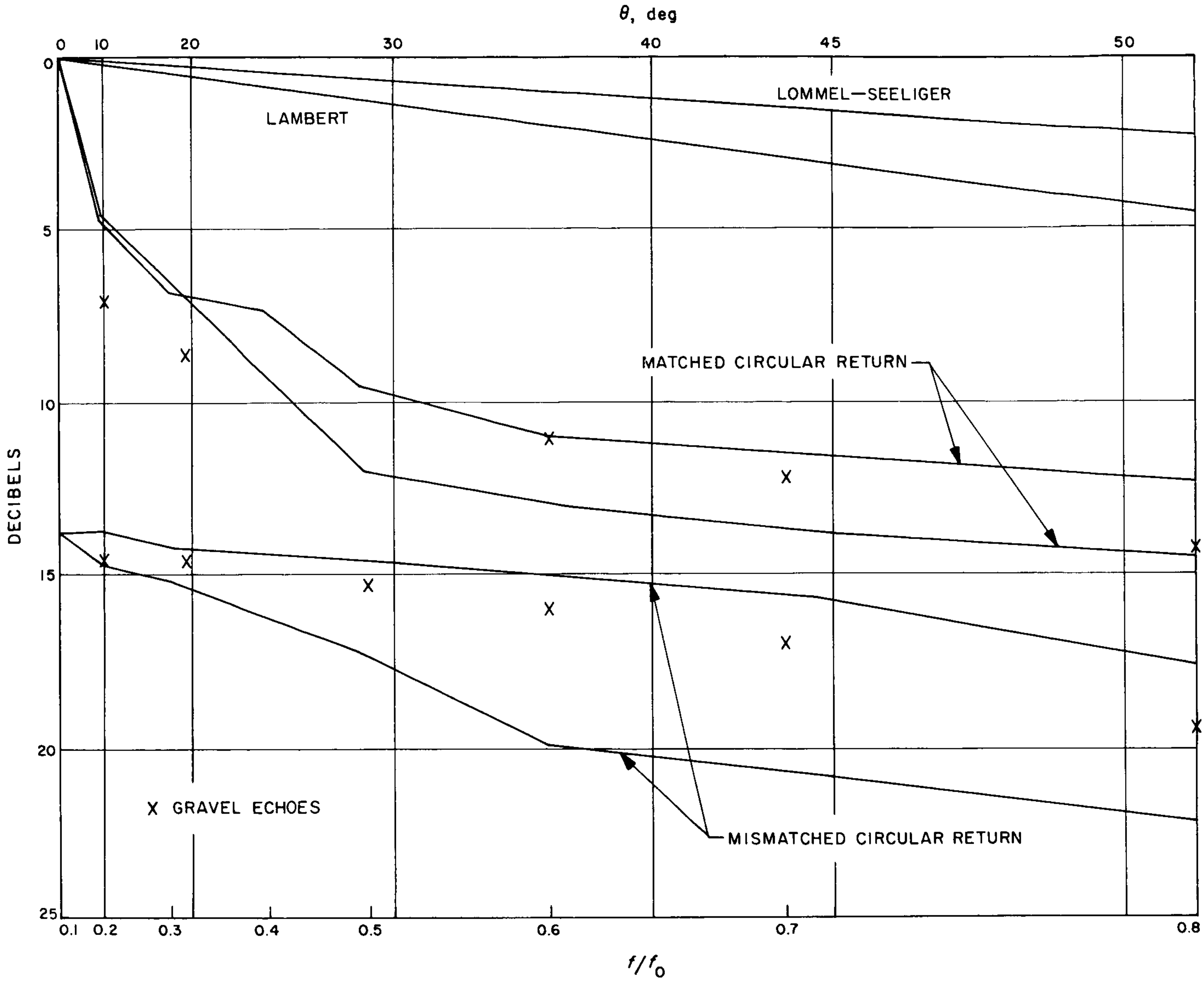

Fig. 91. Integrated matched and mismatched polarized signal on $\cos^n\theta$ plot (SPS 37-20, Vol. IV)

The integration of several days of data has made it necessary to assume a more or less uniform surface distribution. There is not enough data at this time to discuss non-uniformly distributed surface irregularities.

C. *Faraday Rotation Experiments*

G. Levy and D. Schuster

1. Introduction

On November 20, November 27, and December 1, 1962, Venus Radar experiments were conducted using linear polarization for transmission and reception. In these experiments the orientation of the linear transmitted polarization was kept constant with reference to the local vertical. A signal was transmitted for approximately 5 min (the time of 2-way flight), after which the linear rotatable feed was rotated by a remotely controlled servo-drive system in the Cassegrain support cone. When the feed was properly aligned, the receive cycle started. Angular orientation and the depth of the polarization null were the quantities desired from the experiments.

2. Measurements

The actual measurements that were made are summarized in Table 9, where S/N is the computer output of the AM receiver and $T°K$ is the system temperature. Unnormalized signal strength is the product of S/N and

T°K. The first signal-strength level obtained from parallel transmitted and received polarization was used for normalization. The ratios were then converted into db. The transmitted and received polarizations, as well as the transmitter start time and elevation angle, are tabulated for each run.

Table 9. Polarization data

Run	S/N	T°K	Signal strength	Ratio	—db	Polarization, deg		Transmitter start time	El Angle	
						Receiver	Transmitter		Transmitter	Receiver
November 27, 1962										
1	0.161	52.2	2.50	1.0	0	0	0	20:52:36	24.1	
2	0.000309	55.9	1.52	0.00191	27.2	90	0	21:02:29	22.6	
3	0.0275	46.5°	7.77	0.175	7.57	60	0	21:13:07	20.95	
4	0.0508	46.5°	0.171	0.334	4.78	120	0	21:23:31	19.22	
6	0.0295	47.75	7.49	0.203	6.94	100	0	21:44:39	15.54	
7	0.1488	49.25	0.0144	1.03	+0.10	0	0	21:55:12	13.9	
8	0.00306	51.5	1.31	0.0228	16.42	80	0	22:05:39		
December 1, 1962										
6	0.000417	40.3	5.418	0.959	0.2	0	0	15:33:35		31.30
7	NG	40.3	5.75	1.017	+0.04	0	0	15:44:00		32.52
8	0.013007	40.3	1.38	0.244	6.12	60	0	15:54:25		33.67
9	0.015950	37.5	0.485	0.0858	10.65	80	0	16:26:22		36.7
10	NG	37.5	6.03	1.06	+0.2	0	0	16:37:28		37.5
11	0.012895	37.5	0.0156	0.00276	25.6	80	0	16:47:52		38.1
1	0.134456									
2	0.142812	39.0	0.507	0.0897	10.5	80	0	17:09:58		39.2
3	0.034338	39.0	0.622	0.110	9.6	85	0	17:20:56		39.5
4	0.012928									
5	0.160885	38.5	0.496	0.0877	10.6	100	0	17:43:09		39.7
12	0.047132	37.6	1.77	0.313	5.0	120	0	17:54:09		39.6
13	NG									
14	0.022314	37.5	0.836	0.147	8.3	110	0	18:21:00		38.8
15	0.029059	38.3	1.11	0.196	7.1	67	0	18:31:58		38.3
16	0.164521	38.7	6.36	1.13	+0.5	0	0	18:43:03		37.7
17	0.154560	38.1	5.88	1.04	+0.1	90	90	18:56:31		36.7
18	0.054516	39.0	2.13	0.377	4.2	200	90	20:32:44		35.8
19	0.019197	38.1	0.732	0.130	8.8					34.8
20	0.004127	38.8	0.160	0.0283	15.5	220	90	20:51:24		34.3
21	NG					180	90	21:03:01		
22	0.012537	38.5	0.483	0.0854	10.7	270	90	21:15:07		32.0
23	NG					50	0	21:25:50		
24	0.015091	40.3	0.608	0.1076	9.7	65	0	21:36:50		29.2
25	0.002124	34.0	0.0826	0.0146	18.3	110	0	21:47:50		27.0
26	0.027516	41.3	1.14	0.202	7	130	0	21:58:50		25.4
27	NG	41.6				90	0	22:09:51		
28	0.065551	41.8	2.74	0.484	3.2	140	90	19:06:55		23.3
29	0.009989	41.8	0.418	0.0740	11.3	155	90	19:17:41		20.7
30	0.131749	42.7	5.63	0.996	0	170	90	19:28:24		18.7
31	0.042134	42.0	1.77	0.313	5.1					16.8
32	0.012282	44.6	0.548	0.0969	10.1	190	90	19:49:08		14.8
33	0.013876	44.6	0.619	0.110	9.6					13.9
34	0.054807	47.7	2.61	0.462	3.35	190	90	20:11:00		11.0
35	0.004866	52.7	0.257	0.0455	13.4	180	90	20:21:46		9.1
36	0.000789	34.2	0.0270	0.00477	23.2	Cold Sky		22:36:15		87.6
37	−0.008702	34.8	0.303	0.0536	12.7	Calibration		22:46:45		87.6
38	0.000865	34.8	0.0301	0.00533	22.7	Runs		23:02:21		87.6

If there were no surface depolarization, one would expect the returned signal power to obey the following law:

$$P = \frac{C}{2}\left[1 + \cos 2(\psi - \Omega)\right] = C\left[\cos^2(\psi - \Omega)\right]$$

where ψ is the angle between transmitter and receiver polarization orientations, and Ω is the angle of Faraday rotation. If, in addition to Faraday rotation, there was also surface depolarization, then,

$$P = \left[C_1 + C_2 \cos 2(\psi - \Omega)\right]$$

In Fig. 92–97 the signal strength of November 20 has been plotted as a function of ψ, the angle between transmit and receive. The data have been broken up into consecutive time periods through the day. Figure 92 is very nearly a $\cos^2(\psi - \Omega)$ curve where $\Omega \approx 2$ deg. Very little depolarization is indicated because the null depth is between 16 and 21 db. Figures 93 and 94 give approximately the same picture. In Fig. 95 the null appears to be only 13 db deep. The data for Fig. 95 were taken near an angle (ψ) of 270 deg rather than 90 deg to test the symmetry of the antenna system. Figure 96 shows a rotation of approximately five degrees. The data in Fig. 97 shows a great deal of scatter and therefore the rotation angle of 11 deg is assigned a much higher uncertainty than any of the other points.

The data for Fig. 98 were taken November 27 from 2052 to 2205; the rotation angle appears to be about 5 deg. Figures 99–101 represent data for December 1. The period 1533 to 1843 had a 2-deg Faraday rotation. The last two runs had a 5-deg rotation. The very low signal-to-noise ratio in the null is illustrated in Fig. 101 which represents the one-standard-deviation limits. The standard deviation for the AM receiver is calculated from the following equation[2]

$$\sigma = \frac{1}{\sqrt{TB}}$$

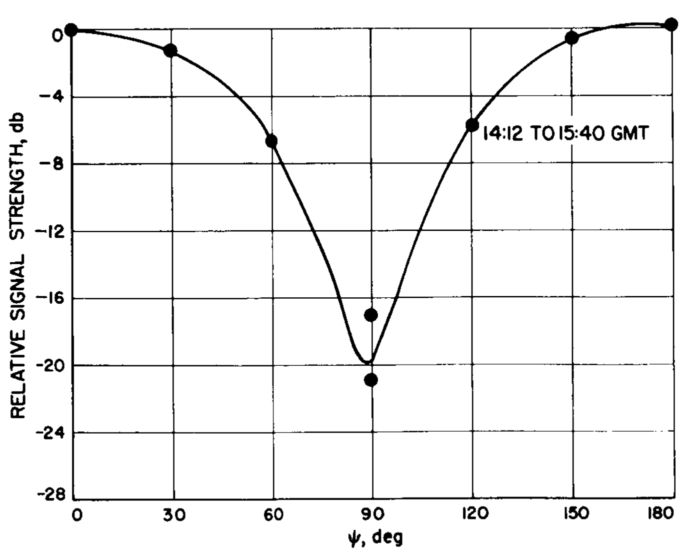

Fig. 92. Received signal polarization angle (ψ) relative to transmitted signal polarization angle

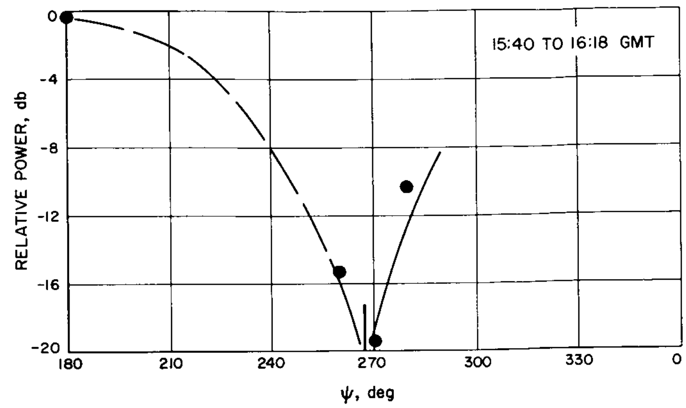

Fig. 93. Relative power vs rotation angle

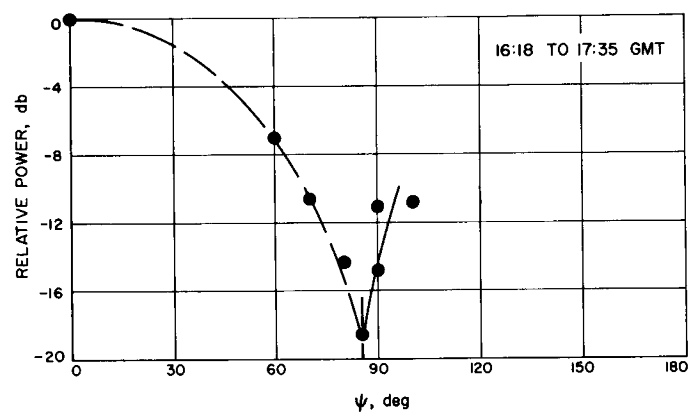

Fig. 94. Relative power vs rotation angle

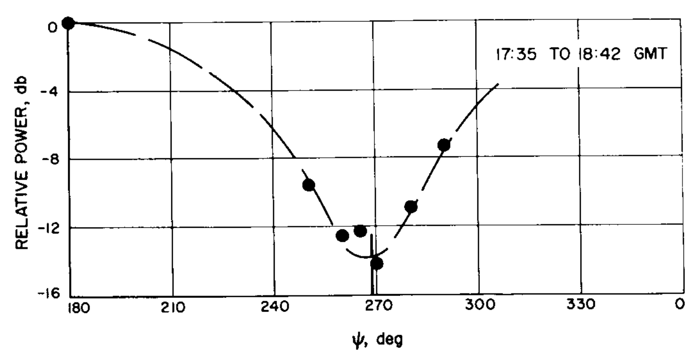

Fig. 95. Relative power vs rotation angle

[2]Private communication from R. Goldstein.

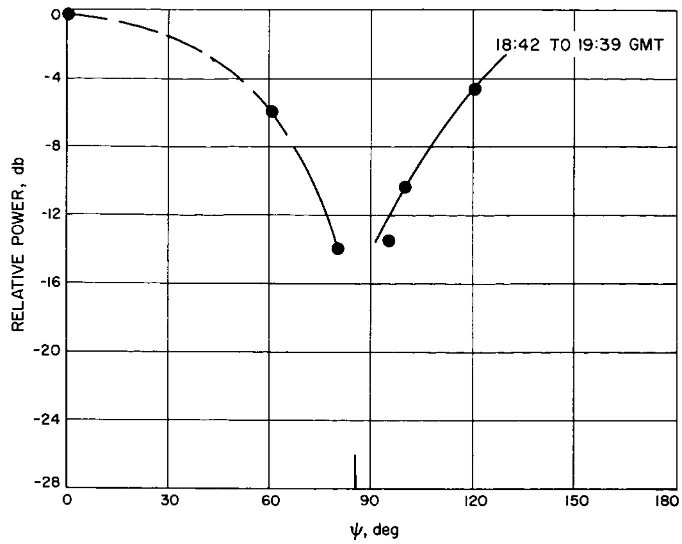

Fig. 96. Relative power vs rotation angle

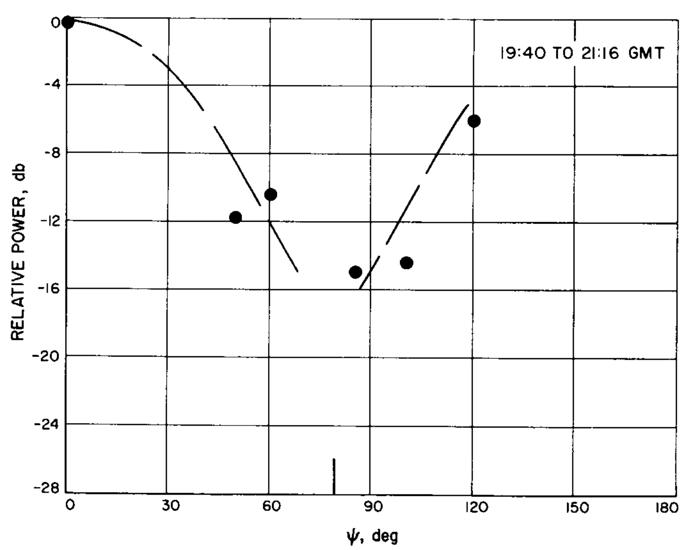

Fig. 97. Relative power vs rotation angle

where T is round-trip flight time in seconds and B is the filter bandwidth. (A 50-cps filter was used November 20, and a 100-cps filter was used November 27 and December 1.) The received power at 90 deg was found to be down 13.4 db from the parallel signal. However, the standard deviation was found to be 1.14 times greater than the power received at 90 deg.

Figure 102 presents all the Faraday rotation angles with their estimated uncertainties as a function of time after Venus rise. The computed value of Faraday rotation based solely on the Earth's ionosphere is also presented.

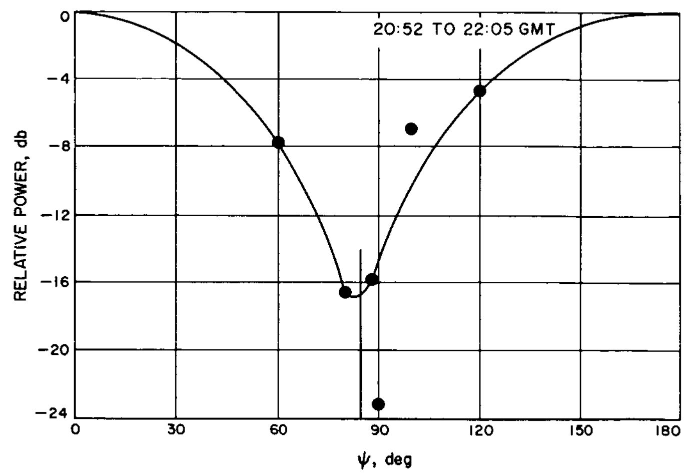

Fig. 98. Relative power vs rotation angle

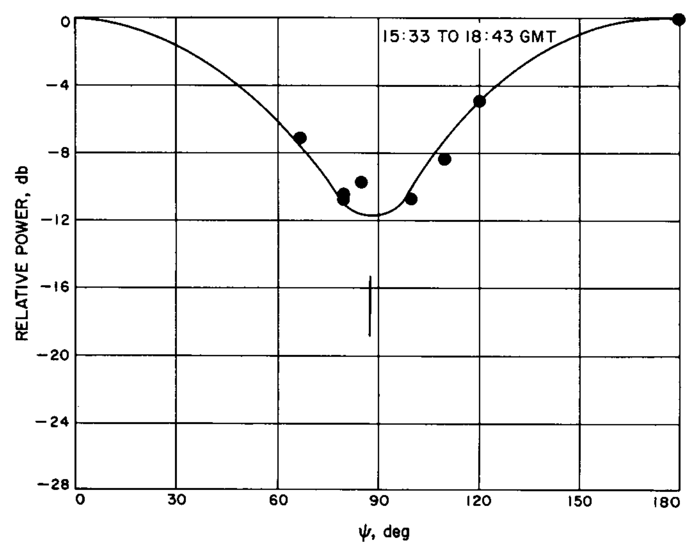

Fig. 99. Relative power vs rotation angle

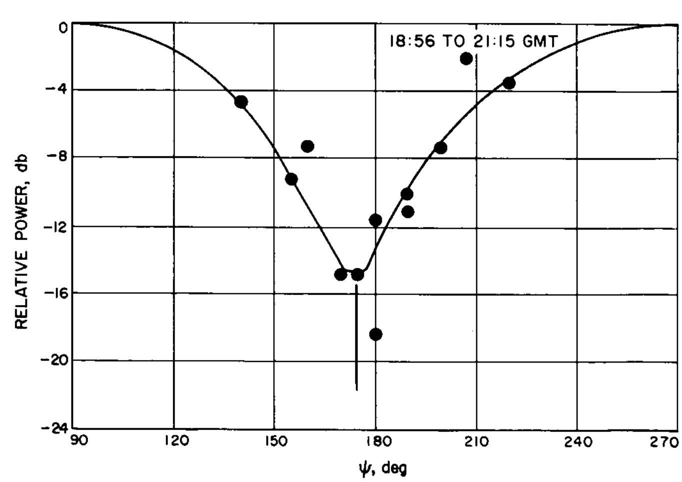

Fig. 100. Relative power vs rotation angle

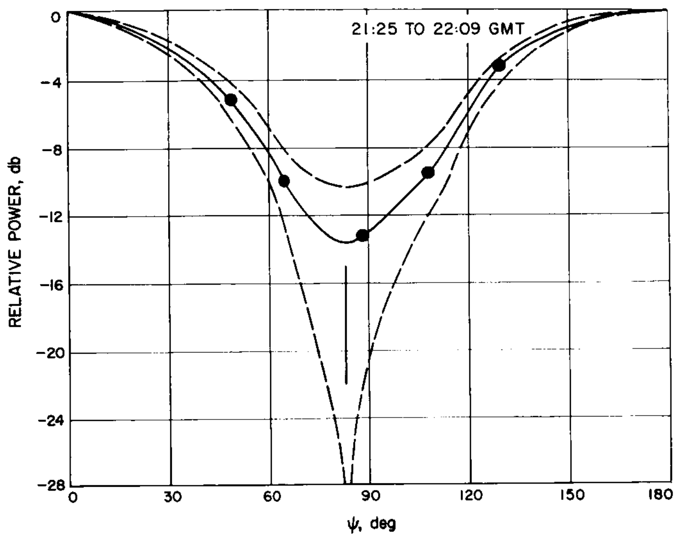

Fig. 101. Relative power vs rotation angle

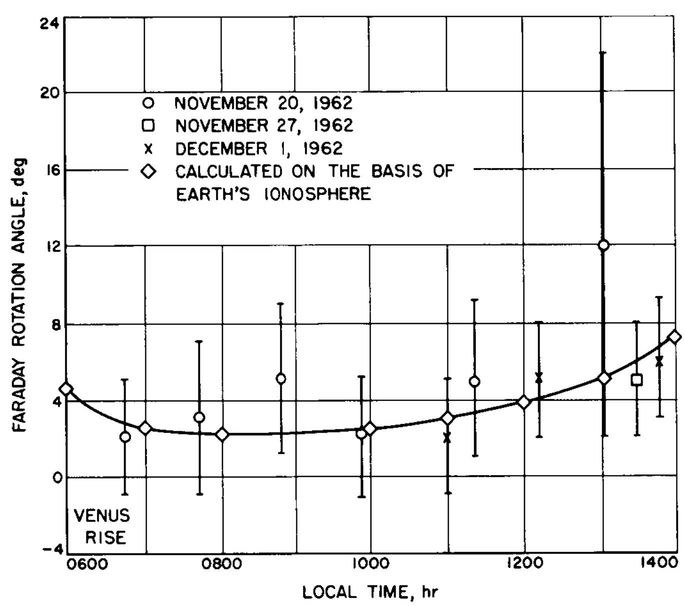

Fig. 102. Faraday rotation vs time of day

3. Discussion

Browne et al (Ref. 27) attributed slow lunar radar fading to Faraday rotation in the ionosphere. This effect was used by Evans (Reg. 28) and others to determine the total electron content of the ionosphere. A somewhat similar technique was employed by Yeh and Swenson (Ref. 29) using the Faraday rotation rate of two frequencies radiated from a satellite.

A medium in which both charged particles and a magnetic field exist can be said to be "optically active." A linearly polarized electromagnetic signal will be split into two circularly polarized components. The refractive index and therefore the velocity of these two components will not be equal. Upon emerging from the magneto-ionic medium there will be a relative phase shift between the two circular components resulting in an apparent rotation of the linearly polarized signal. Bauer and Daniels (Ref. 30) show that the rotation, Ω, in radians for 2-way propagation is

$$\Omega = 4.72 \times 10^{-4} f^{-2} \int_{h_1}^{h_2} NB \cos\theta \sec\delta \, dh$$

where f is frequency in cps, N is electron density (electrons/cm^3), B is the earth's magnetic field in gauss, δ is zenith angle, and θ is the angle between the magnetic field and the direction of propagation. The assumption is generally made that all Faraday rotation takes place within an altitude of 500 km of the Earth. Yeh and Swenson (Ref. 29) found that using the values of B and θ at 350-km altitude gave a good fit to the integration:

$$\Omega = 4.72 \times 10^{-4} f^{-2} B \cos\theta \sec\delta \int_{h_1}^{h_2} N dh$$

Calculations of the rotation expected from the Earth's ionosphere were made using Yeh and Swenson's estimates of the integrated electron density for a period of minimum solar activity. The calculated rotation angle, shown in Fig. 102, has a maximum value occuring near 1400 hr, the time of peak ionospheric electron content. These assumptions were verified in later lunar Faraday rotation measurements.

Preliminary data in the weekly report from the High Altitude Observatory at Boulder, Colorado indicates that there was very little solar activity during this period. The following sunspot numbers were reported: for November 20 and December 1-(11), for November 27-(25). The preliminary data from *Mariner 2* also indicates no unusual magnetic or electron activity.

Considering the probable error assigned to the individual points and the uncertainties involved in the ionospheric parameters, it appears that all the rotation could be ascribed to the Earth's ionosphere. Using preliminary *Mariner* data, it was estimated that interplanetary space would contribute less than 10^{-3} degrees of rotation.

Muhleman (Ref. 31) has postulated an ionosphere on Venus with an integrated electron density of 10^6 electrons/cm^2 and has calculated that the Faraday rotation would be of the order of 6 deg for an average magnetic field of 100 gammas. This would occur if the magnetic axis (assuming a dipole field) was properly aligned with the line of sight. These data then would imply that: (1) there is no magnetic field of the order of 10^{-3} gauss, (2) the alignment of the field is in such a direction that it does not give rise to Faraday rotation, or (3) the electron density is lower than postulated. *Mariner 2* data agrees with the first conclusion.

D. *Black-Body Radiation*

D. Schuster and C. Stelzried

The planetary radar receiving system was used to perform some limited black-body radiation measurements on the planet Venus. Measurements were performed prior to conjunction on September 19, 20, and 21, 1962. The measured temperature was just above the short-term threshold of the radiometer system. After conjunction, measurements were made for approximately one hour a day on 8 days between the December 4 and 14. This period of time was closer to the time of inferior conjunction and therefore the measured temperature was higher.

The combination of a large effective antenna aperture and a low system-noise temperature provided a good system for radio astronomy measurements. However, it was not feasible to modify the feed system to include a synchronous switch (in order to utilize the usual radiometer gain stabilizing techniques) so that it was necessary to operate as a "total power" radiometer. This required that particular emphasis be placed on short term (seconds-minutes) gain stability of the receiving equipment. The system block diagram is shown in Fig. 103.

The receiving system parameters were as shown in Table 10.

Table 10. System parameters

Center frequency, Mc	2388
System noise temperature (Radiometer configuration) °K	45
Bandwidth, Mc	0.9
Post detection time constant, sec	0.2 to 8

The radiometer was calibrated by measuring the system temperature using the Y factor method with the Tucor noise source and the AIL precision attenuator. In this measurement the attenuator is adjusted for the same indicated power level after the noise source is fired as was indicated before firing the noise source. Knowing the system temperature, noise-temperature calibrations can be made with the AIL precision attenuator (see Fig. 103). The measurements consist of determining the increase in antenna temperature when pointed at Venus over that obtained when pointed slightly away from the planet. This on-off source calibration technique has been described in detail by Drake (Ref. 32). All of the usual precautions were observed, such as boresighting frequently and testing the background temperature at various positions away from Venus. Also, the antenna movement rate was slow enough and the time constant short enough so that amplitude-smoothing corrections were not required.

Figure 104 shows a measurement taken on September 20, 1962. The equivalent antenna temperature difference

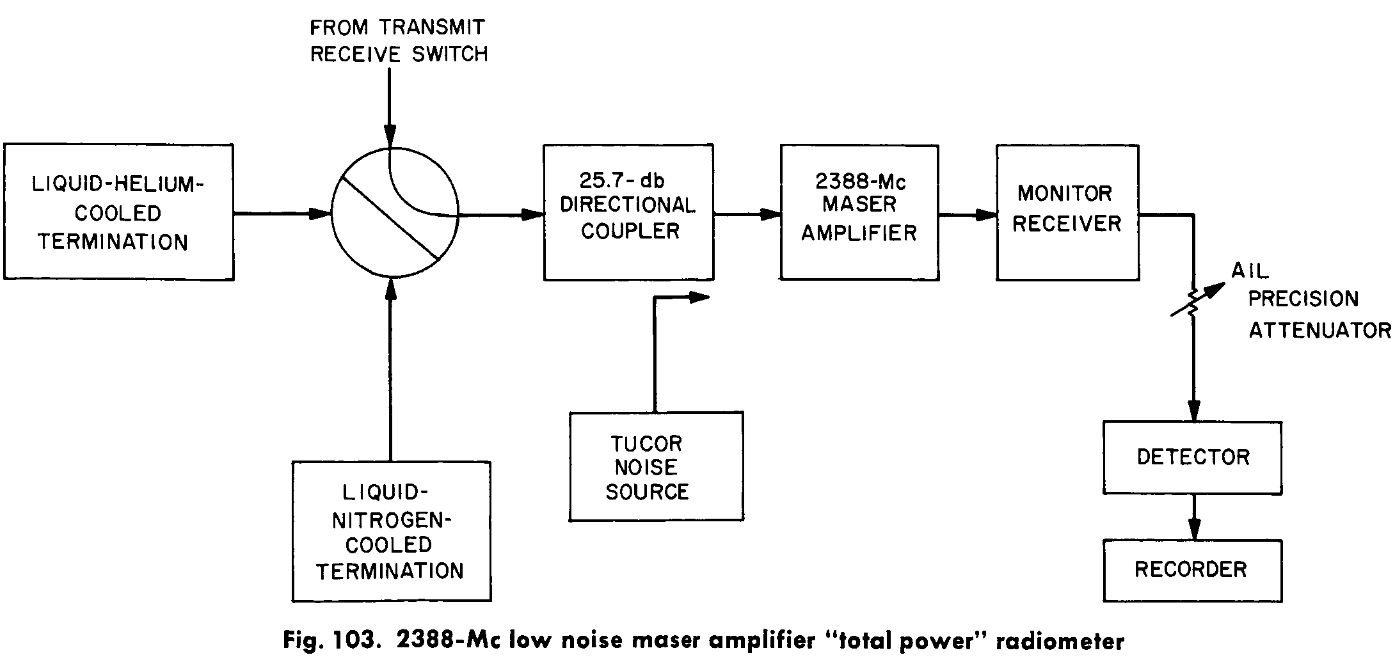

Fig. 103. 2388-Mc low noise maser amplifier "total power" radiometer

for this on-off source calibration (Fig. 104) is about 0.2 deg. The sensitivity of the system used in this manner as a total power radiometer is limited by the system gain stability.

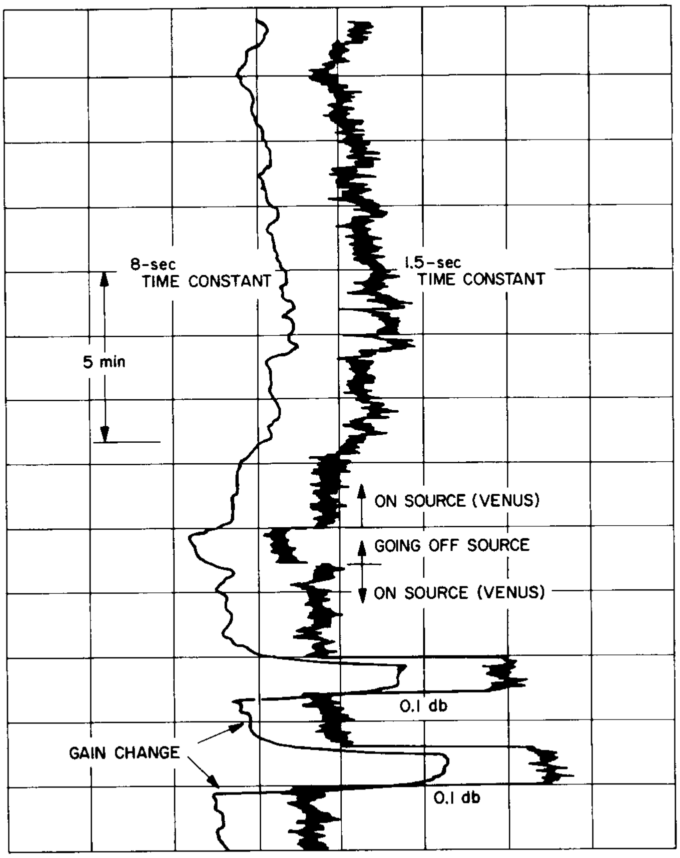

Fig. 104. 2388-Mc Venus black-body radiation (September 20, 1962)

Figure 105 shows a series of measurements taken on December 7, 1962 at 2030 GMT. The elevation angle was 18 deg, and the system temperature 48.5°K. A gain change of about 0.15 db is observed near the center of the record. Again, gain stability is the limiting factor to the system sensitivity.

Due to the width of the antenna beam and small angular size of the source, the measured temperature T may be referred to the temperature at conjunction, T_c, by taking into account the varying Earth-Venus distance with the simple relationship:

$$T_c = T\left(\frac{R}{R_0}\right)^2 \tag{23}$$

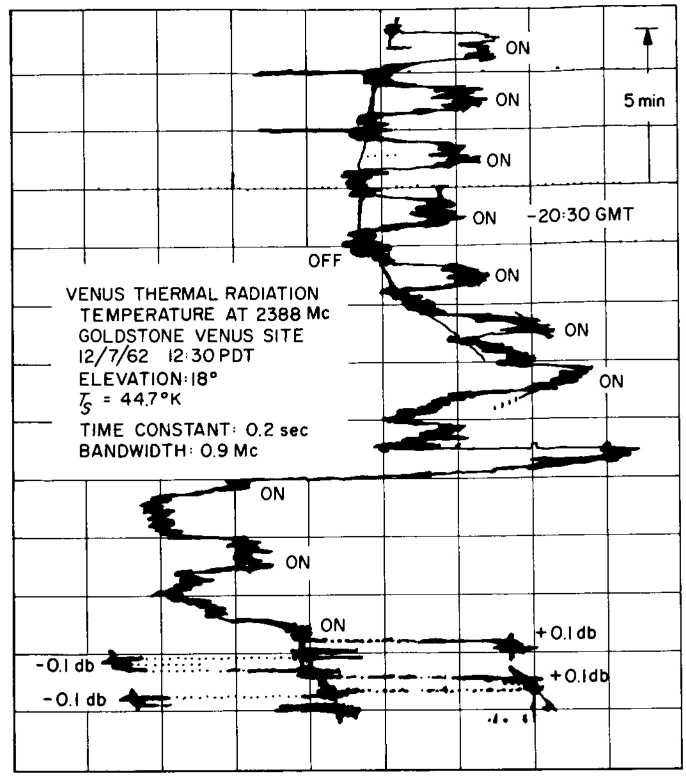

Fig. 105. 2388-Mc radiation (December 7, 1962)

where R and R_0 are the actual and conjunction Earth-Venus distances.

Figure 106 shows a graph of the measured temperatures over the 10-day period, modified by Eq. (23). The

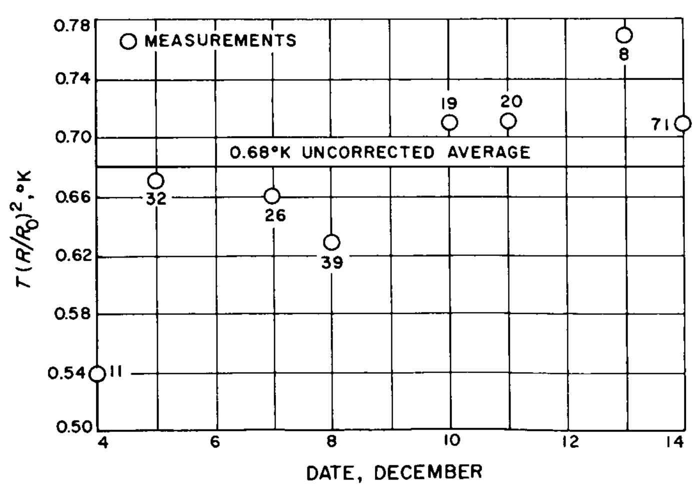

Fig. 106. $\left(\frac{R}{R_0}\right)^2$ normalized antenna temperature due to 2388-Mc Venus radiation over 10-day measurement period

number of measurements for each data point is indicated on the graph; the horizontal straight-line value of 0.68°K is the mean value for all of the data points for this period. Figure 107 shows the measured temperatures taken on December 14, 1962 (the most extensive series of measurements during the 10-day period) as a function of the time of day.

Analysis of the test data to determine the Venus black body disk temperature has not been completed.

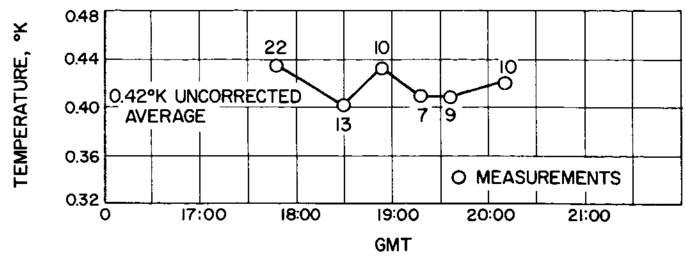

Fig. 107. Measured antenna temperature due to 2388-Mc Venus radiation on December 14, 1962

VII. THE VENUS-EARTH EPHEMERIS

P. Peabody

Calculation of the predicted values of the round-trip signal transit time and of the doppler frequency shift is essentially the same as for the 1961 experiment (Sec. VII of Ref. 1). These calculations are reviewed below. The tables of the motion of Venus are different from those used in the calculations for the 1961 experiment—the difference unfortuitously gives greater ephemeris error. Discussion of the effects of these errors is postponed to Sec. VIII, which describes the provisional calculations of the astronomical unit from the 1962 data, but the details of the construction of the tables are given here.

Desired are the position and velocity vectors $\boldsymbol{R}_{01}$ and $\dot{\boldsymbol{R}}_{01}$ of Venus at epoch T_1 referred to the center of the Earth at the same or some other epoch T_0, as indicated in Fig. 108. But,

$$\boldsymbol{R}_{01} = \boldsymbol{R}_{♀}(T_1) + \boldsymbol{R}_{\odot}(\mathrm{T}_0)$$

$$\dot{\boldsymbol{R}}_{01} = \dot{\boldsymbol{R}}_{♀}(T_1) + \dot{\boldsymbol{R}}_{\odot}(\mathrm{T}_0)$$

where $\boldsymbol{R}_{♀}(T_1)$, $\dot{\boldsymbol{R}}_{♀}(T_1)$ are the heliocentric position and velocity of Venus at T_1 and $\boldsymbol{R}_{\odot}(T_0)$, $\dot{\boldsymbol{R}}_{\odot}(T_0)$ are the geocentric solar position and velocity at T_0. Furthermore,

$$\boldsymbol{R}_{\odot} = -\boldsymbol{R}_{\oplus} + \frac{1}{1+\mu}\boldsymbol{R}_{☾}$$

$$\dot{\boldsymbol{R}}_{\odot} = -\dot{\boldsymbol{R}}_{\oplus} + \frac{1}{1+\mu}\dot{\boldsymbol{R}}_{☾}$$

where $\boldsymbol{R}_{\oplus}$, $\dot{\boldsymbol{R}}_{\oplus}$ are heliocentric position and velocity of the Earth-Moon barycenter, $\boldsymbol{R}_{☾}$, $\dot{\boldsymbol{R}}_{☾}$ are geocentric position and velocity of the Moon, and μ is the Earth-Moon mass ratio, as shown in Fig. 109.

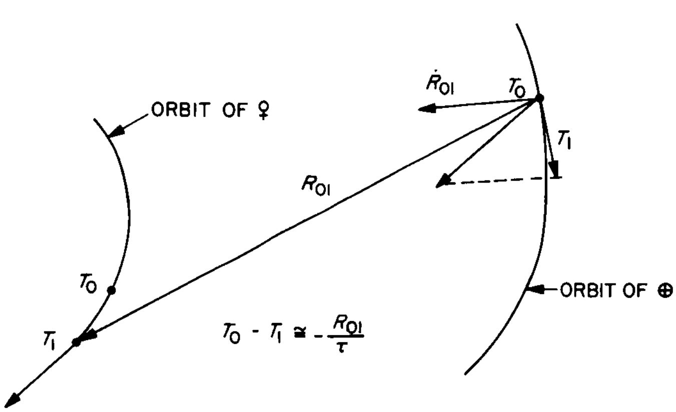

Fig. 108. Earth-Venus orbit geometry

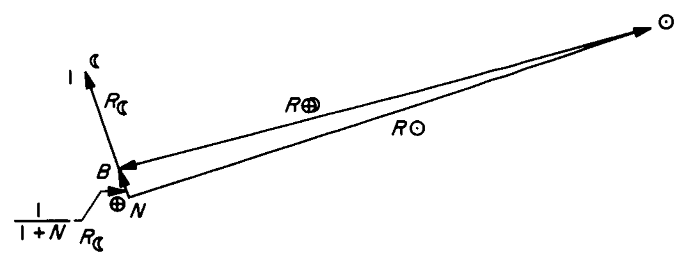

Fig. 109. Earth-Moon-Sun geometry

An ephemeris tape tabulating the equatorial heliocentric position and velocity of the Earth-Moon and of Venus and the equatorial geocentric position of the Moon was prepared as described below, where all quantities were referred to the mean equator and equinox of 1950.0 and tabulated against ephemeris time. The Earth-Moon and Venus tables were expressed in A.U. and in A.U./mean solar day, and the lunar tables in Earth radii. Computation of $\boldsymbol{R}_{01}$ and $\dot{\boldsymbol{R}}_{01}$ for particular epochs T_0 and T_1 expressed as universal time (Greenwich mean time) requires the following steps:

1. Conversion of T_0 and T_1 to ephemeris time by adding the correction $\Delta t_{ll} = 34.0$ sec.
2. Interpolation in the Earth-Moon and lunar tables at T_0 and in the Venus tables at T_1, using Everett's formula with modified second and fourth differences.
3. Numerical differentiation at T_0 in the Lunar tables using the derivitive of Everett's formula.
4. Conversion of the above positions and velocities to km and km/sec, using assigned values of the conversion factors A.U. and the Earth radius R_e.
5. Computation of $\boldsymbol{R}_{01}$ and $\dot{\boldsymbol{R}}_{01}$ referred to 1950.0, using the assigned value of μ.
6. Rotation of $\boldsymbol{R}_{01}$ and $\dot{\boldsymbol{R}}_{01}$ through precession and nutation to the true equator and equinox of date T_0.

Nominal values of the constants are given in Table 11. The value of the A.U. was, of course, recalculated as the purpose of the data reduction.

The lunar tables were constructed directly from Browne's improved lunar theory and are probably correct to at least six figures (less than 1 km). Since errors in the lunar position and velocity are scaled down by the ratio

Table 11. Values of constants used in calculating ephemeris data

Correction to universal time (Δtq), sec	34.0
Earth-Moon mass ratio (μ)	81.450
Earth radius ($R_\oplus$), km	6378.145
Nominal value of astronomical unit, km	149598845
Geocentric radius vector of Golstone (r_G), km	6372.1307
Longitude of Goldstone (θ_G)	243°205989
Geocentric latitude of Goldstone (ϕ_G)	35°064560
Speed of light (c), km/sec	299793
Transmitted frequency (ν_0), Mc	2388
Radius of Venus ($R_♀$), km	6100

82.45 to 1 in computing solar coordinates and velocity, errors in the lunar velocity as obtained by numerical differentiation of lunar positions may be considered negligible compared to errors in the planetary ephemerides.

The best predictions of the motion of Venus and of the Earth-Moon system remain the classical theories of Simon Newcomb, published together with tables of the perturbations to the mean orbit in Ref. 34, with corrections to the mean elements and other parameters in the form A + Bt derived from post-Newcomb optical observations by R. Duncombe. Both the 1961 JPL and MIT radar experiments demonstrated that these corrections were in fact significant (Ref. 2 and 35).

Because of the significant effect of ephemeris errors on observed signal transit time and Doppler shift, it was decided to attempt further corrections to the mean elements from the 1961 and 1962 radar experiments, combining radar observations with optical observations in the form of the normal equations published by Duncombe in Ref. 36. To this end it is necessary to adopt the uncorrected Newcomb theory as the provisional theory.

Cartesian coordinates derived from the Newcomb tables were computed by Paul Herget (Ref. 37). These coordinates, obtained on magnetic tape from the University of California Lawrence Radiation Laboratory in 1958, form the source of Venus and Earth-Moon ephemerides for the 1962 radar experiment.

Velocities obtained by numerical differentiation of these planetary coordinates are too inaccurate to be used in generating the doppler ephemeris, even for the purpose of conducting the experiment; in particular, short period terms neglected in the Newcomb theory as negligible in position prediction become significant to velocity prediction. These terms were essentially recovered and interconsistent position and velocity planetary ephemerides were generated by a numerical integration of the orbits of Venus and the Earth-Moon system, with initial position and velocity chosen so that the resulting positions were the best fit in the least squares sense to the Newcomb-Herget positions over a 10-year interval from July 1960 to July 1970. These are the positions and velocities carried on the ephemeris tape described above. They have proven quite satisfactory for the purpose of conducting the experiment; a discussion of their effect on A.U. calculation is postponed to Sec. VIII.

The Gauss-Jackson method, retaining sixth differences and with an integration step of two days, was used for the numerical integration. Coordinates of the perturbing planets were obtained from the ephemeris tapes prepared as a joint JPL-STL project in 1959 (Ref. 38). Reciprocal mass ratios of the planets were as given in Ref. 1 (p. 79).

These planetary ephemerides were also used in the planning and orbit determination of the *Mariner 2* mission. A more detailed discussion of their development is given in Ref. 39.

Plots of the residuals between the Newcomb-Herget and the numerical integration positions are given in Fig. 110 and 111. Residuals in equatorial x, y, and z and also ecliptic latitude, longitude, and radius vector are shown. The maximum residual in any coordinate over the ten year arc is 4.76×10^{-7} A.U. = 71 km for Venus and 8.11×10^{-7} A.U. = 122 km for the Earth-Moon.

The residuals are well within the stated accuracy of the Newcomb ephemerides. However, the component with sidereal period evident in each case indicates that the mean elements of Newcomb are not reflected into the numerical integration ephemeris with quite the desired accuracy. Machinery for obtaining improved fits to source position tabulations over extended intervals is nearly complete, and position-velocity ephemerides derived as above from new evaluations of the Newcomb theory, with or without corrections in Duncombe's form, will be used for final reduction of the 1962 radar experiment data.

The remaining calculations of Goldstone observables is essentially the same as described in Ref. 1, and is reviewed here. The position vector ρ from the Goldstone transmitter-receiver at T_0 to the center of Venus at T_1 is given by

$$\rho(T_0,T_1) = \mathbf{R}_{01} - \mathbf{R}_G(T_0)$$

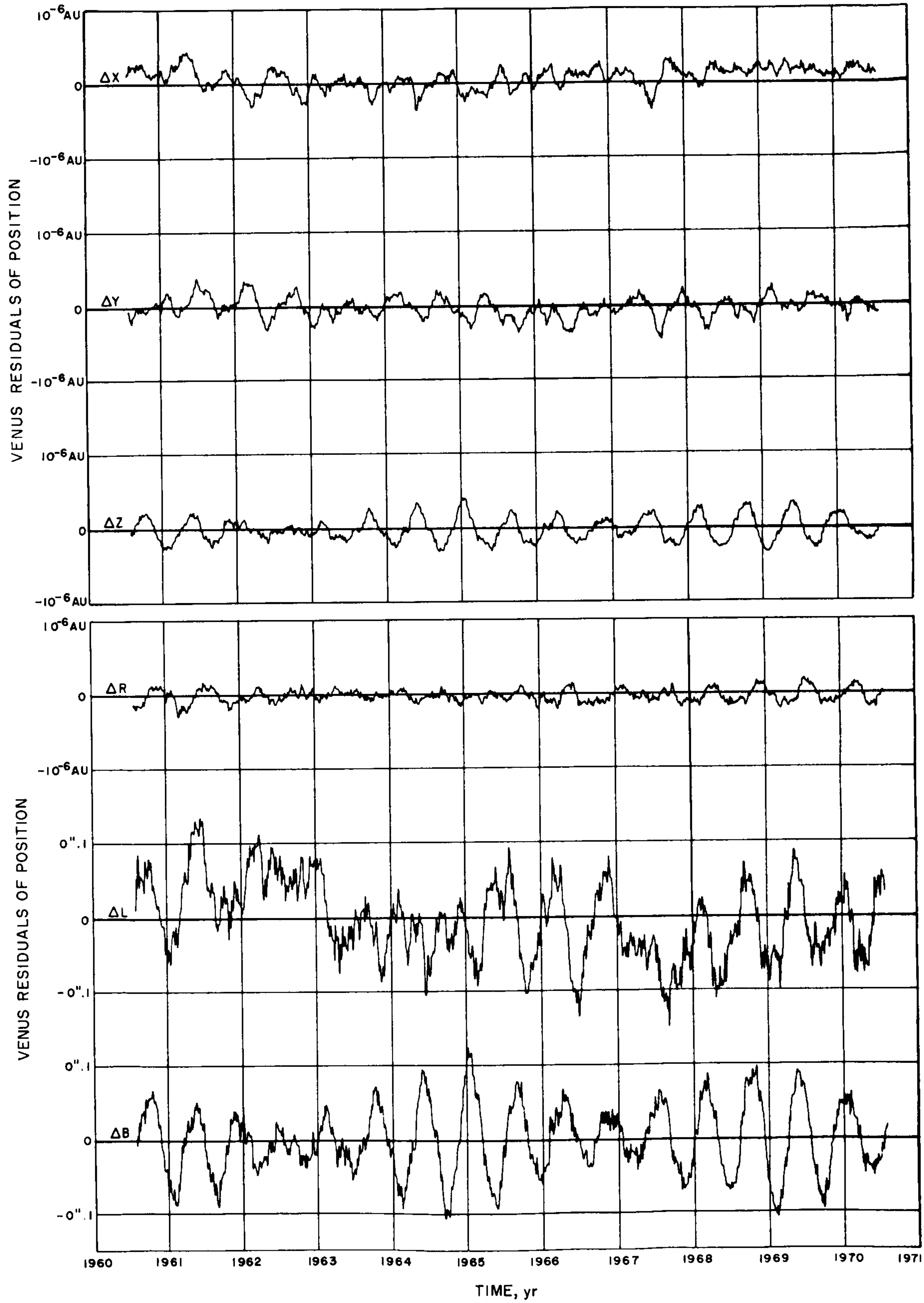

Fig. 110. Venus position residuals

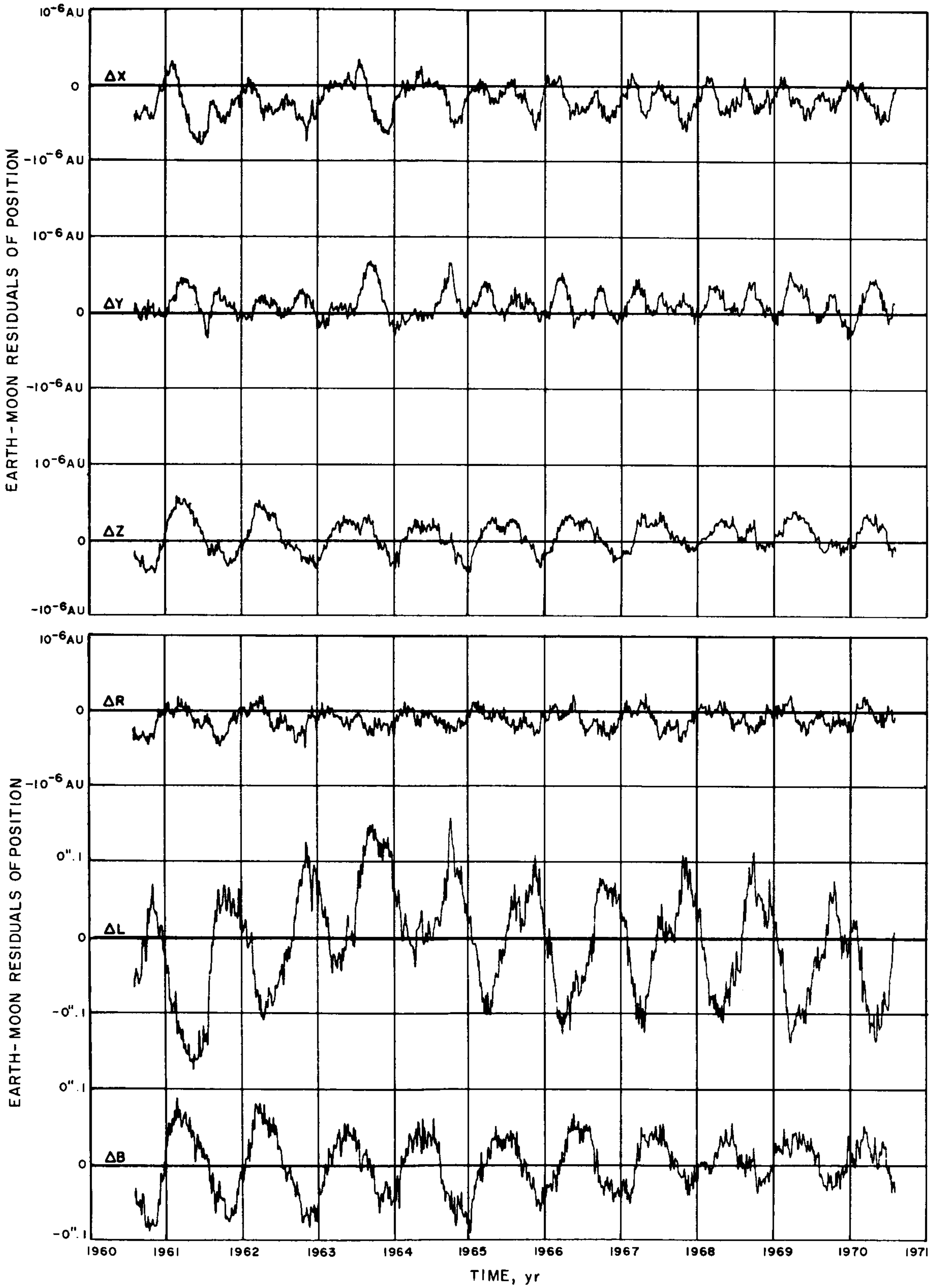

Fig. 111. Earth-Moon position residuals

where $\boldsymbol{R}_G(T_0)$ is the geocentric space-fixed position vector of Goldstone at T_0, and has the components

$$X_G = r_G \cos\phi_G \cos(\theta_G + \gamma(T_0))$$

$$Y_G = r_G \cos\phi_G \sin(\theta_G + \gamma(T_0))$$

$$Z_G = r_G \sin\phi_G$$

where θ_G, ϕ_G, and r_G are the longitude, latitude, and radius vector of the Goldstone transmitter-receiver. The Greenwich hour angle $\gamma\,(T_0)$ is given by

$$\gamma(T_0) = 100\overset{\circ}{.}07554260 + 0\overset{\circ}{.}9856473460\,d + 2\overset{\circ}{.}9015 \times 10^{-13}\,d^2 + \omega t + \delta\alpha\ (\text{mod } 360^\circ)$$

where d is the number of days past JD 2433282.5, t the seconds past 0^h of the epoch T_0, $\delta\,\alpha$ the nutation in right ascension, and ω the rotation rate of the Earth, computed as

$$\omega = \frac{0.00417807417}{1 + 5.21 \times 10^{-13}\,d}\ \frac{\text{deg}}{\text{sec}}$$

Similarly the velocity vector $\rho(T_0, T_1)$ is given by

$$\dot{\rho}(T_0, T_1) = \dot{\boldsymbol{R}}_{01} + \begin{pmatrix} -\omega Y_G \\ \omega X_G \\ 0 \end{pmatrix}$$

Given the epoch T_0 of reception, the epoch T_1 of reflection by Venus and the epoch T_2 of transmission are found by solving the implicit equations

$$T_1 = T_0 - \frac{\rho(T_0, T_1) - R_V}{c}$$

$$T_2 = T_1 - \frac{\rho(T_2, T_1) - R_V}{c}$$

where R_V is the adopted radius of Venus, c the speed of light, and $\rho = ||\rho||$.

The slant range and range rate at the instant of reception are

$$\rho_R = \rho(T_0, T_1) - R_V$$

$$\dot{\rho}_R = \frac{\rho(T_0, T_1) \bullet \rho(T_0, T_1)}{\rho(T_0, T_1)}$$

```
CASE 35                                        1962 VENUS RADAR EXPERIMENT                                                    1
                H.A.(R),  DEC.(R),   AZ.(R),   EL.(R),  RANGE(R), FRQ. SHIFT,ELONG.(R),TM. PLANET,RT. ASCENS.,DECLINATION
                H.A.(T),  DEC.(T),   AZ.(T),   EL.(T), R(R)+R(T),  REF. FRQ.,ELONG.(T),TOTAL TIME, MICRO SEC.,SIGNAL LOSS

EPOCH OF RECEPTION                                JULIAN DATE 2437970.16666666                 NOV. 1,1962   16 00 00.000
RECEIVED     291.69780 -25.01714 122.60691   1.79196  43.082161    95378.66  18.07238  143.70636   231.95277   -25.01045
TRANSMITTED  290.50882 -25.01469 121.90943    .97056  86.162017 2388.000000 18.06519  287.40503   287405032      -1.258

EPOCH OF RECEPTION                                JULIAN DATE 2437970.20833333                 NOV. 1,1962   17 00 00.000
RECEIVED     306.75525 -25.00977 132.16628  11.59452  43.060711    94416.59  18.01687  143.63481   231.93737   -25.00241
TRANSMITTED  305.56683 -25.00733 131.35318  10.87072  86.119115 2388.000000 18.00969  287.26192   287261928      -1.249

EPOCH OF RECEPTION                                JULIAN DATE 2437970.25000000                 NOV. 1,1962   18 00 00.000
RECEIVED     321.81317 -25.00225 143.42718  19.89168  43.039519    93149.18  17.96099  143.56412   231.92191   -24.99433
TRANSMITTED  320.62531 -24.99981 142.46702  19.30787  86.076721 2388.000000 17.95384  287.12052   287120520      -1.241

EPOCH OF RECEPTION                                JULIAN DATE 2437970.29166666                 NOV. 1,1962   19 00 00.000
RECEIVED     336.87149 -24.99453 156.65071  26.07078  43.018641    91644.69  17.90480  143.49448   231.90639   -24.98621
TRANSMITTED  335.68419 -24.99210 155.53667  25.67921  86.034953 2388.000000 17.89767  286.98120   286981200      -1.232

EPOCH OF RECEPTION                                JULIAN DATE 2437970.33333333                 NOV. 1,1962   20 00 00.000
RECEIVED     351.93007 -24.98659 171.59640  29.46422  42.998125    89987.63  17.84833  143.42605   231.89082   -24.97806
TRANSMITTED  350.74332 -24.98418 170.37387  29.31440  85.993904 2388.000000 17.84121  286.84427   286844272      -1.224

EPOCH OF RECEPTION                                JULIAN DATE 2437970.37500000                 NOV. 1,1962   21 00 00.000
RECEIVED       6.98878 -24.97841 187.28704  29.59313  42.977993    88272.97  17.79164  143.35889   231.87518   -24.96987
TRANSMITTED    5.80261 -24.97601 186.05691  29.70833  85.953625 2388.000000 17.78453  286.70991   286709904      -1.216

EPOCH OF RECEPTION                                JULIAN DATE 2437970.41666666                 NOV. 1,1962   22 00 00.000
RECEIVED      22.04749 -24.97000 202.33560  26.43725  42.958242    86599.69  17.73482  143.29301   231.85948   -24.96165
TRANSMITTED   20.86188 -24.96761 201.20369  26.79942  85.914107 2388.000000 17.72771  286.57810   286578096      -1.208

EPOCH OF RECEPTION                                JULIAN DATE 2437970.45833333                 NOV. 1,1962   23 00 00.000
RECEIVED      37.10606 -24.96136 215.71268  20.44804  42.938858    85063.84  17.67794  143.22836   231.84373   -24.95339
TRANSMITTED   35.92102 -24.95898 214.73331  21.00952  85.875326 2388.000000 17.67083  286.44874   286448736      -1.200

EPOCH OF RECEPTION                                JULIAN DATE 2437970.50000000                 NOV. 2,1962   00 00 00.000
RECEIVED      52.16442 -24.95253 227.12559  12.28899  42.919792    83752.08  17.62110  143.16476   231.82792   -24.94509
TRANSMITTED   50.97989 -24.95016 226.29754  12.99652  85.837186 2388.000000 17.61397  286.32151   286321512      -1.192

EPOCH OF RECEPTION                                JULIAN DATE 2437970.54166666                 NOV. 2,1962   01 00 00.000
RECEIVED      67.22237 -24.94353 236.81023   2.58206  42.900989    82735.58  17.56435  143.10204   231.81205   -24.93675
TRANSMITTED   66.03645 -24.94117 236.10390   3.39129  85.799576 2388.000000 17.55720  286.19606   286196064      -1.185
```

Fig. 112. Sample of Venus ephemeris data

with similar equations for slant range and range rate ρ_T and $\dot{\rho}_T$ at the transmitter.

The observed doppler shift is predicted as

$$\Delta\nu = -\frac{75}{80}\nu_0\left(\frac{\dot{\rho}_T + \dot{\rho}_R}{c}\right)\left[1 - ½\left(\frac{\dot{\rho}_T + \dot{\rho}_R}{c}\right)\right]$$

as derived in Ref. 1, and the total signal transit time is

$$T_f = T_0 - T_2$$

These quantities, along with angular data, were printed as auxiliary ephemeris data; a sample is shown in Fig. 112. Paper tapes for driving the antenna servos, tuning the receiver, and operating the transmit-receive switch were also prepared from these calculations.

Values of the constants used in the calculations are given in Table 11.

VIII. THE DETERMINATION OF THE ASTRONOMICAL UNIT FROM THE OBSERVATIONS

D. Muhleman, P. Peabody, and N. Block

A. Introduction

One of the primary scientific goals of the JPL Planetary radar program is to obtain precise measurements of the instantaneous velocities and distances of the various planets relative to the Earth. These data are used to determine the "fundamental constants" of the solar system which include the Astronomical Unit, the orbital elements of the Earth, and certain characteristics of the several planets and the Moon. In the sense that the motion of the Earth is influenced by all the major bodies of the solar system, observations of any object in the system from the Earth yields information about all of the astronomical constants.

Thus far in JPL's program, the Astronomical Unit (AU) determination has received the most attention because of its fundamental importance and also because it is easily determined with high accuracy by radar measurements. However, additional results are expected on the complete system of constants which will be important to workers in planetary theory, space sciences, and, perhaps, relativity.

The actual data obtained from the 1962 Venus radar experiment are the round-trip propagation time of a 2388-Mc radio wave between the Earth station and the surface of Venus, and the doppler frequency shift on the reflected signal. The round trip time is proportional to the distance between the Earth station and the surface of Venus while the doppler frequency shift is proportional to the radial component of velocity of the center of Venus relative to the Earth station.

It is shown below (and elsewhere in this report) that the Earth-Venus distance has been measured to an uncertainty of about 100 km over a single run and that the doppler velocity has been measured to an uncertainty of about 10^{-5} km/sec over a single run.

The Astronomical Unit has been determined by comparing the measured quantities to the corresponding theoretical quantities computed from the astronomical tables (ephemerides) of the Sun and Venus as described in Sec. VII. The rationale of these techniques is described in detail in Ref. 1 and 40. As a consequence of employing the classical comparison methods the results are somewhat dependent on the accuracy of the planetary theory utilized in the construction of the astronomical tables and the numerical techniques used to evaluate the tables. This dependence is apparently not significantly important in determining the AU, but it is critical for extending the work to the determination of other constants, e.g. the elements of the Earth's orbit. In order to complete the task of analyzing the observations to their fullest, it is necessary to essentially abandon the astronomical tables (but not the 200 years of optical observation on Venus). This work is proceeding slowly and is not the subject of this section.

It is important to note that for the purposes of obtaining a value of the AU a value of the speed of light of 299,792.5 km/sec is adopted which is slightly different from the value utilized in the ephemeris computations and the work reported in Ref. 1 and 40. This value is apparently improved according to a study reported in Ref. 41.

Unfortunately, the total set of observations obtained around the 1962 inferior conjunction of Venus is not as precise as obtained in 1961, particularly in the case of the doppler data. This fact is primarily due to the lesser number of observations obtained. Furthermore, at this time the data has not been fully analyzed. Consequently the new results must be considered as preliminary. However, in all cases the values of the AU deduced agree to within the accuracy of the analysis to those found in 1961. This agreement is highly significant and greatly adds to the credence of the radar results.

B. The Calculation of the Astronomical Unit

The AU has been obtained by comparing the observations to the values computed from the astronomical tables using a first guess of the AU for entry into the tables and then computing a second estimate of the AU from the differences by the classical least squares technique. The process is repeated until the rms differences (residuals) obtained in the nth iteration are not significantly smaller than those obtained in the (n-1)th iteration. Thus the AU is found by assuming that the astronomical tables are correct except for one parameter, the AU. In general, a given residual is given by (after a Taylor's expansion to first order)

$$(R_0 - R_c)_i = \left(\frac{\partial R_c}{\partial \alpha_1}\right)_i \delta\alpha_1 + \left(\frac{\partial R_c}{\partial \alpha_2}\right)_i \delta\alpha_2 + \cdots + \left(\frac{\partial R_c}{\partial \alpha_m}\right)_i \delta\alpha_n \qquad (24)$$

where R_0 is the observed range (for example) and R_c is the range computed from the tables with an assumed value of the AU. The $\delta\alpha$'s are the (unknown) errors in the significant parameters of the astronomical theory *including* the AU. Thus, the method employed here assumes that all of the $\delta\alpha$'s are zero except δAU. When the set of equations (Eq. 24) (the normal equations) are solved in a least squares sense the resulting correction for the AU in the case where all of the other $\delta\alpha$'s are zero is

$$\delta \mathrm{AU} = \sum_i \left(\frac{\partial R_c}{\partial \mathrm{AU}}\right)_i (R_0 - R_c)_i \Big/ \sum_i \left(\frac{\partial R_c}{\partial \mathrm{AU}}\right)^2 \qquad (25)$$

A similar expression can be written for δAU for the doppler observations. The solution for a general set of $\delta\alpha$'s merely involves an inversion of the matrix of coefficients from Eq. (25).

The estimates of the AU were computed over each run separately after considerable editing of the raw data to remove "wild" observational points. In the case of the doppler reductions a gauge of ± 8 cps was used on the residuals to further eliminate band points. This device primarily eliminated system transients at the beginning and end of each reception cycle.

A total of 52 doppler runs were made over the period from October 11 to December 17, 1962. The average number of samples per run was 141 and the *average* standard deviation of the final residuals for each run was 2.54 cps. The actual standard deviations are a function of signal-to-noise ratio and they vary from about 3.5 cps at the beginning and end of the observational period to about 1.2 cps at the time of conjunction. Clearly, the uncertainty in a given estimate of the AU from any single run depends further on the total doppler shift at that time and is widely variable. At the points of greatest interest in the case of the doppler, i.e., the further away from conjunction where the doppler shift is the greatest, the following uncertainties in the AU have been computed *based entirely on the above internal statistics* assuming no correlation between samples:

October 12	σAU = 195 km
December 12	σAU = 209 km

The resulting estimates of the AU using the Newcomb ephemerides (see Sec. VII) are shown in Fig. 113. They are discussed in detail below. A representative residual plot is shown in Fig. 114.

A total of ten estimates of the AU have been made from the range data over a period from November 8 to December 15, 1962. The average number of samples per run was 472 and the *average* standard deviation was 614 microseconds, round-trip propagation time. However, the range residuals are highly correlated as can be seen from a typical range residual plot shown in Fig. 115. If we assume that the residuals are correlated over, say, 25 points the average run has an uncertainty of 614 times the square-root of 472/25 or 141 microseconds which corresponds to 42.3 km in round-trip range. Adopting this value for the range uncertainty for a measurement at conjunction gives 79 km in the AU *based on these statistics alone.* The resulting estimates of the AU are shown in Fig. 116.

C. Range and Doppler AU Results

Figures 113 and 116 show the estimates of the AU computed with the Newcomb ephemerides. These ephemerides actually consist of Newcomb's tabulated positions of Venus and the Sun, where the position of the sun has been advanced in its orbit by correcting the Earth's mean anomaly by $+\ 4''.78\ T$ where T is the time in centuries since 1900 (see Ref. 42). Furthermore, the ephemerides have been smoothed by a numerical technique which was described in Sec. VII. This procedure was necessary in order to obtain smooth values of the velocity coordinates for comparison with the doppler observations. The differences between the smoothed position from these ephemerides and Newcomb's tabular positions (corrected by $\Delta M = +\ 4''.78T$) are also shown in Sec. VII. The differences exhibit a significant yearly periodic term that would clearly affect the AU results reported here. However, it is *not* obvious that this periodic term is the fault of the ephemeris fit; it could be an error in the Newcomb theory. This conclusion does not seem likely however, since a new reduction of the 1961 radar observations does violence to the excellent agreement among the AU results from the different data types reported in Ref. 40. The effects of the differences in the two ephemerides (which

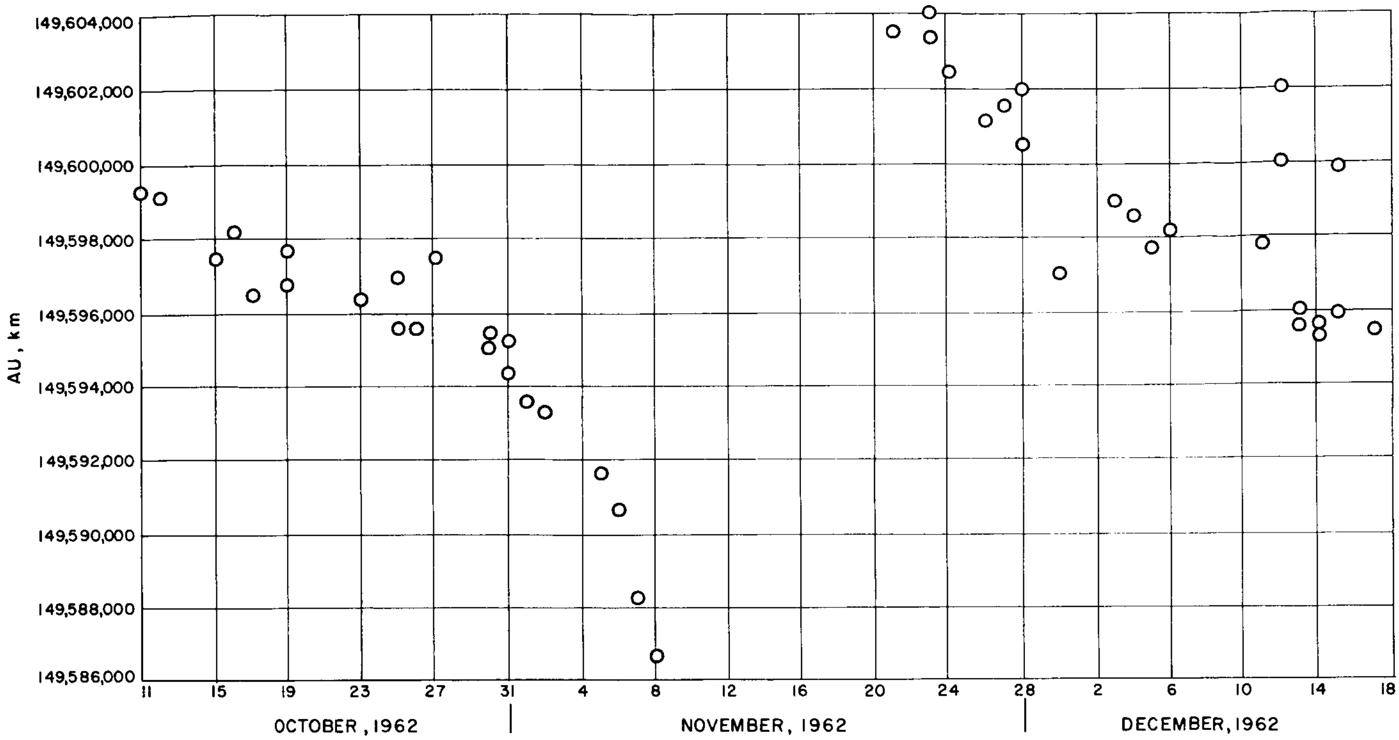

Fig. 113. The AU estimates from the 1962 doppler observations using the Newcomb ephemerides

are truly large, particularly in the latitude and longitude) are not understood at this time but experience with the new reduction of the 1961 data indicate that the effect may be as large as 1000 km in the AU. It is primarily for this reason that the results reported here must be considered "preliminary."

The doppler AU results shown in Fig. 113 exhibit exactly the same variation with date as those reported in Ref. 1 and 40 for 1961. It is certain that this variation is due to errors in the orbital elements of the Earth and Venus employed in Newcomb's tables. In particular, small changes in the mean longitudes and/or the perihelia of the Earth and Venus would essentially remove this variation. A set of corrections to all of the elements has been computed by Duncombe and are reported in Ref. 43. These corrections were computed from optical observations over a 200-year period. The corrections as published in Ref. 43 are as follows:

for the Earth

$$\Delta L'' = -\,0''.39 \pm 0''.05 + (0''.45 \pm 0.15)T,$$

$$\Delta e'' = -\,0''.10 \pm 0''.01 + 0''.00T,$$

$$e''\Delta\pi'' = -\,0''.07 \pm 0.03 - 0''.09T,$$

$$\Delta\epsilon = +\,0''.04 \pm 0''.01 - (0''.29 \pm 0''.03)T,$$

$$\Delta\alpha = +\,0''.02 \pm 0''.09 + (0''.23 \pm 0''.27)T,$$

$$\Delta\delta = -\,0''.03 \pm 0''.04 + (0''.16 \pm 0''.13)T,$$

and for Venus

$$\Delta\ell = +\,0''.10 \pm 0''.06 + (0''.53 \pm 0''.18)T,$$

$$\Delta e = -\,0''.12 \pm 0''.03 + 0''.01T,$$

$$e\Delta\pi = +\,0''.01 \pm 0''.04 - 0''.04T,$$

$$\Delta p = +\,0''.19 \pm 0''.05 + (0''.19 \pm 0.13)T,$$

$$\Delta q = +\,0''.02 \pm 0''.04 + (0''.34 \pm 0.10)T,$$

where all of the notation is conventional, i.e.,

L, ℓ = mean longitudes

e = eccentricities

π = mean longitudes of perihelia

Δp = rotation about the solar vector to the perihelia

Δq = rotation about the solar vector to the "perihelia +90°"

ϵ = obliquity of the ecliptic

$\Delta\alpha$ = the negative of the equinox correction

$\Delta\delta$ = the negative of the equator point corrector

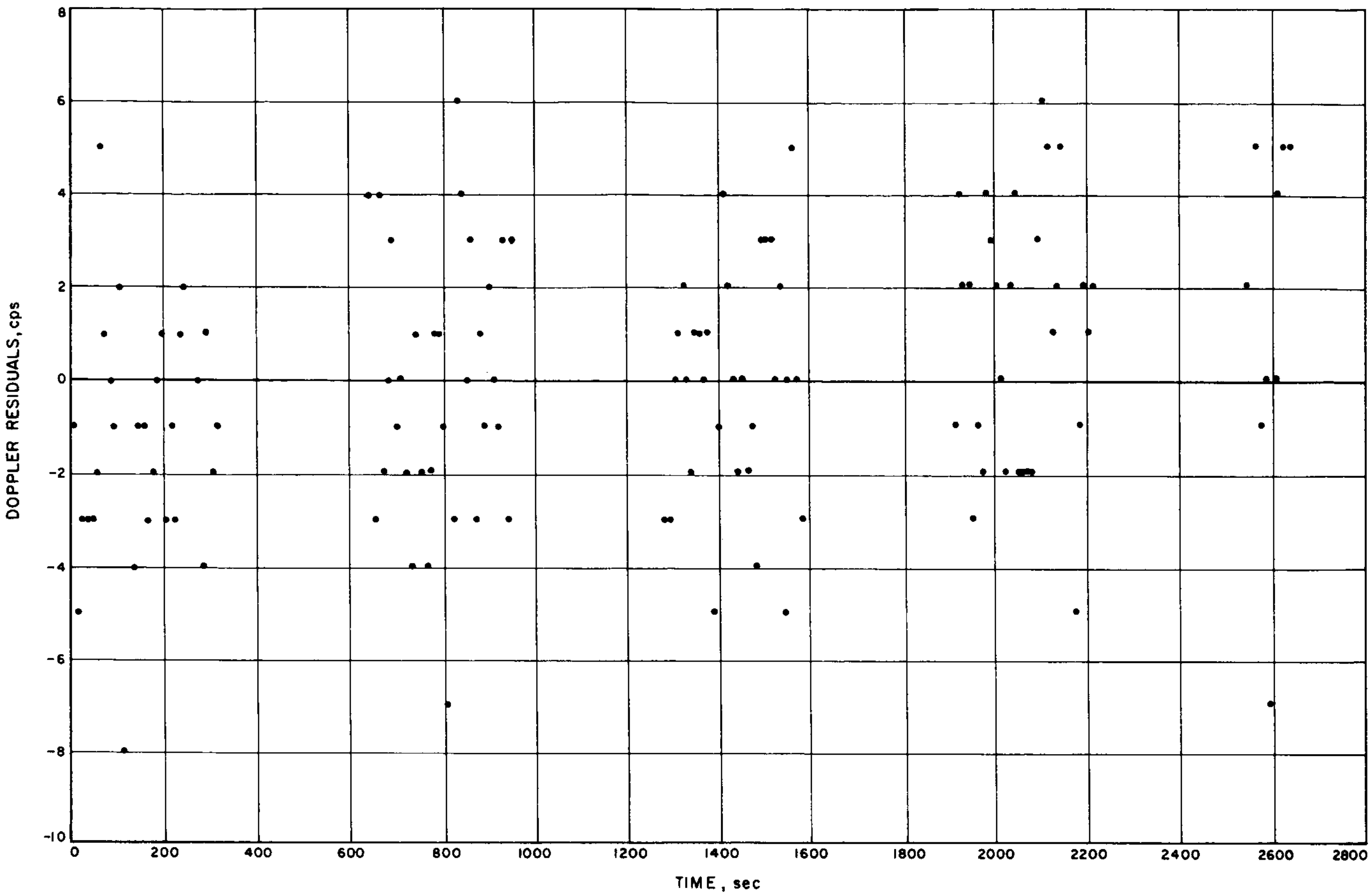

Fig. 114. Representative doppler residual plot

These corrections should be applied to the mean orbital elements used in the Newcomb theory because that theory was the provisional theory utilized by Duncombe in obtaining the corrections. However, several difficulties have been pointed out in this procedure. First of all, Duncombe adopted the concept of "ephemeris time" for

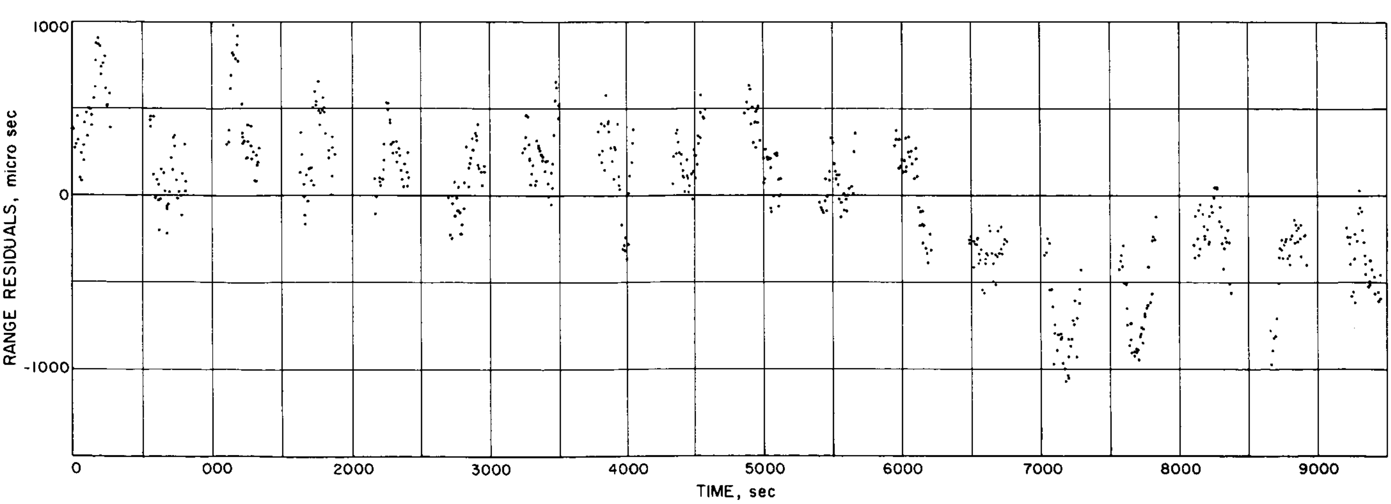

Fig. 115. Representative range residual plot

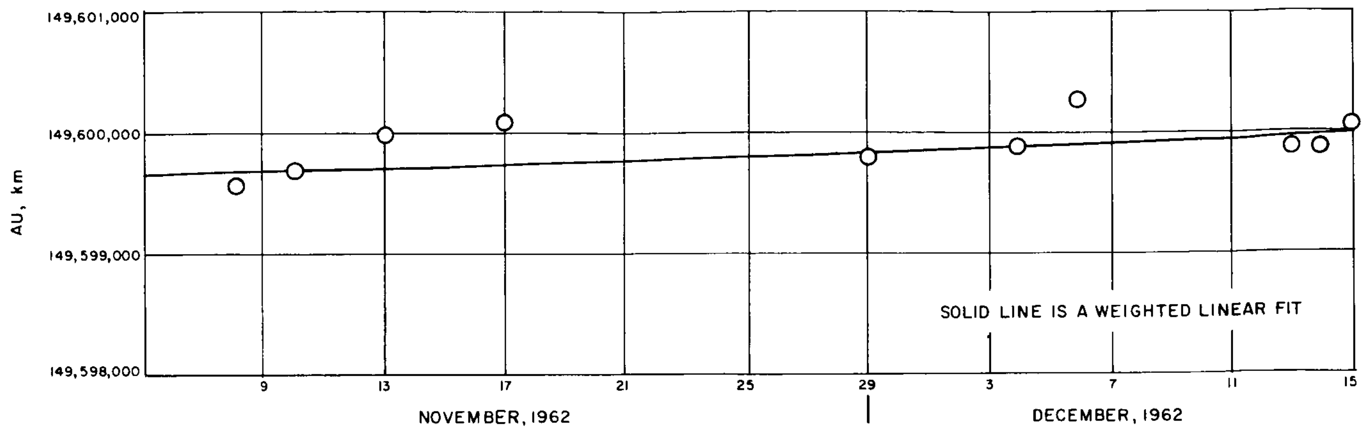

Fig. 116. AU estimates from range observations

his calculations. The ephemeris time is a concept which attempts to utilize a system of time in close accord to Newtonian time, i.e., uniform time associated with the laws of gravitation. However, for practical reasons, the ephemeris time is defined as the time argument for the motion of the Sun (or the Earth) in Newcomb tables of the Sun actually measured utilizing the Moon. Since Duncombe employed this concept, it appears that the correction for the mean longitude of the Earth, $\Delta L''$, should have come out of the calculations as precisely zero (Duncombe, personal communication, May 1963). Consequently, on the advice of Duncombe, we have assumed this correction to be zero (with trepidations). Furthermore, Clemence (Ref. 44) and Morgan (Ref. 45) have obtained a secular correction for the perihelion of the Earth amounting to a correction to the mean anomaly of the Earth of $+4''.78T$ which has already been applied in the reference ephemeris discussed above. On the basis of this, only the correction $\Delta e''$ and $\Delta \epsilon$ were applied to the reference ephemeris of the Earth and all of the above Venus corrections were applied to the Venus ephemeris for the construction of the "Duncombe ephemeris" reported in Ref. 1 and 40.

A Duncombe ephemeris for the 1962 observations has not been computed as yet. Consequently, it was necessary to analytically compute the change in the AU estimate resulting from the Duncombe corrections at each point of interest. It turns out that the effect of the corrections is smallest at specific times in the observational period, i.e., at the points furthest from conjunction for the doppler data and the point at conjunction for the range data. Since these points are the least sensitive to the corrections they are probably the most accurate estimates of the AU, at least for the types of errors that we are considering. The correction procedure follows from Eq. (26). If we identify δc_1 with the correction to the AU we get, upon solving Eq. (24) for δc_1:

$$\delta c_1 = \delta \mathrm{AU} = \frac{\left\{(R_M - R_0) - \frac{\partial R_c}{\partial c_2}\delta c_2 - \cdots - \frac{\partial R_c}{\partial c_M}\delta c_M\right\}}{\left(\frac{\partial R_c}{\partial c_1}\right)} \tag{26}$$

but the term $(R_M - R_0)$ has been iterated to zero. Therefore,

$$\delta \mathrm{AU} = \frac{\left\{- \frac{\partial R_c}{\partial c_2}\delta c_2 - \cdots - \frac{\partial R_c}{\partial c_M}\delta c_M\right\}}{\left(\frac{\partial R_c}{\partial \mathrm{AU}}\right)} \tag{27}$$

where $\delta c_2 = \Delta L''$, $\delta c_3 = \Delta e''$, etc. The partial derivatives in Eq. (27) have been computed from analytical expressions from Ref. 46 with a digital computer program (Ref. 47). An expression similar to Eq. (27) can be written for the doppler data. The individual terms in δAU are shown in Table 12 for the doppler observations on October 12 and December 12 and the range observation of November 12, 1962. The actual AU estimates listed in Table 13 were obtained by computing the weighted mean of the estimates near the date of interest. It is clear from the table that the value for December 12 is anomalously low (also evident from Fig. 113). A similar effect was observed in the observations one month after conjunction in 1961 but of much smaller magnitude (see below). Figure 113 suggests that the observations in this region may have been faulty but no explanation can be offered to support this conjecture. Some insight can be gained by the following analysis, however.

Table 12. The effect of the Duncombe corrections on the AU

	Doppler, Oct. 12	Doppler, Dec. 12	Range, Nov. 12
$\Delta L''$	−119 km	+141 km	− 4 km
$\Delta e''$	+ 75	+132	−191
$e''\Delta\pi''$	−182	−164	+319
Δl	−441	+506	− 1
Δe	+ 97	−169	− 40
$e\Delta\pi$	+ 45	+ 41	− 44
Δp	− 74	− 30	− 68
Δq	− 43	− 44	− 8
Totals	−642	+413	− 37

Table 13. 1962 Astronomical Unit results

	Newcomb Ephemerides[1], km	Duncombe Ephemerides[2], km
Doppler, October 12	149,599,060	149,598,719
Range, November 12	149,599,730	149,599,374
Doppler, December 12	149,596,452	149,596,888

[1] Newcomb ephemerides means Newcomb's tables with a mean anomaly correction of $\Delta M_\oplus = +4''.78\,T$.

[2] Duncombe ephemerides means here that only $\Delta e''$ has been applied for the Earth plus all of the Venus corrections.

The true longitude of the Sun, λ, is computed from Newcomb's tables using the equation

$$\lambda = L'' - (f'' - M'') + \text{perturbation terms} \qquad (28)$$

where f'' and M'' are the true anomaly and mean anomaly of the Sun, respectively, and the combination $(f'' - M'')$ is the equation of center. As is well known (Ref. 49), f'' may be expanded in terms of M''

$$f'' = M'' + (2e'' - \tfrac{1}{4}e^3)\sin M + \frac{5}{4}e^2 \sin 2M + \cdots \qquad (29)$$

and, consequently, to first order in e''

$$f'' - M'' = 2e'' \sin M''. \qquad (30)$$

Then from Eq. (28)

$$\lambda = L'' - 2e'' \sin M'' + \text{perturbation terms}. \qquad (31)$$

Now the only change that was made to Newcomb's tables was $M'' = -4''.78T$. From Eq. (31) for a change of M'' only, we get

$$\Delta\lambda = 2e'' M'' \cos M''.$$

Actually there is a slight change in the perturbation terms due to a change in M, but it is negligible. It turns out that $\cos M''$ for October 12 is 0.135, whereas for December 12 $\cos M'' = 0.922$. Thus any change in M'' has about 7 times the effect on the latter date than on the former date. Actually the inclusion of $-4''.78T$ had an effect on the AU estimate for October 12 of +13 km and on December 12, +111 km. Clearly, it is possible to raise the AU estimate of December 12 by a very large amount without lowering the estimate on October 12 significantly with a correction to M'' (or $e''\Delta\pi''$). However, an impossibly large $\Delta M''$ is required to bring the two estimates into complete agreement. We can conclude from this that the ephemeris errors introduced into the AU computations are probably large compared with the accuracy of the radar observations. These errors include those in the Newcomb tables, Duncombe corrections to this table, and probably the most significant, errors in our numerical representation of the ephemerides.

D. *Weighted Mean Results and Comparison with Previous Radar Results*

We shall adopt the mean of AU estimates reported in the final column of Table 13 weighted by *Estimated* variances based on the noise in Fig. 113 and 114 and estimated ephemeris uncertainties. Adopting

149,598,719 ± 1000 km, October 12, 1962

149,599,026 ± 1000 km, November 12, 1962

149,596,452 ± 2000 km, December 12, 1962

we obtain as our preliminary 1962 result

149,598,757 ± 670 km

The final AU results reported in Ref. 41 and 49 are shown in Table 14. The table is nearly self-explanatory with the possible exception of our revision of the Millstone result. This revision was accomplished by averaging the Mill-

Table 14. 1961 radar results (Ref. 41)

1. Doppler near eastern elongation	149,598,750 ± 200 km
2. Doppler near western elongation	149,598,000 ± 1000 km
3. Range at conjunction (closed loop)	149,598,500 ± 150 km
4. Range at conjunction (radiometer)	149,598,800 ± 150 km
5. Millstone result (Ref. 2)	149,597,850 ± 400 km
6. Muhleman's rework of Millstone data (Ref. 41)	149,598,100 ± 400 km
7. Weighted mean of 1, 2, 3, and 4	149,598,640 ± 200 km

stone estimates over date in a manner significantly different from that reported in Ref. 2. The details of the revision are given in Ref. 41.

E. Conclusions

The preliminary best value of the astronomical unit from the observations of Venus around the 1962 inferior conjunction is

$$149{,}598{,}757 \pm 670 \text{ km}$$

where most of the uncertainties are due to ephemeris errors. This result is in complete agreement with the 1961 Goldstone radar result of

$$149{,}598{,}640 \pm 200 \text{ km}$$

as well as with the results from the 1961 Millstone radar observations.

The remaining uncertainties are primarily linked to the uncertainties in the ephemerides of the Earth and Venus and are of such a nature that the radar observations will ultimately yield definitive corrections to the fundamental ephemerides. This ultimate result is difficult to obtain from an analytical standpoint and will evolve slowy. While it is clear that the observations available at this time are of sufficient quality and quantity to accomplish a good measure of this goal, it should be realized that observations distant from conjunction are required to solve for certain of the corrections that are strongly correlated. In particular, radar observations from the Earth of other planets (or asteroids) are highly desirable for the separation of the effects of the Earth's orbit from those of the orbit of Venus.

IX. SUMMARY AND CONCLUSIONS

A. Science Summary

R. Goldstein

This section gives a highly condensed picture of what the various experiments measured and how these measurements relate to characteristics of Venus. Details on the method of performing these experiments may be found in the appropriate section of this report. In all cases, the conclusions reported here are preliminary ones; and complete reduction and analysis of the data may be expected to refine the conclusions considerably.

Measurement of the total power contained in the radar echo yields a very interesting characteristic of Venus—its radar cross-section. This data was obtained in two ways. One method used the receiver in the configuration of a radiometer, which measured the power directly. In the other method, the total power was obtained by integrating the power spectrum of the signal.

The power measurement was repeated almost daily during the months of the experiment, giving an average radar cross section for Venus of about 10% of its geometric cross section.

There are no periodicities seen in this data, but the signal power does show a Venus-induced variation much larger than can be ascribed to random noise or experimental variations.

Typically, the received signal power, referred to the antenna terminals, was 10^{-21} watts. This extremely feeble signal still provided a good signal-to-noise ratio because of the very high performance of the receiver.

Having sufficient signal strength, another dimension to the data was obtained by analyzing the echo power into its frequency components.

A very pure sinusoid was transmitted, but Venus' rotation, working through the doppler effect, spread the received signal into a broader spectrum. Because of the remarkable geometric properties of a sphere, all of the points on Venus that contribute echos at a given frequency lie on a specific (projected) straight line. Thus a spectrogram can be thought of as the result of scanning Venus with an extremely high resolution fan-beam antenna. This is the extra dimension provided by spectral analysis of the echo.

Spectrograms were taken almost every day of the experiment. Like the power measurements, they also show a variation from day to day.

A feature on Venus, which evidently reflects more strongly than the surrounding area, was found by its signature on the power spectra. This feature was found to move slowly across part of the disk of Venus, hence the rate of rotation may be inferred.

The spectrograms also contain the rotation rate in a different way. The bandwidth at the base equals the product of the surface roughness and the rotation component which is perpendicular to the line of sight. A single measurement is not sufficient to resolve the ambiguity between rotation rate and roughness; but a series of measurements made as Venus sweeps by the Earth is sufficient, and will also yield the direction of the axis of Venus.

The Venus spectrograms showed enough signal-to-noise ratio that the returning power was divided into yet another dimension—that of time delay. This was done with a range-gate, which is a device which accepts echos originating from a specified distance and rejects closer and farther echos. The selected zone was then analyzed for its frequency composition. Thus Venus was divided into concentric rings by the range-gate, and the rings in turn were divided into parallel lines by the spectrometer. Hours of signal integration were required to produce an adequate signal-to-noise ratio for this experiment.

The ambiguity between roughness and perpendicular component of rotation is removed by this technique, as the echos originate from known parts of the surface.

The three methods of determining Venus' rotation period yield essentially the same surprising result—about 240 days *retrograde.*

Knowing the component of rotation, the spectrograms yield the roughness characteristic of Venus. Most of the reflection comes from a central "high light" area, but echos from the limbs are detectable. In this sense, Venus is somewhat smoother than the Moon.

During most of the experiments, the transmitter generated right-handed, circularly polarized, waves. Reflection generally reverses the sense of circular polarization; so to receive the maximum signal strength, the receiver was normally arranged for left-handed waves. A rough reflecting surface will alter this situation, however. By providing multiple reflections, some power will be returned in the original sense of polarization. This phenomenon makes it possible to study surface characteristics of Venus by reversing the sense of polarization accepted by the receiver.

When this was done, it was found that the signal power dropper 11 to 12 db and that most of this loss was from the "highlight" area surrounding the sub-Earth point. Echoes from the limbs (where roughness is more effective in producing multiple reflections) show up stronger, relative to the center, than in the normal polarization case. The data indicates that under reversed polarization, the surface of Venus is nearly a Lambert scatterer.

For further polarization studies, the versatile antenna feed was adjusted to transmit and receive linear polarization of specified orientation. This configuration was used to measure the total amount of polarization rotation suffered by the signal on its round trip flight.

The total rotation was found to be very small, of an amount that can easily be imputed to the Earth's ionosphere. The interesting conclusion is that the combined rotation produced by the interplanetary medium and the atmosphere and ionosphere of Venus is negligible.

The relative velocity between Venus and the radar station was determined by measurement of the change in frequency (doppler shift) of the received signal with respect to the transmitted signal. This was done by tracking the echo with the receiver in the configuration of a phase-locked loop. All reference frequencies were derived from the same stable source, so that extreme accuracy in the measurement was achieved.

Most of the error is attributable to the random character of the Venus echo, the signal having a fade rate of about 10 cps. Even so, the rms velocity error for a single 5-min observation is less than 20 cm/sec.

Radar range to Venus was also observed, not by integrating velocity, but by the independent process of measuring the time-of-flight of the signals. The transmitter was modulated by a pseudorandom waveform and the receiver tracked the timing of the echo by employing a phase-lock (on the modulation) technique. This approach provides a highly accurate method of measuring the time-of-flight. The rms error of a single observation is less than 1 millisec, compared to the total round trip time of about 6 min.

The range and velocity of Venus can be calculated from the standard astronomical ephemerides, hence these independent measurements serve as a powerful tool for checking these tables; and, indeed, improving their accuracy. Both range and velocity calculations require the knowledge of many physical constants. However, one constant is more sensitive by far than the others, and that one is the Astronomical Unit. The JPL radar observations of Venus during the 1961 conjunction yielded data which refined the previously agreed upon value of the A. U. by over two orders of magnitude. The 1962 data has positively confirmed this value, and may improve it still further when the data has been completely analyzed.

Other constants such as the mass and radius of Venus, the mass of Mars, etc. are also accessible to the radar measurements. They cannot be determined by one period of observation, however, but data taken over extended periods will eventually enable these constants to be sorted out.

B. Radar and Communications Technology Results

R. Stevens

There is a direct similarity between a planetary radar station and a deep space communication ground station; it is the same similarity as between skin tracking and active beacon tracking of conventional radars — very often the skin and beacon tracking modes are provided in a single radar. The planetary radar and the deep space communication station both require very high average power transmitters, very low noise receivers, and large high gain ground antennas. Both systems also require very reliable operation 12-16 hr per day, daily for several months. Thus a technological advancement successfully applied in the JPL planetary radar is almost sure to be useful in (and soon applied to) the JPL/NASA Deep Space Instrumentation Facility.

Throughout this report we have discussed equipment and techniques used in the present experiment which are advanced relative to that available in the 1961 JPL Venus Radar (cf. Ref. 1). These are:

1. Completely automatic receiver frequency tuning by punched paper tape. The accuracy of tuning is better than 1 cps at 2388 Mc about 5 times more precise than the 1961 system. Also, the 1961 system required an operator. This new system does not, except for setup prior to a day's operation. Automatic tuning to this accuracy can be applied to increasing the sensitivity of future space communication receivers by decreasing pre-detection bandwidth of either coherent or non-coherent systems through the use of a priori knowledge.

2. Extensive use of digital signal processing in the receiver. To provide a means of accurately integrating through the receiver off-cycles of the time shared monostatic radar, the integration was done digitally with essentially complete accuracy. In the earlier receiver the smoothing was done in an analog filter which would drift between receive cycles. Also, in preference to the previously used square law detector a high level amplitude detector followed by a precise digital squaring computation was used in this experiment. Both of these techniques are applicable to precision processing of very weak and noisy signals as might be received from an extreme distance or low power space probe.

3. A technique was implemented for performing a spectral analysis of a range gated signal. During the experiment range zones on Venus of 111 miles depth were analyzed. This technique is of special interest in planetary and lunar radar astronomy. Also, a technique was implemented for providing a signal spectrum read-out after each receive cycle while retaining the signal for integration with future receive cycles. The technique, which we found quite useful for rapid validation of system performance, is potentially useful for quick identification of weak spacecraft signals.

4. The pseudo-noise planetary ranging system was completely digitized as compared to a hyrbid digital-analog system in the 1961 system The proper time of flight delay for open loop ranging and signal amplitude and spectrum measurement was controlled entirely automatically compared to a manual method in the 1961 system. Also for closed loop ranging, range and range rate was automatically provided during the receiver-off cycle portion and range rate was provided during the receiver-on cycle portion, allowing a decreased range tracking loop bandwidth. The range tracking closed loop was completely digital. These techniques are applicable for use of a priori knowledge in range measurements on a weak spacecraft signal.

5 The monostatic radar involved having both a low noise receiver and a high power transmitter on a single antenna. This is the present standard configuration for the DSIF ground stations. In the radar the receiver and transmitter are connected to the antenna at different times, whereas in the DSIF system they are connected at different frequencies; however, some of the technical and operational problems are the same. By use of very carefully designed waveguide switches and transmission components the losses were only 0.1 db ahead of the maser amplifier, 0.2 db ahead of the transmitter. This technology and experience has been very useful in the design and building of the new S-band system for the DSIF.

6. A cassegrain microwave optics configuration was used on the 85-ft antenna; the 1961 system used a focal point feed system. The operational advantage of the cassegrain configuration for a low noise high power system has been proven by this radar experiment; it is now being used in the design of the S-band system for the DSIF. We obtained an aperture efficiency of 64% and a maximum zenith antenna temperature of 11°K as compared to 56% and 15°K, respectively, for the 1961 focal point installation. Including the effects of waveguide losses which were less in the cassegrain system, the 1962 antenna gain was up by 0.8 db over the 1961 system and the system temperature, which benefitted from a better maser was down from 64 to 40°K average (2.0 db improvement). With the increased flexibility of the cassegrain installation, we were able to include the capability of switchable orthogonal circular polarizations (ellipticity < 0.5 db) or, by a simple (30 min) change in a turnstile junction, precision rotatable orthogonal linear polarizations. The diverse polarization capability was very useful to the planetary radar measurement, as well as to measurements of space propagation phenomena. The improved technical performance provided by the cassegrain system is directly applicable to the DSIF space communication mission.

7. The two-cavity open cycle dewar maser which was located in the cassegrain cone was relatively easy to service compared to the 1961 installation at the 85-ft antenna quadripod apex. It is a mid-way device between the earlier single cavity maser and the traveling wave maser with closed cycle helium refrigeration required by the DSIF. The maser was, in fact, a very reasonable amplifier; it provided about 28.5 db gain, 3 Mc bandwidth, gain stability of ± 0.5 db long term, ± 0.02 db short term, and about 21°K noise temperature. It operated essentially trouble-free for the 3-month experiment. The experience gained in operating this relatively low noise system (40°K total system temperature) has proven very useful in the development of the low noise S-band system for the DSIF.

8. A Rubidium vapor oscillator was used as the basic frequency standard for the transmitter and receiver. It provided a factor of 5 increased stability over the cesium beam controlled oscillator used in 1961. Partly as a result of the experience gained during the radar experiment, this type oscillator has been adopted throughout the DSIF.

The techniques and equipment advances discussed were applied in the field at the Goldstone Venus Site for a continuous period of about 2½ months during the radar experiment. We also accumulated in excess of 300 hr of instrumented deep space "communication" including measurements with various polarizations and with varying local weather conditions at a frequency (2388 Mc) very near that to be used in the future by the DSIF (2295.2115 Mc). This has improved our confidence of obtaining good and predictable performance with the future system.

REFERENCES

1. Victor, W. K., R. Stevens, and S. Golomb, *Radar Exploration of Venus: Goldstone Observatory Report for March-May 1961*, Technical Report No. 32-132, Jet Propulsion Laboratory, Pasadena, California, August 1, 1961.

2. Pettingill, G., et al, "A Radar Investigation of Venus," *Astronomical Journal*, Vol. 67, No. 4, p. 181, May 1962.

3. Maron, I., G. Luchak, and Wm. W. Blitzstein, "Radar Observation of Venus," *Science*, Vol. 134, pp. 1419-1420, 3 November 1961.

4. Thompson, J. H., J. E. B. Ponsonby, G. N. Taylor, and R. S. Roger, "A New Determination of the Solar Parallax by Means of Radar Echoes from Venus," *Nature*, Vol. 190, pp. 519-520, May 6, 1961.

5. Kotelnikov, V. A., and I. Shklovsky, "Radio Location of Venus," *Izvestia*, May 12, 1961.

6. Hannan, P. W., "Microwave Antennas Derived from the Cassegrain Telescope," *IRE Transactions on Antennas and Propagation*, Vol. AP-9, pp. 140-153, March 1961.

7. Potter, P. D., "The Application of the Cassegrainian Principle to Ground Antennas for Space Communications," *IRE Transactions on Space Electronics and Telemetry*, Vol. SET-8, No. 2, June 1962.

8. Potter, P. D., "A New Horn Antenna with Suppressed Sidelobes and Equal Beamwidths," *The Microwave Journal*, Vol. VI, No. 6, pp. 71-78, June 1963.

9. *Space Programs Summary*, No. 37-18, Vol. III, pp. 25-26.

10. Potter, R. S., *The Analysis and Matching of the Trimode Turnstile Junction*, NRL Report No. 4670, Naval Research Laboratories, Washington, D.C., December 1955.

11. Schuster, D., C. T. Stelzried, G. S. Levy, "The Determination of Noise Temperature of Large Antennas," *IRE Transaction on Antennas and Propagation*, AP-3, No. 3, May 1962.

12. *Space Programs Summary* No. 37-17, Vol. 3.

13. *Space Programs Summary* No. 37-9, Vol. 1.

14. *Research Summary* No. 36-4, Vol. 1.

15. Markowitz, W., R. G. Hall, L. Essen, and J. V. L. Parry, "Frequency of Cesium in Terms of Ephemeris Time," *Physical Review Letters*, Vol. 1, No. 3, pp. 705-706, August 1958.

16. *Space Programs Summary* No. 37-15, Vol. III.

17. Stevens, R., and W. K. Victor, editors, *The Goldstone Station Communications and Tracking System for Project Echo*, Technical Report No. 32-59, Jet Propulsion Laboratory, Pasadena, California, December 1, 1960.

18. *The Exploration of Space by Radio*, Hanbury, Brown, and Lovell, Wiley, 1958, p. 29

19. Goldstein, R. M., *Radar Exploration of Venus*, Technical Report 32-280, Jet Propulsion Laboratory, Pasadena, Calif., May 25, 1962.

20. *The Measurement of Power Spectra*, Blackman and Tukey, Dover, 1958.

REFERENCES (Cont'd)

21. Space Programs Summary 37-14, Vol I, p. 111.
22. Research Summary No. 36-14, p. 58, May 1962
23. Price, Robert, *IRE Transactions on Information Theory*, June 1958, p. 71.
24. Grieg, D., S. Metzger, R. Waer, *Proceedings of the Institute of Radio Engineers*, 36, 652, 1948.
25. *Reference Data for Radio Engineers*, 4th Edition (ITT, 1956), Reed and Russell, "Ultra High Frequency Propagation," John Wiley and Son, New York 1953
26. SPS 37-16, Vol III
27. Browne, I. C., J. V. Evans, J. K. Hargreaves, and W. A. S. Murray, "Radio Echoes from the Moon," *Proceedings of the Physical Society*, Vol. B69, p. 901, 1956.
28. Evans, J. V., "The Measurement of the Electron Content of the Ionosphere by the Lunar Radar Echo Method," *Proceedings of the Physical Society*, Vol. B69, p. 953, 1956.
29. Yeh, K. C., and G. W. Swenson, Jr., "Ionospheric Electron Content and its Variation Deduced from Satellite Observation," *Institute of Geophysical Research*, Vol. 66, p. 1061, 1961.
30. Daniels, F. B., and S. J. Bauer, "The Ionospheric Faraday Effect and Its Applications," *Journal of the Franklin Institute*, Vol. 267, p. 187, 1959.
31. Muhleman, D. O., *The Electrical Characteristics of the Atmosphere and Surface of Venus from Radar Observation, Icarus*, Vol. I, no. 5, 6, May 1963.
32. Drake, F. D., *10-CM Observations of Venus in 1961*, publications of the National Radio Astronomy Observatory, Vol. I, No. 11, February 1962.
33. *The American Ephemeris and Nautical Almanac for the Year 1962*, U.S. Government Printing Office, Washington, p. 317.
34. *Astronomical Papers of the National Almanac Office*, Vol. 6, Parts I and III.
35. Muhleman, D. O., D. Holdridge and N. Block, *The Astronomical Unit Determined by Radar Reflections from Venus*, Technical Report 32-221, Jet Propulsion Laboratory, Pasadena, Calif., March 1962.
36. *Astronomical Papers of the National Almanac Office, Vol. 16, Part I.*
37. *Astronomical Papers of the National Almanac Office*, Vol. 14 and 15, Part III.
38. Hudson, R. H., *Subtabulated Lunar and Planetary Ephemerides*, Technical Release No. 34-239, Jet Propulsion Laboratory, Pasadena, November 1960.
39. Peabody, P., and N. Block, *Planetary Position-Velocity Ephemerides Obtained by Special Perturbations*, ARS National Conference, November 1962.
40. Muhleman, D. O., D. Holdridge, and N. Block, "The Astronomical Unit Determined by Radar Reflections from Venus," *Astronomical Journal 67*, 4, 1962.
41. Muhleman, D. O., *The Relationship Between the System of Astronomical Constants and the Radar Determinations of the Astronomical Unit*, Technical Report No. 32-447, Jet Propulsion Laboratory, Pasadena, Calif., January 15, 1964 (presented at the IAU Symposium 21, Paris, May 1963).

REFERENCES (Cont'd)

42. Clemence, G. M., "On the System of Astronomical Constants," *Astronomical Journal* 53, 178, 1948.

43. Duncombe, R. L., Motions of Venus, *Astronomical Papers,* 16, Part I, 1958.

44. Clemence, G. M., Motion of Mercury, *Astronomical Papers,* 11, Part I, 1943.

45. Morgan, H. R., "The Earth's Perihelion Motion," *Astronomical Journal* 51, 127, 1945.

46. Brower, D., and P. Peabody; unpublished data, 1962.

47. Holdridge, D., unpublished data, 1962.

48. Brower, D., and G. M. Clemence, *Methods of Celestial Mechanics,* Academic Press, New York, 1961.

49. Muhleman, D. O., *Radar Investigations of Venus,* Thesis, Harvard University, 1963.

APPENDIX A.

Venus Spectrograms

R. Goldstein

The figures in this Appendix are all spectograms taken with either the spectrometer, or range-gated spectrometer, both of which are described in Sec. IV-A. All of the experimental data is presented here. The first spectrogram was taken October 1, and they were taken almost every day thereafter until the experiment terminated on December 15.

The integration time for these experiments varied from ten minutes to several hours. The arrows marked on the abscissa represent the predicted limb-to-limb bandwidth under the assumption of retrograde rotation with a period of 250 days.

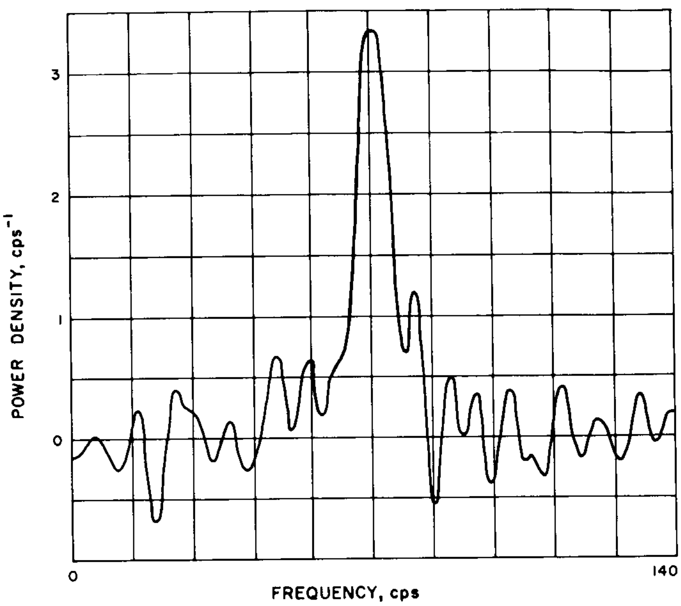

Fig. A-1. Spectrogram for October 1. Integration time: 10 min.

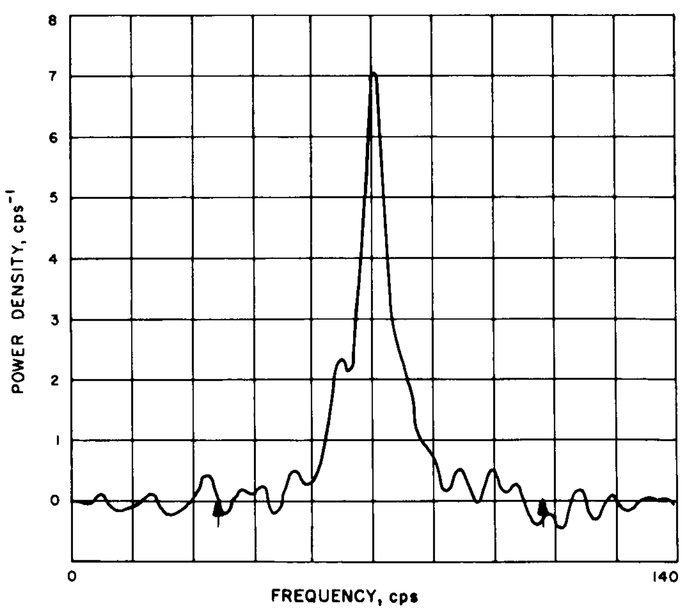

Fig. A-2. Spectrogram for October 8. Integration time: 56 min.

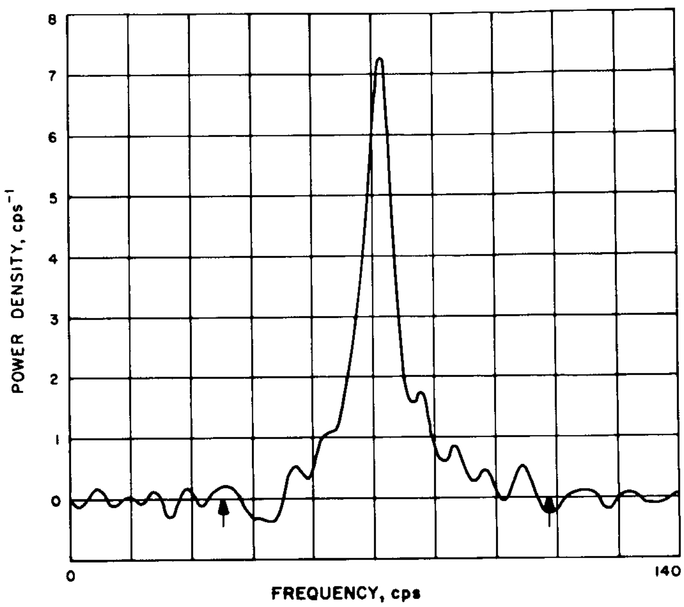

Fig. A-3. Spectrogram for October 9. Integration time: 75 min.

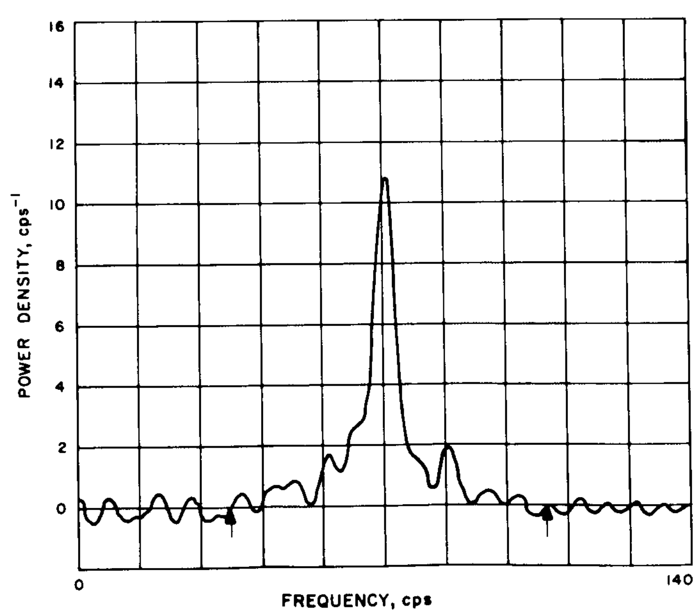

Fig. A-4. Spectrogram for October 10. Integration time: 40 min.

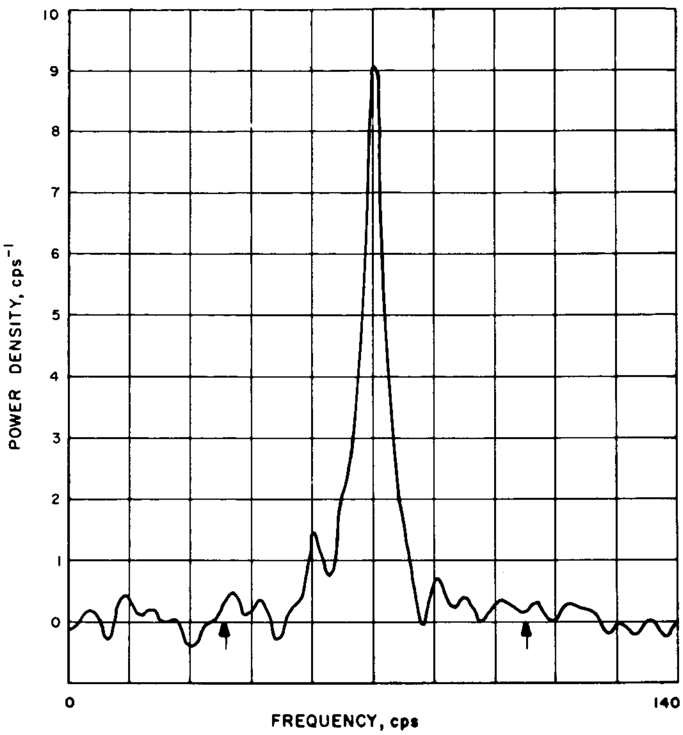

Fig. A-5. Spectrogram for October 12. Integration time: 64 min.

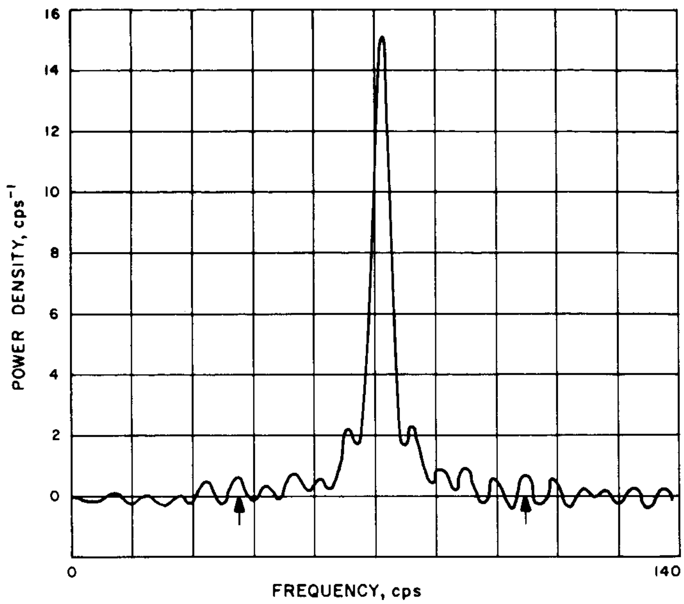

Fig. A-7. Spectrogram for October 16. Integration time: 54 min.

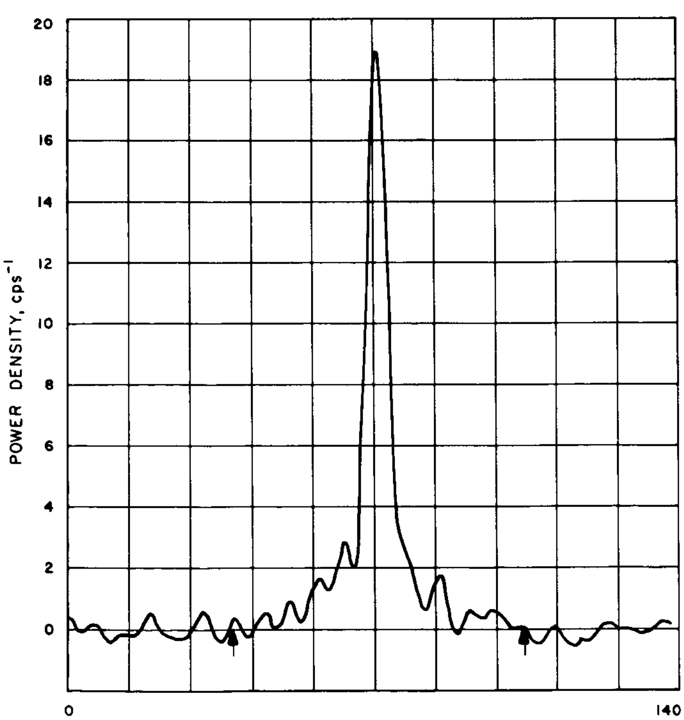

Fig. A-6. Spectrogram for October 15. Integration time: 49 min.

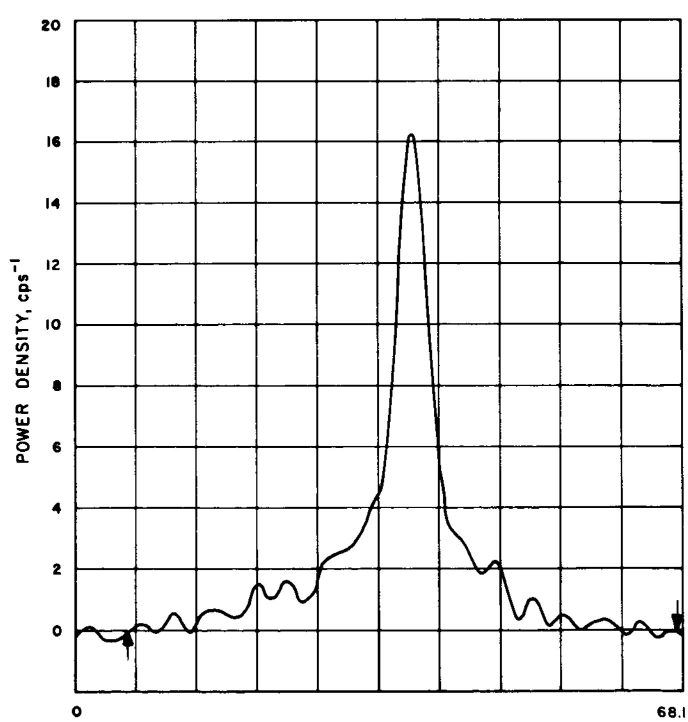

Fig. A-8. Spectrogram for October 17. Integration time: 78 min.

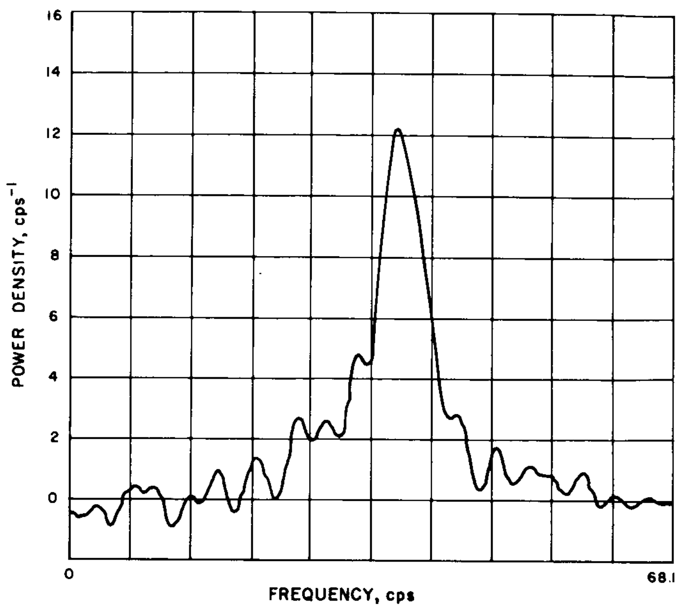

Fig. A-9. Spectrogram for October 18. Integration time: 41 min.

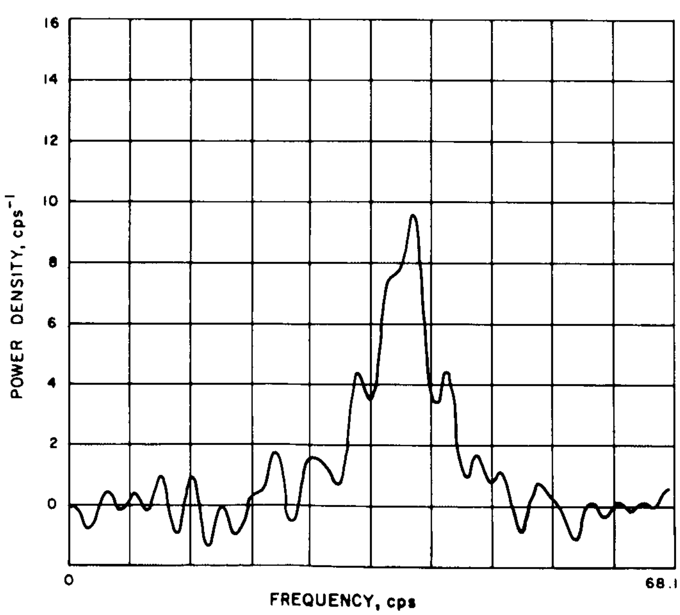

Fig. A-10. Spectrogram for October 19. Integration time: 16 min.

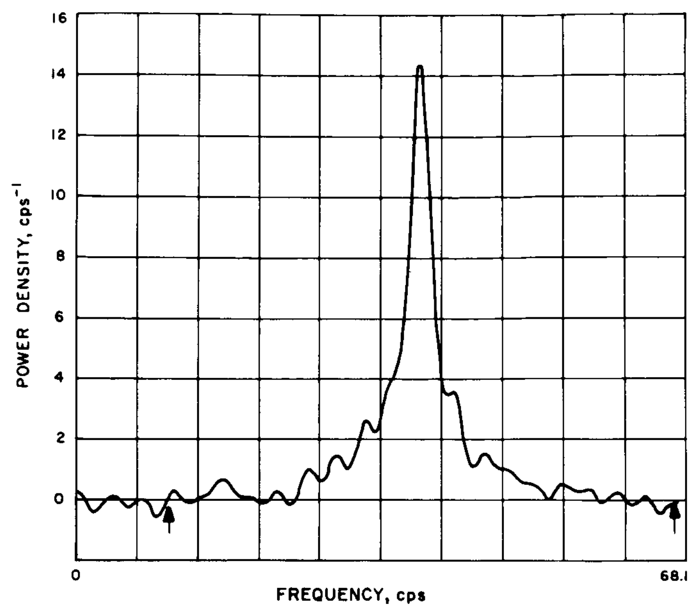

Fig. A-11. Spectrogram for October 22. Integration time: 27 min.

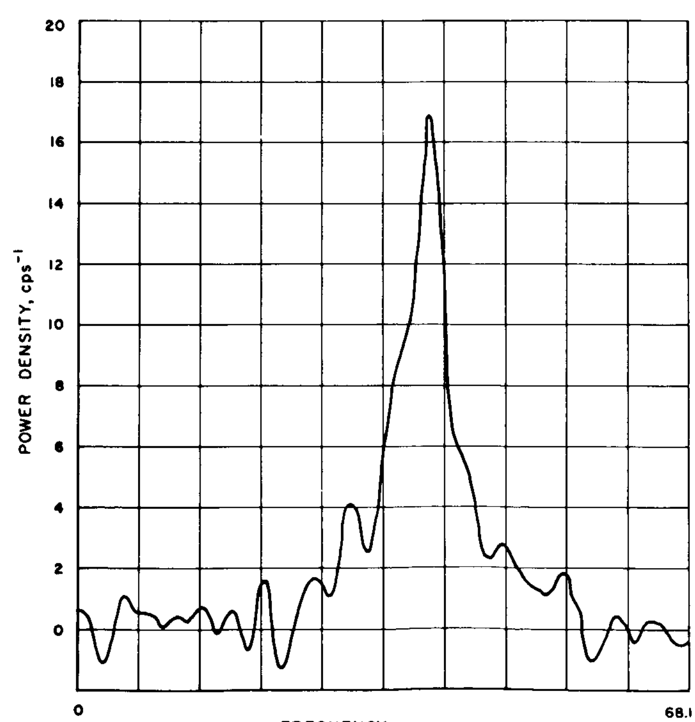

Fig. A-12. Spectrogram for October 23. Integration time: 16 min.

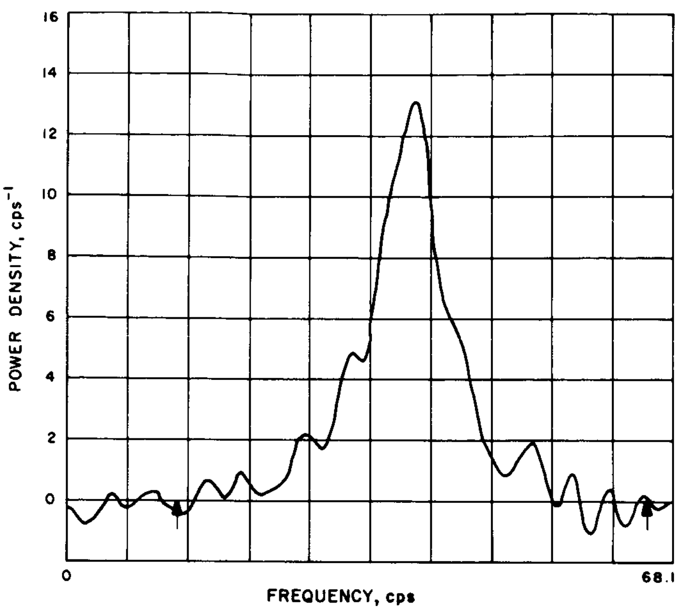

Fig. A-13. Spectrogram for October 24. Integration time: 21 min.

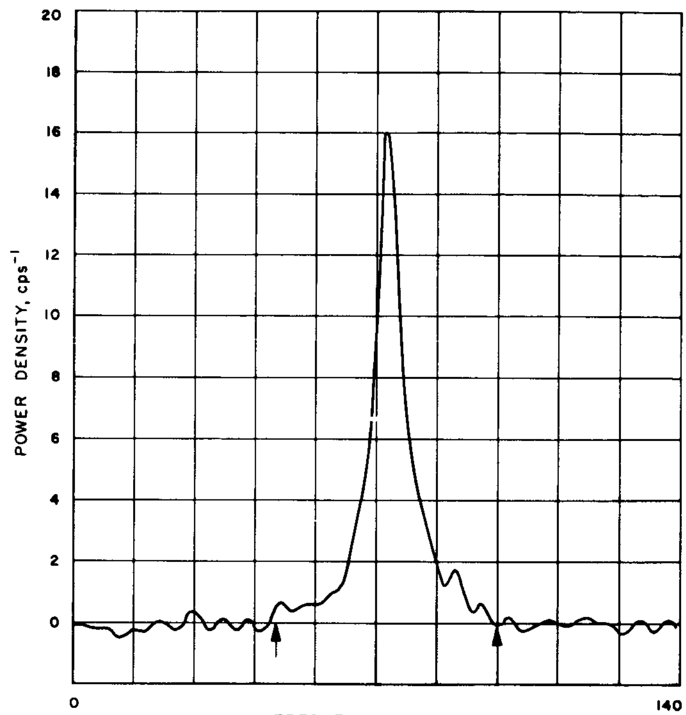

Fig. A-15. Spectrogram for October 26. Integration time: 41 min.

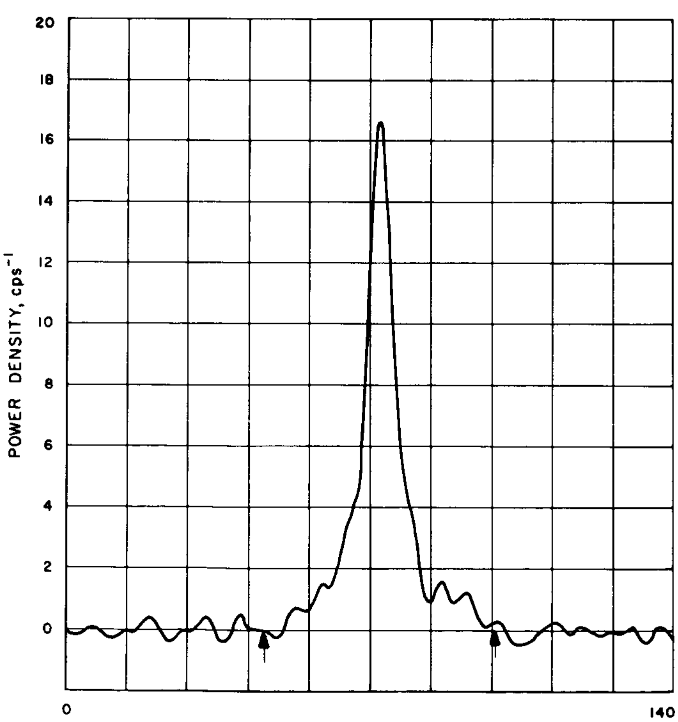

Fig. A-14. Spectrogram for October 25. Integration time: 31 min.

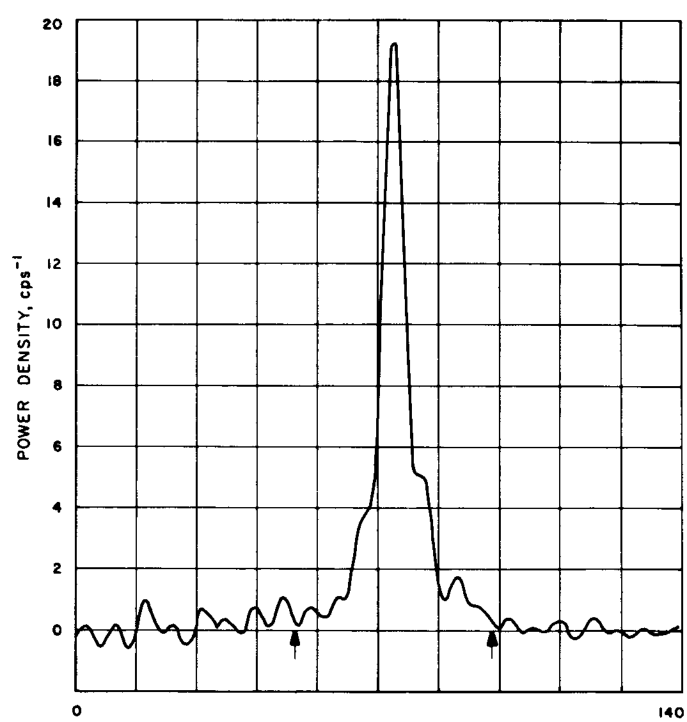

Fig. A-16. Spectrogram for October 29. Integration time: 30 min.

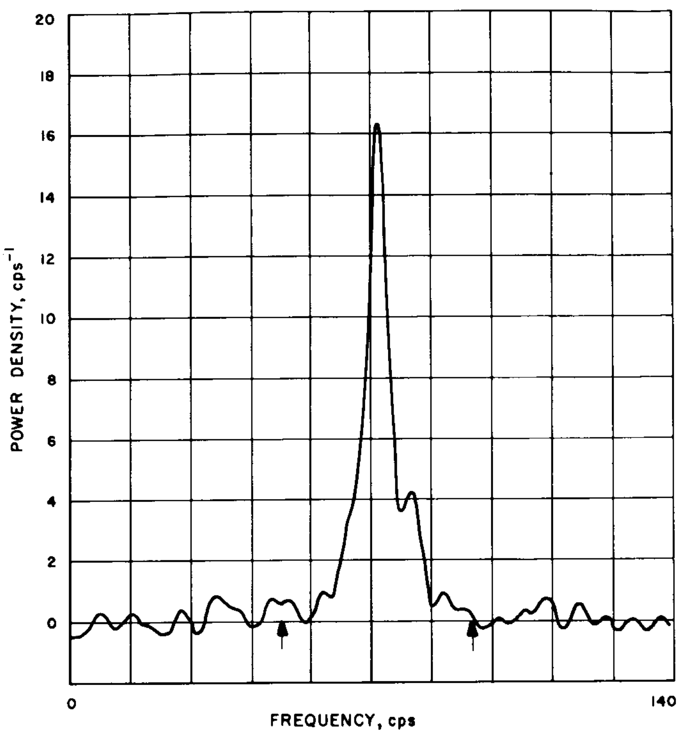

Fig. A-17. Spectrogram for October 30. Integration time: 25 min.

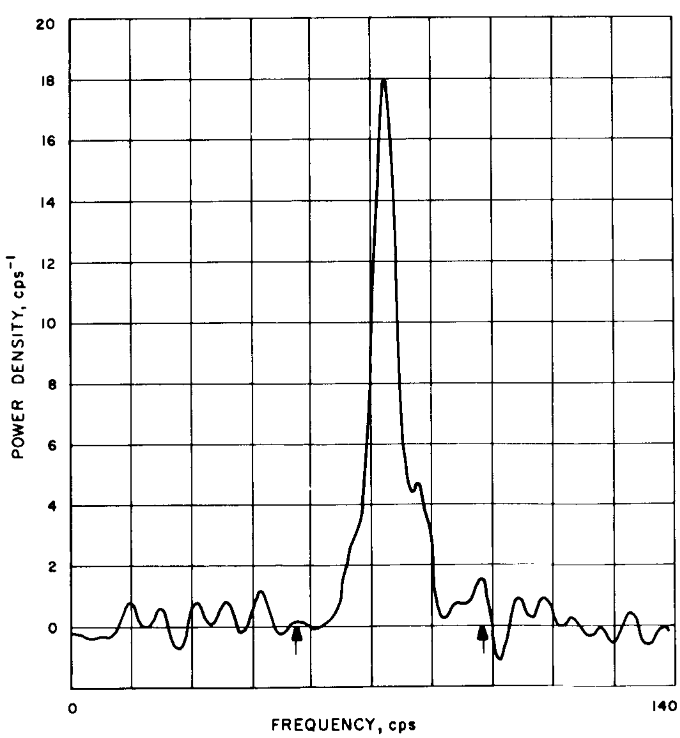

Fig. A-18. Spectrogram for October 31. Integration time: 14 min.

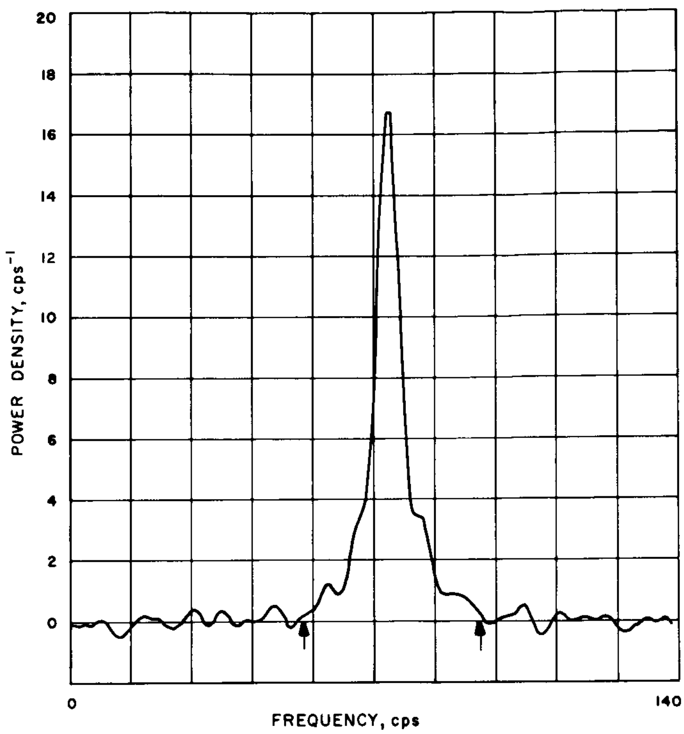

Fig. A-19. Spectrogram for November 1. Integration time: 19 min.

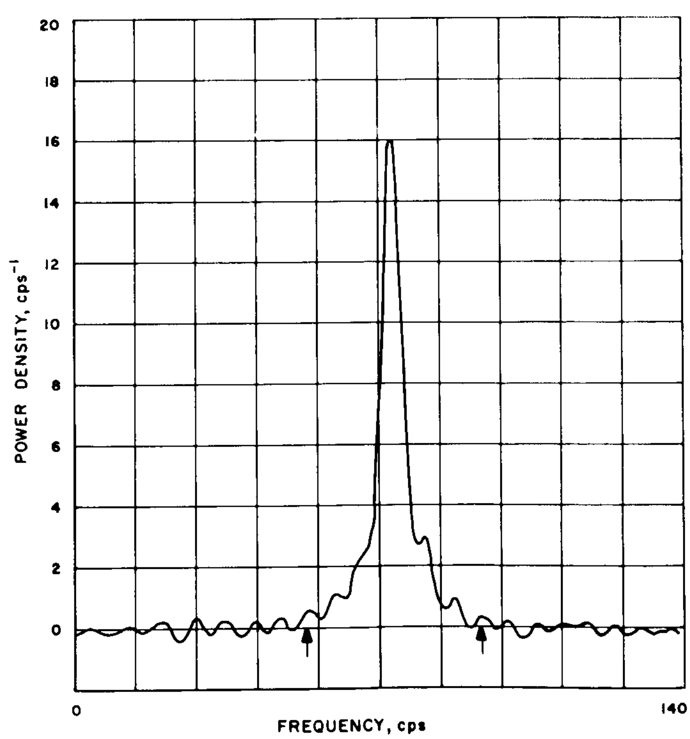

Fig. A-20. Spectrogram for November 2. Integration time: 24 min.

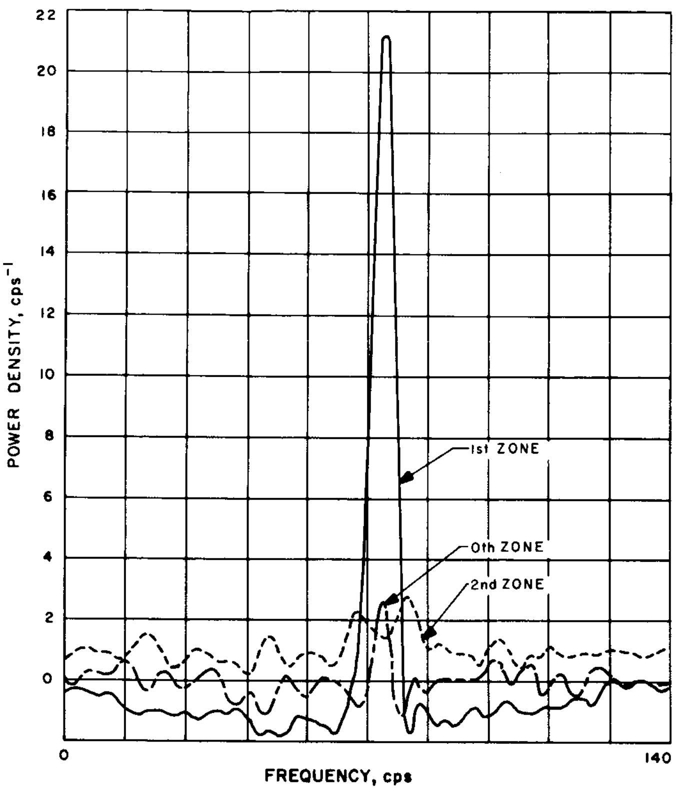

Fig. A-21. Range-gated spectra for November 2

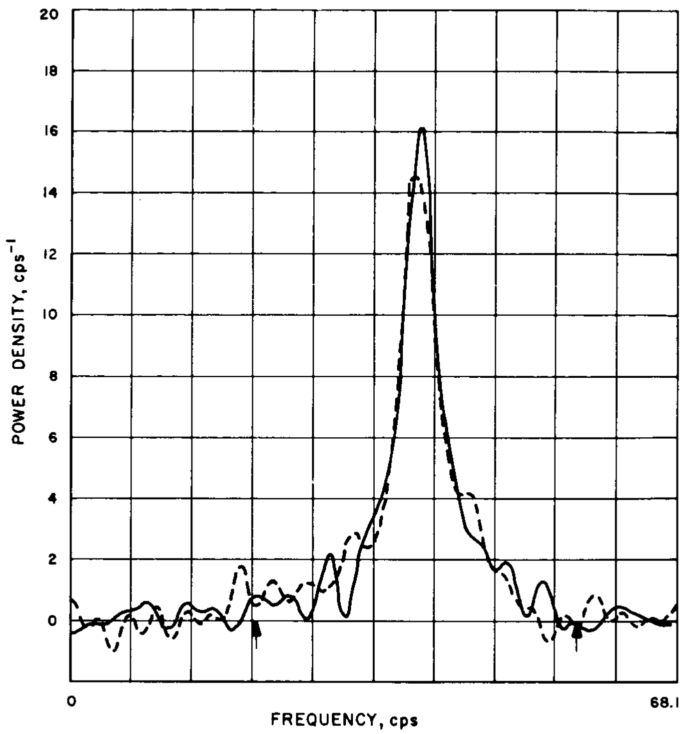

Fig. A-23. Two consecutive spectra, November 6, 4 min. each

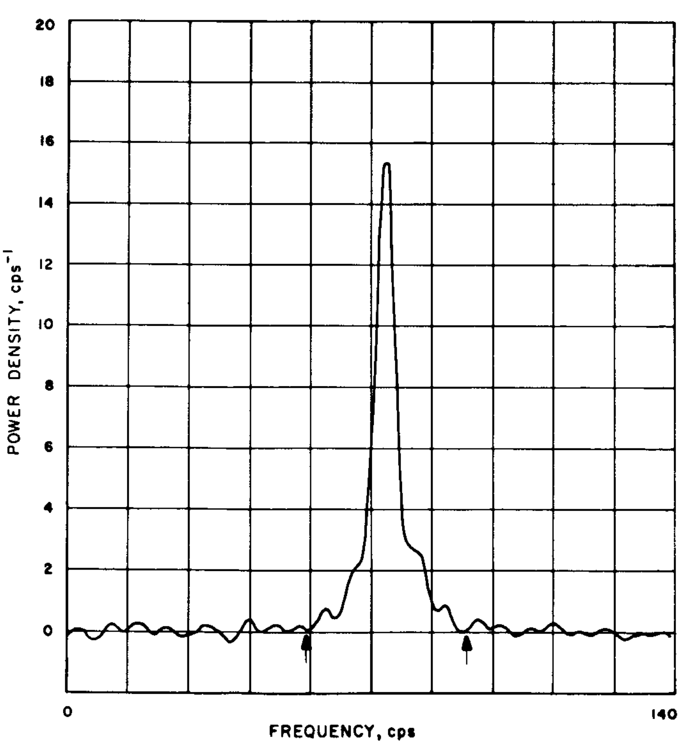

Fig. A-22. Spectrogram for November 5. Integration time: 37 min.

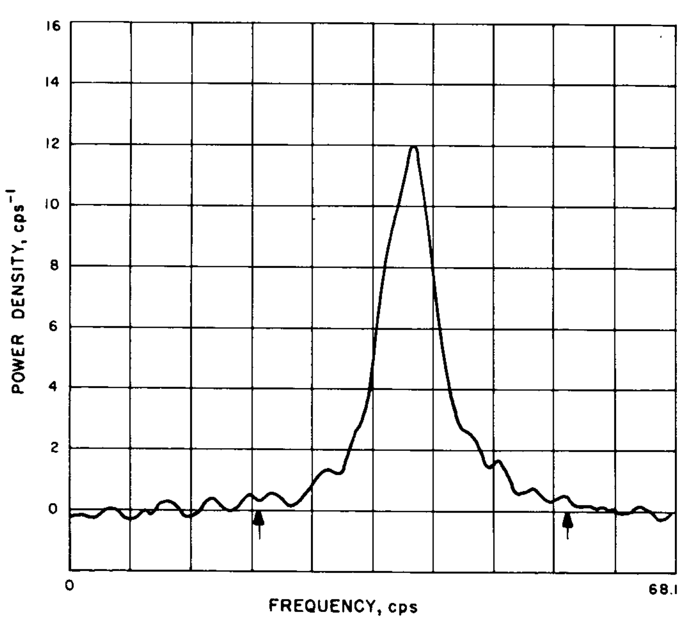

Fig. A-24. Spectrogram for November 7. Integration time: 23 min.

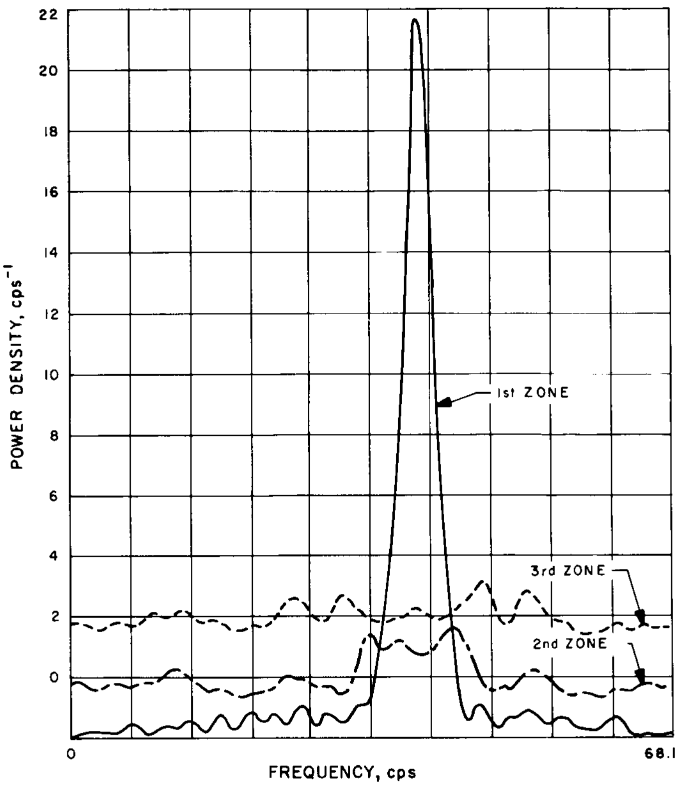

Fig. A-25. Range-gated spectra for November 7

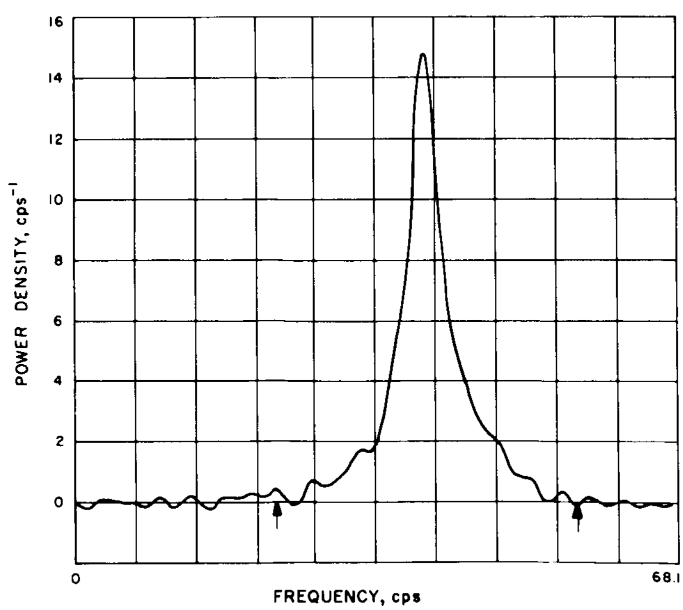

Fig. A-26. Spectrogram for November 9. Integration time: 27 min.

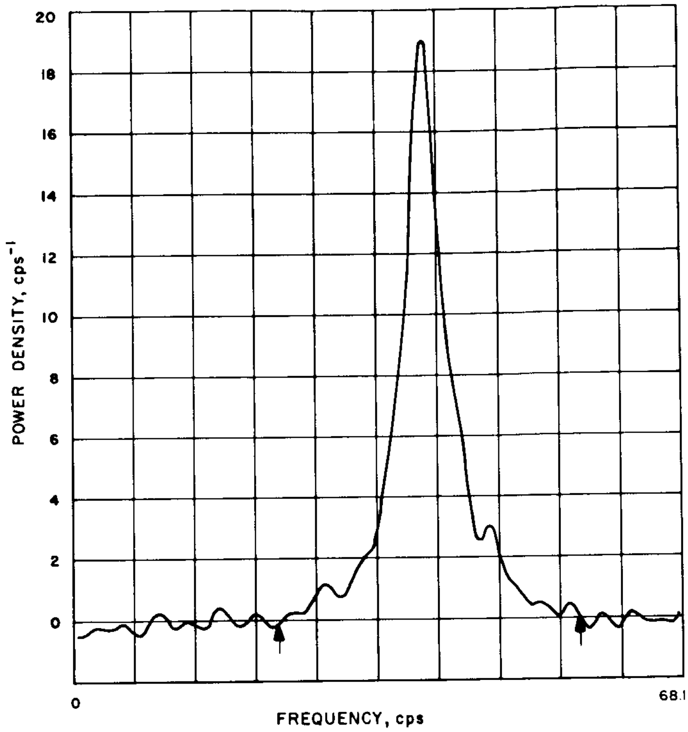

Fig. A-27. Spectrogram for November 10. Integration time: 31 min.

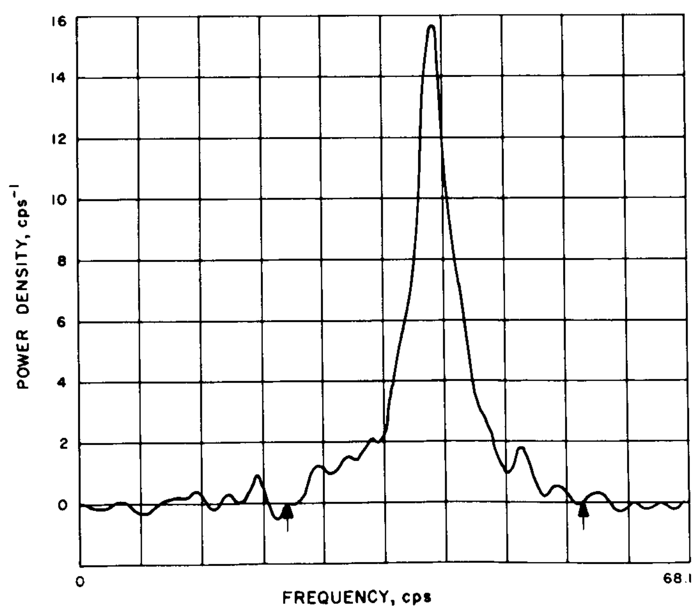

Fig. A-28. Spectrogram for November 12. Integration time: 18 min.

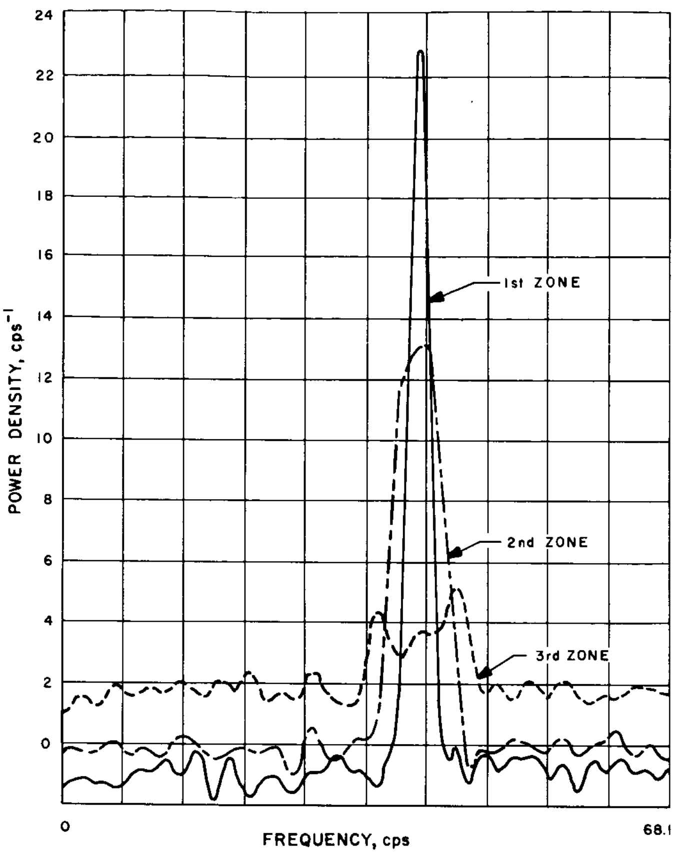

Fig. A-29. Range-gated spectra for November 12

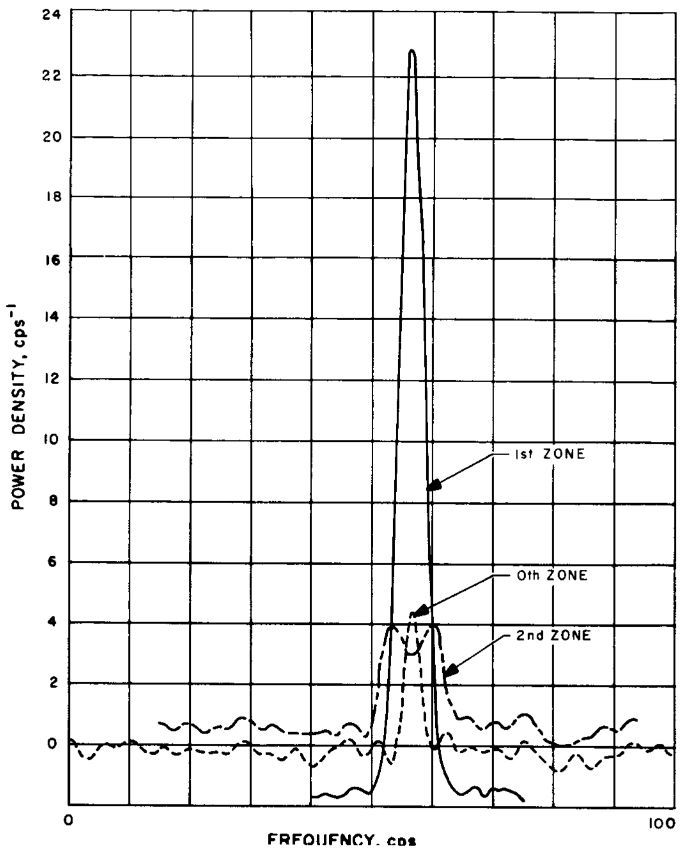

Fig. A-31. Range-gated spectra for November 14

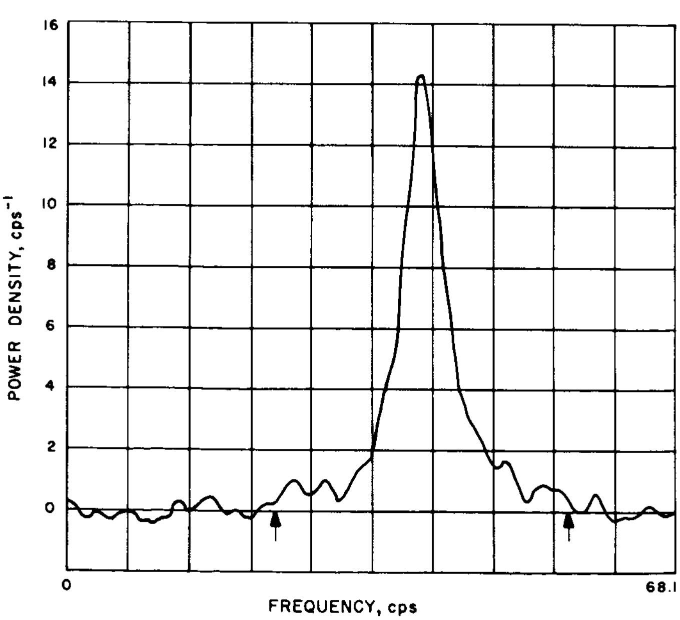

Fig. A-30. Spectrogram for November 14. Integration time: 27 min.

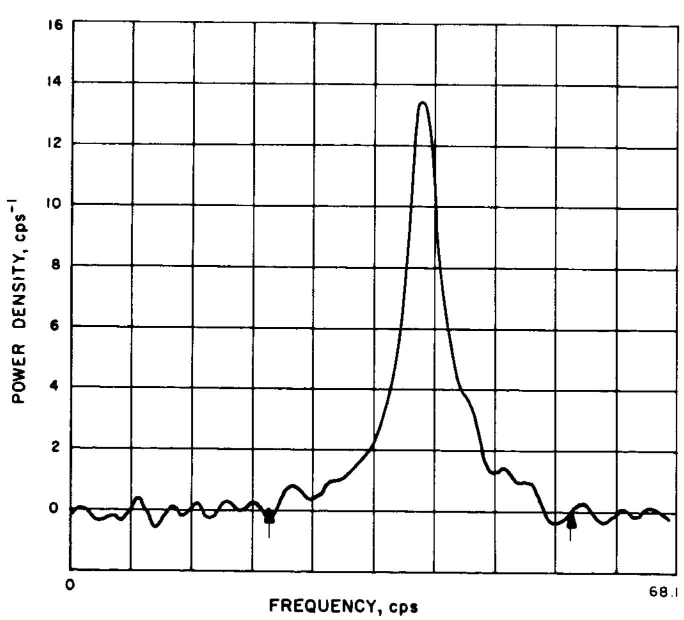

Fig. A-32. Spectrogram for November 15. Integration time: 18 min.

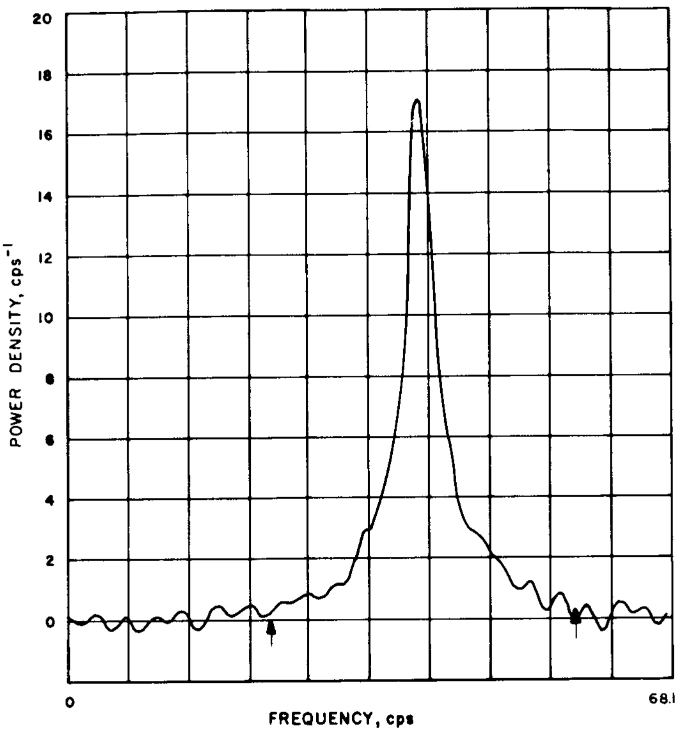

Fig. A-33. Spectrogram for November 17. Integration time: 18 min.

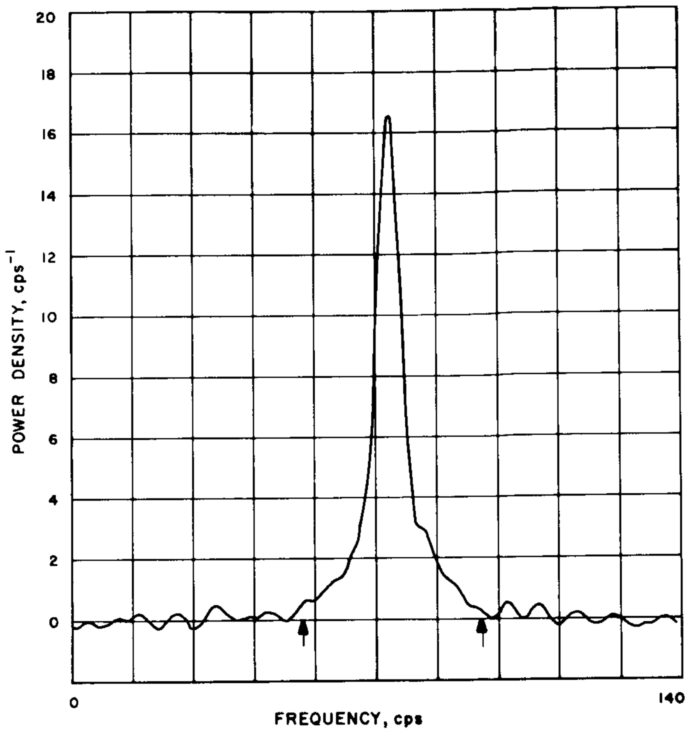

Fig. A-35. Spectrogram for November 23. Integration time: 28 min.

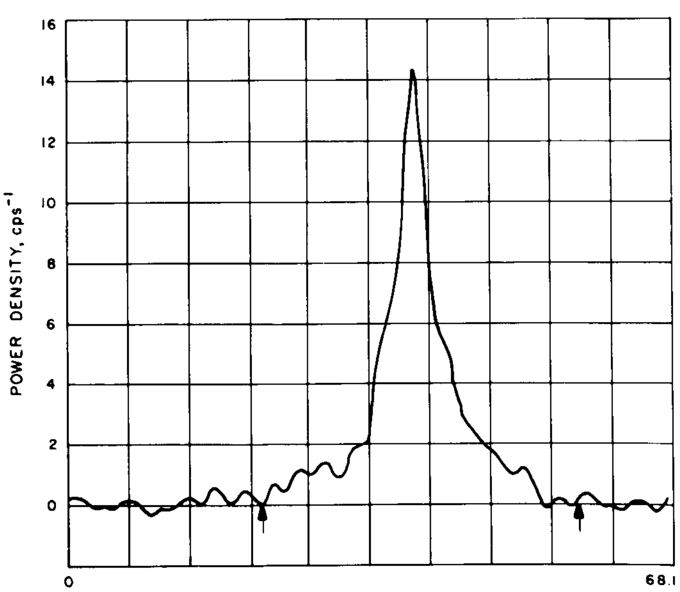

Fig. A-34. Spectrogram for November 19. Integration time: 23 min.

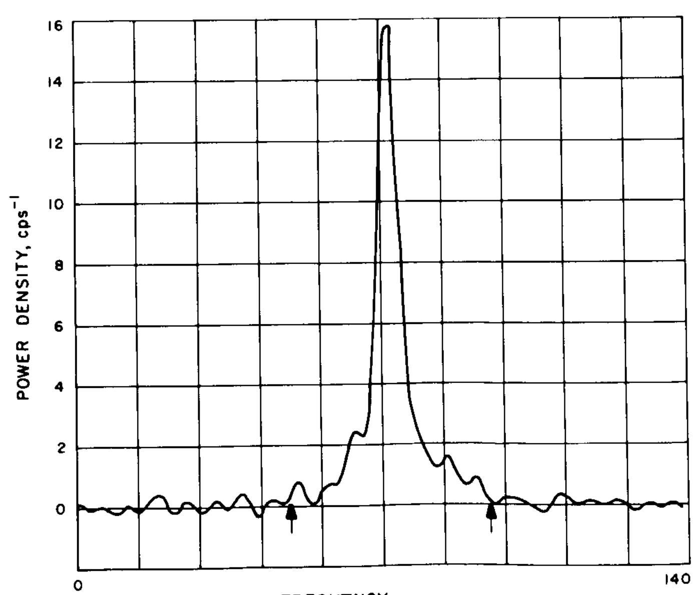

Fig. A-36. Spectrogram for November 26. Integration time: 29 min.

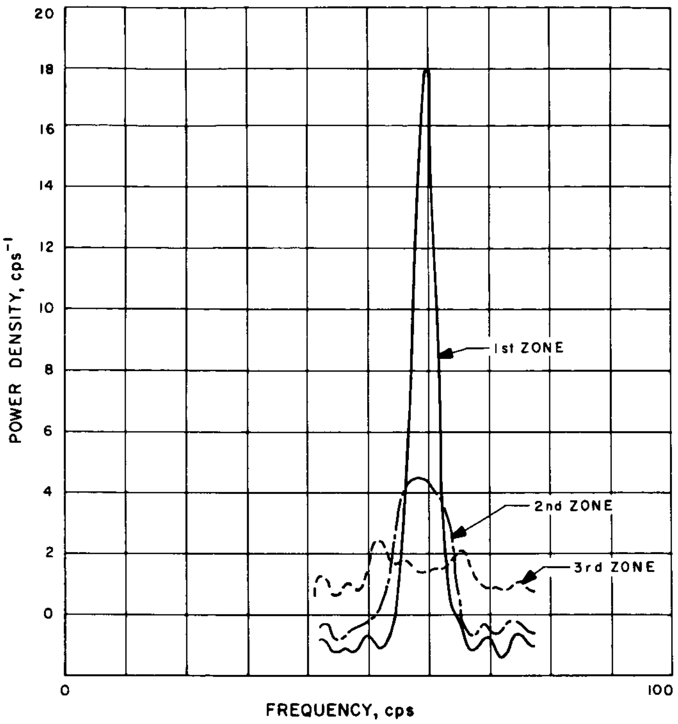

Fig. A-37. Range-gated spectra for November 26

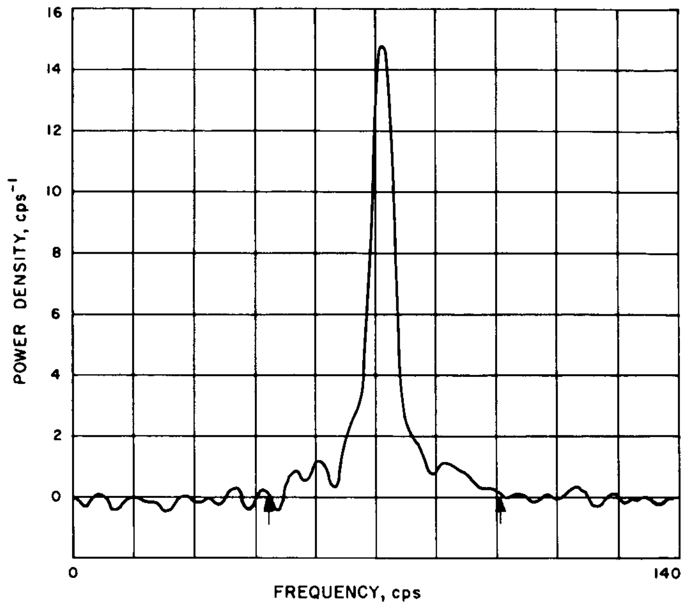

Fig. A-39. Spectrogram for November 30. Integration time: 25 min.

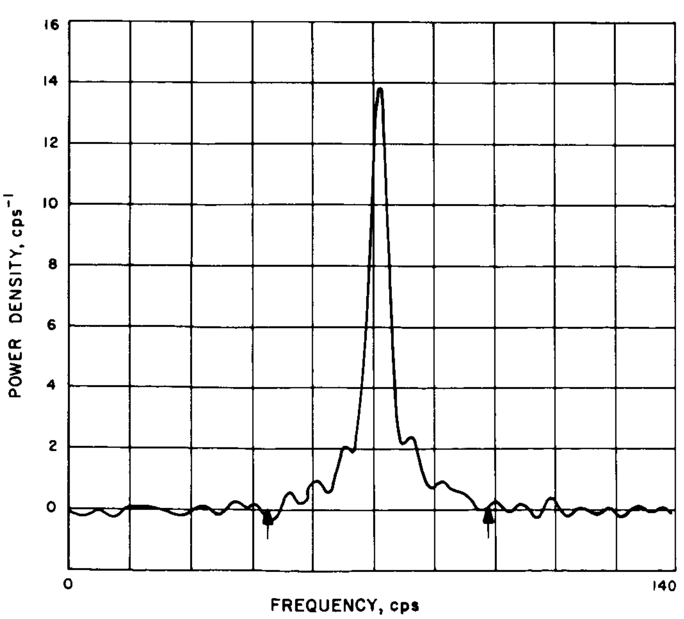

Fig. A-38. Spectrogram for November 29. Integration time: 10 min.

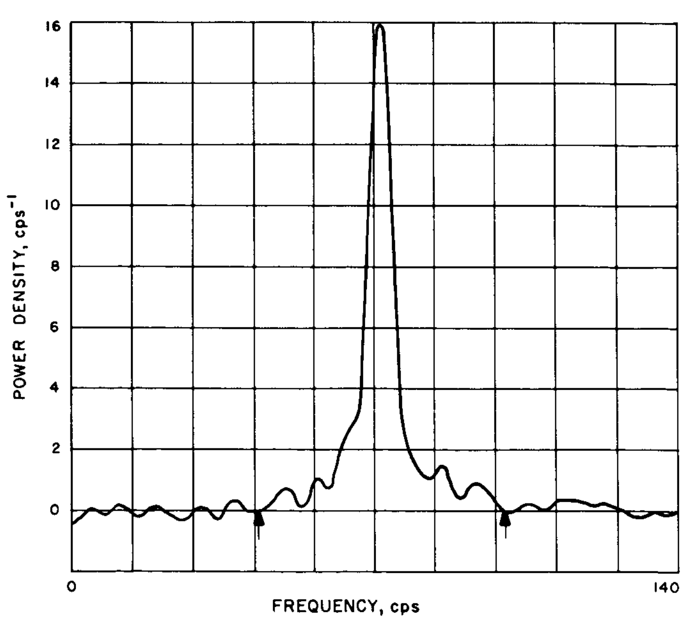

Fig. A-40. Spectrogram for December 3. Integration time: 27 min.

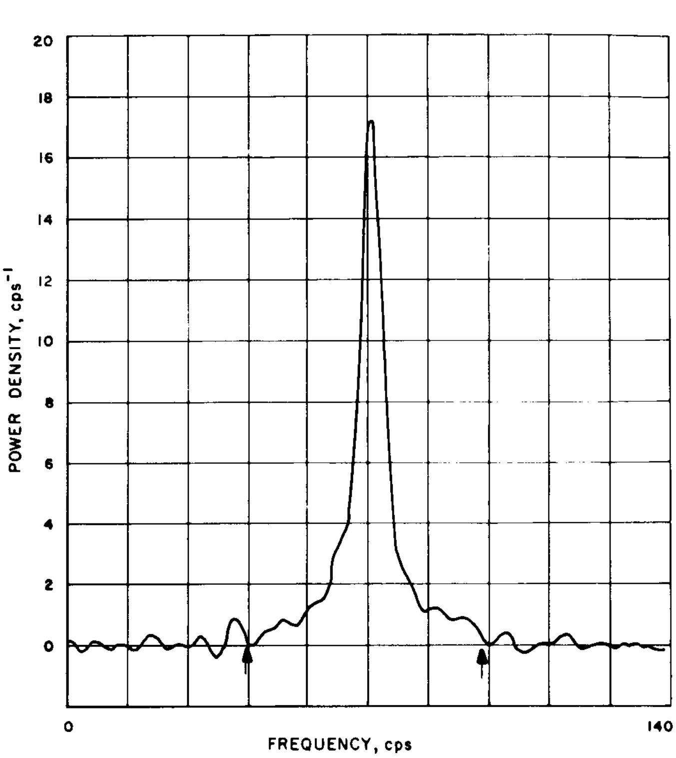

Fig. A-41. Spectrogram for December 4. Integration time: 44 min.

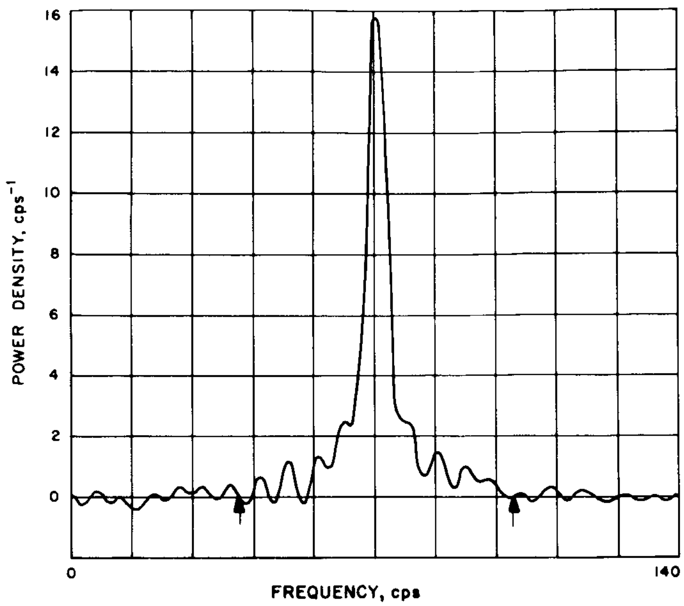

Fig. A-43. Spectrogram for December 7. Integration time: 68 min.

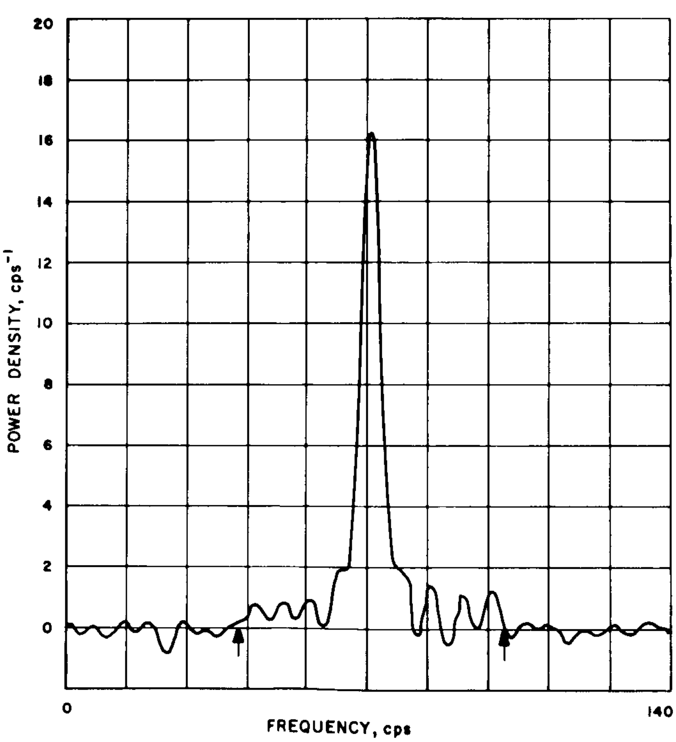

Fig. A-42. Spectrogram for December 6. Integration time: 23 min.

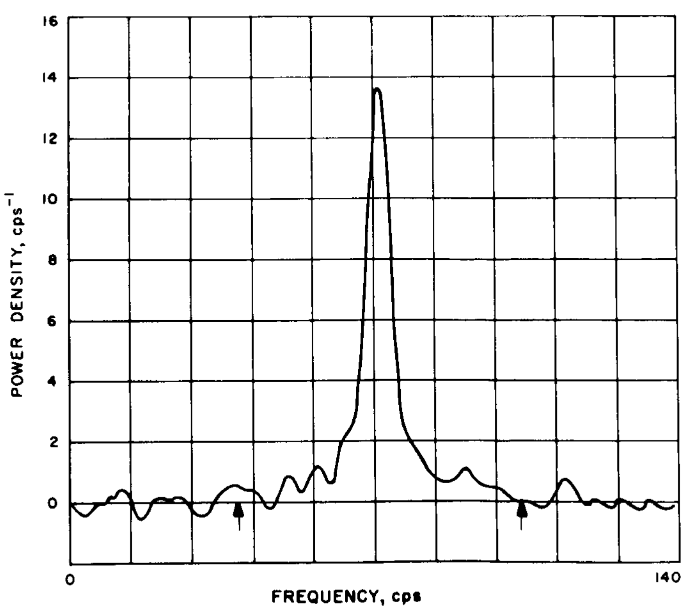

Fig. A-44. Spectrogram for December 8. Integration time: 47 min.

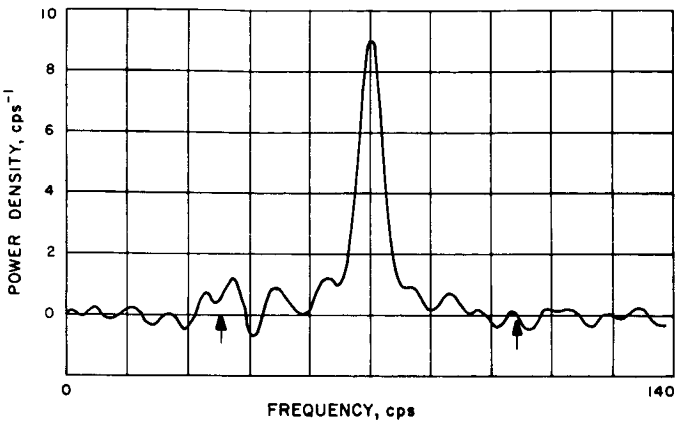

Fig. A-45. Spectrogram for December 11. Integration time: 24 min.

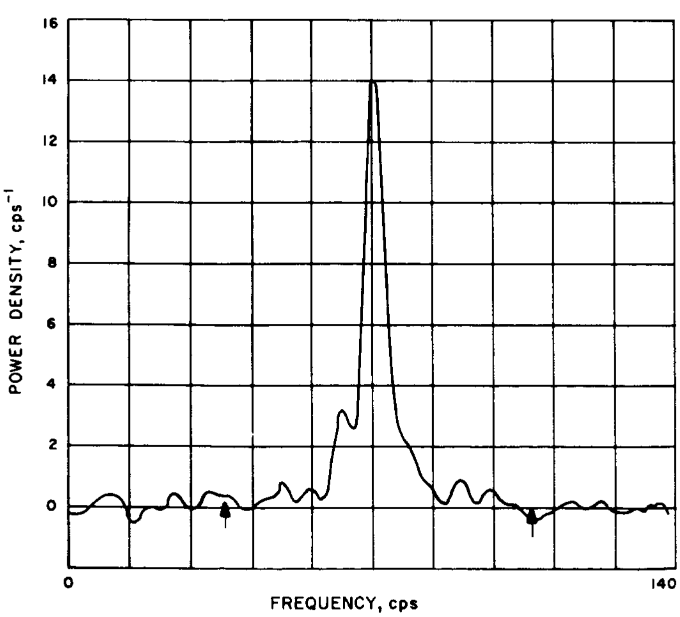

Fig. A-46. Spectrogram for December 12. Integration time: 31 min.

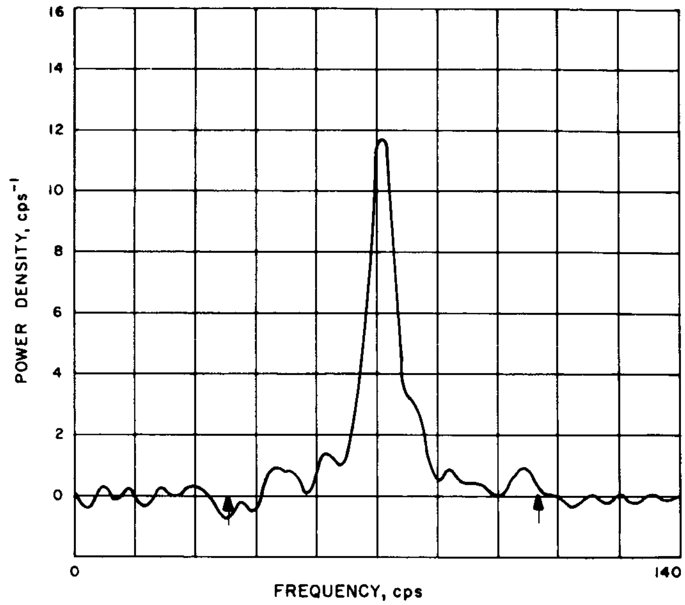

Fig. A-47. Spectrogram for December 13. Integration time: 32 min.

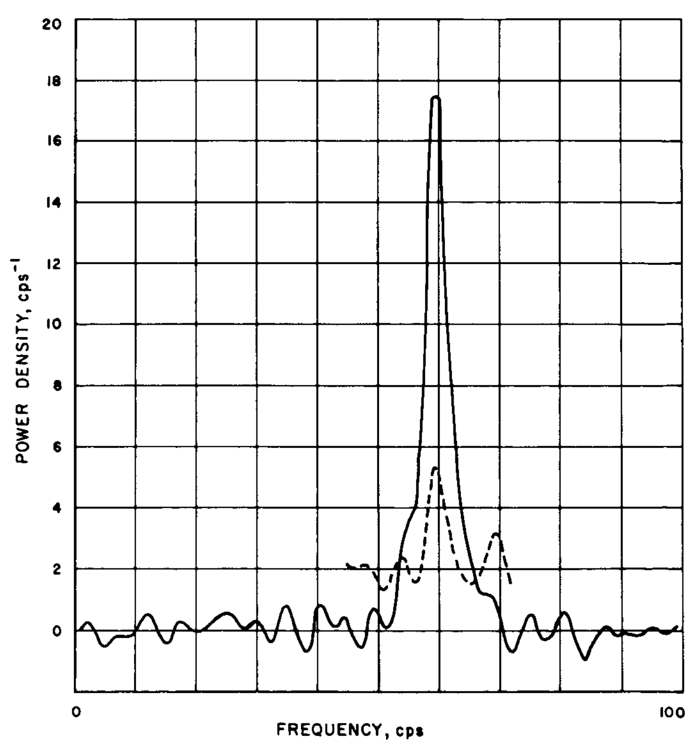

Fig. A-48. Range-gated spectra for December 12

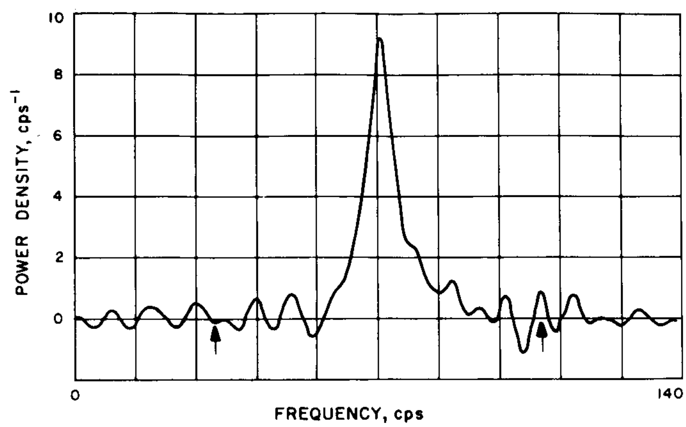

Fig. A-49. Spectrogram for December 15. Integration time: 33 min.

APPENDIX B.

Venus Continuous Wave Spectrum

R. L. Carpenter

Figures B-1 through B-30 show the CW spectra obtained during the 1962 Venus radar experiment. They were computed on the IBM 7094 computer with a frequency resolution of 1 cps. The ordinates are in arbitrary units of power density and the abscissa is frequency. The frequency scale is 2 cps per small division. The abscissa has been oriented so that the high frequency side of the spectrum corresponds to the approaching side of the planet and vice versa. For the spectra obtained from October 23, 1962 on the center frequency should be at 97.6 cps. Small deviations from this frequency indicate instability of the radar system's oscillators ($\sim \pm$ 1 cps) and/or errors in the astronomical unit and the ephemeris of Venus and the Earth.

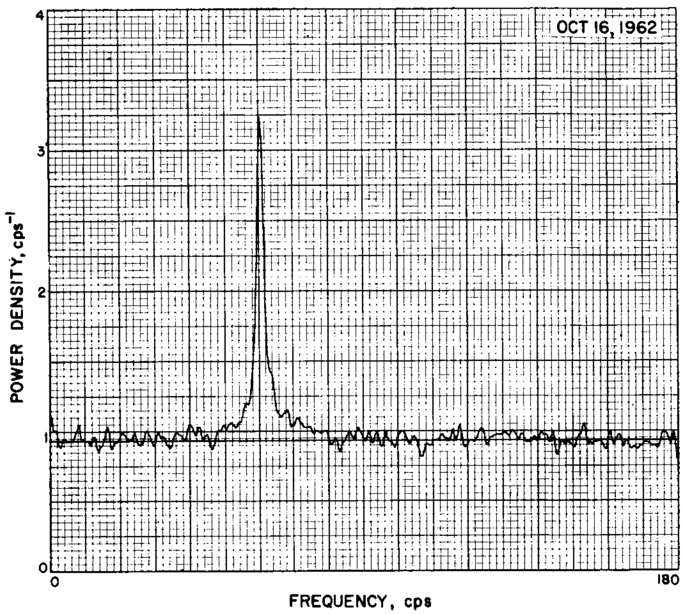

Fig. B-1. Venus CW spectrum, October 16

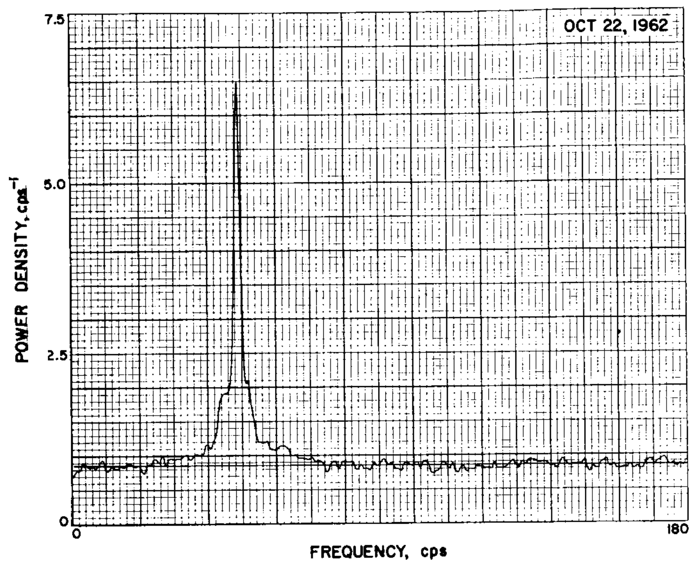

Fig. B-3. Venus CW spectrum, October 22

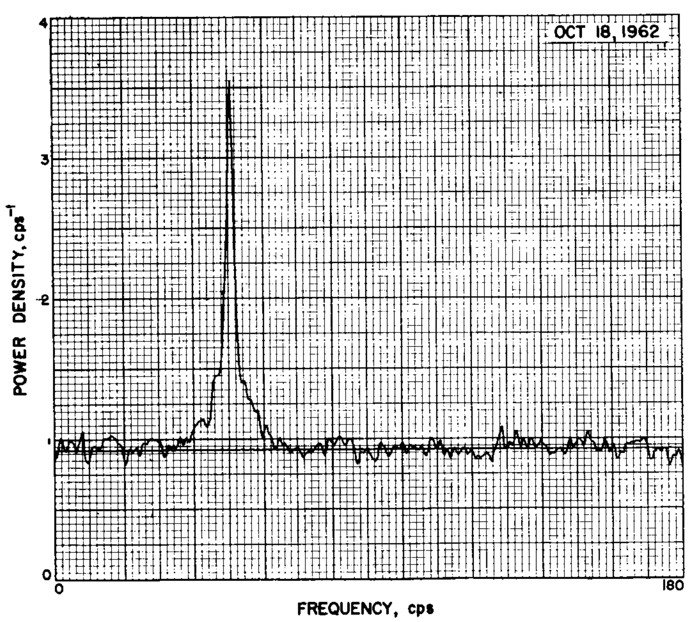

Fig. B-2. Venus CW spectrum, October 18

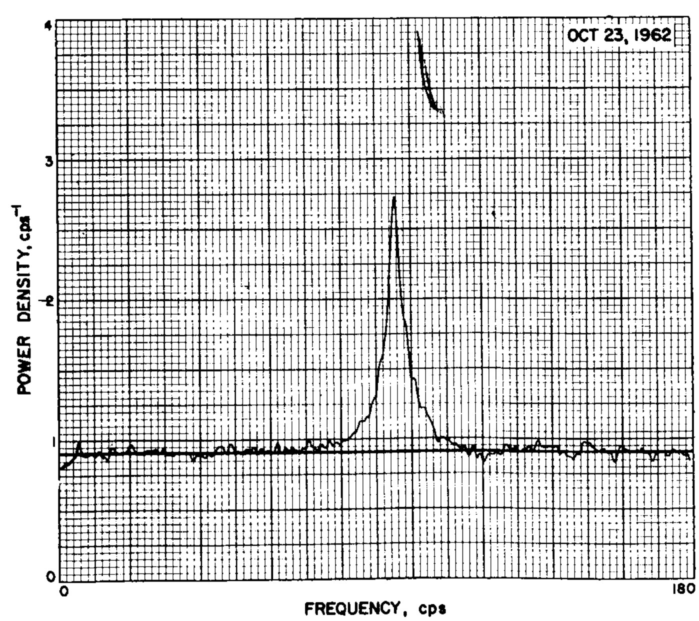

Fig. B-4. Venus CW spectrum, October 23

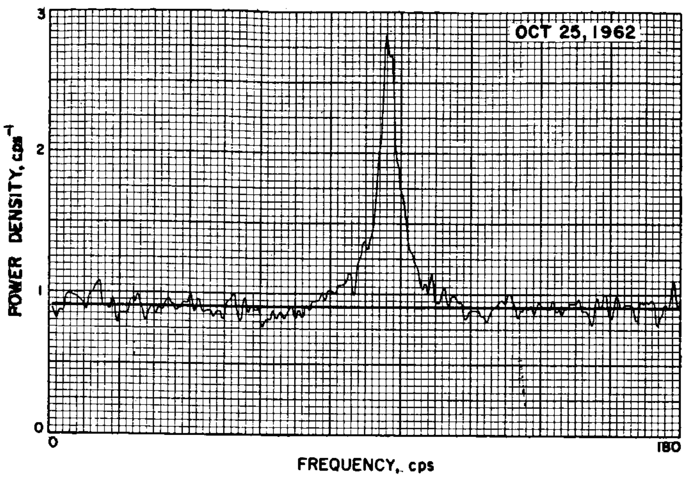

Fig. B-5. Venus CW spectrum, October 25

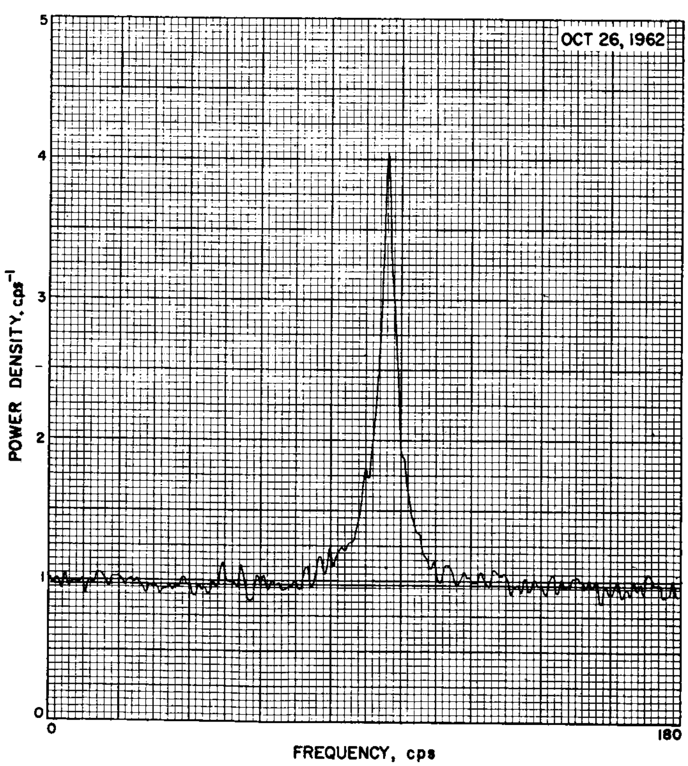

Fig. B-6. Venus CW spectrum, October 26

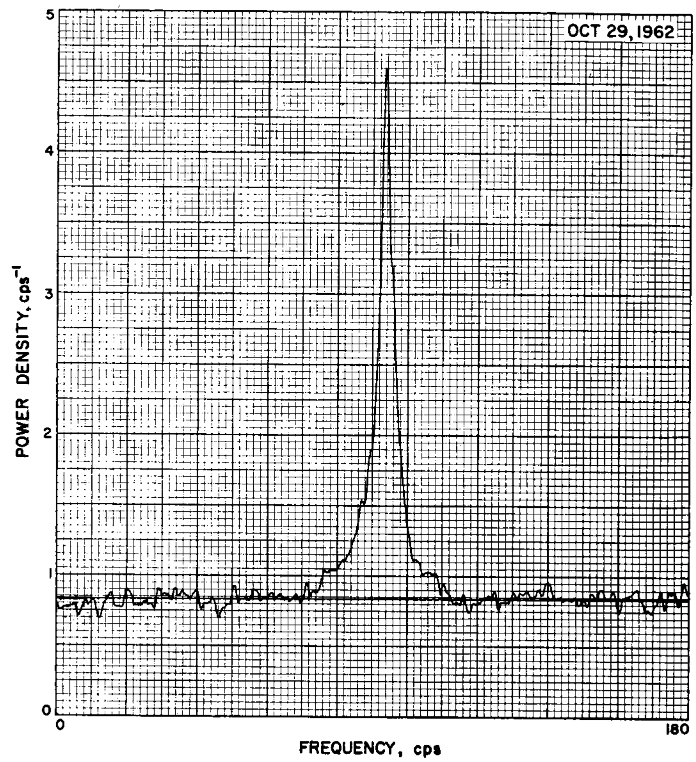

Fig. B-7. Venus CW spectrum, October 29

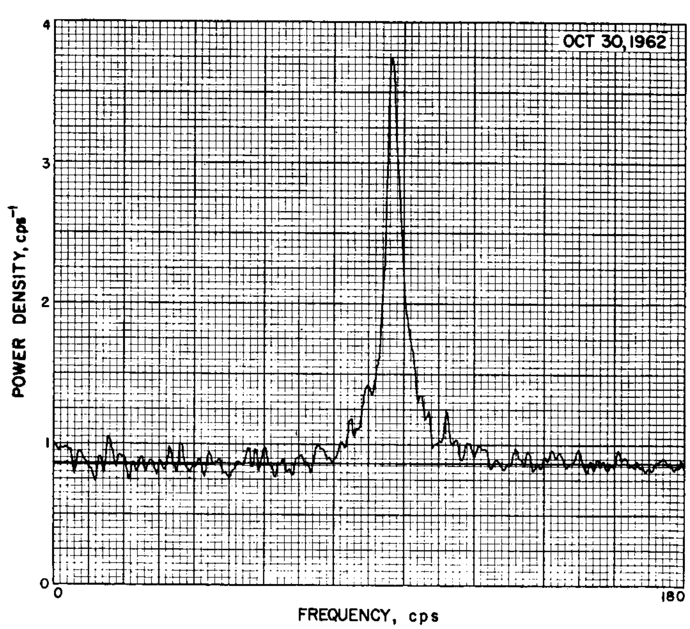

Fig. B-8. Venus CW spectrum, October 30

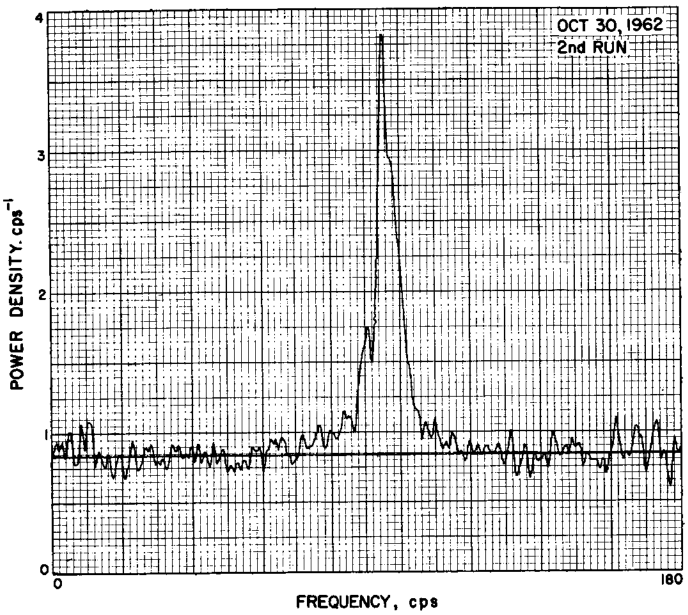

Fig. B-9. Venus CW spectrum, October 30 (2nd run)

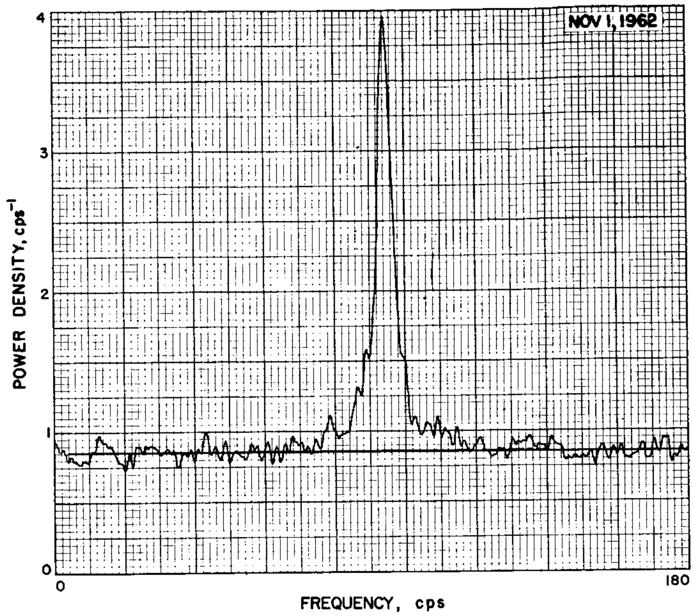

Fig. B-11. Venus CW spectrum, November 1

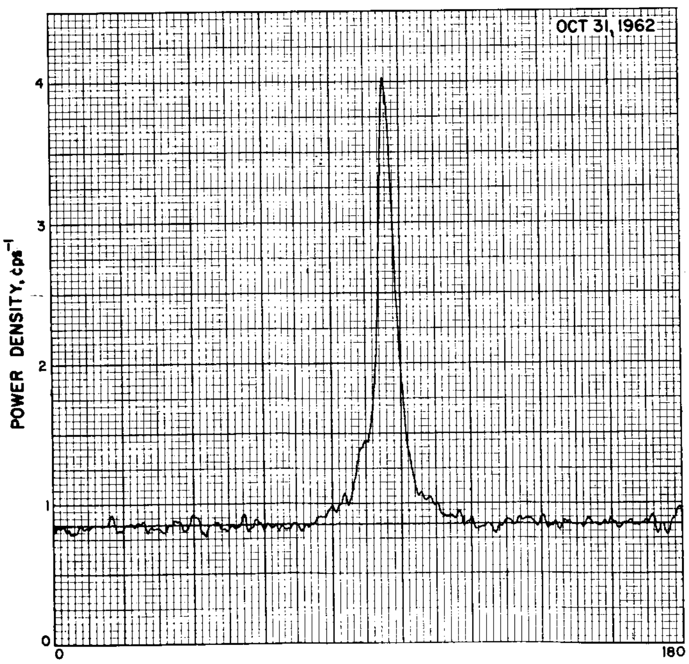

Fig. B-10. Venus CW spectrum, October 31

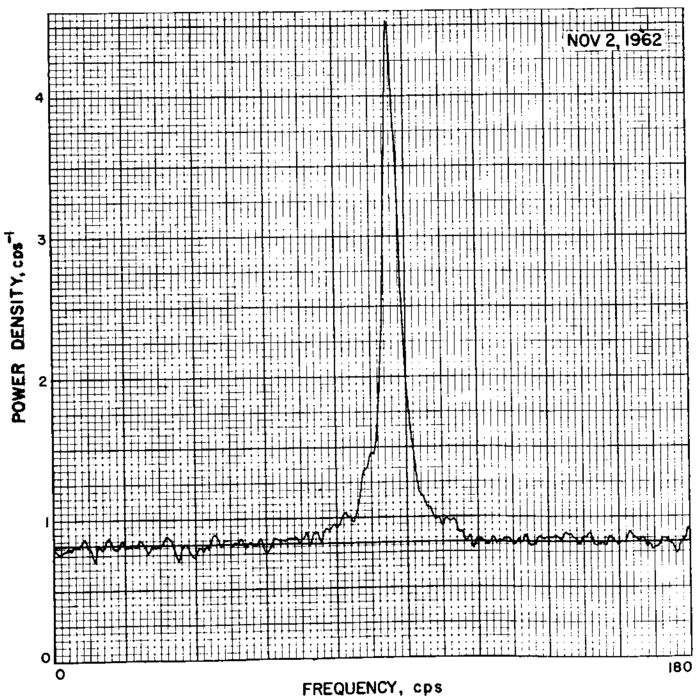

Fig. B-12. Venus CW spectrum, November 2

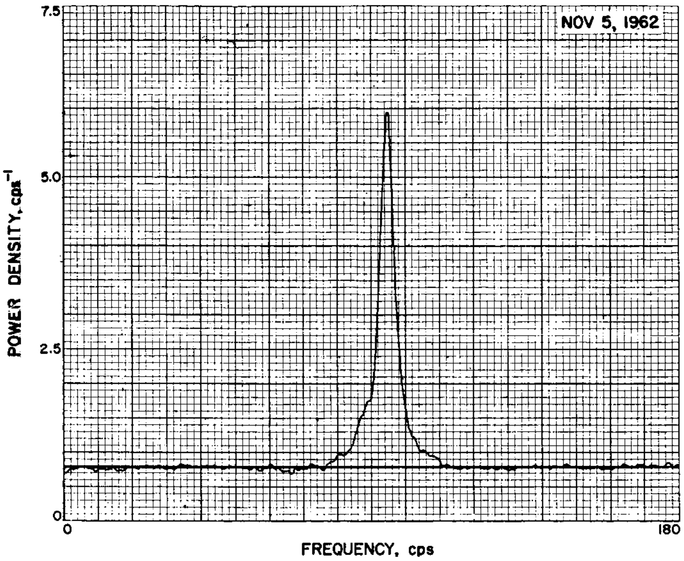

Fig. B-13. Venus CW spectrum, November 5

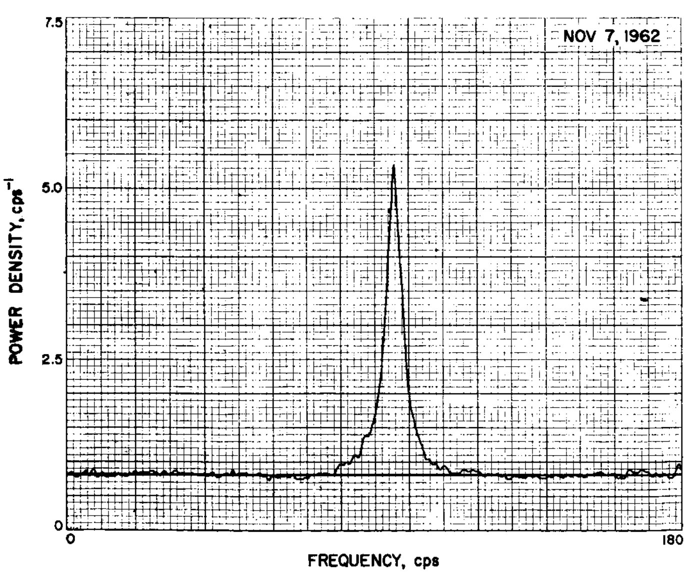

Fig. B-14. Venus CW spectrum, November 7

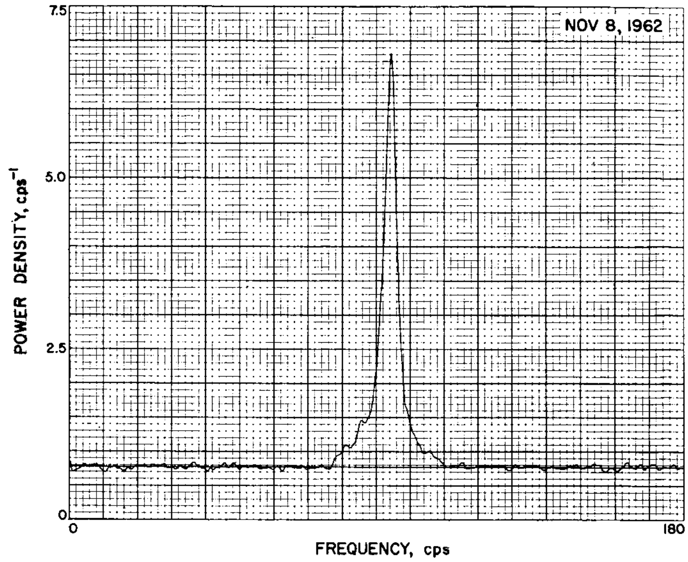

Fig. B-15. Venus CW spectrum, November 8

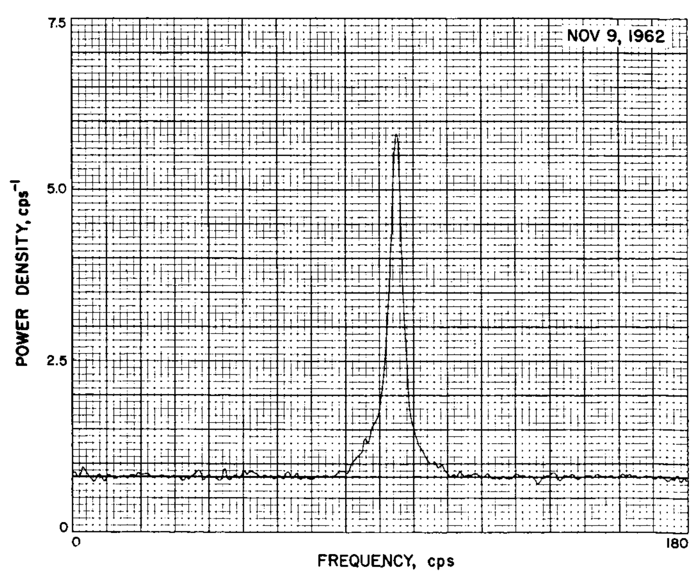

Fig. B-16. Venus CW spectrum, November 9

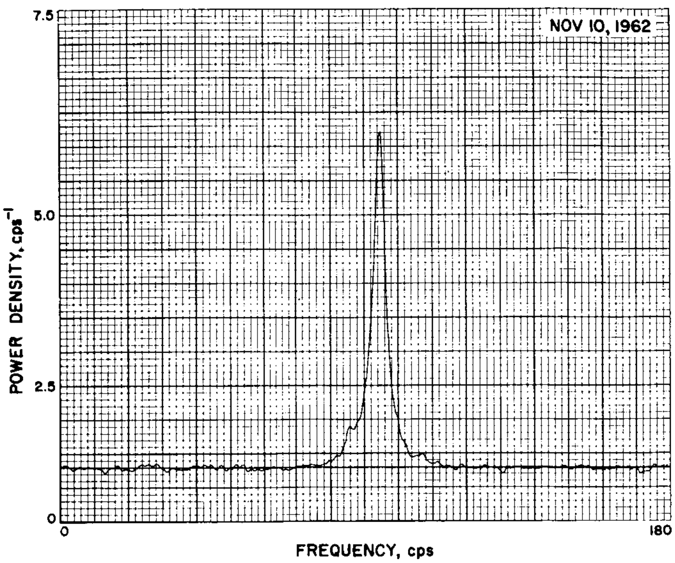

Fig. B-17. Venus CW spectrum, November 10

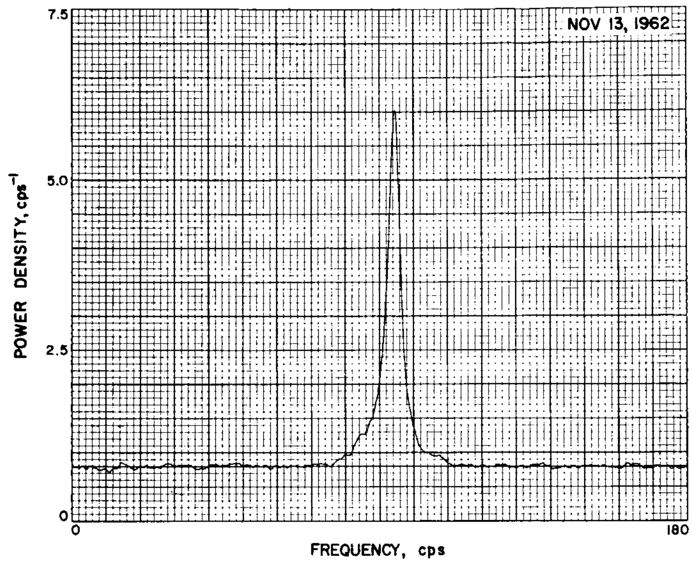

Fig. B-19. Venus CW spectrum, November 13

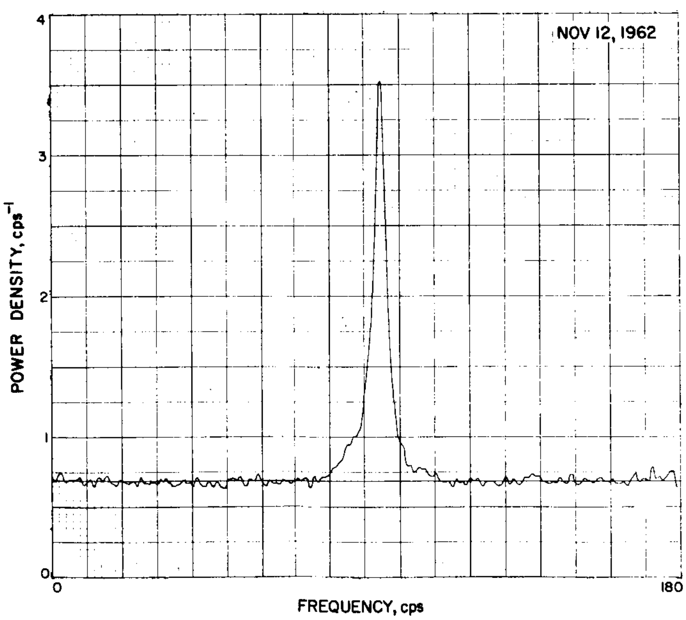

Fig. B-18. Venus CW spectrum, November 12

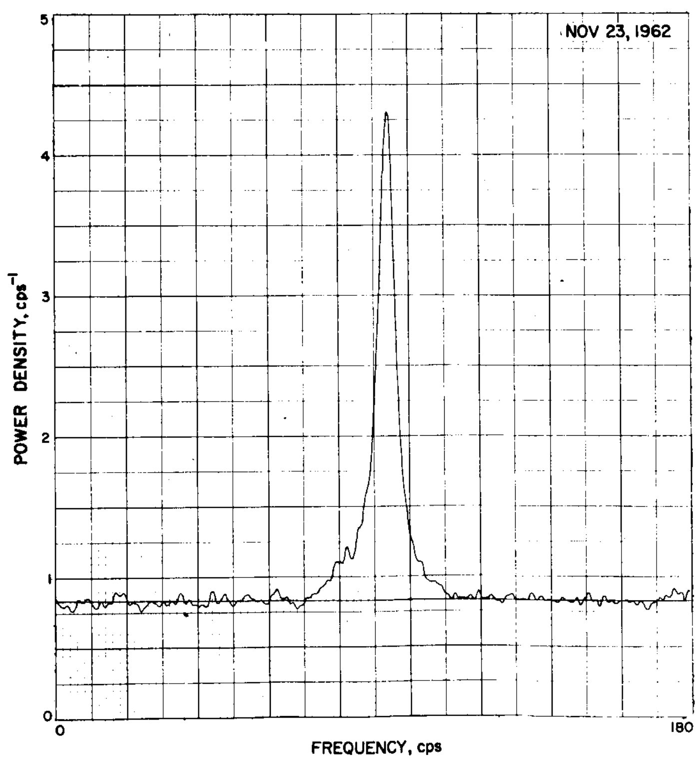

Fig. B-20. Venus CW spectrum, November 23

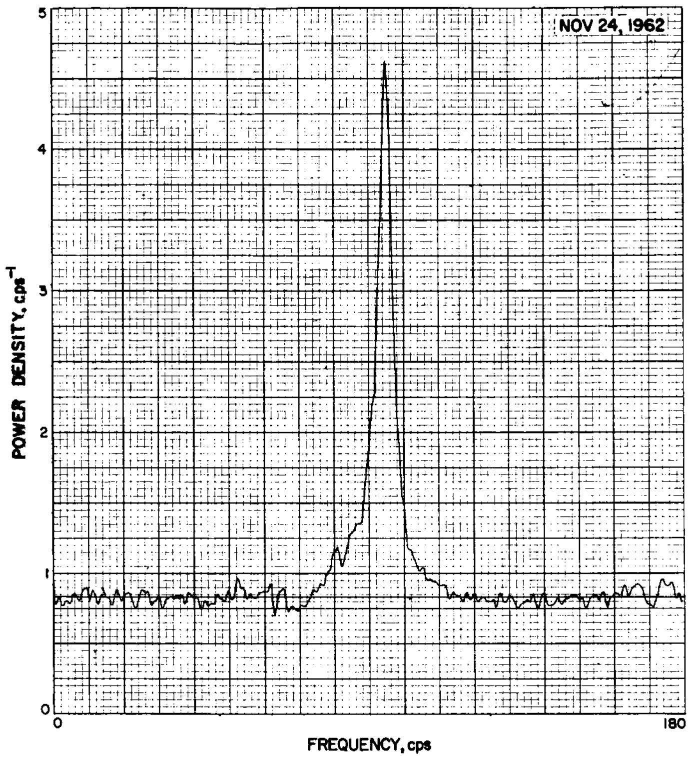

Fig. B-21. Venus CW spectrum, November 24

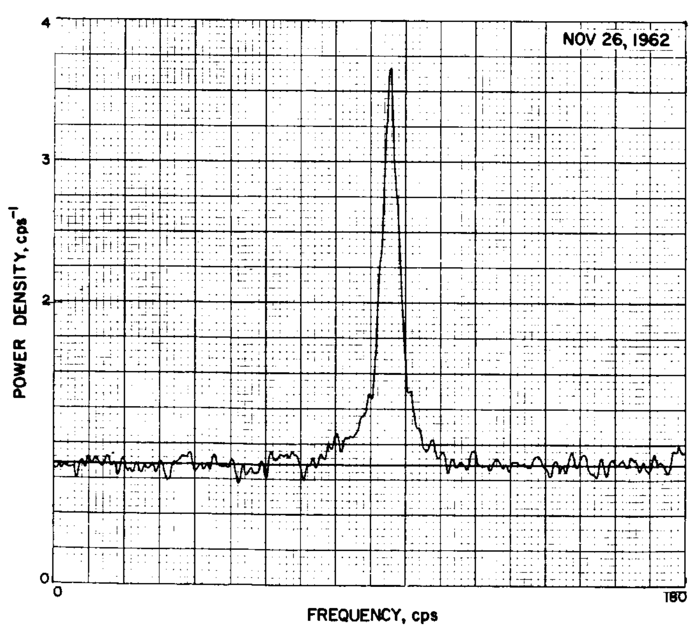

Fig. B-22. Venus CW spectrum, November 26

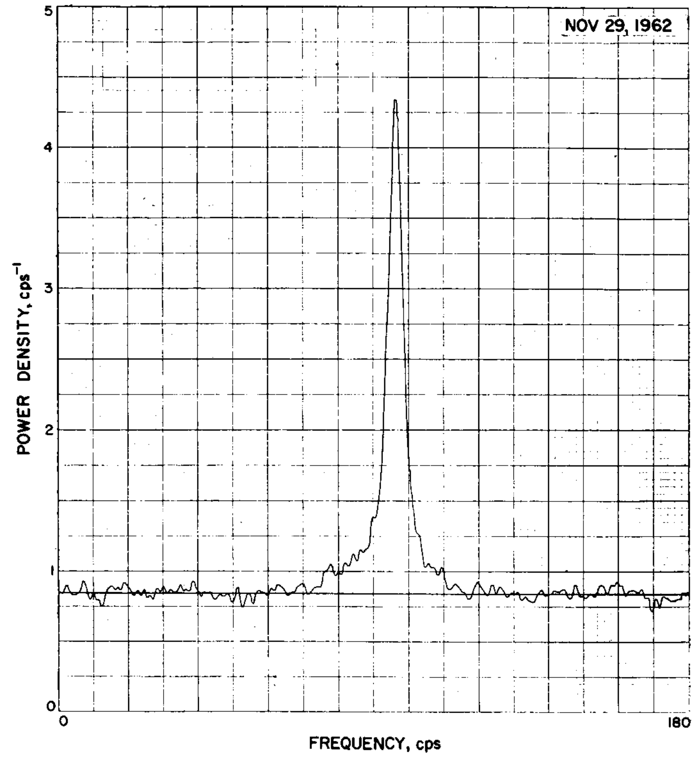

Fig. B-23. Venus CW spectrum, November 29

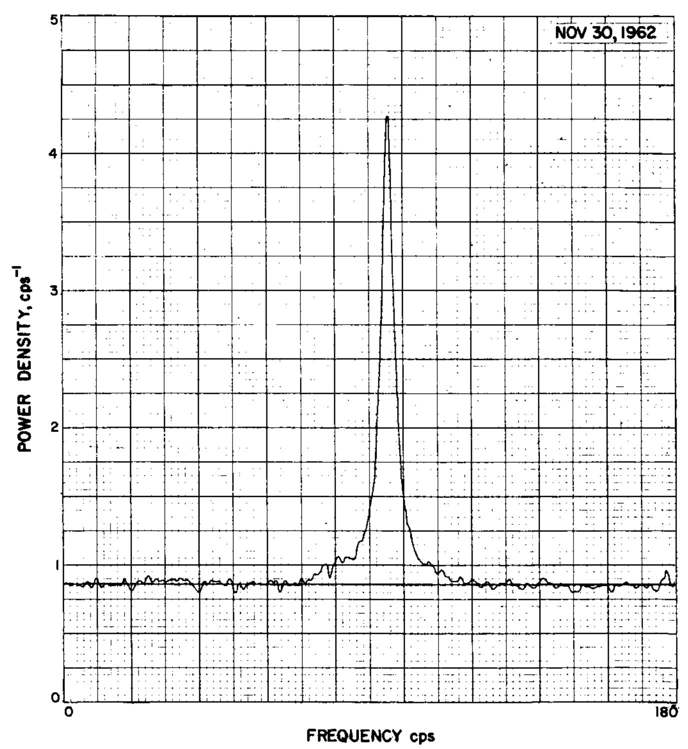

Fig. B-24. Venus CW spectrum, November 30

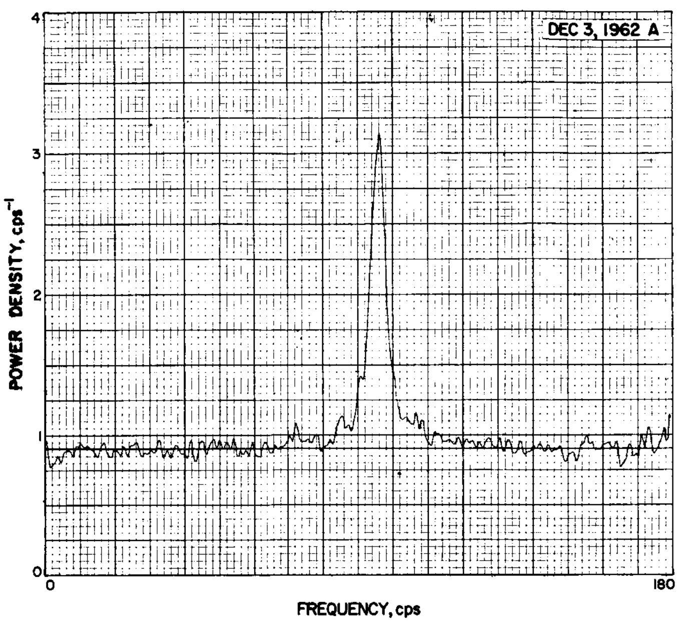

Fig. B-25. Venus CW spectrum, December 3 (A)

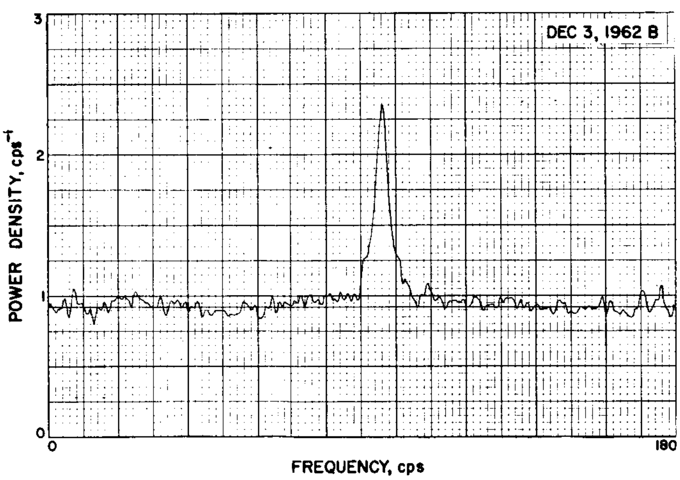

Fig. B-26. Venus CW spectrum, December 3 (B)

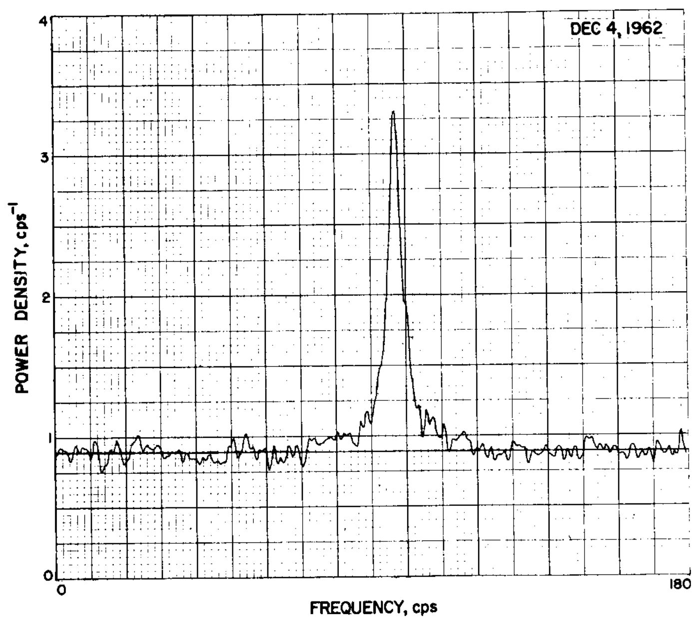

Fig. B-27. Venus CW spectrum, December 4

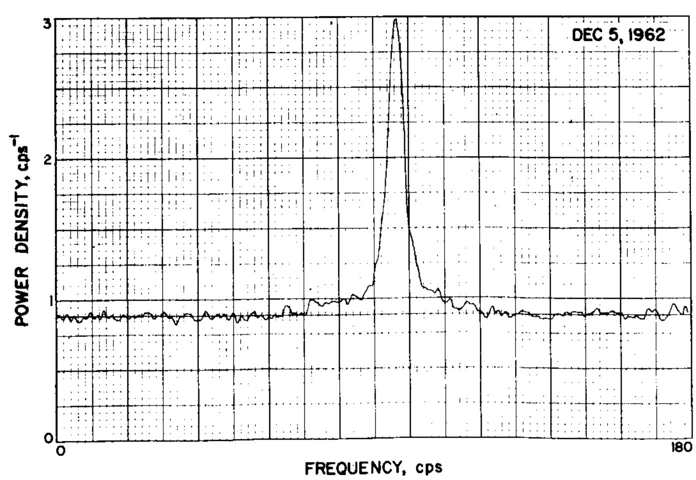

Fig. B-28. Venus CW spectrum, December 5

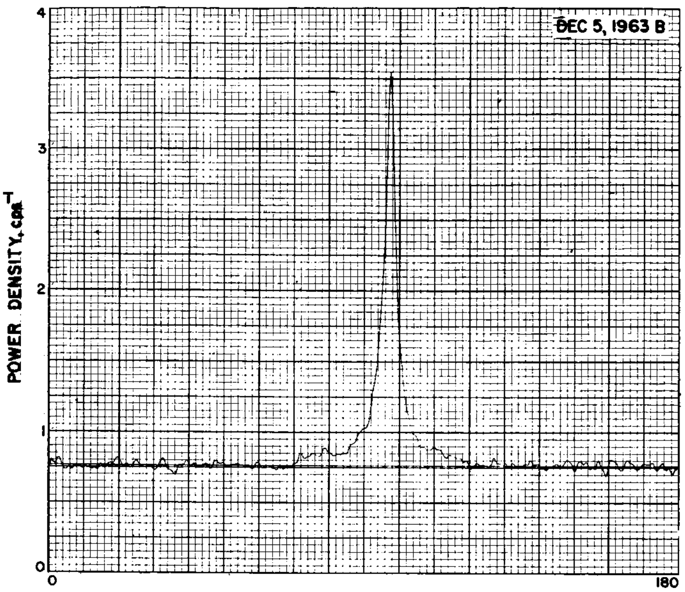

Fig. B-29. Venus CW spectrum, December 5 (B)

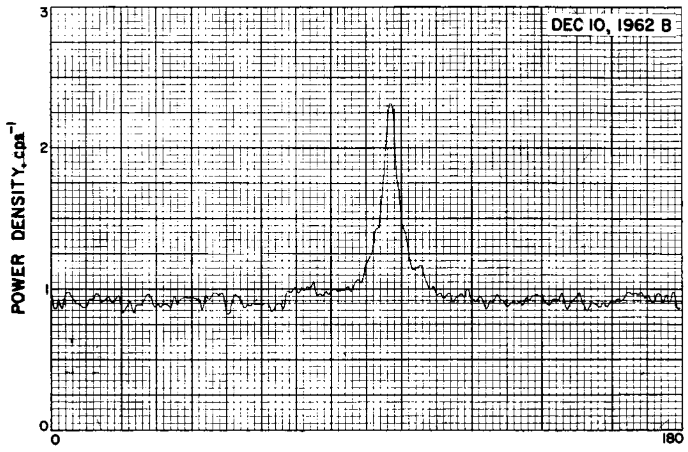

Fig. B-30. Venus CW spectrum, December 10

APPENDIX C.

Data from Closed-Loop Receiver System

C. Wiggins and W. Gillmore

This Appendix contains all of the good doppler data obtained from the closed-loop receiver during the 1962 Venus radar experiment. The data is presented in graphical form to facilitate a detailed look at any particular data run as well as a rapid comparison between different data runs. Each curve represents the results obtained from one particular receive cycle. The length of each cycle was normally equal to the flight time of the radar signal travelling to Venus and back again — usually less than 6 or 7 min.

A large part of the doppler shift in the signal reflected from Venus was due to the relative velocity between Venus and Earth. This velocity is predictable and the frequency shift can be computed quite accurately. Curves for the closed-loop receiver data are most useful if they show only the residual or difference between the recorded and computed values of the doppler shift.

A doppler residual Δ was computed for each data point taken during this experiment. The equation defining Δ is simply

$$\Delta = \frac{75}{80}\left(f_r - f_c \right)$$

where Δ is the doppler residual

f_r is the true doppler shift from the 2388-Mc carrier frequency

f_c is the computed doppler shift from the 2388-Mc carrier frequency

A constant 75/80 appears in this equation because of the frequency multiplication ratio in the circuitry for measuring UHF doppler. Since the basic measurement was (75/80 f_r), it seemed best to multiply the computed values f_c by the same constant and keep the residual Δ in the same arbitrary units as the original data.

The computed values of doppler shift f_c used the following constants in conjunction with a Venus ephemeris:

Astronomical, unit, km	149,598,845
Earth radius for lunar ephemeris, km	6378.145
Velocity of light, km/sec	299,793.0
Earth/Moon mass ratio	81.450
Radius of Venus, km	6100
Rotation rate of Earth, deg/sec	$\dfrac{0.00417807417}{1 + 5.21 \times 10^{-13} d}$
Ephemeris time minus Universal time, sec	34
Geocentric North latitude of radar, deg	35.064560
East longitude of radar, deg	243.205989
Geocentric radius of radar, km	6372.1307

The values for astronomical unit and velocity of light were chosen because they gave results which accurately matched the data obtained during the previous 1961 Venus radar experiment. The parameter d is a decimal number giving the number of days since year 1950.0.

The first group of curves covers the period from October 11 to December 17, 1962. Data plotted on these curves is based on a 1-sec count of the UHF doppler, which occurred every 10 sec. The other 9 sec were used to record the data and reset the counter for the next 1-sec count interval. On the second group of curves the count interval for the UHF doppler was 10 sec. Two counters were used so that a 10-sec count could be taken from one and then the other, alternately. The 10-sec counts were used at various times between November 10, and December 17, 1962.

Each curve is labeled with a file number to identify the data. The first three digits give the sequential number of the day in the year 1962. The last digit is 0 when the coherent receiver experiment is run for the first time, on any particular day. Sometimes the experiment was interrupted by some other experiment or station maintenance. Each time on the same day when the experiment was resumed after such an interruption, the file number was increased by 1. For convenience the time and date of the data run are labeled on each curve.

All of the curves plotted on the following pages use linear interpolation between points. This gives a continuous-looking picture of what happens in the 10-sec interval between data points. The time axes are labeled in minutes past the epoch stated below the curve while the residual axes are symmetrical about zero in units of (75/80 times cycles per second). All curves are plotted with similar scales. A few curves run off scale, but the scales chosen give the best detail on the largest number of curves.

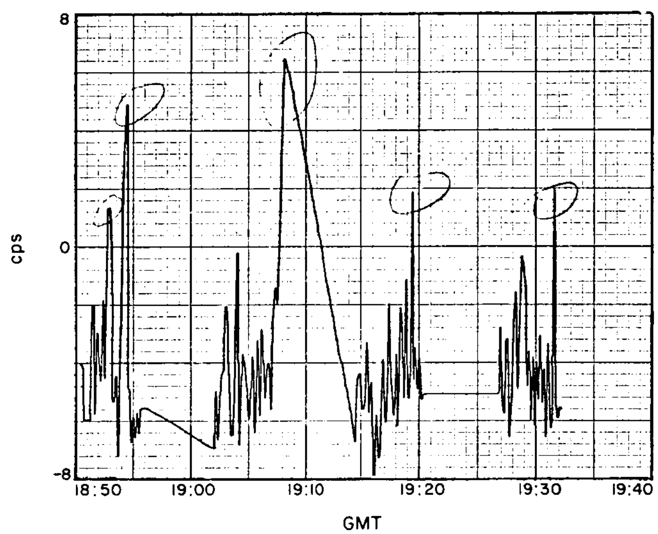

Fig. C-1. Doppler residuals, October 15

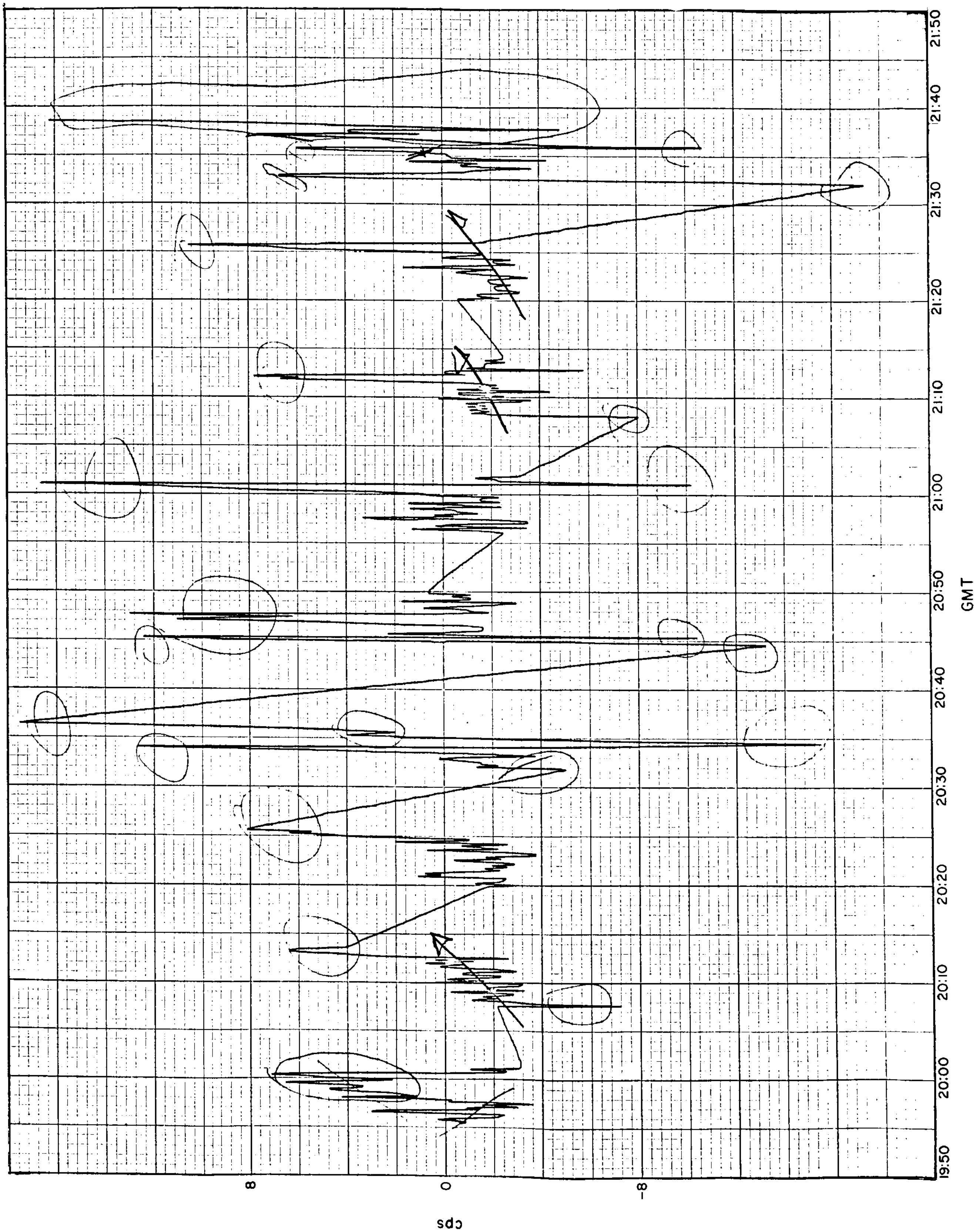

Fig. C-2. Doppler residuals, October 16

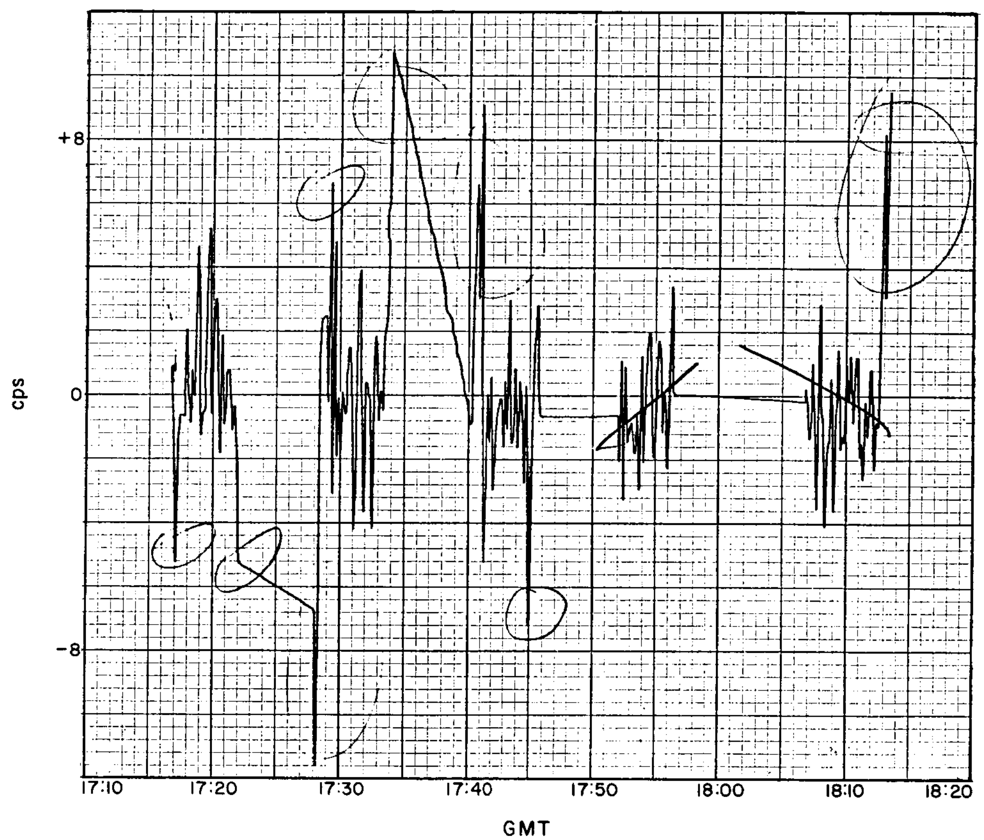

Fig. C-3. Doppler residuals, October 17

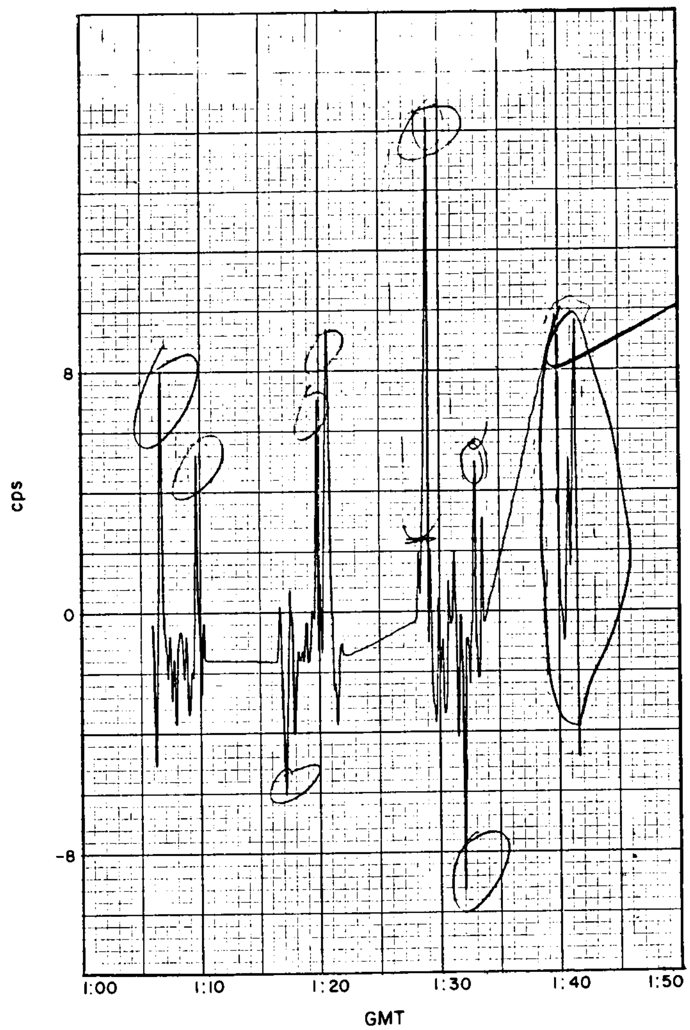

Fig. C-4. Doppler residuals, October 19

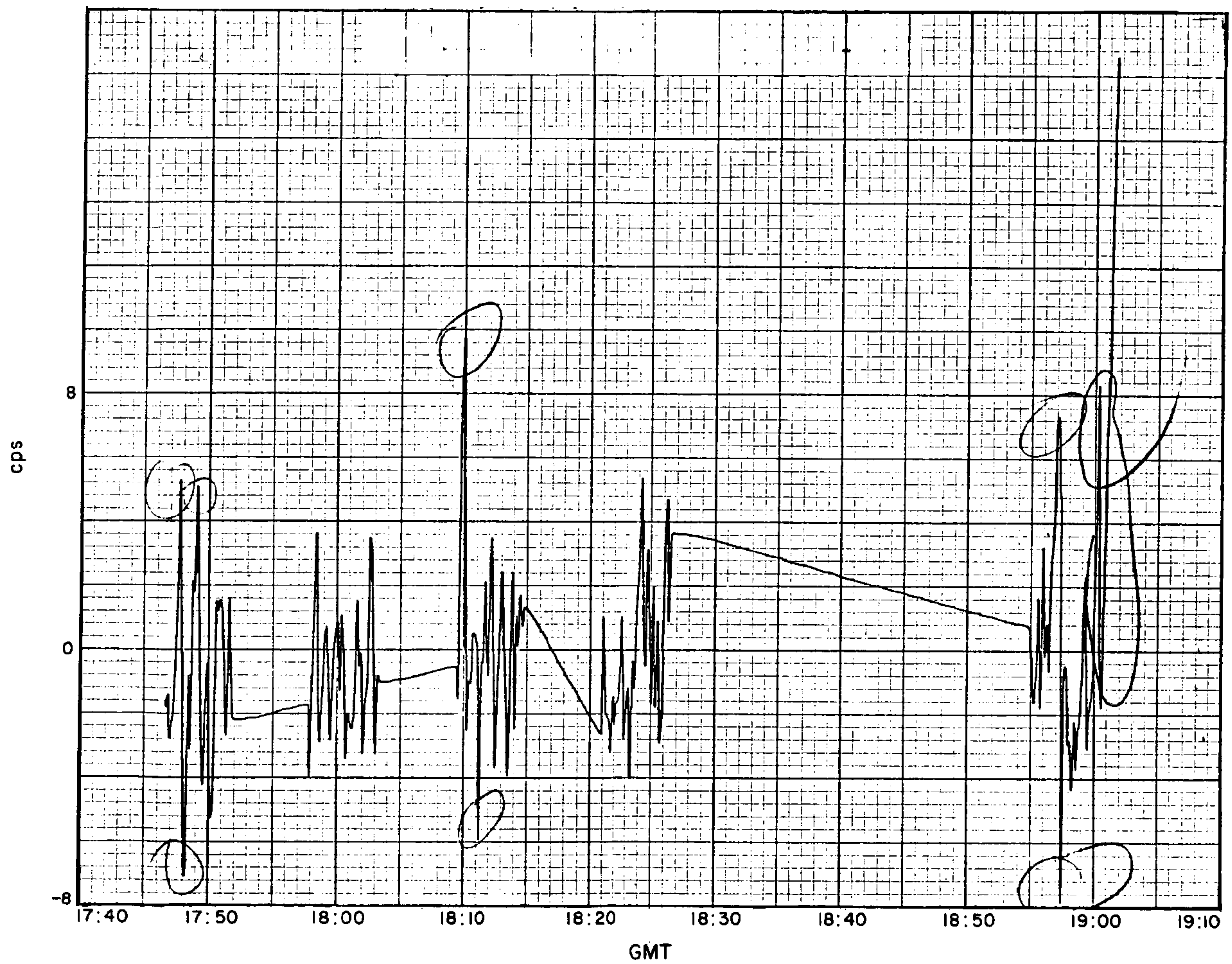

Fig. C-5. Doppler residuals, October 19

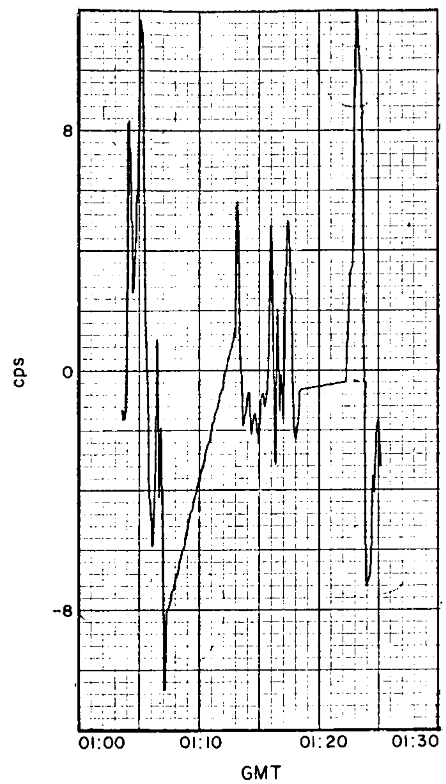

Fig. C-6. Doppler residuals, October 23

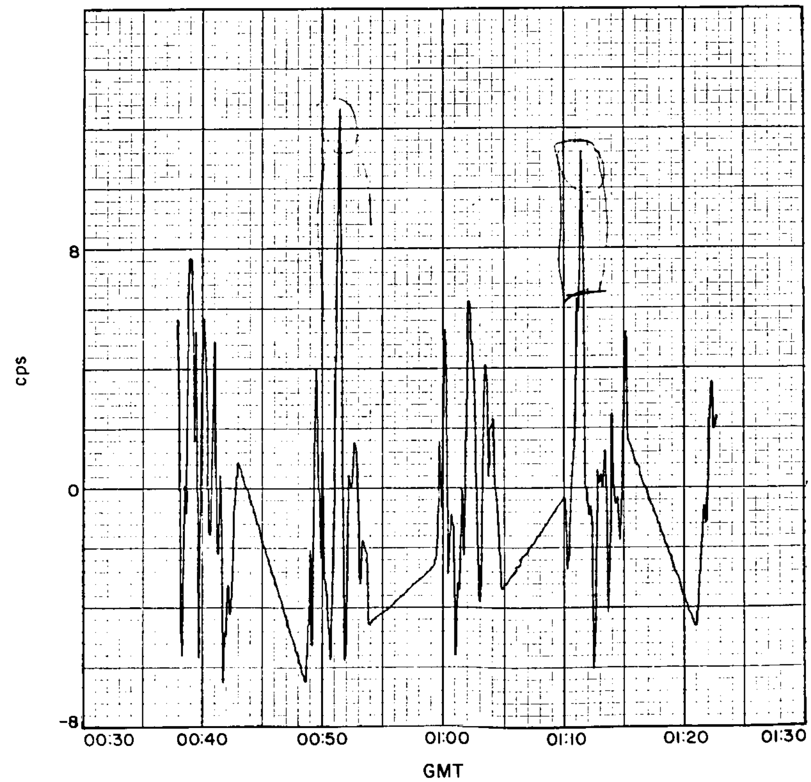

Fig. C-7. Doppler residuals, October 24

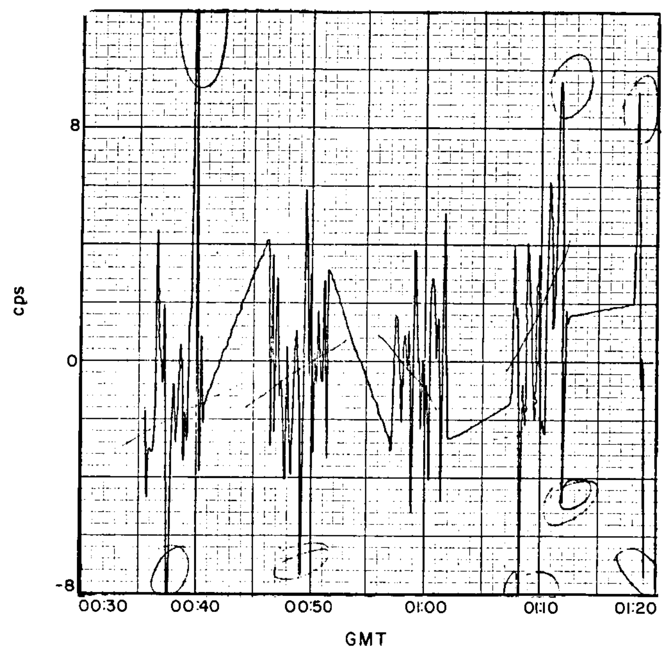

Fig. C-8. Doppler residuals, October 25

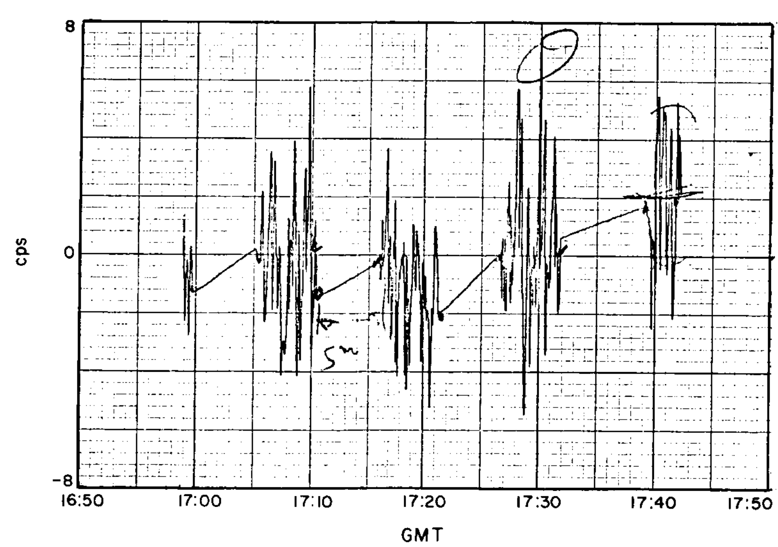

Fig. C-9. Doppler residuals, October 25

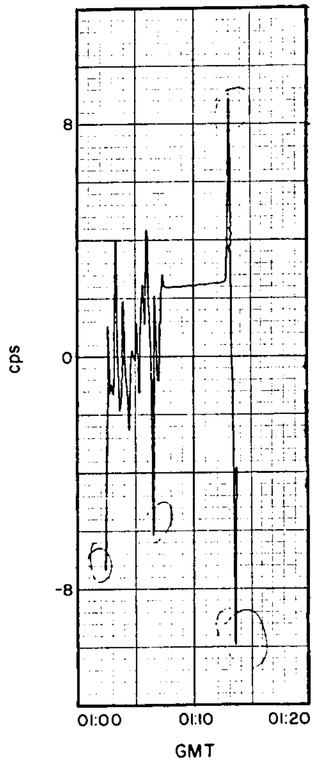

Fig. C-10. Doppler residuals, October 26

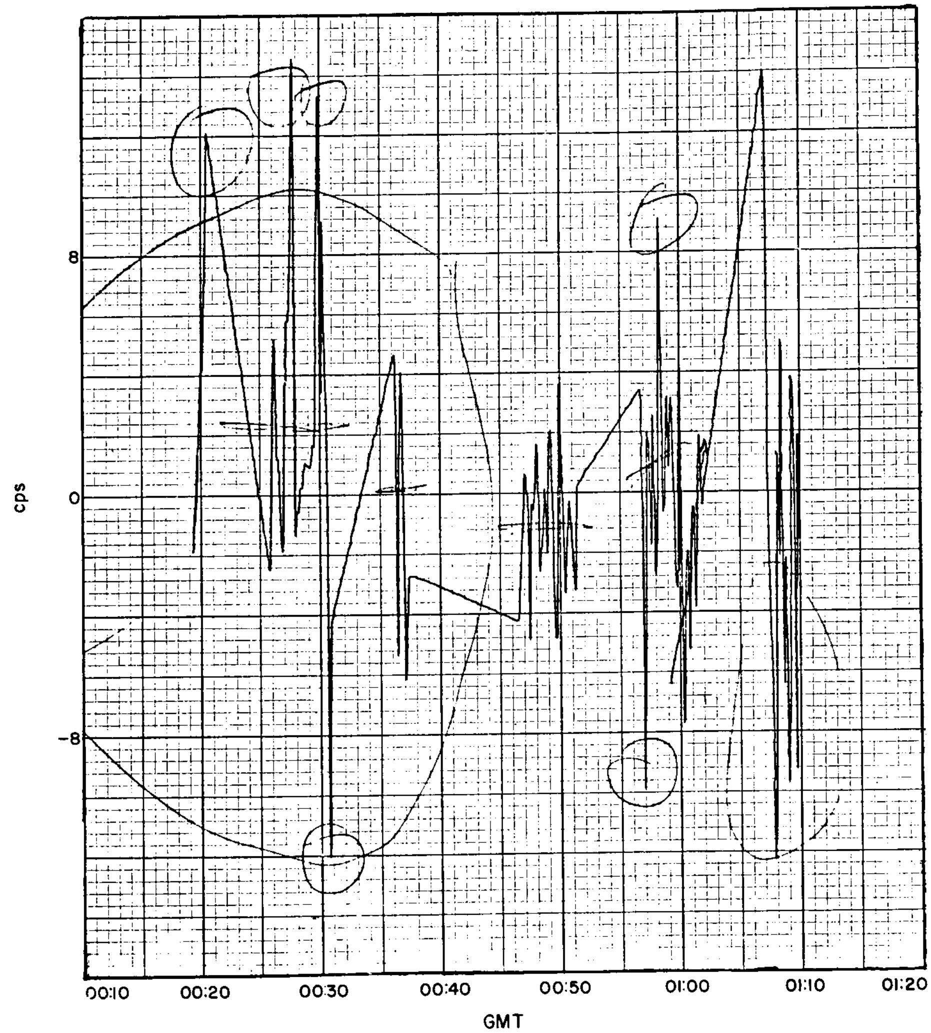

Fig. C-11. Doppler residuals, October 27

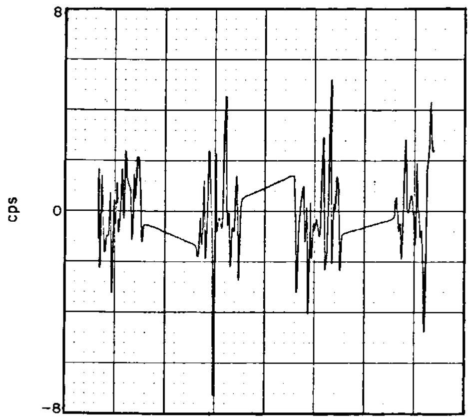

Fig. C-12. Doppler residuals, October 30

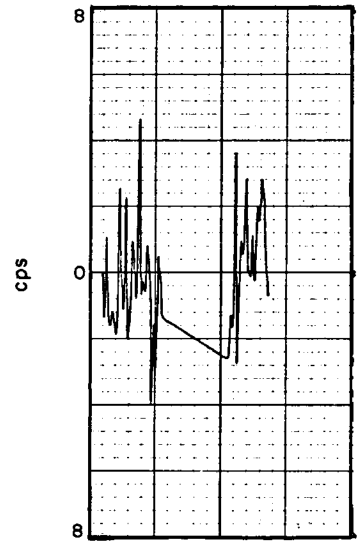

Fig. C-14. Doppler residuals, October 31

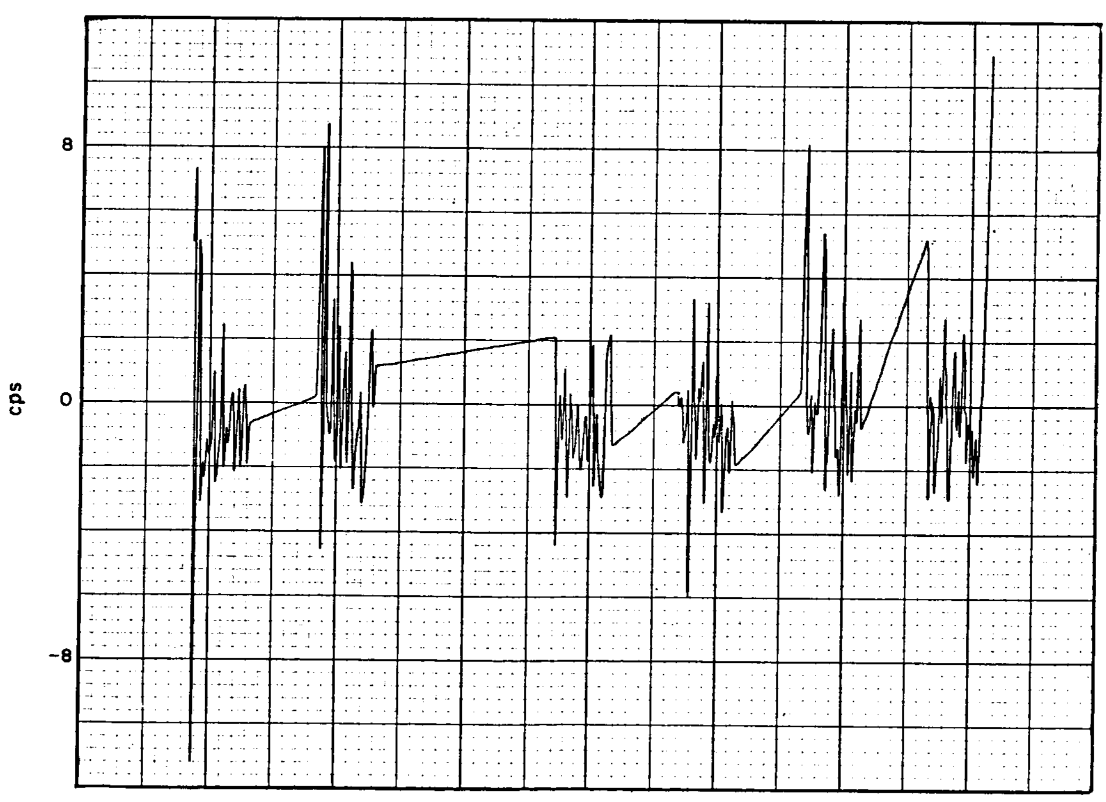

Fig. C-13. Doppler residuals, October 30

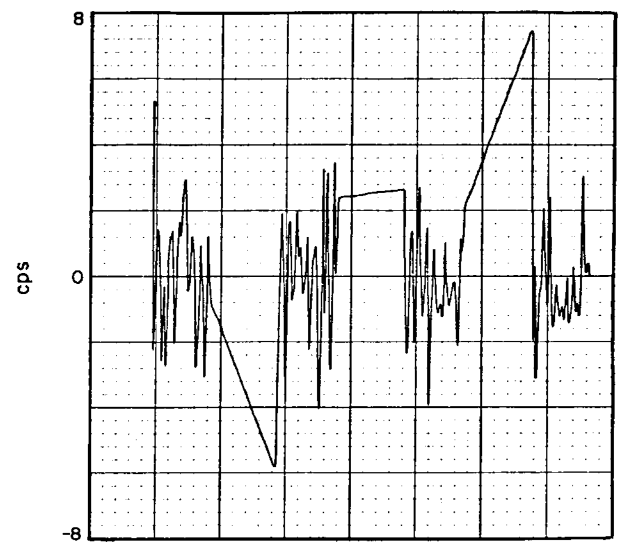

Fig. C-15. Doppler residuals, October 31

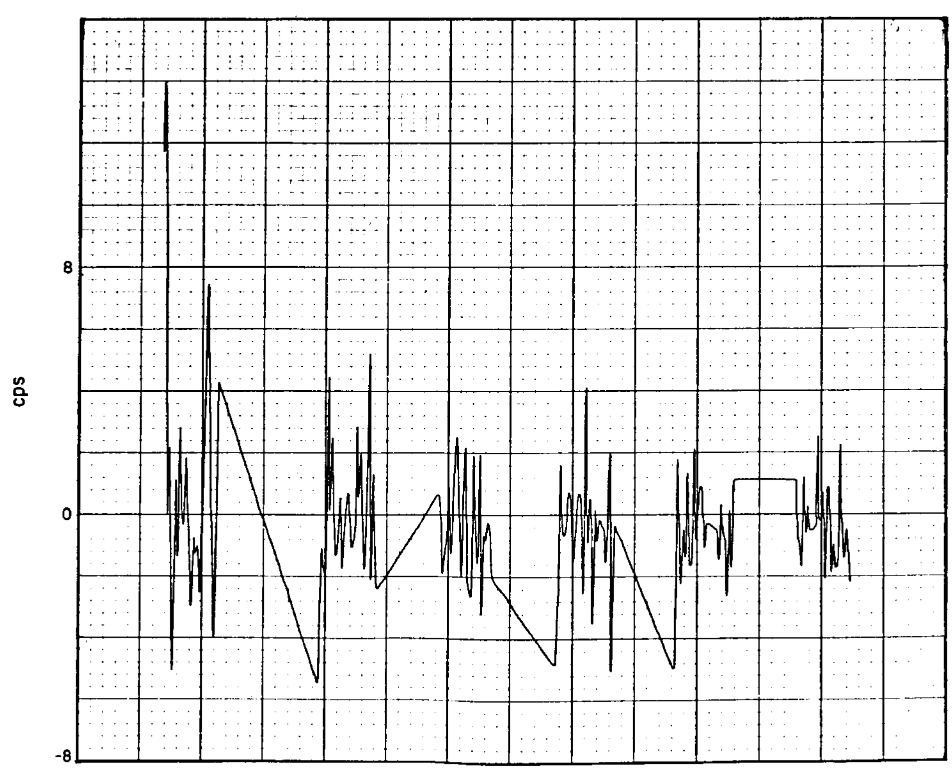

Fig. C-16. Doppler residuals, November 1

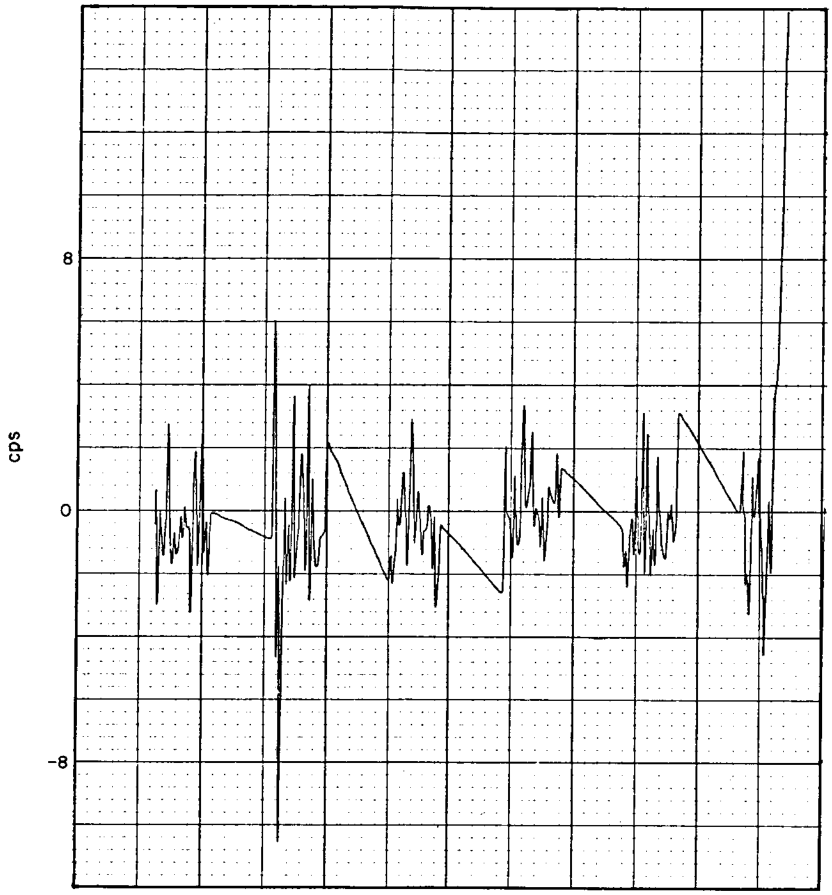

Fig. C-17. Doppler residuals, November 2

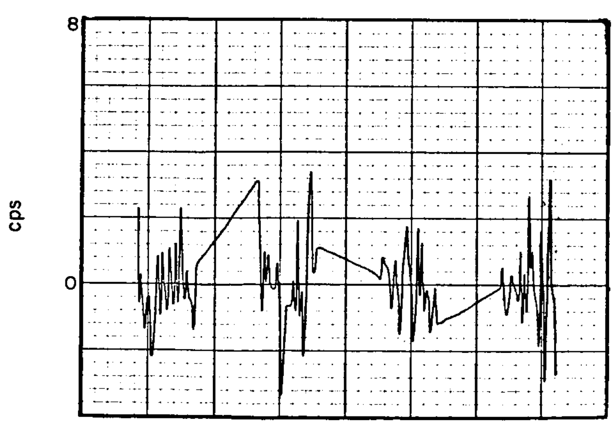

Fig. C-18. Doppler residuals, November 5

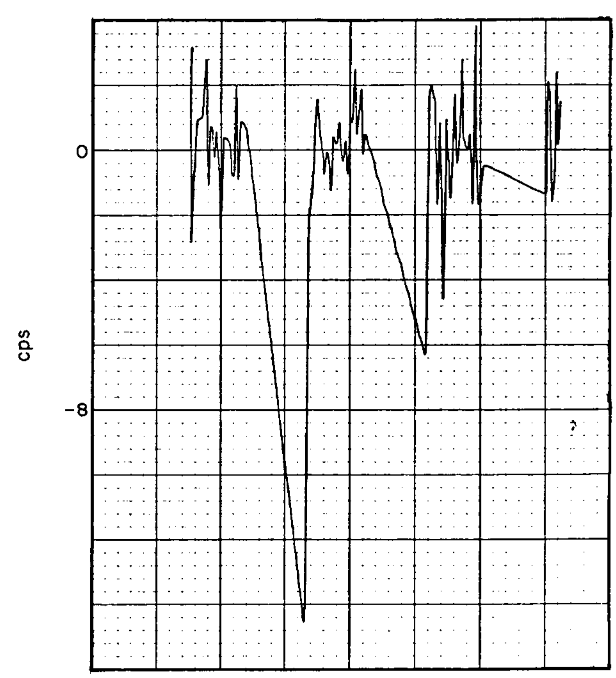

Fig. C-19. Doppler residuals, November 6

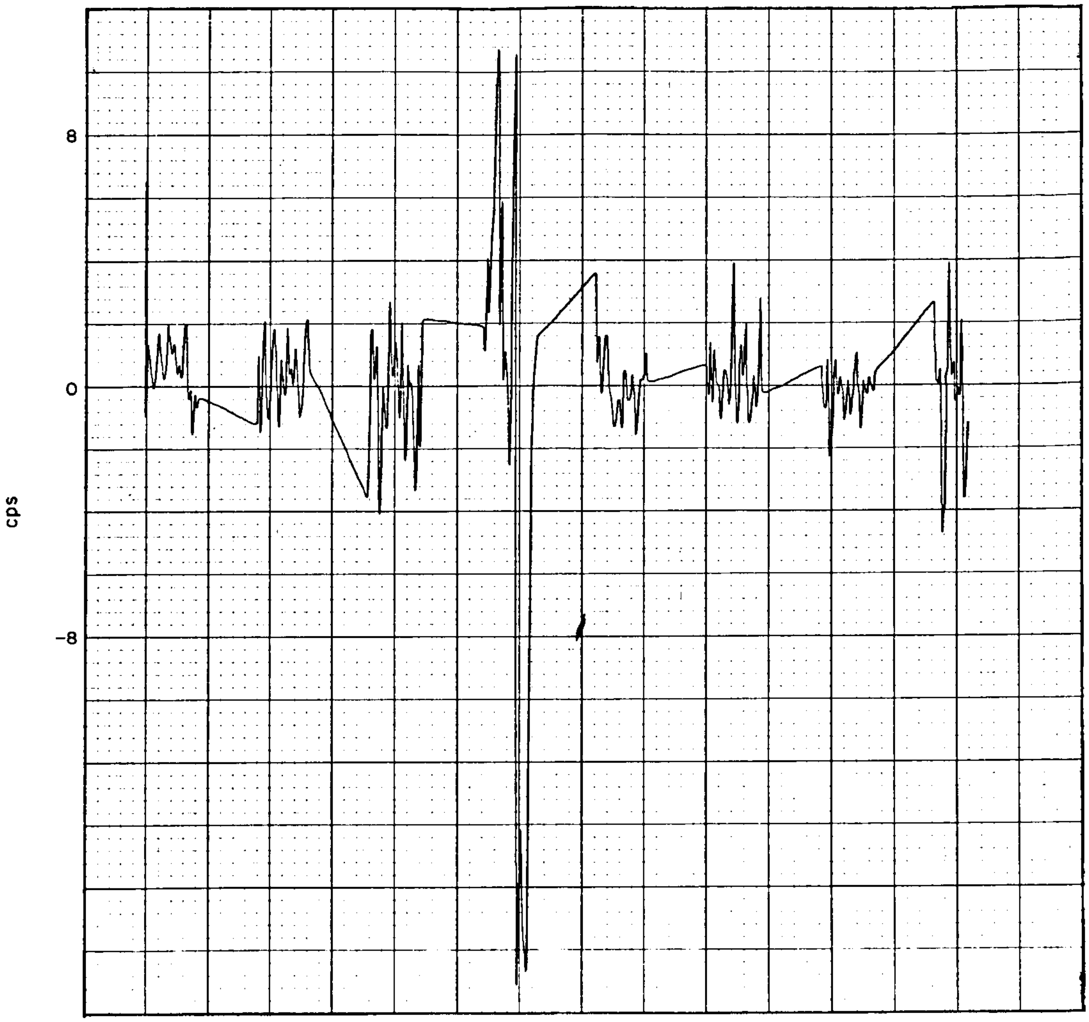

Fig. C-20. Doppler residuals, November 7

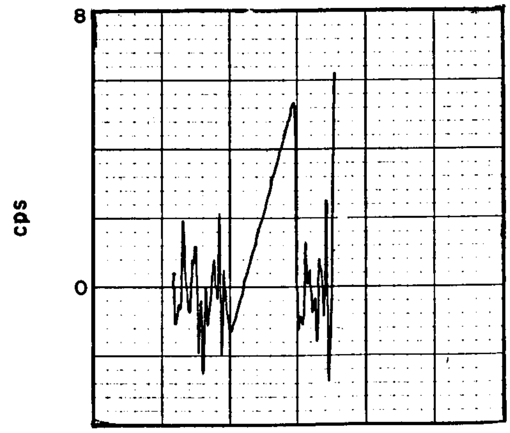

Fig. C-21. Doppler residuals, November 8

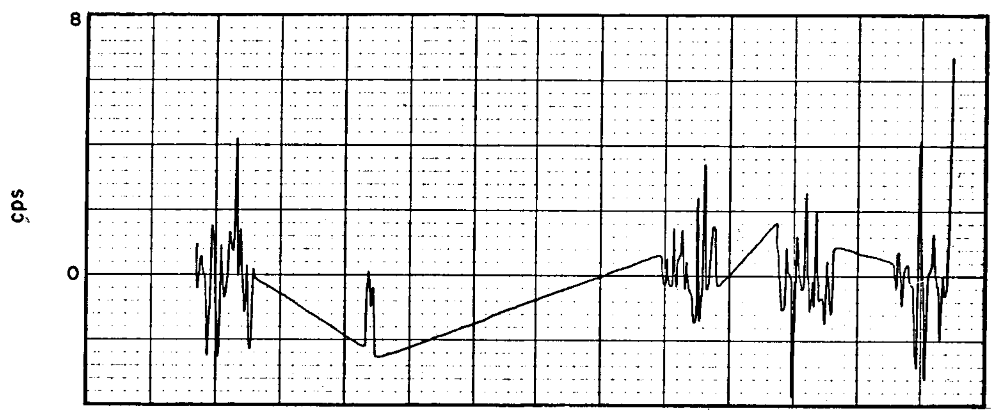

Fig. C-22. Doppler residuals, November 9

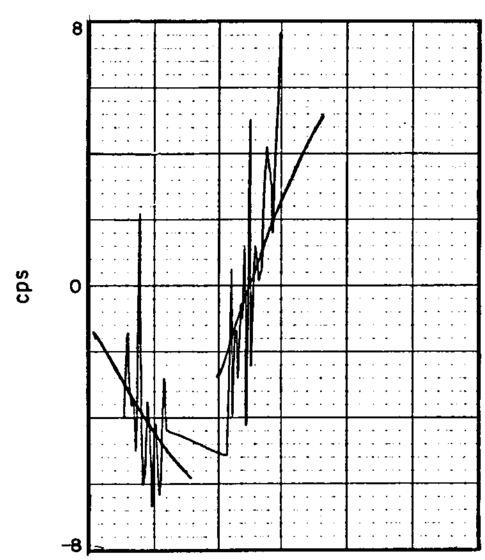

Fig. C-23. Doppler residuals, November 13
(just before conjunction)

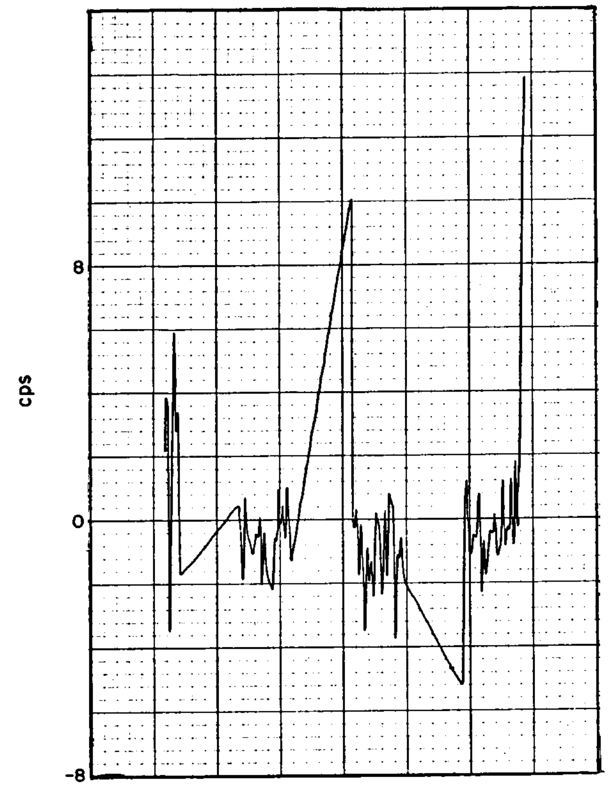

Fig. C-24. Doppler residuals, November 13 (just after conjunction)

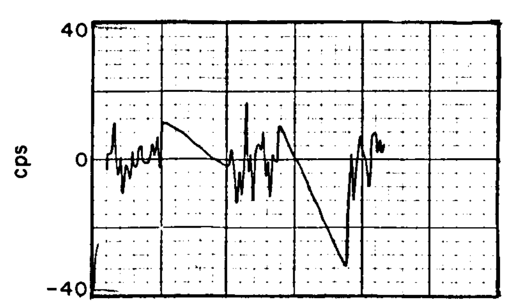

Fig. C-25. Ten-sec doppler residuals, November 10

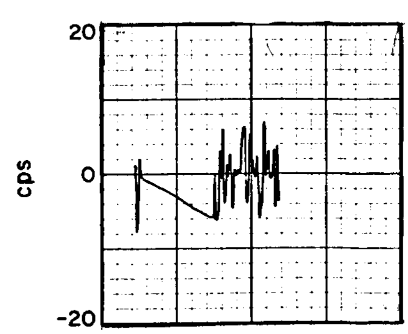

Fig. C-26. Five-sec doppler residuals, November 10

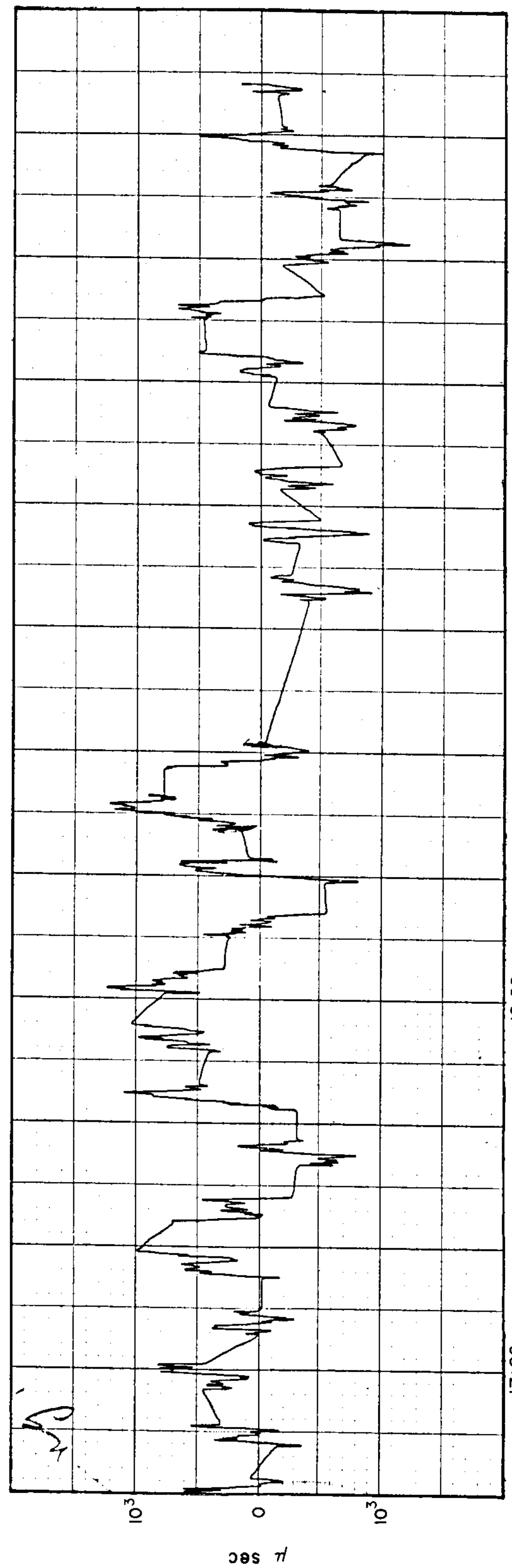

Fig. C-27. Range residuals, November 6

APPENDIX D.

Closed-Loop Ranging Data

M. Easterling

This Appendix is a listing of the round-trip propagation time as measured by the amplitude-modulated range-measuring system. The data listed is edited as described in Sec. V-B, but, as discussed there, should be considered as "raw" data for scientific purposes.

Each row of figures gives one data point. The first group of figures in a row is the day of the year. The second group of figures is Greenwich Mean Time in hours, minutes, and seconds. The time given is the time at which the wave whose propagation time is being measured arrives back at the receiving antenna. The third group of figures is the measured propagation time in microseconds. The fourth group of figures is the measured propagation time minus the ephemeris propagation time. The units are microseconds. The last group of figures is the propagation time given by the ephemeris (see Sec. VII). The listing of the data was made from a deck of IBM cards, copies of which are available for scientific purposes.

FLIGHT TIME 29 NOV 62 01

333	133724	303199121	3137	303195984
333	133732	303199615	3255	303196360
333	133740	303199941	3221	303196720
333	133748	303200208	3120	303197088
333	133756	303200431	2967	303197464
333	133804	303200772	2940	303197832
333	133812	303201195	2987	303198208
333	133820	303201561	2993	303198568
333	133828	303201989	3045	303198944
333	133836	303202578	3274	303199304
333	133844	303203101	3413	303199688
333	133852	303203361	3305	303200056
333	133900	303203806	3382	303200424
333	133908	303204289	3497	303200792
333	133916	303204559	3399	303201160
333	133924	303204966	3438	303201528
333	133932	303205300	3404	303201896
333	133940	303205722	3458	303202264
333	133948	303206076	3444	303202632
333	133956	303206422	3430	303202992
333	134004	303206790	3414	303203376
333	134012	303207233	3497	303203736
333	134020	303207667	3563	303204104
333	134028	303208075	3595	303204480
333	134036	303208469	3621	303204848
333	134044	303208929	3713	303205216
333	134052	303209195	3611	303205584
333	134100	303209594	3642	303205952
333	134108	303209883	3563	303206320
333	134116	303210163	3475	303206688
333	134124	303210473	3417	303207056
333	134132	303210817	3393	303207424
333	134140	303211154	3354	303207800
333	134148	303211632	3464	303208168
333	134156	303211892	3356	303208536
333	134204	303212126	3214	303208912
333	134212	303212499	3219	303209280
333	134724	303225848	2168	303223680
333	134732	303226353	2297	303224056
333	134740	303226847	2423	303224424
333	134748	303227148	2348	303224800
333	134756	303227617	2449	303225168
333	134804	303227882	2346	303225536
333	134812	303228315	2411	303225904
333	134820	303228680	2400	303226280
333	134828	303229002	2362	303226640
333	134836	303229327	2311	303227016
333	134844	303229754	2378	303227376
333	134852	303230154	2402	303227752
333	134900	303230408	2288	303228120
333	134908	303230771	2283	303228488
333	134916	303231193	2329	303228864
333	134924	303231617	2385	303229232
333	134932	303232213	2613	303229600
333	134940	303232656	2696	303229960
333	134948	303233103	2767	303230336
333	134956	303233674	2970	303230704

333	135004	303234029	2949	303231080
333	135012	303234484	3036	303231448
333	135020	303234967	3151	303231816
333	135028	303235315	3131	303232184
333	135036	303235608	3048	303232560
333	135044	303235916	2988	303232928
333	135052	303236293	2997	303233296
333	135100	303236709	3045	303233664
333	135108	303237061	3029	303234032
333	135116	303237431	3023	303234408
333	135124	303237771	2995	303234776
333	135132	303238073	2929	303235144
333	135140	303238350	2838	303235512
333	135148	303238693	2805	303235888
333	135156	303239195	2947	303236248
333	135204	303239595	2963	303236632
333	135212	303239878	2886	303236992
333	135220	303240270	2902	303237368
333	135732	303254158	2374	303251784
333	135740	303254535	2375	303252160
333	135748	303254950	2414	303252536
333	135756	303255293	2389	303252904
333	135804	303255762	2490	303253272
333	135812	303256039	2399	303253640
333	135820	303256249	2241	303254008
333	135828	303256603	2227	303254376
333	135836	303256971	2219	303254752
333	135844	303257320	2192	303255128
333	135852	303257892	2396	303255496
333	135900	303258376	2520	303255856
333	135908	303258624	2384	303256240
333	135916	303259039	2431	303256608
333	135924	303259501	2525	303256976
333	135932	303259815	2471	303257344
333	135940	303260242	2522	303257720
333	135948	303260494	2406	303258088
333	135956	303260849	2393	303258456
333	140004	303261311	2487	303258824
333	140012	303261639	2439	303259200
333	140020	303262052	2484	303259568
333	140028	303262302	2366	303259936
333	140036	303262790	2478	303260312
333	140044	303263075	2395	303260680
333	140052	303263464	2408	303261056
333	140100	303263753	2337	303261416
333	140108	303264120	2328	303261792
333	140116	303264611	2443	303262168
333	140124	303264951	2423	303262528
333	140132	303265336	2432	303262904
333	140140	303265722	2450	303263272
333	140148	303266155	2515	303263640
333	140156	303266480	2464	303264016
333	140204	303266954	2570	303264384
333	140212	303267356	2612	303264744
333	140220	303267810	2690	303265120
333	140228	303268123	2635	303265488
333	140740	303282290	2346	303279944
333	140748	303282803	2499	303280304
333	140756	303283367	2679	303280688

333	140804	303283753	2697	303281056
333	140812	303284278	2846	303281432
333	140820	303284543	2751	303281792
333	140828	303284945	2777	303282168
333	140836	303285327	2799	303282528
333	140844	303285646	2734	303282912
333	140852	303286067	2787	303283280
333	140900	303286420	2772	303283648
333	140908	303286786	2762	303284024
333	140916	303287125	2733	303284392
333	140924	303287546	2778	303284768
333	140932	303287894	2758	303285136
333	140940	303288191	2687	303285504
333	140948	303288626	2754	303285872
333	140956	303288779	2539	303286240
333	141004	303289160	2544	303286616
333	141012	303289461	2477	303286984
333	141020	303289756	2396	303287360
333	141028	303290053	2317	303287736
333	141036	303290501	2397	303288104
333	141044	303290966	2494	303288472
333	141052	303291366	2526	303288840
333	141100	303291702	2486	303289216
333	141108	303292081	2497	303289584
333	141116	303292614	2662	303289952
333	141124	303293083	2755	303290328
333	141132	303293500	2804	303290696
333	141140	303293924	2852	303291072
333	141148	303294152	2712	303291440
333	141156	303294497	2689	303291808
333	141204	303294817	2633	303292184
333	141220	303295419	2491	303292928
333	141228	303295750	2454	303293296
333	141236	303296230	2566	303293664
333	145820	303422999	1575	303421424
333	145828	303423439	1639	303421800
333	145836	303423643	1467	303422176
333	145844	303423967	1423	303422544
333	145852	303424296	1376	303422920
333	145900	303424650	1354	303423296
333	145908	303424939	1275	303423664
333	145916	303425346	1306	303424040
333	145924	303425737	1321	303424416
333	145932	303426141	1357	303424784
333	145940	303426632	1472	303425160
333	145948	303427233	1689	303425544
333	145956	303427723	1811	303425912
333	150004	303428103	1815	303426288
333	150012	303428283	1627	303426656
333	150020	303428525	1493	303427032
333	150028	303428873	1465	303427408
333	150036	303429213	1429	303427784
333	150044	303429599	1447	303428152
333	150052	303429943	1407	303428536
333	150100	303430320	1416	303428904
333	150108	303430754	1474	303429280
333	150116	303431195	1539	303429656
333	150124	303431582	1550	303430032
333	150132	303431950	1542	303430408

333	150140	303432241	1473	303430768
333	150148	303432569	1417	303431152
333	150156	303433078	1558	303431520
333	150204	303433485	1589	303431896
333	150212	303433957	1693	303432264
333	150220	303434225	1585	303432640
333	150228	303434570	1546	303433024
333	150236	303434891	1499	303433392
333	150244	303435346	1570	303433776
333	150252	303435639	1495	303434144
333	150300	303435941	1421	303434520
333	150308	303436293	1405	303434888
333	150316	303436738	1474	303435264
333	151316	303463512	136	303463376
333	151324	303463919	167	303463752
333	151332	303464357	229	303464128
333	151340	303464883	379	303464504
333	151348	303465300	420	303464880
333	151356	303465916	668	303465248
333	151404	303466203	579	303465624
333	151412	303466524	524	303466000
333	151420	303466962	586	303466376
333	151428	303467403	651	303466752
333	151436	303467802	666	303467136
333	151444	303468142	630	303467512
333	151452	303468488	608	303467880
333	151500	303468861	613	303468248
333	151508	303469206	574	303468632
333	151516	303469843	835	303469008
333	151524	303470142	758	303469384
333	151532	303470543	791	303469752
333	151540	303471010	874	303470136
333	151548	303471257	753	303470504
333	151556	303471653	773	303470880
333	151604	303472024	768	303471256
333	151612	303472393	753	303471640
333	151620	303472889	881	303472008
333	151628	303473239	855	303472384
333	151636	303473633	873	303472760
333	151644	303473771	635	303473136
333	151652	303474057	545	303473512
333	151700	303474821	933	303473888
333	151708	303475188	932	303474256
333	151716	303475616	976	303474640
333	151724	303476094	1086	303475008
333	151732	303476493	1109	303475384
333	152244	303492923	2883	303490040
333	152252	303493212	2804	303490408
333	152300	303493427	2643	303490784
333	152308	303493869	2701	303491168
333	152316	303494357	2813	303491544
333	152324	303494809	2889	303491920
333	152332	303495200	2912	303492288
333	152340	303495706	3034	303492672
333	152348	303496047	2999	303493048
333	152356	303496494	3070	303493424
333	152404	303497067	3267	303493800
333	152412	303497376	3200	303494176
333	152420	303497615	3063	303494552

333	152428	303497877	2949	303494928
333	152436	303498097	2793	303495304
333	152444	303498443	2763	303495680
333	152452	303498883	2835	303496048
333	152500	303499190	2758	303496432
333	152508	303499437	2629	303496808
333	152516	303499829	2645	303497184
333	152524	303500273	2713	303497560
333	152532	303500536	2600	303497936
333	152540	303500781	2469	303498312
333	152548	303501076	2388	303498688
333	152556	303501412	2340	303499072
333	152604	303501791	2351	303499440
333	152612	303502155	2339	303499816
333	152620	303502326	2142	303500184
333	152628	303502553	1985	303500568
333	152636	303502820	1868	303500952
333	152644	303503302	1982	303501320
333	152652	303503750	2054	303501696
333	152700	303504245	2173	303502072
333	152708	303504598	2150	303502448
333	152716	303504891	2067	303502824
333	152724	303505154	1946	303503208
333	152732	303505497	1921	303503576
333	152740	303505881	1929	303503952
333	153252	303519304	672	303518632
333	153300	303519793	769	303519024
333	153308	303520197	813	303519384
333	153316	303520486	718	303519768
333	153324	303520733	589	303520144
333	153332	303521264	736	303520528
333	153340	303521561	657	303520904
333	153348	303521927	655	303521272
333	153356	303522334	686	303521648
333	153404	303522603	579	303522024
333	153412	303523216	808	303522408
333	153420	303523729	937	303522792
333	153428	303524250	1090	303523160
333	153436	303524800	1264	303523536
333	153444	303525243	1331	303523912
333	153452	303525682	1394	303524288
333	153500	303526004	1324	303524680
333	153508	303526479	1439	303525040
333	153516	303527080	1656	303525424
333	153524	303527483	1691	303525792
333	153532	303527779	1595	303526184
333	153540	303528233	1681	303526552
333	153548	303528568	1640	303526928
333	153556	303528842	1538	303527304
333	153604	303529249	1569	303527680
333	153612	303529592	1528	303528064
333	153620	303530210	1770	303528440
333	153628	303530894	2070	303528824
333	153636	303531337	2145	303529192
333	153644	303531615	2047	303529568
333	153652	303532269	2325	303529944
333	153700	303532747	2419	303530328
333	153708	303532923	2219	303530704
333	153716	303533364	2284	303531080

333	153724	303533919	2463	303531456
333	153732	303534650	2818	303531832
333	153740	303535217	3009	303532208
333	153748	303535791	3199	303532592
333	154252	303551276	4348	303546928
333	154300	303551748	4444	303547304
333	154308	303551930	4250	303547680
333	154316	303552266	4210	303548056
333	154324	303552524	4092	303548432
333	154332	303552891	4083	303548808
333	154340	303553243	4051	303549192
333	154348	303553467	3899	303549568
333	154356	303553774	3830	303549944
333	154404	303554245	3925	303550320
333	154412	303554694	3998	303550696
333	154420	303555106	4026	303551080
333	154428	303555510	4054	303551456
333	154436	303555958	4126	303551832
333	154444	303556095	3887	303552208
333	154452	303556583	3999	303552584
333	154500	303556782	3814	303552968
333	154508	303557207	3863	303553344
333	154516	303557501	3781	303553720
333	154524	303557928	3824	303554104
333	154532	303558318	3838	303554480
333	154540	303558698	3842	303554856
333	154548	303559108	3876	303555232
333	154556	303559519	3911	303555608
333	154604	303559828	3844	303555984
333	154612	303560202	3834	303556368
333	154620	303560421	3677	303556744
333	154628	303560760	3640	303557120
333	154636	303561026	3522	303557504
333	154644	303561558	3686	303557872
333	154652	303561875	3619	303558256
333	154700	303562223	3591	303558632
333	154708	303562605	3597	303559008
333	154716	303563013	3621	303559392
333	154724	303563385	3617	303559768
333	154732	303563752	3608	303560144
333	154740	303564160	3640	303560520
333	154748	303564538	3642	303560896
333	154756	303564826	3554	303561272
333	155300	303578611	2955	303575656
333	155308	303578764	2740	303576024
333	155316	303579030	2614	303576416
333	155324	303579493	2701	303576792
333	155332	303579923	2755	303577168
333	155340	303580265	2721	303577544
333	155348	303580647	2727	303577920
333	155356	303581080	2776	303578304
333	155404	303581422	2742	303578680
333	155412	303581675	2619	303579056
333	155420	303582155	2707	303579448
333	155428	303582609	2793	303579816
333	155436	303583039	2847	303580192
333	155444	303583381	2813	303580568
333	155452	303583827	2875	303580952
333	155500	303584331	2995	303581336

333	155508	303584728	3024	303581704
333	155516	303585054	2966	303582088
333	155524	303585482	3018	303582464
333	155532	303585787	2947	303582840
333	155540	303586284	3060	303583224
333	155548	303586645	3045	303583600
333	155556	303587106	3130	303583976
333	155604	303587561	3193	303584368
333	155612	303587811	3075	303584736
333	155620	303588238	3118	303585120
333	155628	303588652	3164	303585488
333	155636	303589082	3202	303585880
333	155644	303589442	3194	303586248
333	155652	303589767	3135	303586632
333	155700	303590045	3037	303587008
333	155708	303590450	3058	303587392
333	155716	303590746	2978	303587768
333	155724	303591096	2952	303588144
333	155732	303591432	2904	303588528
333	155740	303591872	2968	303588904
333	155748	303592023	2743	303589280
333	155756	303592269	2605	303589664
333	155804	303592480	2440	303590040
333	160316	303606501	1677	303604824
333	160332	303607368	1784	303605584
333	160340	303607669	1709	303605960
333	160348	303608105	1761	303606344
333	160356	303608612	1892	303606720
333	160404	303609005	1909	303607096
333	160412	303609479	1999	303607480
333	160420	303609727	1871	303607856
333	160428	303610242	2010	303608232
333	160508	303612053	1909	303610144
333	160516	303612281	1769	303610512
333	160524	303612813	1917	303610896
333	160532	303613294	2014	303611280
333	160540	303613646	1990	303611656
333	160548	303613716	1684	303612032
333	160556	303614016	1608	303612408
333	160604	303614388	1596	303612792
333	160612	303614766	1598	303613168
333	160620	303615273	1721	303613552
333	160628	303615596	1660	303613936
333	160636	303616052	1740	303614312
333	160644	303616378	1682	303614696
333	160652	303616868	1796	303615072
333	160700	303617242	1794	303615448
333	160708	303617615	1775	303615840
333	160716	303617969	1761	303616208
333	160724	303618283	1691	303616592
333	160732	303618744	1784	303616960
333	160740	303619071	1727	303617344
333	160748	303619602	1874	303617728
333	160756	303619920	1808	303618112
333	160804	303620326	1830	303618496
333	160812	303620753	1889	303618864
333	161316	303633549	245	303633304
333	161324	303633943	255	303633688
333	161332	303634249	185	303634064

333	161340	303634855	407	303634448
333	161348	303634962	138	303634824
333	161356	303635316	108	303635208
333	161404	303635643	59	303635584
333	161412	303636010	42	303635968
333	161420	303636499	147	303636352
333	161428	303636938	218	303636720
333	161436	303637269	165	303637104
333	161444	303637644	156	303637488
333	161452	303638193	321	303637872
333	161500	303638670	430	303638240
333	161508	303639169	537	303638632
333	161516	303639531	523	303639008
333	161524	303639832	440	303639392
333	161532	303640322	546	303639776
333	161540	303640634	482	303640152
333	161548	303640937	401	303640536
333	161556	303641428	524	303640904
333	161604	303641853	565	303641288
333	161612	303642319	647	303641672
333	161620	303642785	737	303642048
333	161628	303643121	689	303642432
333	161636	303643592	784	303642808
333	161644	303644131	931	303643200
333	161652	303644375	799	303643576
333	161700	303644936	984	303643952
333	161708	303645348	1012	303644336
333	161716	303645741	1021	303644720
333	161724	303646222	1134	303645088
333	161732	303646534	1054	303645480
333	161740	303647012	1156	303645856
333	161748	303647326	1086	303646240
333	161756	303647792	1176	303646616
333	161804	303648101	1101	303647000
333	161812	303648569	1185	303647384
333	161820	303648984	1216	303647768
333	162332	303664173	1557	303662616
333	162340	303664661	1661	303663000
333	162348	303664852	1476	303663376
333	162356	303665324	1564	303663760
333	162404	303665877	1741	303664136
333	162412	303666424	1904	303664520
333	162420	303666920	2016	303664904
333	162428	303667261	1981	303665280
333	162436	303667626	1962	303665664
333	162444	303668101	2045	303666056
333	162452	303668478	2054	303666424
333	162500	303668914	2106	303666808
333	162508	303669320	2120	303667200
333	162516	303669731	2155	303667576
333	162524	303670101	2141	303667960
333	162532	303670530	2202	303668328
333	162540	303671062	2350	303668712
333	162548	303671313	2217	303669096
333	162556	303671792	2312	303669480
333	162604	303672125	2269	303669856
333	162612	303672585	2345	303670240
333	162620	303672983	2359	303670624
333	162628	303673373	2365	303671008

333	162636	303673683	2299	303671384
333	162644	303674009	2241	303671768
333	162652	303674413	2261	303672152
333	162700	303674681	2153	303672528
333	162708	303675126	2214	303672912
333	162716	303675540	2252	303673288
333	162724	303675986	2314	303673672
333	162732	303676412	2356	303674056
333	162740	303676816	2384	303674432
333	162748	303677157	2349	303674808
333	162756	303677538	2338	303675200
333	162804	303677875	2291	303675584
333	162812	303678374	2406	303675968
333	162820	303678689	2345	303676344
333	162828	303678840	2112	303676728
333	163340	303692424	808	303691616
333	163348	303692825	825	303692000
333	163356	303693277	901	303692376
333	163404	303693814	1054	303692760
333	163412	303694045	893	303693152
333	163420	303694193	665	303693528
333	163428	303694421	517	303693904
333	163436	303694846	558	303694288
333	163444	303695290	618	303694672
333	163452	303695608	552	303695056
333	163500	303696120	680	303695440
333	163508	303696519	703	303695816
333	163516	303696979	779	303696200
333	163524	303697287	703	303696584
333	163532	303697644	676	303696968
333	163540	303697977	625	303697352
333	163548	303698564	828	303697736
333	163556	303698929	817	303698112
333	163604	303699371	875	303698496
333	163612	303699736	856	303698880
333	163620	303700081	817	303699264
333	163628	303700544	904	303699640
333	163636	303700926	910	303700016
333	163644	303701341	941	303700400
333	163652	303701728	944	303700784
333	163700	303702010	842	303701168
333	163708	303702435	883	303701552
333	163716	303702691	755	303701936
333	163724	303703050	730	303702320
333	163732	303703583	887	303702696
333	163740	303704002	914	303703088
333	163748	303704252	780	303703472
333	163756	303704769	921	303703848
333	163804	303705470	1238	303704232
333	163812	303705799	1183	303704616
333	163820	303706291	1291	303705000
333	163828	303706638	1262	303705376
333	163836	303707226	1458	303705768
333	164348	303722613	1925	303720688
333	164356	303723022	1942	303721080
333	164404	303723347	1899	303721448
333	164412	303723752	1912	303721840
333	164420	303724193	1977	303722216

333	164428	303724470	1870	303722600
333	164436	303724969	1977	303722992
333	164444	303725276	1908	303723368
333	164452	303725625	1873	303723752
333	164500	303725851	1715	303724136
333	164508	303726252	1732	303724520
333	164516	303726422	1518	303724904
333	164524	303726901	1613	303725288
333	164532	303727499	1827	303725672
333	164540	303727970	1922	303726048
333	164548	303728179	1739	303726440
333	164556	303728709	1893	303726816
333	164604	303728930	1730	303727200
333	164612	303729398	1806	303727592
333	164620	303729840	1872	303727968
333	164628	303730257	1905	303728352
333	164636	303730659	1931	303728728
333	164644	303731159	2039	303729120
333	164652	303731632	2128	303729504
333	164700	303731895	2007	303729888
333	164708	303732176	1912	303730264
333	164716	303732671	2023	303730648
333	164724	303733010	1970	303731040
333	164732	303733410	2002	303731408
333	164740	303733755	1955	303731800
333	164748	303734050	1866	303732184
333	164756	303734367	1799	303732568
333	164804	303734746	1794	303732952
333	164812	303735306	1970	303733336
333	164820	303735698	1978	303733720
333	164828	303736092	1996	303734096
333	164836	303736562	2082	303734480
333	164844	303736928	2064	303734864
333	165348	303751121	1673	303749448
333	165356	303751694	1862	303749832
333	165404	303752009	1793	303750216
333	165412	303752530	1930	303750600
333	165420	303752983	1991	303750992
333	165428	303753339	1971	303751368
333	165436	303753669	1917	303751752
333	165444	303754090	1954	303752136
333	165452	303754314	1794	303752520
333	165500	303754931	2027	303752904
333	165508	303755567	2279	303753288
333	165516	303755996	2316	303753680
333	165524	303756426	2370	303754056
333	165532	303756792	2352	303754440
333	165540	303757145	2321	303754824
333	165548	303757552	2344	303755208
333	165556	303757721	2121	303755600
333	165604	303758151	2175	303755976
333	165612	303758353	1993	303756360
333	165620	303758711	1967	303756744
333	165628	303759048	1912	303757136
333	165636	303759556	2044	303757512
333	165644	303759951	2047	303757904
333	165652	303760289	2009	303758280
333	165700	303760679	2023	303758656
333	165708	303761118	2070	303759048

333	165716	303761487	2055	303759432
333	165724	303761850	2034	303759816
333	165732	303762060	1852	303760208
333	165740	303762337	1753	303760584
333	165748	303762741	1773	303760968
333	165756	303763138	1778	303761360
333	165804	303763610	1866	303761744
333	165812	303763961	1833	303762128
333	165820	303764412	1900	303762512
333	165828	303764735	1839	303762896
333	165836	303765159	1887	303763272
333	165844	303765669	2005	303763664
333	165852	303766043	1995	303764048
333	170404	303780940	1892	303779048
333	170412	303781390	1958	303779432
333	170420	303781778	1962	303779816
333	170428	303782238	2038	303780200
333	170436	303782611	2027	303780584
333	170444	303783045	2077	303780968
333	170452	303783356	1996	303781360
333	170500	303783688	1944	303781744
333	170508	303784025	1897	303782128
333	170516	303784473	1961	303782512
333	170524	303784747	1851	303782896
333	170532	303785101	1813	303783288
333	170540	303785491	1811	303783680
333	170548	303785869	1813	303784056
333	170556	303786197	1757	303784440
333	170604	303786687	1863	303784824
333	170612	303786921	1713	303785208
333	170620	303787385	1785	303785600
333	170628	303787671	1687	303785984
333	170636	303788097	1729	303786368
333	170644	303788700	1956	303786744
333	170652	303789248	2112	303787136
333	170700	303789709	2181	303787528
333	170708	303790195	2291	303787904
333	170716	303790649	2353	303788296
333	170724	303791055	2375	303788680
333	170732	303791486	2422	303789064
333	170740	303791965	2517	303789448
333	170748	303792352	2512	303789840
333	170756	303792831	2607	303790224
333	170804	303793359	2759	303790600
333	170812	303793742	2750	303790992
333	170820	303794105	2729	303791376
333	170828	303794459	2691	303791768
333	170836	303794821	2677	303792144
333	170844	303795065	2537	303792528
333	170852	303795289	2377	303792912
333	170900	303795722	2418	303793304
333	171404	303810495	2535	303807960
333	171412	303810960	2616	303808344
333	171420	303811505	2777	303808728
333	171428	303811799	2687	303809112
333	171436	303812107	2611	303809496
333	171444	303812572	2684	303809888
333	171452	303812880	2608	303810272
333	171500	303813148	2492	303810656

333	171508	303813560	2520	303811040
333	171516	303814009	2585	303811424
333	171524	303814437	2621	303811816
333	171532	303814876	2676	303812200
333	171540	303815300	2716	303812584
333	171548	303815636	2660	303812976
333	171556	303815935	2575	303813360
333	171604	303816163	2419	303813744
333	171612	303816490	2354	303814136
333	171620	303816881	2361	303814520
333	171628	303817241	2345	303814896
333	171636	303817644	2356	303815288
333	171644	303817943	2263	303815680
333	171652	303818437	2373	303816064
333	171700	303818829	2373	303816456
333	171708	303819143	2303	303816840
333	171716	303819508	2292	303817216
333	171724	303820014	2406	303817608
333	171732	303820467	2467	303818000
333	171740	303820712	2328	303818384
333	171748	303821120	2360	303818760
333	171756	303821675	2523	303819152
333	171804	303822181	2645	303819536
333	171812	303822683	2755	303819928
333	171820	303823216	2904	303820312
333	171828	303823411	2715	303820696
333	171836	303823738	2658	303821080
333	171844	303823965	2501	303821464
333	171852	303824260	2404	303821856
333	171900	303824714	2474	303822240
333	171908	303825178	2554	303822624
333	173332	303864783	351	303864432
333	173340	303865170	346	303864824
333	173348	303865644	444	303865200
333	173356	303866347	747	303865600
333	173404	303866817	833	303865984
333	173412	303867231	855	303866376
333	173420	303867812	1044	303866768
333	173428	303868224	1080	303867144
333	173436	303868553	1017	303867536
333	173444	303868866	946	303867920
333	173452	303869222	902	303868320
333	173500	303869626	922	303868704
333	173508	303869962	866	303869096
333	173516	303870362	882	303869480
333	173524	303870624	760	303869864
333	173532	303871009	753	303870256
333	173540	303871588	948	303870640
333	173548	303872001	969	303871032
333	173556	303872407	983	303871424
333	173604	303872902	1094	303871808
333	173612	303873166	966	303872200
333	173620	303873790	1206	303872584
333	173628	303874217	1249	303872968
333	173636	303874424	1072	303873352
333	173644	303874981	1237	303873744
333	175708	303934457	1177	303933280
333	173652	303875179	1051	303874128
333	173700	303875195	667	303874528

333	175340	303923301	157	303923144
333	175348	303923875	339	303923536
333	175356	303924534	614	303923920
333	175404	303925045	733	303924312
333	175412	303925533	829	303924704
333	175420	303925800	712	303925088
333	175428	303926081	601	303925480
333	175436	303926550	678	303925872
333	175444	303926973	709	303926264
333	175452	303927420	780	303926640
333	175500	303927986	946	303927040
333	175508	303928359	927	303927432
333	175516	303928808	992	303927816
333	175524	303929231	1023	303928208
333	175532	303929505	905	303928600
333	175540	303929897	905	303928992
333	175548	303930446	1070	303929376
333	175556	303930903	1135	303929768
333	175604	303931325	1165	303930160
333	175612	303931753	1201	303930552
333	175620	303932167	1231	303930936
333	175628	303932530	1202	303931328
333	175636	303932936	1216	303931720
333	175644	303933437	1333	303932104
333	175652	303933832	1336	303932496
333	175700	303934153	1265	303932888

FLIGHT	TIME	04 DEC 62		01
338	140808	326506501	1621	326504880
338	140816	326506850	1522	326505328
338	140824	326507239	1455	326505784
338	140832	326507588	1356	326506232
338	140840	326508033	1345	326506688
338	140848	326508524	1380	326507144
338	140856	326509037	1437	326507600
338	140904	326509458	1402	326508056
338	140912	326509705	1201	326508504
338	140920	326510073	1105	326508968
338	140928	326510578	1162	326509416
338	140936	326510995	1115	326509880
338	140944	326511370	1042	326510328
338	140952	326511878	1102	326510776
338	141000	326512257	1017	326511240
338	141008	326512759	1071	326511688
338	141016	326513377	1233	326512144
338	141024	326513872	1272	326512600
338	141032	326514474	1418	326513056
338	141040	326514954	1450	326513504
338	141048	326515669	1709	326513960
338	141056	326516081	1665	326514416
338	141104	326516563	1691	326514872
338	141632	326535434	1930	326533504
338	141640	326536093	2125	326533968
338	141648	326536481	2057	326534424
338	141656	326536815	1943	326534872
338	141704	326537174	1838	326535336
338	141712	326537529	1737	326535792
338	140800	326505947	1531	326504416
338	141720	326537964	1724	326536240
338	141728	326538628	1924	326536704
338	141736	326539005	1853	326537152
338	141744	326539511	1903	326537608
338	141752	326540064	2008	326538056
338	141800	326540478	1950	326538528
338	141808	326540874	1898	326538976
338	141816	326541087	1655	326539432
338	141824	326541575	1695	326539880
338	141832	326542053	1717	326540336
338	141840	326542554	1762	326540792
338	141848	326543012	1772	326541240
338	141856	326543536	1832	326541704
338	141904	326544122	1962	326542160
338	141912	326544490	1882	326542608
338	141920	326544865	1801	326543064
338	141928	326545063	1543	326543520
338	141936	326545503	1527	326543976
338	141944	326545910	1486	326544424
338	141952	326546378	1498	326544880
338	142000	326546875	1539	326545336
338	142008	326547393	1601	326545792
338	142016	326547868	1620	326546248
338	142024	326548491	1787	326546704
338	142032	326548994	1834	326547160
338	142040	326549341	1733	326547608
338	142048	326549784	1712	326548072

338	142056	326550296	1768	326548528
338	142104	326550829	1845	326548984
338	142112	326551456	2024	326549432
338	142120	326551940	2052	326549888
338	142128	326552422	2078	326550344
338	142136	326552811	2011	326550800
338	142144	326553216	1960	326551256
338	142152	326553737	2025	326551712
338	142728	326573364	2532	326570832
338	142736	326573956	2660	326571296
338	142744	326574318	2566	326571752
338	142752	326574950	2742	326572208
338	142800	326575435	2779	326572656
338	142808	326575900	2780	326573120
338	142816	326576236	2660	326573576
338	142824	326576479	2447	326574032
338	142832	326576961	2481	326574480
338	142840	326577600	2664	326574936
338	142848	326578070	2678	326575392
338	142856	326578399	2559	326575840
338	142904	326578925	2621	326576304
338	142912	326579222	2454	326576768
338	142920	326579478	2262	326577216
338	142928	326579829	2165	326577664
338	142936	326580260	2140	326578120
338	142944	326580782	2198	326578584
338	142952	326581290	2250	326579040
338	143000	326581694	2206	326579488
338	143008	326582271	2327	326579944
338	143016	326582610	2202	326580408
338	143024	326583255	2399	326580856
338	143032	326583733	2413	326581320
338	143040	326584205	2437	326581768
338	143048	326584562	2338	326582224
338	143056	326585011	2331	326582680
338	143104	326585465	2321	326583144
338	143112	326586206	2606	326583600
338	143120	326586476	2420	326584056
338	143128	326586836	2332	326584504
338	143136	326587170	2202	326584968
338	143144	326587726	2302	326585424
338	143152	326587962	2082	326585880
338	143200	326588471	2135	326586336
338	143208	326588739	1947	326586792
338	143216	326589144	1896	326587248
338	143224	326589737	2041	326587696
338	143232	326590195	2043	326588152
338	143240	326590786	2178	326588608
338	143248	326591143	2079	326589064
338	163528	327013996	1036	327012960
338	163536	327014436	1012	327013424
338	163544	327014957	1061	327013896
338	163552	327015342	982	327014360
338	163600	327015939	1115	327014824
338	163608	327016381	1085	327015296
338	163616	327017070	1310	327015760
338	163624	327017834	1610	327016224
338	163632	327018247	1551	327016696
338	163640	327018852	1692	327017160

338	163648	327019230	1606	327017624
338	163656	327019637	1549	327018088
338	163704	327020196	1636	327018560
338	163712	327020598	1574	327019024
338	163720	327021280	1800	327019480
338	163728	327021781	1821	327019960
338	163736	327022137	1713	327020424
338	163744	327022878	1982	327020896
338	163752	327023308	1956	327021352
338	163800	327023855	2031	327021824
338	163808	327024128	1840	327022288
338	163816	327024670	1918	327022752
338	163824	327024911	1695	327023216
338	163832	327025527	1839	327023688
338	163840	327025911	1759	327024152
338	163848	327026345	1721	327024624
338	163856	327027021	1933	327025088
338	163904	327027543	1991	327025552
338	163912	327028139	2123	327026016
338	163920	327028673	2185	327026488
338	163928	327029166	2214	327026952
338	163936	327029672	2256	327027416
338	163944	327030281	2393	327027888
338	163952	327030808	2456	327028352
338	164000	327031155	2331	327028824
338	164008	327031464	2184	327029280
338	164016	327031738	1986	327029752
338	164024	327032398	2174	327030224
338	164032	327032906	2226	327030680
338	164608	327051889	1601	327050288
338	164616	327052198	1438	327050760
338	164624	327052674	1450	327051224
338	164632	327052997	1301	327051696
338	164640	327053450	1290	327052160
338	164648	327053972	1348	327052624
338	164656	327054485	1389	327053096
338	164704	327054901	1349	327053552
338	164712	327055504	1472	327054032
338	164720	327055921	1425	327054496
338	164728	327056293	1333	327054960
338	164736	327056704	1272	327055432
338	164744	327057121	1233	327055888
338	164752	327057545	1185	327056360
338	164800	327057976	1152	327056824
338	164808	327058467	1171	327057296
338	164816	327058910	1150	327057760
338	164824	327059401	1177	327058224
338	164832	327059779	1075	327058704
338	164840	327060221	1053	327059168
338	164848	327060838	1206	327059632
338	164856	327061335	1231	327060104
338	164904	327061754	1186	327060568
338	164912	327062268	1236	327061032
338	164920	327062820	1316	327061504
338	164928	327063287	1311	327061976
338	164936	327063924	1484	327062440
338	164944	327064385	1473	327062912
338	164952	327064966	1590	327063376
338	165000	327065293	1453	327063840

338	165008	327065822	1510	327064312
338	165016	327066128	1360	327064768
338	165024	327066769	1521	327065248
338	165032	327067334	1622	327065712
338	165040	327067681	1513	327066168
338	165048	327068018	1362	327066656
338	165056	327068650	1538	327067112
338	165104	327069339	1755	327067584
338	165112	327069682	1634	327068048
338	165120	327070234	1722	327068512
338	165128	327070671	1687	327068984
338	165704	327089801	1169	327088632
338	165712	327090306	1210	327089096
338	165720	327090795	1227	327089568
338	165728	327091338	1306	327090032
338	165736	327091729	1225	327090504
338	165744	327092198	1222	327090976
338	165752	327092800	1360	327091440
338	165800	327093072	1160	327091912
338	165808	327093513	1129	327092384
338	165816	327094009	1161	327092848
338	165824	327094411	1099	327093312
338	165832	327094899	1115	327093784
338	165840	327095389	1133	327094256
338	165848	327095926	1206	327094720
338	165856	327096590	1398	327095192
338	165904	327097088	1440	327095648
338	165912	327097651	1523	327096128
338	165920	327098044	1452	327096592
338	165928	327098673	1617	327097056
338	165936	327099294	1758	327097536
338	165944	327099781	1789	327097992
338	165952	327100479	2015	327098464
338	170000	327100965	2029	327098936
338	170008	327101414	2014	327099400
338	170016	327101790	1918	327099872
338	170024	327102371	2043	327100328
338	170032	327102883	2075	327100808
338	170040	327103291	2019	327101272
338	170048	327103612	1860	327101752
338	170056	327103853	1637	327102216
338	170104	327104406	1726	327102680
338	170112	327104797	1645	327103152
338	170120	327105455	1831	327103624
338	170128	327105882	1794	327104088
338	170136	327106507	1947	327104560
338	170144	327106918	1902	327105016
338	170152	327107377	1889	327105488
338	170200	327107947	1987	327105960
338	170208	327108396	1956	327106440
338	170216	327108974	2070	327106904
338	170224	327109442	2066	327107376
338	170800	327128022	966	327127056
338	170808	327128430	902	327127528
338	170816	327129041	1033	327128008
338	170824	327129334	862	327128472
338	170832	327129694	758	327128936
338	170840	327130137	737	327129400
338	170848	327130583	703	327129880

338	170856	327131248	904	327130344
338	170904	327131764	956	327130808
338	170912	327132170	898	327131272
338	170920	327132752	1000	327131752
338	170928	327133334	1110	327132224
338	170936	327133889	1193	327132696
338	170944	327134487	1327	327133160
338	170952	327135124	1492	327133632
338	171000	327135650	1554	327134096
338	171008	327136141	1565	327134576
338	171016	327136562	1530	327135032
338	171024	327136910	1406	327135504
338	171032	327137399	1431	327135968
338	171040	327137811	1363	327136448
338	171048	327138440	1520	327136920
338	171056	327139055	1679	327137376
338	171104	327139391	1543	327137848
338	171112	327139879	1551	327138328
338	171120	327140426	1634	327138792
338	171128	327140914	1650	327139264
338	171136	327141486	1750	327139736
338	171144	327141951	1751	327140200
338	171152	327142351	1679	327140672
338	171200	327142683	1547	327141136
338	171208	327143083	1475	327141608
338	171216	327143631	1551	327142080
338	171224	327144248	1696	327142552
338	171232	327144706	1682	327143024
338	171240	327145004	1516	327143488
338	171248	327145508	1548	327143960
338	171256	327146010	1578	327144432
338	171304	327146490	1594	327144896
338	171312	327147210	1842	327145368
338	171320	327147602	1762	327145840
338	171848	327167205	2093	327165112
338	171856	327167777	2193	327165584
338	171904	327168328	2280	327166048
338	171912	327168671	2159	327166512
338	171920	327169132	2140	327166992
338	171928	327169556	2100	327167456
338	171936	327170114	2186	327167928
338	171944	327170768	2376	327168392
338	171952	327171371	2499	327168872
338	172000	327171641	2305	327169336
338	172008	327172224	2416	327169808
338	172016	327172672	2400	327170272
338	172024	327173057	2313	327170744
338	172032	327173528	2320	327171208
338	172040	327174040	2352	327171688
338	172048	327174550	2390	327172160
338	172056	327175027	2395	327172632
338	172104	327175662	2558	327173104
338	172112	327176201	2633	327173568
338	172120	327176448	2416	327174032
338	172128	327177078	2566	327174512
338	172136	327177555	2571	327174984
338	172144	327177960	2504	327175456
338	172152	327178341	2421	327175920
338	172200	327178617	2225	327176392

338	172208	327179214	2350	327176864
338	172216	327179892	2548	327177344
338	172224	327180217	2409	327177808
338	172232	327180841	2561	327178280
338	172240	327181137	2393	327178744
338	172248	327181616	2400	327179216
338	172256	327182003	2315	327179688
338	172304	327182419	2259	327180160
338	172312	327182953	2329	327180624
338	172320	327183370	2282	327181088
338	172328	327183852	2284	327181568
338	172336	327184371	2331	327182040
338	172344	327184866	2354	327182512
338	172352	327185322	2338	327182984
338	172400	327185838	2382	327183456
338	172408	327186177	2257	327183920

FLIGHT TIME 06 DEC 62 01

340	181704	337884191	1967	337882224
340	181712	337884941	2221	337882720
340	181720	337885304	2072	337883232
340	181728	337885819	2091	337883728
340	181744	337886958	2222	337884736
340	181736	337886428	2196	337884232
340	181752	337887491	2243	337885248
340	181800	337888156	2412	337885744
340	181808	337888629	2381	337886248
340	181816	337889136	2384	337886752
340	181824	337889564	2292	337887272
340	181832	337890032	2272	337887760
340	181840	337890365	2101	337888264
340	181848	337891038	2270	337888768
340	181856	337891487	2215	337889272
340	181904	337892165	2381	337889784
340	181912	337892655	2367	337890288
340	181920	337893006	2222	337890784
340	181928	337893506	2210	337891296
340	181936	337893773	1973	337891800
340	181944	337894282	1978	337892304
340	181952	337894874	2074	337892800
340	182000	337895416	2112	337893304
340	182008	337896034	2226	337893808
340	182016	337896663	2343	337894320
340	182024	337897106	2282	337894824
340	182032	337897635	2307	337895328
340	182040	337898178	2346	337895832
340	182048	337898901	2565	337896336
340	182056	337899606	2766	337896840
340	182104	337900191	2839	337897352
340	182112	337900651	2803	337897848
340	182120	337901262	2910	337898352
340	182128	337901875	3011	337898864
340	182136	337902346	2978	337899368
340	182144	337902881	3009	337899872
340	182152	337903586	3210	337900376
340	182200	337904184	3304	337900880
340	182208	337904691	3307	337901384
340	182216	337905123	3227	337901896
340	182224	337905613	3213	337902400
340	182232	337906132	3236	337902896
340	182808	337927487	3383	337924104
340	182816	337927903	3287	337924616
340	182824	337928544	3432	337925112
340	182832	337928878	3254	337925624
340	182840	337929408	3288	337926120
340	182848	337929810	3178	337926632
340	182856	337930351	3215	337927136
340	182904	337930773	3133	337927640
340	182912	337931548	3404	337928144
340	182920	337931977	3329	337928648
340	182928	337932535	3375	337929160
340	182936	337932937	3281	337929656
340	182944	337933653	3485	337930168
340	182952	337933773	3101	337930672
340	183000	337934299	3123	337931176

340	183008	337934787	3107	337931680
340	183016	337935153	2969	337932184
340	183024	337935699	3011	337932688
340	183032	337936234	3034	337933200
340	183040	337936706	3002	337933704
340	183048	337937237	3029	337934208
340	183056	337937632	2920	337934712
340	183104	337938269	3045	337935224
340	183112	337938782	3054	337935728
340	183120	337939234	3002	337936232
340	183128	337939761	3017	337936744
340	183136	337940212	2972	337937240
340	183144	337940751	2999	337937752
340	183152	337941305	3049	337938256
340	183200	337941737	2977	337938760
340	183208	337942447	3175	337939272
340	183216	337942830	3054	337939776
340	183224	337943437	3157	337940280
340	183232	337943827	3043	337940784
340	183240	337944341	3053	337941288
340	183248	337944739	2947	337941792
340	183256	337945378	3082	337942296
340	183304	337945802	3002	337942800
340	183312	337946411	3099	337943312
340	183320	337947127	3311	337943816
340	183328	337947435	3115	337944320
340	183336	337948021	3189	337944832
340	190120	338053398	3126	338050272
340	190128	338053816	3032	338050784
340	190136	338054251	2955	338051296
340	190144	338054610	2818	338051792
340	190152	338055383	3079	338052304
340	190200	338055981	3165	338052816
340	190208	338056467	3147	338053320
340	190216	338056946	3114	338053832
340	190224	338057451	3107	338054344
340	190232	338058076	3236	338054840
340	190240	338058663	3311	338055352
340	190248	338059135	3279	338055856
340	190256	338059677	3293	338056384
340	190304	338060146	3258	338056888
340	190312	338060844	3452	338057392
340	190320	338061363	3459	338057904
340	190328	338061818	3402	338058416
340	190336	338062305	3377	338058928
340	190344	338062715	3283	338059432
340	190352	338063241	3297	338059944
340	190400	338063680	3240	338060440
340	190408	338064322	3378	338060944
340	190416	338064815	3359	338061456
340	190424	338065357	3397	338061960
340	190432	338066002	3522	338062480
340	190440	338066304	3320	338062984
340	190448	338066946	3458	338063488
340	190456	338067410	3402	338064008
340	190504	338068181	3677	338064504
340	190512	338068675	3659	338065016
340	190520	338069280	3752	338065528
340	190528	338069821	3781	338066040

340	190536	338070177	3641	338066536
340	190544	338070796	3748	338067048
340	190552	338071266	3706	338067560
340	190600	338071853	3781	338068072
340	190608	338072396	3820	338068576
340	190616	338072883	3795	338069088
340	190624	338073473	3881	338069592
340	190632	338073966	3862	338070104
340	190640	338074386	3778	338070608
340	190648	338074902	3782	338071120
340	191224	338094802	2306	338092496
340	191232	338095294	2294	338093000
340	191240	338095907	2395	338093512
340	191248	338096594	2578	338094016
340	191256	338097340	2804	338094536
340	191304	338097674	2634	338095040
340	191312	338098399	2847	338095552
340	191320	338098919	2847	338096072
340	191328	338099304	2736	338096568
340	191336	338099878	2798	338097080
340	191344	338100216	2624	338097592
340	191352	338100575	2471	338098104
340	191400	338101158	2550	338098608
340	191408	338101762	2650	338099112
340	191416	338102138	2506	338099632
340	191424	338102767	2631	338100136
340	191432	338103395	2747	338100648
340	191440	338104056	2904	338101152
340	191448	338104603	2939	338101664
340	191456	338105403	3227	338102176
340	191504	338105849	3169	338102680
340	191512	338106334	3142	338103192
340	191520	338106749	3053	338103696
340	191528	338107310	3102	338104208
340	191536	338107985	3265	338104720
340	191544	338108698	3474	338105224
340	191552	338109317	3581	338105736
340	191600	338109809	3561	338106248
340	191608	338110223	3463	338106760
340	191616	338110556	3284	338107272
340	191624	338111052	3268	338107784
340	191632	338111580	3292	338108288
340	191640	338112044	3244	338108800
340	191648	338112711	3407	338109304
340	191656	338113376	3560	338109816
340	191704	338114021	3693	338110328
340	191712	338114659	3819	338110840
340	191720	338115096	3752	338111344
340	191728	338115527	3671	338111856
340	191736	338115919	3559	338112360
340	191744	338116491	3611	338112880
340	191752	338116908	3524	338113384
340	192328	338138783	3983	338134800
340	192336	338139355	4051	338135304
340	192344	338139808	3992	338135816
340	192352	338140271	3951	338136320
340	192400	338140872	4032	338136840
340	192408	338141147	3803	338137344
340	192416	338141741	3893	338137848

340	192424	338142507	4139	338138368
340	192432	338142903	4023	338138880
340	192440	338143423	4039	338139384
340	192448	338144017	4113	338139904
340	192456	338144589	4173	338140416
340	192504	338145148	4228	338140920
340	192512	338145664	4232	338141432
340	192520	338146170	4234	338141936
340	192528	338146673	4217	338142456
340	192536	338147244	4284	338142960
340	192544	338147670	4198	338143472
340	192552	338148071	4087	338143984
340	192600	338148487	3999	338144488
340	192608	338149054	4054	338145000
340	192616	338149698	4186	338145512
340	192624	338150302	4278	338146024
340	192632	338150767	4231	338146536
340	192640	338151345	4305	338147040
340	192648	338151707	4155	338147552
340	192656	338152191	4135	338148056
340	192704	338152775	4199	338148576
340	192712	338153293	4205	338149088
340	192720	338153718	4134	338149584
340	192728	338154254	4142	338150112
340	192736	338154548	3940	338150608
340	192744	338155141	4013	338151128
340	192752	338155709	4069	338151640
340	192800	338156200	4056	338152144
340	192808	338156674	4018	338152656
340	192816	338157064	3904	338153160
340	192824	338157665	3985	338153680
340	192832	338158127	3935	338154192
340	192840	338158464	3768	338154696
340	192848	338159017	3801	338155216

FLIGHT	TIME	13 DEC 62	01	
347	122032	377299553	1985	377297568
347	122040	377299996	1868	377298128
347	122048	377300646	1958	377298688
347	122056	377301209	1969	377299240
347	122104	377301901	2101	377299800
347	122112	377302407	2063	377300344
347	122120	377303042	2138	377300904
347	122128	377303534	2062	377301472
347	122136	377304092	2068	377302024
347	122144	377304507	1931	377302576
347	122152	377305088	1952	377303136
347	122200	377305598	1910	377303688
347	122208	377306021	1773	377304248
347	122832	377332656	1688	377330968
347	122840	377333229	1693	377331536
347	122848	377333597	1509	377332088
347	122856	377334211	1563	377332648
347	122904	377334665	1465	377333200
347	122912	377335195	1443	377333752
347	122920	377335595	1275	377334320
347	122928	377336217	1345	377334872
347	122936	377336835	1411	377335424
347	122944	377337464	1480	377335984
347	122952	377338037	1501	377336536
347	123000	377338674	1578	377337096
347	123008	377339284	1628	377337656
347	123016	377339906	1698	377338208
347	123024	377340274	1506	377338768
347	123032	377340796	1476	377339320
347	123040	377341286	1398	377339888
347	123048	377341942	1502	377340440
347	123056	377342431	1431	377341000
347	123104	377342951	1399	377341552
347	123112	377343285	1173	377342112
347	123120	377343859	1195	377342664
347	123128	377344593	1377	377343216
347	123136	377345141	1365	377343776
347	123144	377345696	1360	377344336
347	123152	377346371	1475	377344896
347	123200	377347125	1669	377345456
347	123208	377347838	1838	377346000
347	123216	377348338	1770	377346568
347	123224	377348874	1754	377347120
347	123232	377349411	1739	377347672
347	123240	377349848	1608	377348240
347	123248	377350432	1640	377348792
347	123256	377351009	1657	377349352
347	123304	377351535	1623	377349912
347	123312	377352132	1668	377350464
347	123320	377352717	1693	377351024
347	123328	377353248	1664	377351584
347	123336	377353846	1710	377352136
347	123344	377354556	1852	377352704
347	123352	377355179	1923	377353256
347	123400	377355776	1976	377353800
347	123408	377356247	1887	377354360
347	123416	377356864	1936	377354928

347	123424	377357448	1968	377355480
347	123432	377357915	1875	377356040
347	123440	377358390	1798	377356592
347	124112	377385741	1845	377383896
347	124120	377386218	1770	377384448
347	124128	377386796	1796	377385000
347	124136	377387404	1836	377385568
347	124144	377387969	1849	377386120
347	124152	377388563	1883	377386680
347	124200	377388984	1736	377387248
347	124208	377389592	1792	377387800
347	124216	377390191	1839	377388352
347	124224	377390737	1825	377388912
347	124232	377391224	1752	377389472
347	124240	377391773	1749	377390024
347	124248	377392190	1606	377390584
347	124256	377392634	1498	377391136
347	124304	377393199	1503	377391696
347	124312	377393735	1471	377392264
347	124320	377394281	1465	377392816
347	124328	377394624	1256	377393368
347	124336	377395174	1246	377393928
347	124344	377395787	1291	377394496
347	124352	377396328	1288	377395040
347	124400	377397016	1416	377395600
347	124408	377397577	1425	377396152
347	124416	377398075	1363	377396712
347	124424	377398763	1491	377397272
347	124432	377399433	1609	377397824
347	124440	377400058	1674	377398384
347	124448	377400846	1902	377398944
347	124456	377401368	1864	377399504
347	124504	377401974	1926	377400048
347	124512	377402417	1809	377400608
347	124520	377403153	1977	377401176
347	124528	377403626	1890	377401736
347	124536	377404173	1885	377402288
347	124544	377404771	1923	377402848
347	124552	377405438	2030	377403408
347	124600	377405994	2042	377403952
347	124608	377406450	1938	377404512
347	124616	377406977	1905	377405072
347	124624	377407554	1922	377405632
347	124632	377408239	2039	377406200
347	124640	377408709	1965	377406744
347	124648	377409286	1982	377407304
347	124656	377409704	1848	377407856
347	124704	377410455	2031	377408424
347	124712	377410985	2009	377408976
347	125344	377438305	2001	377436304
347	125352	377439020	2156	377436864
347	125400	377439576	2160	377437416
347	125408	377440296	2320	377437976
347	125416	377440789	2253	377438536
347	125424	377441343	2255	377439088
347	125432	377441931	2291	377439640
347	125440	377442385	2169	377440216
347	125448	377442873	2105	377440768
347	125456	377443433	2113	377441320

347	125504	377444010	2130	377441880
347	125512	377444663	2223	377442440
347	125520	377445155	2155	377443000
347	125528	377445847	2295	377443552
347	125536	377446491	2379	377444112
347	125544	377446989	2317	377444672
347	125552	377447576	2344	377445232
347	125600	377448047	2255	377445792
347	125608	377448782	2446	377446336
347	125616	377449150	2246	377446904
347	125624	377449736	2272	377447464
347	125632	377450401	2385	377448016
347	125640	377451076	2500	377448576
347	125648	377451567	2431	377449136
347	125656	377452243	2547	377449696
347	125704	377452895	2647	377450248
347	125712	377453370	2554	377450816
347	125720	377453797	2437	377451360
347	125728	377454360	2440	377451920
347	125736	377454766	2286	377452480
347	125744	377455227	2187	377453040
347	125752	377455784	2192	377453592
347	125800	377456387	2235	377454152
347	125808	377457078	2366	377454712
347	125816	377457652	2372	377455280
347	125824	377458017	2185	377455832
347	125832	377458439	2055	377456384
347	125840	377459077	2133	377456944
347	125848	377459726	2214	377457512
347	125856	377460336	2264	377458072
347	125904	377460809	2185	377458624
347	125912	377461397	2221	377459176
347	125920	377461962	2226	377459736
347	125928	377462633	2337	377460296
347	125936	377463202	2354	377460848
347	125944	377463577	2169	377461408
347	125952	377464173	2213	377461960
347	130616	377490981	2221	377488760
347	130624	377491602	2282	377489320
347	130632	377492239	2359	377489880
347	130640	377492827	2387	377490440
347	130648	377493345	2345	377491000
347	130656	377493846	2294	377491552
347	130704	377494401	2289	377492112
347	130712	377495053	2381	377492672
347	130720	377495503	2279	377493224
347	130728	377496102	2310	377493792
347	130736	377496810	2466	377494344
347	130744	377497563	2659	377494904
347	130752	377498330	2858	377495472
347	130800	377499058	3026	377496032
347	130808	377499522	2938	377496584
347	130816	377500065	2929	377497136
347	130824	377500486	2782	377497704
347	130832	377500960	2704	377498256
347	130840	377501533	2717	377498816
347	130848	377502026	2650	377499376
347	130856	377502530	2594	377499936
347	130904	377503072	2584	377500488

347	130912	377503494	2446	377501048
347	130920	377504207	2607	377501600
347	130928	377504700	2532	377502168
347	130936	377505154	2426	377502728
347	130944	377505875	2595	377503280
347	130952	377506502	2670	377503832
347	131000	377507074	2674	377504400
347	131008	377507571	2611	377504960
347	131016	377508128	2608	377505520
347	131024	377508845	2773	377506072
347	131032	377509410	2778	377506632
347	131040	377510136	2944	377507192
347	131048	377510619	2867	377507752
347	131056	377511180	2868	377508312
347	131104	377511835	2963	377508872
347	131112	377512472	3040	377509432
347	131120	377513143	3159	377509984
347	131128	377513744	3200	377510544
347	131136	377514305	3201	377511104
347	131144	377514826	3170	377511656
347	131152	377515555	3339	377512216
347	131200	377516125	3341	377512784
347	131208	377516542	3206	377513336
347	131216	377517125	3229	377513896
347	131224	377517609	3153	377514456
347	131856	377544888	3048	377541840
347	131904	377545270	2870	377542400
347	131912	377545791	2831	377542960
347	131920	377546445	2933	377543512
347	131928	377547103	3031	377544072
347	131936	377547767	3135	377544632
347	131944	377548412	3212	377545200
347	131952	377548990	3238	377545752
347	132000	377549379	3067	377546312
347	132008	377550164	3300	377546864
347	132016	377550668	3236	377547432
347	132024	377551124	3140	377547984
347	132032	377551628	3084	377548544
347	132040	377552153	3049	377549104
347	132048	377552630	2974	377549656
347	132056	377553178	2946	377550232
347	132104	377553724	2932	377550792
347	132112	377554318	2974	377551344
347	132120	377555015	3111	377551904
347	132128	377555425	2961	377552464
347	132136	377556054	3030	377553024
347	132144	377556659	3083	377553576
347	132152	377557247	3111	377554136
347	132200	377557712	3016	377554696
347	132208	377558202	2946	377555256
347	132216	377558625	2801	377555824
347	132224	377559174	2798	377556376
347	132232	377559707	2771	377556936
347	132240	377560196	2700	377557496
347	132248	377560713	2657	377558056
347	132256	377561301	2693	377558608
347	132304	377562013	2837	377559176
347	132312	377562486	2758	377559728
347	132320	377563004	2716	377560288

347	132328	377563742	2886	377560856
347	132336	377564272	2864	377561408
347	132344	377564757	2789	377561968
347	132352	377565254	2726	377562528
347	132400	377566050	2962	377563088
347	132408	377566721	3073	377563648
347	132416	377567263	3055	377564208
347	132424	377567853	3093	377564760
347	132432	377568517	3197	377565320
347	132440	377568985	3105	377565880
347	132448	377569412	2972	377566440
347	132456	377569894	2886	377567008
347	133128	377597079	2663	377594416
347	133136	377597700	2724	377594976
347	133144	377598270	2742	377595528
347	133152	377598754	2658	377596096
347	133200	377599294	2638	377596656
347	133208	377599824	2608	377597216
347	133216	377600457	2681	377597776
347	133224	377601095	2767	377598328
347	133232	377601596	2700	377598896
347	133240	377602284	2828	377599456
347	133248	377602791	2783	377600008
347	133256	377603371	2803	377600568
347	133304	377603914	2786	377601128
347	133312	377604437	2741	377601696
347	133320	377604907	2651	377602256
347	133328	377605408	2592	377602816
347	133336	377605872	2504	377603368
347	133344	377606369	2441	377603928
347	133352	377607049	2553	377604496
347	133400	377607767	2719	377605048
347	133408	377608296	2688	377605608
347	133416	377608738	2578	377606160
347	133424	377609371	2651	377606720
347	133432	377609965	2677	377607288
347	133440	377610608	2760	377607848
347	133448	377611203	2795	377608408
347	133456	377611779	2811	377608968
347	133504	377612380	2860	377609520
347	133512	377612873	2785	377610088
347	133520	377613530	2882	377610648
347	133528	377614161	2953	377611208
347	133536	377614761	2993	377611768
347	133544	377615481	3153	377612328
347	133552	377616139	3251	377612888
347	133600	377616542	3094	377613448
347	133608	377617161	3153	377614008
347	133616	377617588	3020	377614568
347	133624	377618097	2969	377615128
347	133632	377618773	3085	377615688
347	133640	377619320	3072	377616248
347	133648	377620027	3211	377616816
347	133656	377620842	3474	377617368
347	133704	377621464	3536	377617928
347	133712	377621990	3502	377618488
347	133720	377622566	3518	377619048
347	133728	377623220	3612	377619608
347	133736	377623836	3668	377620168

347	134400	377650690	3634	377647056
347	134408	377651217	3601	377647616
347	134416	377651724	3548	377648176
347	134424	377652290	3554	377648736
347	134432	377652929	3633	377649296
347	134440	377653442	3586	377649856
347	134448	377654091	3675	377650416
347	134456	377654597	3613	377650984
347	134504	377655053	3509	377651544
347	134512	377655792	3688	377652104
347	134520	377656326	3670	377652656
347	134528	377656794	3578	377653216
347	134536	377657249	3473	377653776
347	134544	377657813	3469	377654344
347	134552	377658437	3541	377654896
347	134600	377659065	3601	377655464
347	134608	377659492	3468	377656024
347	134616	377660178	3594	377656584
347	134624	377660717	3573	377657144
347	134632	377661224	3528	377657696
347	134640	377661625	3361	377658264
347	134648	377662419	3587	377658832
347	134656	377662824	3432	377659392
347	134704	377663519	3567	377659952
347	134712	377664161	3649	377660512
347	134720	377664865	3801	377661064
347	134728	377665162	3530	377661632
347	134736	377665826	3634	377662192
347	134744	377666426	3674	377662752
347	134752	377666992	3688	377663304
347	134800	377667427	3555	377663872
347	134808	377668042	3602	377664440
347	134816	377668582	3590	377664992
347	134824	377669257	3705	377665552
347	134832	377669631	3519	377666112
347	134840	377670239	3567	377666672
347	134848	377670669	3437	377667232
347	134856	377671197	3405	377667792
347	134904	377671755	3403	377668352
347	134912	377672222	3310	377668912
347	134920	377672913	3441	377669472
347	134928	377673438	3398	377670040
347	134936	377674159	3559	377670600
347	134944	377674842	3682	377671160
347	134952	377675156	3444	377671712
347	135000	377675768	3480	377672288
347	135008	377676334	3494	377672840
347	135632	377703212	3444	377699768
347	135640	377703763	3435	377700328
347	135648	377704437	3541	377700896
347	135656	377705216	3768	377701448
347	135704	377705837	3821	377702016
347	135712	377706304	3736	377702568
347	135720	377706897	3761	377703136
347	135728	377707372	3668	377703704
347	135736	377707933	3685	377704248
347	135744	377708352	3536	377704816
347	135752	377708765	3389	377705376
347	135800	377709444	3508	377705936

347	135808	377709942	3438	377706504
347	135816	377710414	3350	377707064
347	135824	377710984	3368	377707616
347	135832	377711488	3312	377708176
347	135840	377712054	3310	377708744
347	135848	377712664	3352	377709312
347	135856	377713246	3382	377709864
347	135904	377713692	3260	377710432
347	135912	377714310	3310	377711000
347	135920	377714927	3375	377711552
347	135928	377715574	3462	377712112
347	135936	377716139	3459	377712680
347	135944	377716669	3429	377713240

FLIGHT	TIME	14 DEC 62	01	
348	123540	383626476	1948	383624528
348	123548	383627170	2074	383625096
348	123556	383627648	1992	383625656
348	123604	383628285	2053	383626232
348	123612	383628774	1974	383626800
348	123620	383629286	1918	383627368
348	123628	383629730	1810	383627920
348	123636	383630303	1807	383628496
348	123644	383630710	1654	383629056
348	123652	383631380	1756	383629624
348	123700	383631956	1772	383630184
348	123708	383632586	1826	383630760
348	123716	383633217	1889	383631328
348	123724	383633736	1848	383631888
348	123732	383634292	1836	383632456
348	123740	383634676	1652	383633024
348	123748	383635337	1753	383633584
348	123756	383636051	1891	383634160
348	123804	383636696	1968	383634728
348	123812	383637074	1786	383635288
348	123820	383637583	1727	383635856
348	123828	383638156	1740	383636416
348	123836	383638718	1726	383636992
348	123844	383639168	1608	383637560
348	123852	383639895	1783	383638112
348	123900	383640406	1726	383638680
348	123908	383641041	1793	383639248
348	123916	383641612	1788	383639824
348	123924	383641865	1481	383640384
348	123932	383642424	1472	383640952
348	123940	383643240	1728	383641512
348	123948	383643866	1786	383642080
348	123956	383644465	1825	383642640
348	124004	383645220	2004	383643216
348	124012	383645684	1908	383643776
348	124020	383646085	1741	383644344
348	124028	383646556	1644	383644912
348	124036	383647005	1525	383645480
348	124044	383647494	1454	383646040
348	124052	383648072	1456	383646616
348	124100	383648643	1475	383647168
348	124108	383649293	1557	383647736
348	124116	383649903	1591	383648312
348	124124	383650441	1569	383648872
348	124132	383651038	1598	383649440
348	124140	383651548	1540	383650008
348	124148	383652223	1647	383650576
348	124828	383680585	1689	383678896
348	124836	383681174	1718	383679456
348	124844	383681767	1743	383680024
348	124852	383682279	1687	383680592
348	124900	383682743	1583	383681160
348	124908	383683279	1551	383681728
348	124916	383684000	1704	383682296
348	124924	383684439	1575	383682864
348	124932	383685135	1703	383683432
348	124940	383685577	1585	383683992

348	124948	383686066	1506	383684560
348	124956	383686714	1586	383685128
348	125004	383687321	1633	383685688
348	125012	383687902	1638	383686264
348	125020	383688571	1739	383686832
348	125028	383689113	1721	383687392
348	125036	383689658	1698	383687960
348	125044	383690167	1639	383688528
348	125052	383690641	1545	383689096
348	125100	383691169	1505	383689664
348	125108	383691659	1443	383690216
348	125116	383692151	1359	383690792
348	125124	383692657	1305	383691352
348	125132	383693269	1341	383691928
348	125140	383694166	1670	383692496
348	125148	383694880	1824	383693056
348	125156	383695481	1857	383693624
348	125204	383696141	1957	383694184
348	125212	383696806	2054	383694752
348	125220	383697434	2106	383695328
348	125228	383698170	2282	383695888
348	125236	383698695	2239	383696456
348	125244	383699160	2136	383697024
348	125252	383699611	2019	383697592
348	125300	383700254	2094	383698160
348	125308	383700722	1994	383698728
348	125316	383701251	1963	383699288
348	125324	383701926	2070	383699856
348	125332	383702589	2157	383700432
348	125340	383703170	2170	383701000
348	125348	383703706	2138	383701568
348	125356	383704153	2025	383702128
348	125404	383704715	2027	383702688
348	125412	383705373	2117	383703256
348	125420	383705928	2096	383703832
348	125428	383706428	2036	383704392
348	125436	383707086	2126	383704960
348	130116	383735381	2069	383733312
348	130124	383735950	2070	383733880
348	130132	383736470	2030	383734440
348	130140	383737012	2004	383735008
348	130148	383737547	1971	383735576
348	130156	383738102	1958	383736144
348	130204	383738504	1800	383736704
348	130212	383739170	1898	383737272
348	130220	383739854	2014	383737840
348	130228	383740489	2081	383738408
348	130236	383741039	2063	383738976
348	130244	383741625	2081	383739544
348	130252	383742284	2172	383740112
348	130300	383742808	2128	383740680
348	130308	383743347	2099	383741248
348	130316	383744094	2278	383741816
348	130324	383744632	2248	383742384
348	130332	383745192	2240	383742952
348	130340	383745807	2295	383743512
348	130348	383746578	2490	383744088
348	130356	383747101	2453	383744648
348	130404	383747588	2372	383745216

348	130412	383748207	2423	383745784
348	130420	383748849	2497	383746352
348	130428	383749294	2374	383746920
348	130436	383749790	2294	383747496
348	130444	383750310	2254	383748056
348	130452	383750788	2172	383748616
348	130500	383751224	2032	383749192
348	130508	383751983	2223	383749760
348	130516	383752677	2349	383750328
348	130524	383753126	2238	383750888
348	130532	383753566	2110	383751456
348	130540	383754196	2172	383752024
348	130548	383754798	2206	383752592
348	130556	383755425	2265	383753160
348	130604	383756085	2365	383753720
348	130612	383756595	2307	383754288
348	130620	383757117	2261	383754856
348	130628	383757740	2308	383755432
348	130636	383758255	2255	383756000
348	130644	383758650	2090	383756560
348	130652	383759337	2201	383757136
348	130700	383759991	2295	383757696
348	130708	383760749	2485	383758264
348	130716	383761363	2523	383758840
348	130724	383761932	2532	383759400
348	131412	383790887	2551	383788336
348	131420	383791621	2701	383788920
348	131428	383792070	2590	383789480
348	131436	383792669	2613	383790056
348	131444	383793242	2626	383790616
348	131452	383793819	2635	383791184
348	131500	383794198	2446	383791752
348	131508	383794641	2321	383792320
348	131516	383795207	2319	383792888
348	131524	383795959	2503	383793456
348	131532	383796404	2388	383794016
348	131540	383797257	2673	383794584
348	131548	383797981	2821	383795160
348	131556	383798516	2788	383795728
348	131604	383799140	2844	383796296
348	131612	383799730	2866	383796864
348	131620	383800155	2723	383797432
348	131628	383800770	2770	383798000
348	131636	383801403	2835	383798568
348	131644	383802197	3061	383799136
348	131652	383802777	3073	383799704
348	131700	383803338	3074	383800264
348	131708	383803846	3006	383800840
348	131716	383804405	3005	383801400
348	131724	383804948	2972	383801976
348	131732	383805713	3177	383802536
348	131740	383806466	3354	383803112
348	131748	383807032	3352	383803680
348	131756	383807767	3519	383804248
348	131804	383808317	3501	383804816
348	131812	383808887	3503	383805384
348	131820	383809557	3605	383805952
348	131828	383810217	3705	383806512
348	131836	383810850	3762	383807088

348	131844	383811534	3886	383807648
348	131852	383811928	3712	383808216
348	131900	383812550	3758	383808792
348	131908	383813210	3850	383809360
348	131916	383813624	3696	383809928
348	131924	383814211	3723	383810488
348	131932	383814826	3762	383811064
348	131940	383815487	3863	383811624
348	131948	383816085	3893	383812192
348	131956	383816736	3976	383812760
348	132004	383817282	3954	383813328
348	132012	383817814	3918	383813896
348	132652	383846255	3943	383842312
348	132700	383846681	3801	383842880
348	132708	383847445	3997	383843448
348	132716	383848029	4013	383844016
348	132724	383848567	3983	383844584
348	132732	383849177	4025	383845152
348	132740	383849703	3983	383845720
348	132748	383850231	3943	383846288
348	132756	383850813	3949	383846864
348	132804	383851430	4006	383847424
348	132812	383852030	4038	383847992
348	132820	383852752	4192	383848560
348	132828	383853335	4207	383849128
348	132836	383853890	4194	383849696
348	132844	383854423	4159	383850264
348	132852	383854991	4151	383850840
348	132900	383855467	4067	383851400
348	132908	383855966	3998	383851968
348	132916	383856446	3902	383852544
348	132924	383857036	3924	383853112
348	132932	383857647	3967	383853680
348	132940	383858291	4043	383854248
348	132948	383858900	4084	383854816
348	132956	383859540	4156	383855384
348	133004	383859862	3902	383855960
348	133012	383860427	3907	383856520
348	133020	383861026	3938	383857088
348	133028	383861562	3906	383857656
348	133036	383862065	3841	383858224
348	133044	383862384	3584	383858800
348	133052	383862825	3465	383859360
348	133100	383863310	3382	383859928
348	133108	383863823	3327	383860496
348	133116	383864373	3309	383861064
348	133124	383864761	3121	383861640
348	133132	383865407	3199	383862208
348	133140	383865889	3113	383862776
348	133148	383866419	3075	383863344
348	133156	383867058	3146	383863912
348	133204	383867517	3045	383864472
348	133212	383868297	3249	383865048
348	133220	383868771	3155	383865616
348	133228	383869363	3171	383866192
348	133236	383870014	3254	383866760
348	133244	383870474	3146	383867328
348	133252	383871277	3381	383867896
348	133300	383871795	3339	383868456

348	133940	383900152	3248	383896904
348	133948	383900791	3311	383897480
348	133956	383901288	3240	383898048
348	134004	383901797	3181	383898616
348	134012	383902312	3128	383899184
348	134020	383902854	3102	383899752
348	134028	383903477	3157	383900320
348	134036	383903993	3097	383900896
348	134044	383904336	2880	383901456
348	134052	383904863	2831	383902032
348	134100	383905461	2861	383902600
348	134108	383906046	2878	383903168
348	134116	383906729	2993	383903736
348	134124	383907185	2881	383904304
348	134132	383907847	2975	383904872
348	134140	383908444	2996	383905448
348	134148	383909006	2990	383906016
348	134156	383909622	3038	383906584
348	134204	383910219	3067	383907152
348	134212	383910832	3112	383907720
348	134220	383911344	3056	383908288
348	134228	383911849	2993	383908856
348	134236	383912299	2875	383909424
348	134244	383912962	2962	383910000
348	134252	383913361	2793	383910568
348	134300	383913977	2833	383911144
348	134308	383914570	2858	383911712
348	134316	383915160	2880	383912280
348	134324	383915842	2994	383912848
348	134332	383916297	2881	383913416
348	134340	383916804	2812	383913992
348	134348	383917250	2698	383914552
348	134356	383917813	2685	383915128
348	134404	383918564	2876	383915688
348	134412	383919079	2823	383916256
348	134420	383919791	2959	383916832
348	134428	383920177	2777	383917400
348	134436	383921002	3034	383917968
348	134444	383921468	2940	383918528
348	134452	383921987	2883	383919104
348	134500	383922601	2921	383919680
348	134508	383923136	2888	383920248
348	134516	383923663	2847	383920816
348	134524	383924250	2874	383921376
348	134532	383924939	2987	383921952
348	134540	383925452	2932	383922520
348	134548	383926063	2967	383923096

FLIGHT	TIME	15 DEC 62	01	
349	131424	390151330	2922	390148408
349	131424	390151330	2922	390148408
349	131432	390152094	3110	390148984
349	131440	390152690	3138	390149552
349	131448	390153378	3242	390150136
349	131456	390153900	3188	390150712
349	131504	390154451	3155	390151296
349	131512	390155008	3152	390151856
349	131520	390155656	3224	390152432
349	131528	390156091	3075	390153016
349	131536	390156633	3041	390153592
349	131544	390157079	2903	390154176
349	131552	390157573	2829	390154744
349	131600	390158167	2847	390155320
349	131608	390158852	2956	390155896
349	131616	390159455	2983	390156472
349	131624	390160128	3080	390157048
349	131632	390160725	3093	390157632
349	131640	390161270	3070	390158200
349	131648	390161774	2990	390158784
349	131656	390162351	2991	390159360
349	131704	390162822	2886	390159936
349	131712	390163318	2814	390160504
349	131720	390163833	2745	390161088
349	131728	390164547	2883	390161664
349	131736	390165209	2969	390162240
349	131744	390165810	2994	390162816
349	131752	390166452	3060	390163392
349	131800	390167192	3224	390163968
349	131808	390167798	3246	390164552
349	131816	390168283	3163	390165120
349	131824	390168690	2994	390165696
349	131832	390169350	3078	390166272
349	131840	390169726	2878	390166848
349	131848	390170172	2748	390167424
349	131856	390170709	2709	390168000
349	131904	390171294	2726	390168568
349	131912	390172069	2917	390169152
349	131920	390172662	2934	390169728
349	131928	390173238	2934	390170304
349	131936	390173847	2967	390170880
349	131944	390174471	3015	390171456
349	131952	390175215	3183	390172032
349	132000	390175946	3330	390172616
349	132008	390176654	3470	390173184
349	132016	390176963	3195	390173768
349	132024	390177476	3132	390174344
349	132032	390178146	3226	390174920
349	132040	390178720	3224	390175496
349	132728	390207839	2927	390204912
349	132736	390208370	2890	390205480
349	132744	390208952	2888	390206064
349	132752	390209587	2955	390206632
349	132800	390210264	3056	390207208
349	132808	390210753	2961	390207792
349	132816	390211347	2987	390208360
349	132824	390212008	3072	390208936

349	132832	390212608	3080	390209528
349	132840	390213168	3064	390210104
349	132848	390213802	3122	390210680
349	132856	390214286	3030	390211256
349	132904	390214849	3017	390211832
349	132912	390215414	3006	390212408
349	132920	390216152	3168	390212984
349	132928	390216775	3215	390213560
349	132936	390217454	3318	390214136
349	132944	390218260	3548	390214712
349	132952	390218709	3421	390215288
349	133000	390219337	3465	390215872
349	133008	390220044	3596	390216448
349	133016	390220519	3503	390217016
349	133024	390221276	3676	390217600
349	133032	390221731	3555	390218176
349	133040	390222305	3545	390218760
349	133048	390222813	3477	390219336
349	133056	390223406	3494	390219912
349	133104	390224024	3544	390220480
349	133112	390224649	3593	390221056
349	133120	390225282	3650	390221632
349	133128	390225732	3508	390222224
349	133136	390226321	3537	390222784
349	133144	390226696	3336	390223360
349	133152	390227186	3242	390223944
349	133200	390227886	3366	390224520
349	133208	390228507	3403	390225104
349	133216	390229116	3444	390225672
349	133224	390229645	3397	390226248
349	133232	390230202	3370	390226832
349	133240	390230935	3527	390227408
349	133248	390231515	3531	390227984
349	133256	390232062	3502	390228560
349	133304	390232597	3461	390229136
349	133312	390233154	3434	390229720
349	133320	390233568	3264	390230304
349	133328	390234183	3303	390230880
349	133336	390234932	3484	390231448
349	133344	390235290	3258	390232032
349	134024	390264176	3288	390260888
349	134032	390264817	3353	390261464
349	134040	390265192	3144	390262048
349	134048	390265836	3204	390262632
349	134056	390266412	3212	390263200
349	134104	390267032	3256	390263776
349	134112	390267473	3113	390264360
349	134120	390268073	3137	390264936
349	134128	390268695	3175	390265520
349	134136	390269277	3181	390266096
349	134144	390269854	3182	390266672
349	134152	390270470	3222	390267248
349	134200	390271037	3213	390267824
349	134208	390271646	3246	390268400
349	134216	390272194	3218	390268976
349	134224	390272798	3246	390269552
349	134232	390273357	3221	390270136
349	134240	390273873	3161	390270712
349	134248	390274736	3448	390271288

349	134256	390275369	3497	390271872
349	134304	390275841	3393	390272448
349	134312	390276416	3392	390273024
349	134320	390276810	3202	390273608
349	134328	390277482	3290	390274192
349	134336	390278060	3300	390274760
349	134344	390278373	3037	390275336
349	134352	390279035	3115	390275920
349	134400	390279609	3113	390276496
349	134408	390280019	2947	390277072
349	134416	390280439	2799	390277640
349	134424	390281072	2840	390278232
349	134432	390281705	2897	390278808
349	134440	390282283	2899	390279384
349	134448	390282941	2981	390279960
349	134456	390283622	3086	390280536
349	134504	390284163	3051	390281112
349	134512	390284724	3020	390281704
349	134520	390285255	2975	390282280
349	134528	390285854	3006	390282848
349	134536	390286538	3114	390283424
349	134544	390287218	3210	390284008
349	134552	390287855	3271	390284584
349	134600	390288405	3245	390285160
349	134608	390288884	3140	390285744
349	134616	390289564	3252	390286312
349	134624	390290080	3184	390286896
349	134632	390290680	3208	390287472
349	134640	390291225	3177	390288048
349	134648	390291723	3099	390288624
349	135328	390320600	3056	390317544
349	135336	390321087	2975	390318112
349	135344	390321511	2823	390318688
349	135352	390321993	2721	390319272
349	135400	390322417	2569	390319848
349	135408	390322873	2441	390320432
349	135416	390323564	2556	390321008
349	135424	390324112	2528	390321584
349	135432	390324787	2627	390322160
349	135440	390325219	2483	390322736
349	135448	390325790	2470	390323320
349	135456	390326430	2526	390323904
349	135504	390326822	2342	390324480
349	135512	390327440	2384	390325056
349	135520	390328037	2405	390325632
349	135528	390328662	2446	390326216
349	135536	390329405	2613	390326792
349	135544	390330066	2690	390327376
349	135552	390330603	2651	390327952
349	135600	390331200	2672	390328528
349	135608	390331940	2836	390329104
349	135616	390332636	2956	390329680
349	135624	390333300	3036	390330264
349	135632	390333943	3103	390330840
349	135640	390334530	3114	390331416
349	135648	390335167	3167	390332000
349	135656	390335759	3183	390332576
349	135704	390336355	3203	390333152
349	135712	390337012	3276	390333736

349	135720	390337566	3254	390334312
349	135728	390338129	3241	390334888
349	135736	390338781	3309	390335472
349	135744	390339229	3189	390336040
349	135752	390339851	3227	390336624
349	135800	390340363	3163	390337200
349	135808	390340813	3037	390337776
349	135816	390341321	2961	390338360
349	135824	390342025	3081	390338944
349	135832	390342702	3190	390339512
349	135840	390343210	3106	390340104
349	135848	390343905	3233	390340672
349	135856	390344519	3263	390341256
349	135904	390345242	3410	390341832
349	135912	390345947	3523	390342424
349	135920	390346484	3492	390342992
349	135928	390347217	3641	390343576
349	135936	390347901	3749	390344152
349	135944	390348347	3619	390344728